TRANSACTIONS
OF THE ASME
Series C

Journal of HEAT TRANSFER

May 1959

RADIATION • CONDUCTION • CONVECTION • COMPLEX SYSTEMS • PHASE CHANGES AND MIXTURES • TRANSIENT PHENOMENA • THERMOPHYSICAL PROPERTIES • EXPERIMENTAL TECHNIQUES • THERMOMETRY • ANALOG METHODS • ANALYTICAL AND NUMERICAL METHODS • APPLICATIONS • DESIGN TECHNIQUES • HEAT EXCHANGERS • INSULATION • ECONOMIC FACTORS BIOTECHNOLOGY • ASTRONAUTICS

Published Quarterly by
THE AMERICAN SOCIETY OF MECHANICAL ENGINEERS

TRANSACTIONS OF THE ASME
Series C

Journal of
HEAT TRANSFER

VOL. 81 • SERIES C • NO. 2
May 1959

CONTENTS

95 **Heat and Mass Transfer From a Rotating Disk**
F. Kreith, J. H. Taylor, and J. P. Chong

106 **Numerical and Machine Solutions of Transient Heat-Conduction Problems Involving Melting or Freezing, Part I**
W. D. Murray and Fred Landis

113 **A Theory of Rotating Condensation**
E. M. Sparrow and J. L. Gregg

121 **Laminar Heat Transfer in Rectangular Channels**
L. S. Han

129 **Heat Transfer to Water in Thin Rectangular Channels**
S. Levy, R. A. Fuller, and R. O. Niemi

144 **Combined Geometric and Network Analog Computer for Transient Heat Flow**
Victor Paschkis

151 **Heat Transfer From an Annular Fin of Constant Thickness**
H. H. Keller and E. V. Somers

157 **A Variational Method for Fully Developed Laminar Heat Transfer in Ducts**
E. M. Sparrow and R. Siegel

168 **The Effect of Surface Roughness on the Convection Heat-Transfer Coefficient for Fully Developed Turbulent Flow in Ducts With Uniform Heat Flux**
R. T. Lancet

EDITORIAL DEPARTMENT
Editor, J. J. JAKLITSCH, JR.
Editor Emeritus, GEORGE A. STETSON
Consulting Editor, LEO BLODGETT
Production, JEAN NORTH
Art Editor, HENRY BALFOUR

HEAT TRANSFER DIVISION
Chairman, W. E. HAMMOND
Secretary, J. F. WACHUNAS
Consulting Editor, S. P. KEZIOS

OFFICERS OF THE ASME
President, G. B. WARREN
Secretary, O. B. SCHIER, II
Treasurer, E. J. KATES
Assistant Treasurer, H. J. BAUER

PUBLICATIONS COMMITTEE
Chairman, JOHN de S. COUTINHO
B. G. A. SKROTZKI
HENDLEY N. BLACKMON
R. D. MINDLIN
MARTIN GOLAND
Junior Representatives
A. T. WUSKA
A. S. GOLDSTEIN

REGIONAL ADVISORY BOARD
Region I, ROY L. PARSELL
Region II, GLENN R. FRYLING
Region III, F. J. HEINZE
Region IV, FRANCIS C. SMITH
Region V, H. M. CATHER
Region VI, C. R. EARLE
Region VII, M. POPOVICH
Region VIII, LINN HELANDER

Published quarterly by The American Society of Mechanical Engineers. Publication office at 20th and Northampton Streets, Easton, Pa. The editorial department is located at the headquarters of the Society, 29 West Thirty-Ninth Street, New York 18, N. Y. Cable address, "Mechaneer," New York. Price $3.00 a copy, $10.00 annually; to members, $1.50 a copy, $5.00 annually. Add 50 cents for postage to all countries outside the United States, Canada, and Pan American Union. Changes of address must be received at Society headquarters seven weeks before they are to be effective on the mailing list. Please send old as well as new address. . . . By-Law: The Society shall not be responsible for statements or opinions advanced in papers or . . . printed in its publications (B13, Par. 4). . . . Second-class mail privileges authorized at Easton, Penna. . . . This publication is authorized to be mailed at the special rates of postage prescribed by Section 132.122 . . . © Copyrighted, 1959, by The American Society of Mechanical Engineers. Reprints from this publication may be made on condition that full credit be given the Transactions of the ASME, Series C—Journal of Heat Transfer, and the author, and that date of publication be stated.

TRANSACTIONS OF THE ASME
is indexed by the Engineering Index, Inc.

TRANSACTIONS OF THE ASME Series D

Journal of
BASIC ENGINEERING

Vol. 81 • Series D • No. 1

CONTENTS FOR MARCH, 1959

1 Ball Motion and Sliding Friction in Ball Bearings, by A. B. Jones. (58—AV-14)
13 A Variational Approach to Lubrication Problems and the Solution of the Finite Journal Bearing, by D. F. Hays. (58—SA-54)
24 On the Necessity of Unsteady Flow in Fluid Machines, by R. C. Dean, Jr.
29 Prediction of Choking Flow in Centrifugal Impellers, by Harold Lown and F. J. Wiesner, Jr. (58—SA-15)
37 Concerning Subharmonic Oscillations Which May Exist in Nonlinear Systems Having Odd Restoring Forces, by C. A. Ludeke and William Pong.
41 An Analytic Frequency-Response Solution for a Higher Order Servomechanism With a Nonlinear Control Element, by A. M. Hopkin and K. Ogata. (58—SA-35)
46 Antifriction Instrument-Bearing Torque Testing and the Resistance to Motion of Such Bearings, by A. B. Asch. (58—SA-34)
49 Analysis and Characteristics of the Three-Lobe Bearing, by O. Pinkus. (58—LUB-2)
56 An Investigation of Dry Adhesive Wear, by R. P. Steijn. (58—LUB-8)
67 Sliding Wear and Metal Transfer Under Unlubricated Conditions, by R. P. Steijn. (58—LUB-9
79 On the Mechanism of Gear Lubrication, by V. N. Borsoff. (58—LUB-4)
94 The Influence of the Molecular Mean Free Path on the Performance of Hydrodynamic Gas Lubricated Bearings, by Albert Burgdorfer. (58—LUB-7)

TRANSACTIONS OF THE ASME Series E

Journal of
APPLIED MECHANICS

Vol. 81 • Series E • No. 1

CONTENTS FOR MARCH, 1959

TECHNICAL PAPERS

3 Experimental Surface-Wave Method for Recording Force-Time Curves, J. N. Goodier, W. E. Jahsman, and E. A. Ripperger. (58—A-51)
8 Forced Torsional Vibration of Systems With Distributed Mass and Damping, K. E. Bisshopp. (58—A-8)
13 Frequencies of a Flexible Circular Plate and Light Elastic Half-Space, G. N. Bycroft. (58—A-37)
18 Analytical Design of Disk Cams by Independent Position Equations, F. H. Raven. (58—A-17)
25 Stress Distribution and Plastic Deformation in Rotating Cylinders, E. A. Davis and F. M. Connelly. (58—A-10)
31 Transient and Residual Stresses in Heat-Treated Cylinders, J. H. Weiner and J. V. Huddleston. (58—A-21)
40 The Nonlinear Bending of Thin Rods, T. P. Mitchell. (58—A-50)
44 Stresses and Deflections in Circular Plate Loaded Over a Segment, W. A. Bassali and M. Nassif. (58—A-27)
55 Transverse Flexure of a Thin Plate Containing Two Circular Holes, O. Tamate. (58—A-35)
61 Limit Analysis of Symmetrically Loaded Thin Shells of Revolution, D. C. Drucker and R. T. Shield. (58—A-26)
69 On Influence Coefficients and Nonlinearity for Thin Shells of Revolution, Eric Reissner. (58—A-33)
73 A Theorem of Maximum Strain Energy, E. H. Brown. (58—A-40)
77 Plastic Stress-Strain Relationships—Effect of Loading Path and History, S. S. Gill and J. Parker. (58—A-11)
88 A Stress-Strain Relation for Hexagonal Close-Packed Array of Spheres, J. Duffy. (58—A-53)
95 A Mathematical Model of the Stress-Strain Diagram and Hysteresis Loop, I. R. Whiteman. (58—A-68)
101 A Definition of Stable Inelastic Material, D. C. Drucker. (58—A-31)
107 Retarded Flow of Bingham Materials, Alfred Slibar and P. R. Paslay. (58—A-34)
114 An Experiment on Compressible-Flow Perturbations, T. A. D'Ews Thomson and R. E. Meyer. (58—A-52)
120 Transient Film Condensation, E. M. Sparrow and Robert Siegel. (58—A-13)
122 Effect of Turbulence on Slider-Bearing Lubrication, Y. T. Chou and Edward Saibel. (58—A-30)
127 Theory of Flight of the Sounding Rocket, V. C. Liu. (58—A-32)

DESIGN DATA AND METHODS

130 Stress-Concentration Factors for T-Heads, M. Hetényi.

BRIEF NOTES

133 Buoyancy Effects in Forced-Convection Flow, E. M. Sparrow and J. L. Gregg. 134 Thermally Induced Twists in Thin Plates, L. S. Han and K. L. Bergman. 136 Deflections and Vibrations of Clamped Sectorial Plates, M. Ben-Amoz. 137 Thermal Distributions Without Thermal Stresses, H. H. Hilton. 138 Thin-Walled Cylinders Under Torsion and Pressure, H. S. Suer and L. A. Harris. 140 Transient Heat Transfer for Flow in Ducts, Robert Siegel. 142 Upper and Lower Bounds for Stiffness of Plates, Eric Reissner. 143 Cross-Section Distortion and the Timoshenko Beam Equation, A. D. S. Barr. 144 Analysis of Paraboloidal Shells, Robert Schmidt. 145 Natural Frequencies of Two Nonlinear Systems, E. W. Gaylord. 146 Response of a Slab to Impact, J. N. Goodier and E. A. Ripperger. 147 Thermal Stresses in Long Cylindrical Shells, C. H. Tsao. 148 Dynamic Characteristics of Undamped Vibration Systems, M. E. Gurtin.

DISCUSSION

150 Discussion of previously published papers by A. J. Durelli and A. S. Kobayashi; J. W. Dally, A. J. Durelli, and W. F. Riley; R. Plunkett; J. W. Miles; T. H. Lin.

154 BOOK REVIEWS

TRANSACTIONS OF THE ASME
Series A

Journal of
ENGINEERING FOR POWER
Volume 81 • Series A • Number 2

CONTENTS FOR APRIL, 1959

111 The Control System of a 225,000-Kw Double-Automatic Extraction Steam Turbine and Related Reducing Stations, by M. A. Eggenberger and P. G. Ipsen. (58—SA-36)

123 Design of 321-Mw Cross-Compound Steam Turbine—River Rouge Unit No. 3, by C. D. Wilson. (58—SA-22)

133 Five Years' Experience on the Consolidated Edison System With Protection of Turbine Generators and Boilers by Automatic Tripping, by W. C. Beattie, H. A. Bauman, J. M. Driscoll, P. T. Onderdonk, and R. L. Webb. (58—Pwr-8)

142 A Simplified Regenerator Theory, by W. F. Schalkwijk. (58—A-135)

151 Development of a Smooth Running, Double-Spool, Gas-Turbine Rotor System, by J. R. Schnittger. (58—A-197)

161 M-252 Alloy for Heavy-Duty Gas-Turbine Buckets, by G. R. Fusner and D. L. Newhouse. (58—A-191)

177 The Calibration of Thermocouples by Freezing-Point Baths and Empirical Equations, by R. P. Benedict. (58—A-175)

189 Theoretical Stresses Near a Circular Opening in a Flat Plate, Reinforced With a Cylindrical Outlet, by E. O. Waters. (58—A-171)

201 Effect of Steam-Turbine Reheat on Speed-Governor Performance, by Charles Concordia. (58—A-36)

208 Load Capacity Tests on Tapered-Land and Pivoted-Shoe Thrust Bearings for Large Steam-Turbine Application, by R. E. Brandon and H. C. Bahr. (58—A-172)

TRANSACTIONS OF THE ASME
Series B

Journal of
ENGINEERING FOR INDUSTRY
Volume 81 • Series B • Number 2

CONTENTS FOR MAY, 1959

93 The Strength of Thick-Walled Cylinders, by B. Crossland, S. M. Jorgensen, and J. A. Bones. (58—Pet-20)

115 Steady-State Creep Analysis of the Weight Loadings of Furnace Tubes on Multiple Supports, by J. L. Jacobowitz and C. K. Mader. (58—Pet-14)

126 How to Replace Gears by Mechanisms (Linkages), by Kurt Hain and Gerhard Marx. (58—SA-33)

131 The Effect of a Lead Additive on the Machinability of Alloy Steels, by Norman Zlatin and J. V. Gould. (58—SA-53)

139 Controlled Contact Cutting Tools, by B. T. Chao and K. J. Trigger. (58—SA-42)

152 A Study of the Effects of Tool Flank Wear on Tool Chip Interface Temperature, by D. R. Olberts. (58—SA-41)

159 Synthesis of Path-Generating Mechanisms by Means of a Programmed Digital Computer, by Ferdinand Freudenstein and G. N. Sandor. (58—A-85)

169 Synthesis of the Four-Bar Linkage to Match Prescribed Velocity Ratios, by Philip Barkan and E. J. Tuohy. (58—A-115)

178 High-Range Plasticity of Metals Beyond Normal Work-Hardening, by E. V. Crane and W. S. Wagner. (58—A-132)

183 Self-Excited Vibrations in Metal Cutting, by N H. Cook. (58—A-189)

F. KREITH[1]
J. H. TAYLOR[2]
J. P. CHONG[3]

Heat and Mass Transfer From a Rotating Disk

The analogy between heat, mass, and momentum transfer is applied to a rotating disk. Experimentally measured mass-transfer rates from a disk rotating in an infinite environment under laminar and turbulent conditions are related to the corresponding heat-transfer process by means of an analogy method. The experimental analog is shown to eliminate difficulties associated with accurate measurements of heat-transfer coefficients.

Experimental data on the effect of an adiabatic surface placed at various distances parallel to the disk on the transfer rate from the disk are presented. Observations of some unusual flow patterns resulting from Goertler type vortexes in the transition regime and from some as yet unexplained turbulent vortex phenomena are also reported.

I Introduction

HEAT TRANSFER BY CONVECTION from a rotating body is of importance in the thermal analysis of rotating components of various types of machinery. The rotating disk is one of a number of geometrical configurations of interest because many practical systems can be idealized in terms of a disk rotating in an infinite environment or in a housing.

The hydrodynamic phenomena associated with a disk rotating in an infinite environment have been investigated theoretically by von Karman [1],[4] Cochran [2], Goldstein [3], and Stuart [4]; and experimentally by Theodorsen and Regier [5], Smith [6], and Gregory and Walker [4]. Heat transfer by convection has been investigated theoretically by Wagner [7] and Millsaps and Pohlhausen [8] for laminar flow and by Kreith and Taylor [9] for turbulent flow, and experimental data for cooling in air have been obtained by Young [10] in laminar flow, and by Cobb and Saunders [11] in the laminar as well as in the turbulent flow regime.

For a disk rotating in an enclosure Pantell [12] and Jimbo [13] have measured skin friction and velocity profiles experimentally, and Soo [14] and Schultz-Grunow [15] have investigated the boundary layer and flow characteristics theoretically; neither experimental nor theoretical work on heat transfer are available to date.

This paper contains the results of one phase of a long range research program designed to investigate transfer phenomena in rotating systems. In this phase of the work mass-transfer rates from a disk rotating at various speeds in an infinite environment in laminar and turbulent flow were measured and compared with the results of an analysis which is also applicable to heat transfer. The effect of placing a stationary surface at various distances parallel to the rotating disk surface was investigated experimentally in the laminar flow regime. Some unusual observations of flow patterns resulting from transitional "Goertler vortexes" and from some as yet unexplained turbulent vortex phenomena are also reported.

II Experimental Procedure

During the initial stages of developing equipment suitable for

[1] Professor of Aeronautical Engineering, University of Colorado, Boulder, Colo., formerly, Associate Professor of Mechanical Engineering, Lehigh University, Bethlehem, Pa. Mem. ASME.

[2] Supervisor of Dispersion Research, National Printing Ink Research Institute, Lehigh University, Bethlehem, Pa.

[3] Research Assistant in Mechanical Engineering, Lehigh University, Bethlehem, Pa.

[4] Numbers in brackets designate References at end of paper.

Contributed by the Heat Transfer Division of THE AMERICAN SOCIETY OF MECHANICAL ENGINEERS and presented at the ASME–AIChE Heat Transfer Conference, Chicago, Ill., August 18–21, 1958.

NOTE: Statements and opinions advanced in papers are to be understood as individual expressions of their authors and not those of the Society. Manuscript received at ASME Headquarters, November 7, 1958.

Nomenclature

A = heat or mass-transfer area, sq ft
C_{Dr} = local drag coefficient at r
$\bar{C}_D$ = average drag coefficient, $\frac{1}{\pi r_o^2}\int_0^{r_o} C_{Dr}\, 2\pi\, rdr$
c_p = specific heat at constant pressure, Btu/lb F
d = diameter of disk, ft
D_v = diffusivity of vapor in mass transfer, sq ft/hr
g_c = conversion factor, $32.2 \times (3600)^2$ ft lb/# hr^2
h_c = local convection heat-transfer coefficient at r, Btu/hr sq ft F
$\bar{h}_c$ = average convection heat-transfer coefficient, $\frac{1}{\pi r_o^2}\int_0^{r_o} h_c\, 2\pi rdr$, Btu/hr sq ft F
k = thermal conductivity, Btu/hr ft F
k_c = local mass-transfer coefficient at r, lb/hr sq ft (lb/cu ft)
$\bar{k}_c$ = average mass-transfer coefficient $= \frac{1}{\pi r_o^2}\int_0^{r_o} k_c\, 2\pi rdr$, lb/hr sq ft (lb/cu ft)
M = mass-flux parameter $(m/A)_s$, lb/hr sq ft
m = rate of mass transfer, lb/hr
p_v = partial pressure of vapor component A, #/sq ft
P = total pressure, #/sq ft
q_c = rate of heat transfer by convection, Btu/hr
Q = heat-flux parameter $(q/A)_s/c_p\rho$, ft F/hr
r = radial distance, ft
r_c = critical radius at which transition from laminar to turbulent flow begins, ft
r_o = outside radius of disk, ft
R_v = ideal gas constant for naphthalene vapor, ft #/lb R
S = $\sqrt{g_c\tau_s/\rho}$, shear velocity, ft/hr
T = temperature, F
$V(r)$ = net velocity at r relative to disk velocity at r, ft/hr
u_r = radial velocity component, ft/hr
u = peripheral velocity component, ft/hr
y = distance from disk surface, ft
α = thermal diffusivity, $k/\rho c_p$, sq ft/hr

(*Continued on next page*)

studying transfer processes from a rotating disk, an electrically heated test section was considered. The design of this test section involved the use of a guard heater at the rim of the rotating disk and sliprings for thermocouple or thermistor leads as well as for the electrical heating element. The initial cost of constructing this type of test section was estimated to be quite high and the reliability of measured heat-transfer coefficients appeared to be uncertain. In order to circumvent the experimental difficulties involved in taking heat-transfer and surface temperature measurements, it was decided to use a mass-transfer analogy, similar to one employed by Sogin [16]. This decision shifted the experimental difficulties to finding a suitable material which could withstand rotative speeds up to 10,000 rpm, but eliminated the need for taking heat flux and temperature measurements in a rotating body, and also obviated the necessity of correcting for heat leakages.

The arrangement of the equipment used in the experimental part of this study is shown in Fig. 1. An 8-in-diameter aluminum disk was mounted horizontally on a Serval "Superspeed" centrifuge which could be adjusted to and maintained at speeds ranging from 400 to 10,000 rpm. The speed was measured by means of a stroboscope. The temperature of the air above the disk was determined with a precision thermometer. The tests were carried out in a large closed room to eliminate stray air currents.

Before each test run crystal grade naphthalene ($C_{10}H_8$, molecular weight 128.2, melting point 79–81 C, residue after ignition less than 0.001 per cent) was melted in a covered flask in an electrically heated oven at about 120 F. The molten naphthalene was then cast into the undercut and recessed center of the aluminum disk on whose rim a split retaining ring was mounted. The disk with the molten naphthalene was then cooled in air at room temperature. After the naphthalene had solidified the retainer ring was removed and the surface of the naphthalene was machined on a lathe to obtain a smooth surface raised about $^1/_{32}$ in. above the rim of the disk.

Prior to each test the surface of the naphthalene was carefully cleaned of loose particles and the aluminum disk with the cast naphthalene coating was weighed on a precision balance to within 0.002 gm. The disk was then mounted on the centrifuge and brought up to speed. The time was recorded at initial weighing, at centrifuge start, at attainment of the desired speed, at centrifuge power off, at centrifuge stop, and at reweighing.

Since the measured weight difference between initial and final weighings included losses between weighing and mounting, be-

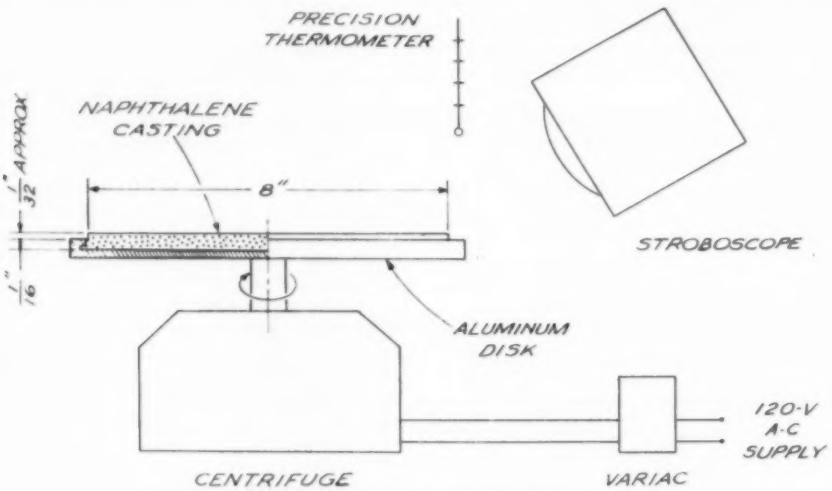

Fig. 1 Schematic sketch of experimental equipment

Nomenclature

ϵ_M = eddy diffusivity for momentum, sq ft/hr
ϵ_H = eddy diffusivity for heat, sq ft/hr
ϵ_m = eddy diffusivity for mass, sq ft/hr
δ = hydrodynamic boundary-layer thickness, ft
δ_H = thermal boundary-layer thickness, ft
δ_m = mass-transfer boundary-layer thickness, ft
ν = kinematic viscosity, $g_o\mu/\rho$, sq ft/hr
ω = rotational speed, rad/hr
ρ = fluid density, lb/cu ft
τ = fluid shear stress, #/sq ft
μ = fluid viscosity, # hr/sq ft
V^+ = nondimensional velocity in the boundary layer, V/S
y = distance from disk surface, ft
Y = clearance between disk surface and stationary shroud surface, ft
y^+ = nondimensional distance from the surface, yS/ν
Nu = local Nusselt number, $h_c r/k$
$\overline{\text{Nu}}$ = average Nusselt number, $\bar{h}_c r_o/k$
Sc = Schmidt number, ν/D_v
β_M = ratio of eddy diffusivities of mass and momentum, ϵ_m/ϵ_M
β_H = ratio of eddy diffusivities of heat and momentum, ϵ_H/ϵ_M
Sh = local Sherwood number, $k_c r/D_v$
$\overline{\text{Sh}}$ = average Sherwood number, $\bar{k}_c r_o/D_v$
$\overline{\text{Sh}}_Y$ = average Sherwood number for a shrouded disk with clearance Y
St = local Stanton number, $h_c/\omega r\rho c_p$
$\overline{\text{St}}$ = average Stanton number, $\bar{h}_c/\omega r_o\rho c_p$
Re = local rotational Reynolds number, $\omega r^2/\nu$
Re_o = rotational Reynolds number, $\omega r_o^2/\nu$
Pr = Prandtl number, ν/α

Subscripts

H = heat transfer
l = laminar
M = momentum transfer
m = mass transfer
o = outside radius of disk
s = surface of disk
t = turbulent
∞ = far away from disk
b = buffer layer

tween dismounting and weighing, and during the start-up and slow-down periods, appropriate corrections had to be applied to obtain the difference in weight due to mass transfer at the test speed. The losses before mounting and after dismounting were due to natural convection transfer. Mass-transfer rates during natural convection were therefore measured independently, multiplied by the total time elapsed between the initial weighing and mounting and between dismounting and the final weighing, and the resulting quantity subtracted from the measured weight difference. To correct similarly for losses during speeding up and slowing down of the disk, it was assumed that the mass-transfer rate varied linearly with time and that the rates of mass transfer were independent of the acceleration. These assumptions were checked by repeating test runs at a given rotational speed, but varying their total duration. Since the results were reproducible within the estimated accuracy of the experimental data, the method of correction was considered satisfactory. All test runs were of sufficient duration that the total of the mass loss corrections necessary for any of them was less than 1.5 per cent of the measured weight difference.

The average mass-transfer coefficient for the system $\bar{k}_c$ is defined by the equation

$$\bar{k}_c = mR_v T_s / p_{v,s} A \qquad (1)^5$$

where m is the total rate of mass transfer in lb/hr

R_v is the ideal gas constant of the vapor in ft #/lb R
T_s is the surface temperature of the solid naphthalene in R
P_{v_s} is the vapor pressure of the naphthalene at T_s in #/sq ft
A is the surface area of the naphthalene in sq ft. and
$\bar{k}_c$ is the average mass-transfer coefficient in lb/hr sq ft (lb/ft^3)

In Equation (1) the vapor pressure P_{v_s} is the saturation pressure corresponding to the temperature T_s which was not actually measured. However, as shown in Reference [17], the temperature measured by the thermometer differs from the disk surface temperature only by two small corrective terms. One accounts for the surface temperature depression by cooling due to sublimation. Its numerical value is about 0.1 F. The other term corrects for the difference between the recovery temperature indicated by the thermometer and that of the cylinder surface. For the rotating disk this term is $[(\omega r)^2/2Jg_c c_p](1 - \eta_r)$ where η_r is the recovery factor. Assuming that the recovery factor for a rotating disk is of the same order of magnitude as for a flat plate at the same velocity, this correction term never exceeds 1 deg F. The omission of these correction terms does therefore not introduce an appreciable error in the results. An analysis of the accuracy of the experimental results in terms of uncertainty intervals based on 20 to 1 odds [18], indicates that the value of any of the mass-transfer coefficients is accurate to within ±6 per cent without applying a surface temperature correction.

The physical properties used in the reduction of the experimental data, including the diffusion coefficient of naphthalene vapor in air, the specific gravity of solid naphthalene, and the vapor pressure of solid naphthalene, were taken from Table 2 of Reference [19] which is based on the best available data.

In the tests designed to study the effect of a shroud on the transfer process, the experimental procedure described here was followed, but after the disk was mounted a 2-ft-square glass plate was placed parallel to and at a predetermined distance above the disk surface on an adjustable stand. The same data reduction method as for the free disk was used.

[5] The concentration of naphthalene vapor in the air above the plate is so small that no correction need to be made to distinguish the process from equimolar counterdiffusion.

III Evaluation of Average Mass and Heat-Transfer Coefficients for a Disk Rotating in an Infinite Environment

The experimental technique used in this investigation as well as that in the heat-transfer measurements of Cobb and Saunders [11] yielded average coefficients of mass and heat transfer. To compare the measured values with those calculated analytically it is therefore necessary to evaluate average values of the coefficients.

As shown in Appendix I as well as in References [7 and 8], the theory predicts that in the laminar flow regime mass and heat-transfer coefficients are uniform over the entire surface of a rotating disk. For the system used in the experiments, i.e., for a Schmidt number of 2.4, the approximate analysis presented in Appendix I yields the equation

$$\mathrm{Sh} = k_x x/D_v = 0.67\mathrm{Re}^{0.5} \qquad (2)$$

Equation (2) applies also to heat transfer for a fluid having a Prandtl number of 2.4 if the Sherwood number is replaced by the Nusselt number $h_x x/k$.

An exact solution of the complete Navier-Stokes and energy equations for the rotating disk was obtained by Millsaps and Pohlhausen [8]. For cases where viscous dissipation can be neglected, the usual situation in laminar flow, their results can be reduced to the equation

$$\mathrm{Nu} = \mathrm{Sh} = C\mathrm{Re}^{0.5} \qquad (3)$$

where the constant C depends on the Schmidt or Prandtl number as shown in Table 1

Table 1

Pr or Sc	0.74	1.0	2.5	5.0	7.5	10
C in Eq. (3)	0.33	0.39	0.60	0.80	1.0	1.1

As shown in Reference [4], laminar flow exists at Reynolds numbers $\omega r^2/\nu$ below about 2×10^5. At about this value of Reynolds number disturbances in the laminar boundary layer on the disk are amplified and rapidly cause transition to turbulent flow. At a Reynolds number $\omega r_o^2/\nu$ larger than about 2.8×10^5 the flow is completely turbulent. On a rotating disk having a Reynolds number larger than 2.8×10^5 there exists therefore a laminar inner core surrounded by a ring shaped transition region and a ring shaped turbulent regime.

In the turbulent regime mass and heat-transfer coefficients increase with increasing radius. As shown in Appendix II, a modified mass, heat, and momentum-transfer analogy predicts local values of Sherwood or Nusselt numbers given by the equations

$$\mathrm{Sh} = \frac{\mathrm{Re}\,\mathrm{Sc}\,\beta_m\sqrt{C_{Dr}/2}}{5\beta_m\mathrm{Sc} + 5\ln(5\beta_m\,\mathrm{Sc} + 1) + \sqrt{2/C_{Dr}} - 14} \qquad (4)$$

and

$$\mathrm{Nu} = \frac{\mathrm{Re}\,\mathrm{Pr}\,\beta_H\sqrt{C_{Dr}/2}}{5\beta_H\mathrm{Pr} + 5\ln(5\beta_H\mathrm{Pr} + 1) + \sqrt{2/C_{Dr}} - 14} \qquad (5)$$

respectively, where the symbols are defined in the nomenclature.

To evaluate average values of the mass coefficients the local values must be integrated over the entire disk surface according to the equation

$$\bar{k}_c = \frac{1}{\pi r_o^2}\left(\int_{r_0}^{r_o} k_{c_l} 2\pi r\,dr + k_{c_l}\pi r_c^2\right) \qquad (6)$$

Table 2 Summary of results for mass transfer from disk rotating in an infinite environment

Test run no.	Speed, rpm	Temperature of air, deg F	Rate of mass transfer, gm/min	Average Sherwood number	Reynolds number based on disk radius
1	2900	79.7	0.02546	293	1.98×10^5
2	4500	77	0.04074	545	3.10
3	5500	77	0.05776	773	3.78
4	2000	77.4	0.01762	231	1.37
5	7000	77.4	0.08817	1154	4.81
6	7200	76.6	0.08520	1216	4.96
7	1000	75.9	0.01137	162	0.691
8	2000	72.9	0.01421	240	1.40
9	3000	72.9	0.01812	305	2.09
10	6520	74.9	0.06238	937	4.52
11	500	69.8	0.00568	114	0.352
12	1200	72.1	0.0101	179	0.839
13	3600	79.6	0.03364	388	2.45
14	3300	77.9	0.02931	373	2.26
15	8300	78.0	0.10949	1397	5.69
16*	10300	77.2	0.15111	2005	7.08
17	700	72.8	0.00852	144	0.488
18	1500	70.8	0.01065	202	1.05
19	1730	70.9	0.01169	220	1.21
20	2250	76.7	0.01896	258	1.55
21	2600	77.7	0.02144	275	1.78

* In this test a small piece of solid naphthalene chipped off near the rim and it was estimated that the actual mass-transfer rate is about 6 per cent less than the measured value.

where r_c is the radius corresponding to the critical Reynolds number.

The same procedure must be followed to evaluate the average heat-transfer coefficient. Since the expressions for k_{ci} and h_{ci} derived in Appendix II cannot be integrated analytically, the averaging was done numerically according to

$$\bar{k}_c = k_{ci}\left(\frac{r_c}{r_o}\right)^2 + 2\sum_{n=1}^{n=N} k_{ci}\left(\frac{r_n}{r_o}\right)\frac{\Delta r}{r_o} \qquad (7)$$

where Δr was taken as 0.2 in. and

$$N = (r_o - r_c)/\Delta r$$

In the averaging procedure the transition region was neglected and it was assumed that turbulent flow sets in at the radial distance corresponding to the critical Reynolds number (see Fig. 2).

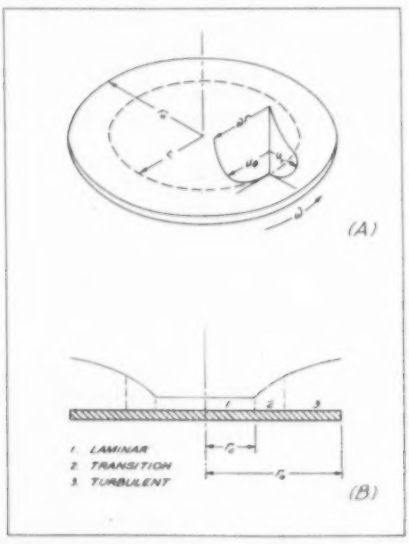

Fig. 2 (A) Velocity profile with observer riding on disk; (B) boundary layer profile

The average Sherwood number corresponding to the average value of the mass-transfer coefficient was then evaluated according to

$$\overline{\mathrm{Sh}} = \bar{k}_{r_o}/D, \qquad (8)$$

A similar procedure was followed in the evaluation of the average Nusselt numbers.

IV Presentation and Discussion of Results

The experimental results for mass transfer from the disk rotating in an infinite environment are summarized in Table 2. The speed was varied from about 500 to 10,000 rpm, corresponding to a rotational Reynolds number variation from about 3.5×10^4 to 7×10^5. At the highest Reynolds number about 70 per cent of the total disk surface was covered by a turbulent boundary layer.

The test results are presented graphically in Fig. 3 where the average Sherwood number is plotted as a function of the rotational Reynolds number. Also shown in Fig. 3 are the results of theoretical analyses for the laminar flow regime and the results of the analogy calculations according to Equations (7) and (8). In addition to the mass-transfer results, averaged heat-transfer data obtained by Cobb and Saunders [11] with a disk rotating in air are compared with the results of the analogy calculations in Fig. 3.

In the laminar regime the experimental data fall slightly below the curve predicted by the analysis in Appendix I, but slightly above Millsaps and Pohlhausen's theory [8]. When the Reynolds number exceeds the critical value and part of the disk surface is covered by a laminar boundary and part by a turbulent boundary layer, the experimental mass-transfer data fall slightly below the results predicted by the analogy if a critical Reynolds number of 2×10^5 is used, but above the calculated curve if 2.5×10^5 is taken to be the critical Reynolds number. In view of the numerous assumptions made in the analysis the agreement between theory and experiment is quite satisfactory for a Schmidt number of 2.4.

The experimental heat-transfer data, that is the average Nusselt numbers for the disk, agree in the laminar regime within 5 per cent with the results predicted theoretically in References [7 and 8]. At turbulent Reynolds numbers the heat-transfer data fall as much as 10 per cent below the result predicted on the basis of the analogy calculations for a Prandtl number of 0.74 and a β_H of

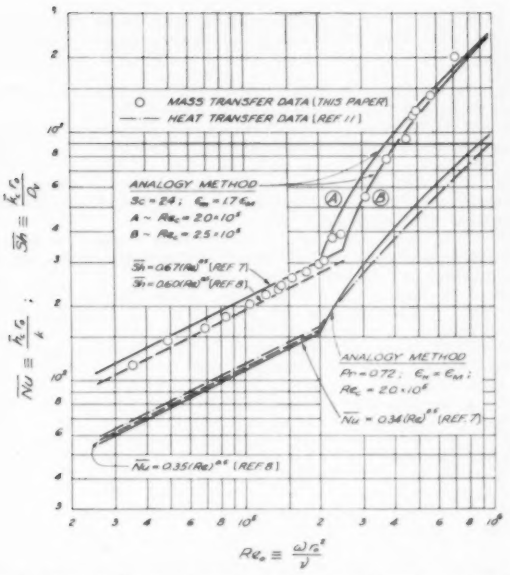
MASS TRANSFER DATA (THIS PAPER)
HEAT TRANSFER DATA (REF 11)
ANALOGY METHOD
Sc = 2.4; $\epsilon_m = 1.7\epsilon_M$
A ~ $Re_c = 2.0\times10^5$
B ~ $Re_c = 2.5\times10^5$
$\overline{Sh} = 0.671(Re)^{0.5}$ (REF 7)
$\overline{Sh} = 0.601(Re)^{0.5}$ (REF 8)
ANALOGY METHOD
Pr = 0.72; $\epsilon_m = \epsilon_M$;
$Re_c = 2.0\times10^5$
$\overline{Nu} = 0.34(Re)^{0.6}$ (REF 7)
$\overline{Nu} = 0.35(Re)^{0.6}$ (REF 8)
$\overline{Sh} \equiv \frac{\bar{h}r_0}{\mathcal{D}_M}$
$\overline{Nu} \equiv \frac{\bar{h}r_0}{k}$
$Re_\omega \equiv \frac{\omega r_0^2}{\nu}$

Fig. 3 Average Sherwood number and average Nusselt number as a function of rotational Reynolds number for a disk rotating in an infinite environment

unity. One possible reason for this deviation is that the analogy calculations take no account of variations in physical properties which are insignificant in mass transfer, but should be taken into account in heat transfer. Moreover, since the disk with which the heat-transfer data were obtained was electrically heated, the surface temperature may not have been uniform. It is of course also possible that the assumptions made in the analogy calculations could be responsible for the deviation between theory and experiment.

Some observations incidental to the primary objective of the research are worth mentioning. At the end of several tests in the turbulent Reynolds number range the imprints of certain features of the flow could be observed on the naphthalene surface. These traces corroborate the observations made by Gregory and Walker [4] by means of the china-clay evaporation technique in the transition regime. According to these authors a vortex system is generated in the region of flow upstream of transition, and between two critical radii vortexes occur which are stationary relative to the moving surface. Also the imprints left on the naphthalene surface indicate the presence of fairly level scale vortex patterns locked to the surface in the transition regime. However, whereas in the British experiments [4] no traces of the vortex pattern were visible in the turbulent regime, the imprints on the naphthalene suggest that also in the fully developed turbulent regime vortexes remain attached to the disk surface and penetrate the so-called laminar sublayer in a more or less regular manner. The scale of the vortexes in the turbulent regime appears to be much smaller than in the transition regime. To verify the existence of stationary vortexes in the turbulent zone the tests should be repeated with a disk whose surface is covered with china-clay, but instead of looking for traces merely after completion of a test, the streak pattern should be recorded photographically throughout the test. It is planned to perform such tests in the future.

The effect of a shroud on the mass-transfer process from a rotating disk was studied experimentally in the laminar flow regime at rotational speeds of 1000 and 2000 rpm, corresponding to rotational Reynolds numbers of about 7×10^4 and 1.4×10^5. The test results are summarized in Table 3 and presented graphically in Fig. 4 where the ratio of the average Sherwood number for the shrouded disk to the Sherwood number for the free disk at the same rotational Reynolds number $\overline{Sh}_Y/\overline{Sh}_\infty$ is plotted versus the ratio of the distance between the disk and the shroud surface and the disk diameter, Y/d.

An inspection of the results shows that within the range of Reynolds number covered in the experiments the effect of the Reynolds number on the Sherwood number ratio is less than the scatter of the data. The presence of a shrouding surface decreases the rate of mass transfer. At a clearance to diameter ratio of 0.25 the mass transfer for the shrouded disk is only about 10 per cent less than that for a comparable free disk, but drops to 80 per cent of the free disk mass-transfer rate at a clearance ratio of 0.05. As the clearance is further decreased the mass-transfer rate decreases rapidly.

These observations are in qualitative agreement with analyses of the boundary characteristics in this sort of system [14, 15]. When the fixed boundary is sufficiently far away from the surface of the rotating disk there will be two distinct boundary layers, one on the stationary, the other one on the rotating surface, leaving between them a "core" of finite width which rotates at approximately one half the velocity of the disk. In this regime the presence of the stationary surface would not be expected to affect the heat or mass transfer appreciably. However, as the clearance is decreased a point is reached where the two boundary layers meet. Any further decrease in clearance will impede the circulation appreciably and eventually cause choking of the central core. In this regime the rate of heat or mass transfer would be expected

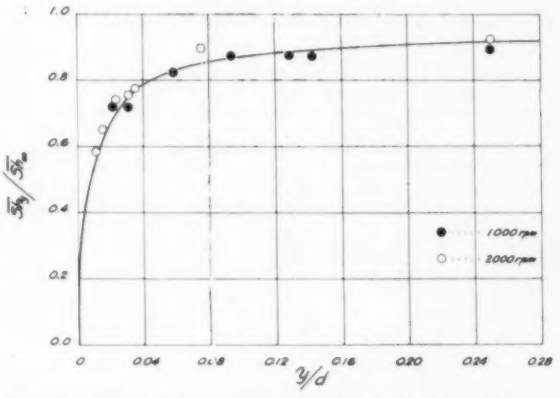

Fig. 4 Ratio of Sherwood number for shrouded disk to Sherwood number for free disk as a function of clearance ratio

Table 3 Summary of results for mass transfer from a disk rotating in a shroud

Test run no.	Speed, rpm	Dimensionless shrouding distance (Y/d)	Sherwood no. ratio ($\overline{Sh}_Y/\overline{Sh}_\infty$)
a	1000	0.143	0.871
b	1000	0.059	0.823
c	1000	0.129	0.878
d	1000	0.031	0.717
e	1000	0.094	0.872
f	1000	0.250	0.896
h	2000	0.079	0.898
i	2000	0.031	0.754
j	2000	0.035	0.776
k	2000	0.023	0.741
l	2000	0.016	0.651
m	2000	0.012	0.585
n	2000	0.250	0.926

to drop off rapidly with decreasing clearance. The experimental results corroborate these phenomena qualitatively, but additional studies of the flow and boundary layer characteristics are necessary before the various flow regimes can be delineated quantitatively.

V Conclusions

1 The analogy between heat, mass, and momentum transfer can be applied to a disk rotating in an infinite environment to calculate heat and mass-transfer coefficient from friction coefficients in the range of Prandtl and Schmidt numbers between 0.7 and 2.5.

2 In the laminar regime of rotational Reynolds numbers, a stationary surface placed parallel to the surface of a rotating disk reduces the rate of mass transfer, but the reduction is less than 20 per cent of the transfer rate for a free disk at clearance to diameter ratios larger than 0.05.

3 Traces left by the air flowing over a disk rotating in an infinite environment suggest that stationary vortexes occur in the turbulent as well as in the transition regime.

Acknowledgment

The work reported here was accomplished as a part of a research program at Lehigh University supported by a grant from the National Science Foundation.

References

1 Th. von Karman, "Über Laminare und Turbulente Reibung," *Zeitschrift für Angewandte Mathematik und Mechanik*, vol. 1, 1921, p. 233.

2 W. G. Cochran, "The Flow Due to a Rotating Disk," *Proceedings, Cambridge Philosophical Society*, vol. 30, 1934, p. 365.

3 S. Goldstein, "On the Resistance of a Disk Immersed in a Fluid," *Proceedings, Cambridge Philosophical Society*, vol. 31, 1935, p. 232.

4 N. Gregory, J. T. Stuart, and W. S. Walker, "On the Stability of Three-Dimensional Boundary Layers With Application to Flow Due to a Rotating Disk," *Philosophical Transactions of the Royal Society of London, Mathematical and Physical Sciences*, series A, vol. 248, 1956, p. 155.

5 T. Theodorsen and A. Regier, "Experiments on Drag of Revolving Disks, Cylinders, and Streamlined Rods at High Speeds," NACA Rep. No. 793, 1944.

6 N. S. Smith, "Exploratory Investigation of Laminar Boundary Layer Oscillations on a Rotating Disk," NACA TN No. 1227, 1947.

7 C. Wagner, "Heat Transfer From a Rotating Disk to Ambient Air," *Journal of Applied Physics*, vol. 19, 1948, p. 837.

8 K. Millsaps and K. Pohlhausen, "Heat Transfer by Laminar Flow From a Rotating Plate," *Journal of the Aeronautical Sciences*, vol. 19, 1952, p. 120.

9 F. Kreith and J. H. Taylor, "Heat Transfer From a Rotating Disk in Turbulent Flow," ASME Paper No. 56—A-146, 1956.

10 R. L. Young, "Heat Transfer From a Rotating Plate," TRANS. ASME, vol. 78, 1956, p. 1163.

11 E. C. Cobb and O. A. Saunders, "Heat Transfer From a Rotating Disk," *Proceedings, Royal Society*, vol. 236, 1956, p. 343.

12 K. Pantell, "Versuche über Scheibenreibung," *Forschung auf dem Gebiete des Ingenieurwesens*, vol. 16, 1949 p. 97.

13 H. Jimbo, "Investigation of the Interaction of Windage and Leakage Phenomena in a Centrifugal Compressor," ASME Paper No. 56—A-47.

14 S. L. Soo, "Laminar Flow Over an Enclosed Rotating Disk," TRANS. ASME, vol. 80, 1958, p. 287.

15 F. Schultz-Grunow, "Der Reibungswiderstand rotierender Scheiben in Gehausen," *Zeitschrift für Angewandte Mathematik und Mechanik*, vol. 15, 1935, p. 191.

16 H. H. Sogin, "Sublimation From Disks to Air Streams Flowing Normal to Their Surface," TRANS. ASME, vol. 80, 1958, p. 593.

17 Shao-Yen Ko and H. H. Sogin, "Laminar Mass and Heat Transfer From Ellipsoidal Surfaces of Fineness Ratio 4 in Axisymmetric Flow," TRANS. ASME, vol. 80, 1958, pp. 387–390.

18 S. J. Kline and F. A. McClintock, "Describing Uncertainties in Single-Sample Experiments," *Mechanical Engineering*, vol. 75, 1953, p. 3.

19 W. J. Christian and S. P. Kezios, "Experimental Investigation of Mass Transfer by Sublimation From Sharp-Edged Cylinders in Axisymmetric Flow With Laminar Boundary Layer," 1957 Heat Transfer and Fluid Mechanics Institute, Pasadena, Calif., June, 1957.

20 Th. von Karman, "The Analogy Between Fluid Friction and Heat Transfer," TRANS. ASME, vol. 61, 1939, p. 705.

21 E. R. G. Eckert, "Introduction to the Transfer of Heat and Mass," McGraw-Hill Book Company, Inc., New York, N. Y., 1950, pp. 120–125.

22 R. G. Deissler, "Analysis of Turbulent Heat Transfer, Mass Transfer, and Friction in Smooth Tubes at High Prandtl and Schmidt Numbers," NACA TN 3145, 1954.

23 T. K. Sherwood, "Heat Transfer, Mass Transfer, and Fluid Friction—Relationships in Turbulent Flow," *Industrial and Engineering Chemistry*, vol. 42, 1950, p. 2077.

24 J. G. Knudsen and D. L. Katz, "Fluid Dynamics and Heat Transfer," Engineering Research Bulletin, no. 37, Engineering Research Institute, University of Michigan, Ann Arbor, Mich., 1953.

25 W. M. Kays and I. S. Bjorklund, "Heat Transfer From a Rotating Cylinder With and Without Crossflow," TRANS. ASME, vol. 80, 1958, p. 70.

26 A. M. Dhanak, "Momentum and Mass Transfer by Eddy Diffusion in a Wetted-Wall Channel," ASME Paper No. 57—HT-32.

27 J. P. Opfell and B. H. Sage, "Turbulence in Thermal and Material Transport," in "Advances in Chemical Engineering," vol. 1, T. B. Drew and J. W. Hoopes, Jr., editors, Academic Press, Inc., New York, N. Y., 1956.

28 U. Grigull, "Die Grundegesetze der Wärmeübertragung," Springer Verlag, Berlin, Germany, 1955.

29 H. E. Brown, B. H. Amstead, and B. E. Short, "The Transfer of Heat and Momentum in a Turbulent Stream of Mercury," condensed in TRANS. ASME, vol. 79, 1957, pp. 279–285.

30 R. Jenkins, "Variation of the Eddy Conductivity With Prandtl Modulus and Its Prediction of Turbulent Heat Transfer Coefficients," Heat Transfer and Fluid Mechanics Institute, Stanford, Calif., 1951, p. 147.

APPENDIX I

Approximate Calculations of Rates of Heat and Mass Transfer From a Disk Rotating in an Infinite Environment in Laminar Flow

In cylindrical co-ordinates the steady-state equation for mass transfer of component A by molecular diffusion through an inert gas in laminar motion is

$$D_v\left(\frac{\partial^2 c}{\partial r^2}+\frac{1}{r}\frac{\partial c}{\partial r}+\frac{\partial^2 c}{\partial y^2}\right)-u_r\frac{\partial c}{\partial r}-u_y\frac{\partial c}{\partial y}=0 \quad (9)$$

where D_v is the diffusivity of component A in ft²/hr and c is the concentration of component A in the inert gas in lb/cu ft.

The corresponding equation for heat transfer to or from a rotating plate is

$$\alpha\left(\frac{\partial^2 T}{\partial r^2}+\frac{1}{r}\frac{\partial T}{\partial r}+\frac{\partial^2 T}{\partial y^2}\right)-u_r\frac{\partial T}{\partial r}-u_y\frac{\partial T}{\partial y}=0 \quad (10)$$

if viscous dissipation is neglected and the fluid properties are uniform. Assuming that the temperature or the concentration at the surface of the rotating plate is uniform and that the temperature or the concentration in the fluid far away from the plate is zero, the boundary conditions pertaining to the system are

$$\text{at } y=0: \quad T=T_s \quad \text{or } c=c_s$$

$$\text{at } y=\infty: \quad T=0 \quad \text{or } c=0$$

Von Karman [1] and Millsaps and Pohlhausen [8] have shown that the boundary layer thickness δ is constant over the entire plate, provided the small influence of flow toward the plate is neglected; and, that the radial flow velocity u_r at a given distance y from the disk surface is proportional to r. Consequently, the total mass rate of fluid flowing outward in the radial direction at any distance r is proportional to the area πr^2. Thus a concentration or temperature distribution dependent on y, but independent

of r may be assumed [7]. Equations (9) and (10) reduce then to the ordinary differential equations

$$(D_v)\left(\frac{d^2c}{dy^2}\right) - (u_y)\left(\frac{dc}{dy}\right) = 0 \tag{11}$$

and

$$(\alpha)\left(\frac{d^2T}{dy^2}\right) - (u_y)\left(\frac{dT}{dy}\right) = 0 \tag{12}$$

respectively. Equations (11) and (12) yield upon integration,

$$\frac{dc}{dy} = -\exp\left(\frac{1}{D_v}\int_0^y u_y dy + c\right) \tag{13}$$

and

$$\frac{dT}{dy} = -\exp\left(\frac{1}{\alpha}\int_0^y u_y dy + c\right) \tag{14}$$

Another integration gives

$$c = \int_y^\infty \exp\left(\frac{1}{D_v}\int_0^y u_y dy + C\right)\cdot dy \tag{15}$$

and

$$T = \int_y^\infty \exp\left(\frac{1}{\alpha}\int_0^y u_y dy + C\right)\cdot dy \tag{16}$$

The integration constant C can be evaluated from the boundary condition at $y = 0$ while the boundary condition at $y = \infty$ is automatically satisfied by the upper limit of the first integral in Equations (15) and (16). The concentration or the temperature at the plate surface are according to Equations (15) and (16), respectively

$$c_s = \int_0^\infty \exp\left(\frac{1}{D_v}\int_0^y u_y dy + C\right)\cdot dy \tag{17}$$

and

$$T_s = \int_0^\infty \exp\left(\frac{1}{\alpha}\int_0^y u_y dy + C\right)\cdot dy \tag{18}$$

On division of Equation (13) by Equation (17) or Equation (14) by Equation (18) the integration constant C drops out and

$$\frac{dc}{dy} = -c_s \frac{\exp\left(\frac{1}{D_v}\int_0^y u_y dy\right)}{\int_0^\infty \exp\left(\frac{1}{D_v}\int_0^y u_y dy\right)\cdot dy} \tag{19}$$

or

$$\frac{dT}{dy} = -T_s \frac{\exp\left(\frac{1}{\alpha}\int_0^y u_y dy\right)}{\int_0^\infty \exp\left(\frac{1}{\alpha}\int_0^y u_y dy\right)\cdot dy} \tag{20}$$

For naphthalene vapor diffusing from the solid naphthalene-air interface at the disk surface into the surrounding air the concentration in the gas phase is related to the partial pressure p_v by the equation

$$c = p_v/R_vT \tag{21}$$

where p_v is the partial pressure of the naphthalene vapor in the air in psf, R_v is the ideal gas constant in ft #/lb R, and T is the absolute temperature in deg R. The mass-transfer coefficient k_c and the heat-transfer coefficient h_c are given by

$$k_c = \frac{1}{c_s}\left[-D_v\left(\frac{\partial c}{\partial y}\right)_{y=0}\right] = \frac{1}{p_{v,s}}\left[-D_v\left(\frac{\partial p_v}{\partial y}\right)_{y=0}\right] = D_v\Big/\int_0^\infty \exp\left(\frac{1}{D_v}\int_0^y u_y dy\right)\cdot dy \tag{22}$$

and

$$h_c = \frac{1}{T_s}\left[-k\left(\frac{\partial T}{\partial y}\right)_{y=0}\right] = k\Big/\int_0^\infty \exp\left(\frac{1}{\alpha}\int_0^y u_y dy\right)\cdot dy \tag{23}$$

The corresponding dimensionless numbers, the Sherwood number and the Nusselt number, are

$$\mathrm{Sh} = \frac{k_c r}{D_v} = r\Big/\int_0^\infty \exp\left(\frac{1}{D_v}\int_0^y u_y dy\right)\cdot dy \tag{24}$$

and

$$\mathrm{Nu} = \frac{h_c r}{k} = r\Big/\int_0^\infty \exp\left(\frac{1}{\alpha}\int_0^y u_y dy\right)\cdot dy \tag{25}$$

The integrals of Equations (24) and (25) can be evaluated graphically with the aid of von Karman's solution [1] of the hydrodynamical problem according to which

$$\text{for } y \le \delta, \quad u_y = -2\omega\int_0^y \left[1.026\left(\frac{y}{\delta}\right)\left(1-\frac{y}{\delta}\right)^2\left(1+2\frac{y}{\delta}\right) - \frac{1}{2}\left(\frac{y}{\delta}\right)^2\left(1-\frac{y}{\delta}\right)^2\right] dy = -2\omega y\left[0.31\left(\frac{y}{\delta}\right)^4 - 0.52\left(\frac{y}{\delta}\right)^3 - 0.17\left(\frac{y}{\delta}\right)^2 + 0.51\left(\frac{y}{\delta}\right)\right] \tag{26}$$

and for

$$y > \delta, \quad u_y = -0.708(\nu\omega)^{1/2} \tag{27}$$

where

$$\delta = 2.58\left(\frac{\nu}{\omega}\right)^{1/2} \tag{28}$$

The mean temperature during the experiments was 74 F. At atmospheric pressure and 74 F the kinematic viscosity of air ν is 0.60 ft²/hr [19] and the vapor diffusivity D_v is 0.25 ft²/hr [19], so that Sc = 2.4. With this value for D_v Equation (24) becomes upon evaluation of the integral in the denominator

$$\mathrm{Sh} = 0.67\left(\frac{\omega r^2}{\nu}\right)^{1/2} = 0.67\,\mathrm{Re}^{1/2} \tag{29}$$

Similarly, for Pr = 2.4 the Nusselt number is

$$\mathrm{Nu} = 0.67\left(\frac{\omega r^2}{\nu}\right)^{1/2} = 0.67\,\mathrm{Re}^{1/2} \tag{30}$$

Wagner [7] evaluated the heat-transfer coefficient in air (Pr = 0.74) and found

$$\mathrm{Nu} = 0.34\left(\frac{\omega r^2}{\nu}\right)^{1/2} = 0.34\,\mathrm{Re}^{1/2} \tag{31}$$

It should be noted that both heat and mass-transfer coefficients are uniform over the entire surface in laminar flow.

APPENDIX II

Approximate Calculation of Rates of Heat and Mass Transfer From a Disk Rotating in an Infinite Environment in Turbulent Flow

The analogy between heat, mass, and momentum transfer has been used successfully to predict heat and mass-transfer coefficients from experimentally measured friction coefficients. Typical analogy solutions for flow inside of tubes or ducts and for flow over plane surfaces are described in References [20, 21, 22, 23, and 24]. Kays and Bjorklund [25] obtained recently an analogy solution for a circular cylinder rotating in an infinite environment and found that the solution agreed satisfactorily with experimental data for air.

The analogy method is based on the assumption that the transfer mechanisms for heat, mass, and momentum are physically similar, or can at least be described by similar equations of the form

$$g_c\tau_s/\rho = (\epsilon_M + \nu)\left(\frac{dV}{dy}\right) \tag{32}$$

for the momentum transfer and resulting shearing stress, by

$$\left(\frac{q}{A}\right)_s \Big/ \rho c_p = (\epsilon_H + \alpha)\left(\frac{dT}{dy}\right) \tag{33}$$

for the rate of heat transfer, and by

$$\left(\frac{m}{A}\right)_s = (\epsilon_m + D_v)\left(\frac{dc}{dy}\right) \tag{34}$$

for the rate of mass transfer, where ϵ_M, ϵ_H, and ϵ_m are dependent on the amount and kind of turbulent mixing at a point. To complete the analogy one assumes that $\epsilon_H = \beta_H\epsilon_M$ and $\epsilon_m = \beta_m\epsilon_M$ where β_H and β_m must be determined theoretically or experimentally inasmuch as the equation of motions for a fluid contains terms which are not present in the diffusion equation. In the vicinity of the surface the shear stress, the heat flux, and the mass flux are nearly constant and if the fluid properties are uniform, Equations (32), (33), and (34) can be written with reference to conditions at the surface as

$$\nu = (\epsilon_M + \nu)\cdot\frac{dV^+}{dy^+} \tag{35}$$

$$Q = \left(\beta_H\epsilon_M + \frac{\nu}{\mathrm{Pr}}\right)\cdot\frac{dT}{dy^+}\cdot\frac{S}{\nu} \tag{36}$$

and

$$M = \left(\beta_m\epsilon_M + \frac{\nu}{\mathrm{Sc}}\right)\cdot\frac{dc}{dy^+}\cdot\frac{S}{\nu} \tag{37}$$

The application of the analogy method to heat and mass transfer from a rotating disk is greatly simplified if one assumes that the flow in the immediate vicinity of the disk surface is similar to the flow near the wall of a pipe. This assumption can be partly justified on the basis of available data on the drag coefficients in the turbulent regime [5] which are well correlated by the equation

$$\frac{1}{\sqrt{C_{Dr}}} = \text{constant} + 4.07\log_{10}\left(\mathrm{Re}\sqrt{C_{Dr}}\right) \tag{38}$$

Equation (38) is of the same form as the well known von Karman-Nikuradse resistance equation for pipe flow and the coefficient 4.07 corresponds to a magnitude of 0.4 for the universal nondimensional profile constant for turbulent flow near a surface.

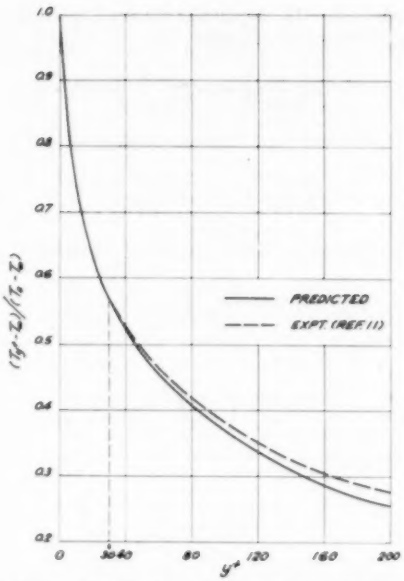

Fig. 5 Evaluation of buffer layer thickness by comparison of $(T_{y^+} - T_\infty)/(T_s - T_\infty)$ versus Y^+ calculated from analogy theory with experimental temperature profile measured by Cobb and Saunders, Reference [11]

Moreover, measurements by Gregory and Walker [4] and Theodorsen and Regier [5] indicate that the velocity profile near a disk is logarithmic outside the so-called laminar sublayer and that the radial velocity component is of a smaller order of magnitude than the tangential velocity component.

Although boundary layers on rotating disks are three dimensional and the differential equations for energy and momentum as well as the boundary conditions are dissimilar, for the purpose of the following approximate calculations a conventional analogy approximation was made. The flow field was divided into a so-called laminar sublayer extending from $y^+ = 0$ to $y^+ = 5$, a buffer layer from $y^+ = 5$ to $y^+ = 30$, and a turbulent region beyond $y^+ = 30$. The upper limit of the buffer layer thickness was estimated by comparing the temperature distribution predicted on the basis of strict analogy calculations [25] with the temperature profile measured by Cobb and Saunders [11]. The solid line in Fig. 5 represents the calculated temperature profile while the dashed line was faired through experimental data taken from Reference [11]. The experimental data follow the predicted curve quite well up to a value of y^+ of about 30, but beyond this point the experimental temperature gradient becomes less than the calculated value. On the basis of similar observations in experiments on heat transfer from a rotating cylinder Kays and Bjorklund [25] suggested that in the region beyond $y^+ = 20$ the transfer mechanism could be approximated by the simple Reynolds analogy. Although the two systems are dissimilar in many respects, the Reynolds analogy was found to be a satisfactory approximation for heat and mass transfer from a rotating disk beyond $y^+ = 30$. Although the following derivation is for mass transfer, it applies equally well to heat transfer since Equations (33) and (34) are analogous.

In the laminar sublayer $V^+ = y^+$, $\epsilon_M = 0$ and integration of Equation (37) gives therefore

$$\Delta c_l = 5M\,\mathrm{Sc}/S \tag{39}$$

In the buffer layer between $y^+ = 5$ and $y^+ = 30$ the von Karman-Nikuradse profile [21] is

$$V^+ = -3.05 + 5.0 \ln y^+ \tag{40}$$

which gives a dimensionless velocity gradient $dV^+/dy^+ = 5/y^+$ substituting $5/y^+$ for the velocity gradient in Equation (35) and solving for ϵ_M yields

$$\epsilon_M = \left(\frac{\nu y^+}{5} - \nu\right)$$

so that

$$\epsilon_m = \beta_m \nu \left(\frac{y^+}{5} - 1\right)$$

Equation (37) can then be written as

$$M = \left(\beta_m \frac{y^+}{5} - \beta_m + \frac{1}{\mathrm{Sc}}\right) \cdot S \cdot \frac{dc}{dy^+}$$

so that

$$dc_b = \frac{5M}{\beta_m s} \cdot \frac{dy^+}{y^+ - 5(1 - 1/\beta_m \mathrm{Sc})}$$

Integration between $y^+ = 5$ and 30 yields the concentration potential drop in the buffer layer Δc_b, or

$$\Delta c_b = \frac{5M}{\beta_m S} \cdot \ln(5\beta_m \mathrm{Sc} + 1) \tag{41}$$

In the flow regime outside of $y^+ = 30$ it will be assumed that the intensity of transfer processes by eddy diffusion is much greater than by molecular diffusion and that the shear stress and mass flux are the same function of y so that

$$\frac{\nu}{M} = \frac{1}{\beta_m} \cdot \frac{\nu}{S} \cdot \frac{dV^+}{dc}$$

Integration between $y^+ = 30$ and ∞ yields Δc_t, the concentration potential at the outer edge of the buffer layer, or

$$\Delta c_t = \frac{M}{\beta_m s} \int_{V^+=14}^{V^+=\frac{\omega r}{s}} dV^+ = \frac{M}{\beta_m S}\left(\frac{\omega r}{S} - 14\right) \tag{42}$$

Adding the concentration potentials and noting that $\omega r/S = \sqrt{2/C_{Dr}}$ gives

$$\Delta c = c_s - 0 = \frac{M}{\beta_m s}\left[5\beta_m \mathrm{Sc} + 5\ln(\beta_m \mathrm{Sc} + 1) + \sqrt{2/C_{Dr}} - 14\right]$$

so that

$$\frac{\mathrm{Sh}}{\mathrm{ReSc}} = \frac{M}{\Delta c \omega r} = \frac{\beta_m \sqrt{C_{Dr}/2}}{5\beta_m \mathrm{Sc} + 5\ln(5\beta_m \mathrm{Sc} + 1) + \sqrt{2/C_{Dr}} - 14} \tag{43}$$

For the calculations in this paper, the experimental results of Dhanak [26] were used to evaluate β_m and the local drag coefficients were taken from Reference [5].

Similarly, the analogy gives for heat transfer

$$\mathrm{St} = \frac{\mathrm{Nu}}{\mathrm{RePr}} = \frac{\beta_H \sqrt{C_{Dr}/2}}{5\beta_H \mathrm{Pr} + 5\ln(5\beta_H \mathrm{Pr} + 1) + \sqrt{2/C_{Dr}} - 14} \tag{44}$$

The selection of an appropriate value of β_H for the numerical evaluation of Equation (4) was difficult because even for a pipe or a duct available experimental results are inconclusive [27, 28, 29, 30]. Experimental measurements of β_H taken with air flowing in rectangular channels are summarized in Reference [27]. They indicate that the space average value of β_H increases with Reynolds number from about 1.1 at a Reynolds number of 2×10^7 to 1.4 at a Reynolds number of 9×10^7 but varies also with the distance from the surface at any given Reynolds number [27, 28]. Data obtained with liquid metals [29] give values of β_H in the range from 0.7 to 0.9.

In the past a value of unity for β_H [20, 22, 25] has been used with good success for heat-transfer analogy calculations. Also in this study a value of β_H equal to unity was found to yield satisfactory results, giving agreement within 10 per cent between the Nusselt numbers calculated from Equation (14) and the experimental results of Reference [11]. For comparison the calculations were repeated with β_H equal to 1.4, the other extreme. This caused the calculated Nusselt numbers to deviate about 27 per cent from the measured values.

In passing it is interesting to note that semiempirical methods deduced originally from experimental data on the basis of a thought model implying a strictly two-dimensional structure of the turbulent boundary layer have in this work and in Reference [25] been applied to systems in which the boundary layer structure must be three dimensional in nature. Since these methods are apparently applicable to cases in which the structure of the boundary layer can by no stretch of the imagination be considered two dimensional, it seems appropriate to question the hypothesis of a two-dimensional turbulent boundary layer in the other cases. The penetration of the so-called laminar sublayer by vortexes should supply additional food for thought.

DISCUSSION

S. L. Soo[6]

Professor Kreith and his associates have presented an interesting study with a rather unique experimental approach. Professor Kreith did not elaborate on the matter involving a stationary surface placed parallel to the disk. It might be worth pointing out that as far as heat-transfer analogy is concerned, his system provides an analog of a constant disk surface temperature, an insulated stationary surface, and the fluid drawn in and out from a constant temperature reservoir following the flow depicted in Fig. 9(*c*) of his reference [14]. Such a system is probably not of practical interest from disk cooling point of view. The discusser would like to suggest the following two different experiments for the constant disk temperature application:

(1) Insulated stationary surface with radial outflow cooling with mass-transfer analogy provided by a nonevaporating stationary surface but carry a central hole to pump air through the gap: Based on Fig. 10 of his reference [14], 1-in-diam hole, nonrecirculating flow can be maintained for a system at $^1/_{32}$-in. gap, 8-in. radius, and 1000 rpm.

(2) Constant stationary surface with recirculation cooling: The mass-transfer analogy can be provided by an intensely cooled stationary surface such that condensation of the evaporating medium can occur at the stationary surface.

Case (1) in practical application is source-flow cooling of a disk enclosed in an insulated housing; case (2) is a disk cooled by water-jacketed housing. Experimental data on such cases will not only furnish useful design reference, but also provide the experimental approximation for analytical study with infinite disk and infinite stationary plate. These data will help improve our understanding of the heat transfer of these significant systems.

[6] Associate Professor of Mechanical Engineering, Princeton University, Princeton, N. J.

Myron Tribus[7]

The use of the analogy between heat transfer and mass transfer in the case of the rotating disk is a very attractive method for getting around the problem of measuring temperatures and providing power through slip rings. If one is to rely upon the analogy, however, it is necessary that the boundary conditions for the mass-transfer system and the heat-transfer system be identical. The writer therefore is concerned with whether or not the surface of the disk was isothermal. If there occurred a variation in temperature over the disk surface, an even larger variation in vapor pressure is to be expected (because of the sensitivity of vapor pressure to temperature). These variations could very well change the mass transfer and therefore the corresponding dimensionless heat and mass-transfer moduli by 50 per cent or more. Does the author have any information concerning the temperature distribution which might have occurred over his disks? In addition, the writer would be interested to learn how the effects of aerodynamic heating were taken into account.

If we can have some assurance that this use of mass transfer to deduce heat transfer can be applied to the rotating disk, a number of important problems can be solved, for example, the disk rotating within housing, the disk with heat or mass transfer at selected points on the radius, and so on.

Authors' Closure

The authors wish to express their appreciation to Dr. Soo and Dr. Tribus for their interesting and constructive discussions.

The experiments in which a stationary surface was placed parallel to that of the rotating disk were of an exploratory nature and are being continued. The heat-transfer analog of the system investigated in the tests reported in the paper corresponds, as Dr. Soo has pointed out, to an isothermally heated rotating disk with an insulated surface placed parallel to the surface of the disk with fluid drawn in from, and discharged into, a constant temperature reservoir. However, subsequent studies of the fluid flow [31][8] have shown that the flow pattern in the space between the rotating disk and the stationary surface does not correspond to that predicted theoretically and depicted in Fig. 9(*c*) of Ref. [14]. As reported at the Symposium on Stall at the 1958 ASME Annual Meeting in New York [32], when the stationary surface is larger than the rotating disk the flow is periodic in nature with distinct inflow and outflow regions rotating in the space between the disk and the stationary surface. On the other hand, if the stationary surface is of the same size or smaller than the rotating disk, the flow is steady as assumed in Ref. [14]. The results of the investigation of the fluid flow mechanism in the space between a rotating disk and a stationary parallel surface will be presented in detail in a forthcoming paper [33].

The results of some preliminary experiments on the influence of the size of the stationary surface on the rate of mass transfer are shown in Fig. 6. Rates of mass transfer in a system consisting of an 8-in. diameter rotating disk with an 8-in. diameter stationary disk placed parallel to the rotating surface were measured with various clearances at speeds of 1000 and 2000 rpm. The results of these tests are presented graphically in Fig. 6 where the ratio of the average Sherwood number for the shrouded disk to the Sherwood number for the free disk at the same Reynolds number Sh_Y/Sh_∞ is plotted versus the clearance ratio Y/d. The dotted line represents a faired average for the 8-in-diameter stationary surface while the solid line, reproduced from Fig. 4, represents the average for the case of a very large stationary surface. Although the number of tests is not sufficient to allow any generalized conclusions, it is apparent that the size of the stationary surface affects the rate of mass transfer appreciably. For a given clearance ratio and speed, the rate of mass transfer is larger with the 8-in. stationary surface, i.e., in steady flow, than with a large stationary surface where the flow is periodic.

Following Dr. Soo's suggestions, a few test runs were also made with a radial outflow system. An 8-in-diameter stationary disk with a 1-in. diameter hold was placed at various distances from the rotating disk and rates of mass transfer were measured at 1000 and 2000 rpm. The results of these tests are plotted in Fig. 7. An inspection of the data shows that even at clearance ratios as small as 0.02 the rate of mass transfer in the radial outflow system is equal to that for a free disk. At 2000 rpm and clearance ratios between 0.01 and 0.02 the Sherwood number in

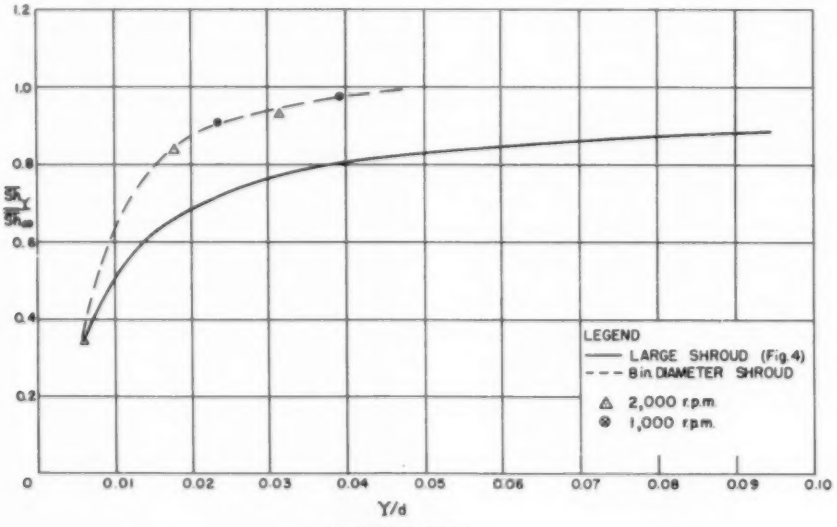

Fig. 6 Ratio of Sherwood number for shrouded disk to Sherwood number for free disk as a function of clearance ratio—comparison of 8-in. shroud with large 4 ft × 4 ft shroud

[7] Associate Professor, Engineering Department, University of California, Los Angeles, Calif. Mem. ASME.

[8] Numbers from 31–33 in brackets designate Additional References at end of this closure.

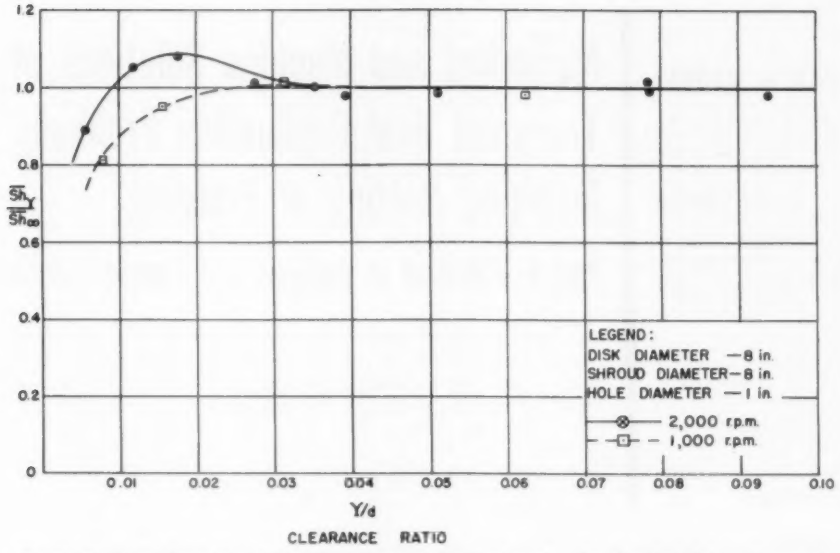

Fig. 7 Mass transfer with radial outflow—ratio of Sherwood number for shrouded disk to Sherwood number for free disk as a function of clearance ratio

the radial outflow system with naturally induced flow was found to be actually larger than the corresponding Sherwood number for a free disk. These results indicate that radial outflow systems may indeed be of practical interest in turbines and other types of rotating machines where disk cooling is a problem. A test program designed to investigate the effect of forced flow through the central hole on the flow and transfer mechanisms will be undertaken at the University of Colorado in the near future.

Dr. Tribus' question regarding the influence of aerodynamic heating on the temperature distribution over the disk surface can be answered by the following analysis. Although the surface temperature T_s was not measured directly, it can be calculated by means of a heat balance. Assuming that conduction within the solid and radiation to and from the surroundings are negligible compared to convection and sublimation, the rate of heat transfer by convection (including aerodynamic heating) to the surface equals the rate of heat transfer as a result of sublimation. For an observer riding on the disk the heat balance becomes therefore

$$h_c[T_\infty + (\eta V^2/2g_cJc_p) - T_s] = k_c p_v \lambda / R_v T_s \qquad (45)$$

where

η is the recovery factor
J is 778 ft #/Btu
λ is the latent heat of sublimation in Btu/lb

Applying the conventional heat-mass transfer analog and approximating ρ_{air} by $P/R_{air}T_s$ we get

$$k_c = (h_c/\rho_{air}c_p)(\mathrm{Pr}/\mathrm{Sc})^{2/3} = (h_c R_{air} T_s/Pc_p)(\mathrm{Pr}/\mathrm{Sc})^{2/3} \qquad (46)$$

Replacing k_c in Equation (45) by this expression yields

$$T_s = T_\infty + (\eta V^2/2g_cJc_p) - K_1 p_v/P \qquad (47)$$

where $K_1 = (R_{air}/R_v)(\mathrm{Pr}/\mathrm{Sc})^{2/3}\lambda/c_p = 1860$ F for the air-naphthalene system.

Introducing now the stagnation temperature $T_{0,\infty}$ we get

$$T_s = T_{0,\infty} - (V^2/2g_cJc_p)(1 - \eta) - K_1 p_v/P \qquad (48)$$

The temperature recorded by a thermometer placed in the air reservoir above the disk is $T_{0,\infty}$. The surface temperature of the disk T_s will therefore be less than $T_{0,\infty}$ as can be seen from Equation (48). The first correction term accounts for viscous dissipation and aerodynamic heating, the second for the cooling due to sublimation. The temperature depression caused by sublimation is less than 0.2 F and can be neglected in most cases. The correction term which accounts for the viscous forces in the boundary layer depends on the local disk velocity and may therefore produce a radial temperature variation over the disk surface. However, assuming that the recovery factor for a rotating disk is, as for turbulent flow over a flat plate, approximately equal to the third root of the Prandtl number, even at the highest speed used in the tests, the maximum temperature variation was less than 0.5 F. The effects of aerodynamic heating could therefore be neglected for the range of variables covered in this study, but they may become significant at higher speeds. The preceding analysis could then be used to calculate the temperature distribution over the surface and to make the corrections necessary for the proper reduction of the data and application of the mass-transfer analog to a heat-transfer problem.

References

31 L. A. Maroti, "Friction and Flow Phenomena Between a Rotating Disk and Parallel Plates," thesis, Lehigh University, September, 1958.

32 L. A. Maroti, G. Deak, and F. Kreith, "Unsteady Flow Induced by a Disk Rotating Between Two Plates," Symposium on Stall, December, 1958, Ingersoll-Rand Co., pp. 103–104.

33 L. A. Maroti, G. Deak, and F. Kreith, "Friction and Flow Phenomena of Partially Enclosed Disks," paper submitted to ASME for publication.

WILLIAM D. MURRAY

Senior Project Engineer, Burroughs Corporation, Paoli, Pa. Assoc. Mem. ASME

FRED LANDIS

Associate Professor of Mechanical Engineering, New York University, New York, N. Y. Mem. ASME

Numerical and Machine Solutions of Transient Heat-Conduction Problems Involving Melting or Freezing[1]

Part I—Method of Analysis and Sample Solutions

Previously published methods for the solution of one-dimensional heat-conduction problems with melting or freezing are briefly reviewed and weaknesses of previous analytic and numerical methods are outlined. Two new and more generally applicable numerical methods, applicable to digital and analog computation, are developed in the paper. Sample problems using these new techniques are solved and compared with the results of a widely used conventional method. An evaluation of the various methods and recommendations on areas of application are included.

1 Introduction

MANY PRACTICAL HEAT-TRANSFER PROBLEMS involve a change of phase of the material due to either melting or freezing. Applications include the solidification of castings, freezing or thawing of soil, ice formation, "ablation" of missile skins under aerodynamic heating, and others. In general, all these problems can be reasonably well described by unidimensional heat flux.

Despite the importance of the topic, a literature search reveals relatively few solutions which may be extended to practical problems. Analytical solutions are limited due to the mathematical complexity, while most numerical solutions have not been developed in a convenient and general form which combines good accuracy with computational ease.

The present paper briefly reviews the existing solutions and their range of applicability and introduces two novel numerical approaches which extend the range of initial and boundary conditions that can be covered. They will also permit a continuous determination of the fusion front travel and indicate the internal temperature distribution with a greater degree of accuracy than the previously published numerical methods. The utility of the new methods will be discussed in terms of both digital and analog mechanizations. Details of the actual implementation on digital and analog equipment and questions of stability, accuracy, and convergence will be presented in a subsequent companion paper.

2 Review of Methods and Solutions Presented in the Literature

The applicable differential equations for one-dimensional heat flow with constant thermal properties in both the solid and the liquid region (as found in most standard references, such as Carslaw and Jaeger [1])[2], are:

$$\frac{\partial \theta_s}{\partial t} = \alpha_s \frac{\partial^2 \theta_s}{\partial x^2} \tag{1a}$$

in the solid region, and:

[1] Abstracted from the thesis submitted by Mr. Murray in partial fulfillment of the requirements of the Eng ScD degree at New York University.

Contributed by the Heat Transfer Division of THE AMERICAN SOCIETY OF MECHANICAL ENGINEERS and presented at the ASME–AIChE Heat Transfer Conference, Chicago, Ill., August 18–21, 1958.

NOTE: Statements and opinions advanced in papers are to be understood as individual expressions of their authors and not those of the Society. Manuscript received at ASME Headquarters, June 4, 1958. Paper No. 58—HT-16.

[2] Numbers in brackets designate References at end of paper.

Nomenclature

c = specific heat, Btu-lb^{-1}-deg F^{-1}
E = half thickness of a finite slab, ft
k = thermal conductivity, Btu-ft^{-1}-deg F^{-1}-sec^{-1}
L = latent heat of fusion, Btu-lb^{-1}
L^* = latent to specific heat effect ratio $= \dfrac{L}{c(T_a - T_F)}$, dimensionless
n = increment of space, or "lump" number, dimensionless
N = number of space increments, or lumps, in E, dimensionless
p = space increment undergoing fusion (conventional method), dimensionless
q = space increment containing the fusion front (Method II), dimensionless
Q = heat flux (positive in direction of increasing x), Btu-sec^{-1} ft^{-2}
r = number of space increments in the solid region (Method I), dimensionless
t = time variable or instant, sec
T = temperature, deg F
T_a = ambient temperature ($= T_{x=0}$ for Stefan problem), deg F
x = space variable or location, ft
α = thermal diffusivity $= k/c\rho$, ft^2-sec^{-1}
ϵ = position of the fusion front, ft
θ = temperature excess above the fusion temperature ($= T - T_F$), deg F
$\theta_{x,t}$ = temperature excess at position x, time t, deg F
$\theta_{n,m}$ = temperature excess at space point n, time point m, deg F
ρ = density of the material, lb/ft^3

Subscripts

F = referring to fusion condition
L = referring to liquid material
m = evaluated at time $m\Delta t$
n = evaluated at $x = n\Delta x$
N = evaluated at $x = E$
0 = evaluated at $x = 0$
s = referring to solid material

$$\frac{\partial \theta_L}{\partial t} = \alpha_L \frac{\partial^2 \theta_L}{\partial x^2} \tag{1b}$$

in the liquid region, if internal natural convection can be neglected. If convection within the liquid is not negligible, an effective liquid conductivity must be defined, which accounts for both convection and conduction. In soil thawing or freezing problems, k_s and k_L are bulk-average values to account for both the soil and the ice or water, respectively.

At the fusion point, these equations are coupled due to the latent heat of fusion by:

$$\frac{d\epsilon}{dt} = \frac{1}{\rho L}\left\{k_s \left.\frac{\partial \theta_s}{\partial x}\right|_{x=\epsilon} - k_L \left.\frac{\partial \theta_L}{\partial x}\right|_{x=\epsilon}\right\} \tag{2}$$

where $d\epsilon/dt$ is the rate of travel on the fusion front, and L the latent heat of fusion, taken as positive for a freezing process. To avoid changes in the physical dimensions as the fusion front progresses, $\rho_s = \rho_L = \rho$ will be specified.

Methods of solution previously published can be grouped into analytical solutions, complete difference methods (where both space and time variables are written in difference form), and into "lumped parameter" methods, wherein the region is grouped into a finite number of discrete space lumps, but time is retained as a continuous variable. In the lumped parameter method the partial differential equations are reduced to a set of coupled ordinary differential equations, which can then be continuously integrated in time by active or inactive analog computers. For solutions on a digital computer, the complete difference method results in the required set of algebraic equations.

The earliest analytical solutions, given by Neumann [1, 2], were limited to a semi-infinite region, initially either all solid or liquid, and subject to a temperature step-input at the boundary. Stefan [2, 3] obtained direct solutions for the semi-infinite solid initially at fusion temperature with a step-input temperature at the boundary or for the specific heat flux distribution resulting in a constant fusion front velocity. Other Neumann or Stefan type solutions are given in References [4 through 12], which also include Lightfoot and Lachmann's analyses for the region bounded by parallel planes. A more recent extension for the case of constant fusion velocity was given by Kreith and Romie [13] for cylinders and spheres.

Weiner [14] analytically treated the case of constant freezing front velocity in a finite slab of metal bounded by semi-infinite molds. In practice, his generalization to consider successive different velocities will require numerical means to obtain a solution. An approximate solution for the fusion front travel in semi-infinite slabs, cylinders, and spheres was obtained by London and Seban [15], who assumed negligible subcooling effects in the solid, limiting the solutions to cases where $L^* = \dfrac{L}{c(T_a - T_F)} \gg 1.0$. Cochran [16] compared the London and Seban results to the Stefan solution and also indicated correction factors as a function of L^* to permit a qualitative extension of the method to other solidification problems. Landau [17] formulated the governing equations in a very general form and gave analytic solutions for the limiting cases of infinite or negligible latent heat effects.

The severe limitations imposed on the available analytical solutions can be lifted by either fully numerical or by lumped parameter techniques. Depending on the method selected, the problem can be extended to include nonuniform initial temperatures, more arbitrary boundary conditions, and, in certain instances, temperature dependent material properties.

The most complete analysis of numerical methods was presented by Eyres and his associates [18] in a pioneer paper. Eyres proposed three separate methods and computed examples on an electromechanical differential analyzer. The most powerful and most accurate of the three methods is a conventional finite difference procedure which was also used by a number of other authors. Since it forms the principal basis for comparison with the suggested new methods, it will be reviewed briefly.

In this analysis the total region is divided into N equally spaced intervals of length Δx. The temperature of each lump, as expressed at its center or nodal point, is considered to be uniform over the lump at each instant of time. For $N-1$ internal nodal points, the temperature corresponds to a lump extending $\pm \Delta x/2$ from the nodal point, while the boundary temperatures at points $n = 0, N$ are characteristic of a half lump of size $\Delta x/2$.

The lumped parameter equations for this case become [from equation (1)] for the nth internal lump:

$$\frac{d\theta_n}{dt} = \alpha \frac{(\theta_{n-1} - 2\theta_n + \theta_{n+1})}{\Delta x^2} \tag{3}$$

with α_s or α_L used, depending on whether the point is in the solid or liquid region.

The complete difference form of this equation is obtained when $\dfrac{\theta_{n,m+1} - \theta_{n,m}}{\Delta t}$ is substituted for $d\theta_n/dt$. Both regions are coupled by the common boundary condition $\theta_p = \theta_F = 0$, where p is the lump containing the fusion front. This boundary condition is maintained for a period such that the heat lost by the lump p equals the latent heat capacity $L\rho$.

Using either an R-C network analog or an electronic differential analyzer, lumped parameter solutions similar to the method given were presented by Martin and Bromberg [19], Kreith and Romie [13], and Aldrich and Paynter [20]. Dusinberre [21], Price and Slack [22], and Liebmann [23] used the fully numerical difference technique. Liebmann further developed a simple resistance analog to implement his solution.

To evaluate the advantages and shortcomings of the conventional method, which forms the basis of most published examples, the authors checked it for two critical sample problems. These will be discussed in detail in section 4, but it should be noted at this time that the method fails to describe the travel of the fusion front continuously and to give reliable indications of material temperatures near the fusion point. This becomes of practical importance in the solidification of many metals where mechanical and thermal problems may be significantly affected by the rate of solidification.

These objections are partially overcome by the remaining methods available in the literature. Cochran [16] simplified the analysis by using a single lump of variable size to represent the complete solid region (between the input boundary and the fusion front) for semi-infinite slabs, cylinders, and spheres all initially at the fusion temperature. While the technique leads to a continuous freezing front solution, the inaccuracies due to single lumping and the limited results available severely restrict its utility.

Otis [24] adapted the concept of a moving heat source to account for the latent heat as initially suggested by the work of Lightfoot and Landau. He subdivided the region into a finite number of space increments, which vary in size with time, but where the temperature in each lump is again considered to be uniform at any instant. The method requires a co-ordinate transformation in terms of an artificial time variable, which limits the analysis to materials initially or finally at the fusion temperature.

Forster [25] extended the conventional complete difference equations for fixed network spacing for the case of materials either initially or finally at the fusion temperature [equation (3)]. The fusion front travel was computed continuously by using a quadratic through the interface and at two adjoining points to obtain the slope of temperature at the fusion point.

Although the method yields accurate results and allows extension to include a variety of boundary conditions, initial (or final) conditions are limited to the fusion point temperature, and computation with the particular choice of the quadratic expansion is cumbersome.

Douglas and Gallie [26, 27] presented a stable, unique numerical analysis of Stefan type problems using a three-point approximation for the time derivative, which requires an implicit iteration of the temperature distribution (see also Reference [28]). However, the method imposes considerable mathematical complexity and requires that $\Delta\epsilon$ be evaluated in large finite steps rather than continuously.

3 Proposed New Methods

The two generalized methods suggested by the authors will yield considerably greater accuracy than the conventional method especially near the fusion point, while requiring only moderate increases in computational complexity. One approach utilizes a traveling space network where the fusion point travel can be accurately determined, but local temperature-time histories within the medium must be interpolated. The second method extends and generalizes the work of Forster; it leads to a more accurate prediction of the transient temperatures at any internal point, continuously computes the fusion front travel, but is subject to a small and rapidly decaying starting error.

Both methods will be applicable to a region with arbitrary initial temperatures and will permit arbitrary boundary conditions for specified surface temperature, convective or radiation heat exchange, or for a prescribed heat flux. The only restrictions are that only one liquid and one solid region be present, and that the material thickness is finite (except in the case where $\theta_{x,0} = \theta_F = 0$, when the Stefan problem may again be analyzed).

(a) Method I. Variable Space Network. Presenting first the variable space network method, it is assumed that the solid region ($x < \epsilon$) is divided into r equally sized space increments of thickness $\Delta x_s = \epsilon/r$, increasing as the freezing front progresses. Similarly, the liquid region ($x > \epsilon$) remains also divided into $N-r$ equally spaced intervals of thickness $\Delta x_L = (E-\epsilon)/(N-r)$ which shrink in time. This is illustrated in Fig. 1 for the special case of $N = 2r = 8$ network intervals.

The method focuses attention on the substantial temperature-time derivative of each internal point, given by:

$$\left.\frac{d\theta}{dt}\right|_n = \left.\frac{\partial\theta}{\partial x}\right|_n \frac{dx}{dt} + \left.\frac{\partial\theta}{\partial t}\right|_n \tag{4}$$

where the rate of travel of each point is related to the fusion front velocity in the solid by:

$$\left.\frac{dx/dt}{x}\right|_n = \frac{d\epsilon/dt}{\epsilon} \tag{5}$$

for a uniform solid network spacing.

Combination of equations (1), (4), and (5) leads to:

$$\left.\frac{d\theta}{dt}\right|_n = \frac{x_n}{\epsilon}\frac{\partial\theta_n}{\partial x}\frac{d\epsilon}{dt} + \alpha_s\frac{\partial^2\theta_n}{\partial x^2} \tag{6a}$$

in the solid region for the network points $n = 1, 2, \ldots, (r-1)$.

The corresponding equation in the liquid region will be:

$$\left.\frac{d\theta}{dt}\right|_n = \frac{E-x_n}{E-\epsilon}\frac{\partial\theta_n}{\partial x}\frac{d\epsilon}{dt} + \alpha_L\frac{\partial^2\theta_n}{\partial x^2} \tag{6b}$$

for $n = r+1, r+2, \ldots, N-1$. At the fusion point ϵ these equations are again coupled by equation (2).

If these equations be written in a difference form, all terms on the right-hand side should be expressed with a consistent approximation. A consistent three-point approximation will result in:

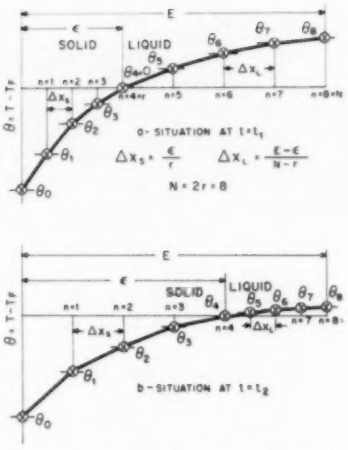

Fig. 1 Description of variables in Method I

$$\frac{d\theta_n}{dt} = \frac{n}{\epsilon}\frac{(\theta_{n+1}-\theta_{n-1})}{2}\frac{d\epsilon}{dt} + \alpha_s r^2\frac{(\theta_{n-1}-2\theta_n+\theta_{n+1})}{\epsilon^2} \tag{7a}$$

$$\frac{d\theta_n}{dt} = \frac{(N-n)}{(E-\epsilon)}\frac{(\theta_{n+1}-\theta_{n-1})}{2}\frac{d\epsilon}{dt} + \alpha_L(N-r)^2\frac{(\theta_{n-1}-2\theta_n+\theta_{n+1})}{(E-\epsilon)^2} \tag{7b}$$

for the solid and liquid regions in the lumped parameter form with the coupling equation:

$$\frac{d\epsilon}{dt} = \frac{1}{\rho L}\left\{k_s r\frac{(\theta_{r-2}-4\theta_{r-1})}{2\epsilon} + k_L(N-r)\frac{(\theta_{r+2}-4\theta_{r+1})}{2(E-\epsilon)}\right\} \tag{8}$$

The equivalent statement for the full difference form is obtained by substituting

$$\frac{\theta_{n,m+1}-\theta_{n,m}}{\Delta t} \text{ for } \left.\frac{d\theta}{dt}\right|_n \text{ and } \frac{\epsilon_{m+1}-\epsilon_m}{\Delta t} \text{ for } \frac{d\epsilon}{dt}.$$

These same substitutions will also apply to all subsequent equations which are given for the lumped parameter case only.

In addition to the differential equations, two boundary conditions must be prescribed. These may include temperature at the boundary or heat flux at the boundary as determined from:[3]

$$\frac{d\theta_0}{dt} = \frac{2\alpha_s}{\Delta x_s}\left\{\frac{\theta_1-\theta_0}{\Delta x_s} + \frac{Q_0(t)}{k_s}\right\} \tag{9a}$$

$$\frac{d\theta_N}{dt} = \frac{2\alpha_L}{\Delta x_L}\left\{\frac{\theta_{N-1}-\theta_N}{\Delta x_L} - \frac{Q_N(t)}{k_L}\right\} \tag{9b}$$

The boundary heat flux can be a function of time, surface temperature or external temperature, as would be the case with convective or radiation boundary conditions.

When $\epsilon = 0$, some terms of equations (7) and (8) become either infinite or indeterminate. Therefore, the problem must be started with a small assumed initial value ϵ_0, and a starting temperature must be assigned to the points in the solid region. By the same argument, the solution must be stopped before $(E-\epsilon) = 0$ and the final time period be extrapolated. Thereafter, the

[3] Further details of these derivations may be found in Reference [29].

subsequent time history of the solid can be continued by an analysis of the conventional diffusion equation.

In the fully numerical solution the choice of the initial fusion front distance ϵ_0 will have considerable effect on the solution time required; due to stability requirements a small initial Δt, corresponding to the initial values of Δx_s, materially increases the solution time for the early (and late) stages. This problem will not arise in the lumped parameter solution, where stability considerations do not enter and the starting value, ϵ_0, is determined by the equipment capacity in R-C network analyzers or by the number of scale changes desired in electronic differential analyzers.

(b) Method II. Fixed Space Network. This alternate method which permits the same range of boundary and initial conditions as the previous technique utilizes a fixed lump size as illustrated on Fig. 2 for the specific case of an eight space network.

At some intermediate time the fusion front ϵ will be in the qth lump $\left(\text{i.e., at a location } q\Delta x + \delta x, \text{ where } -\frac{\Delta x}{2} < \delta_s < \frac{\Delta x}{2}\right)$. For all points except 0, q, and N the conventional fixed space network equations will still apply:

$$\frac{d\theta_n}{dt} = \alpha \frac{\theta_{n-1} - 2\theta_n + \theta_{n+1}}{\Delta x^2} \tag{3}$$

In the conventional method, the whole fusion point lump was assumed to remain at the fixed fusion point temperature $\theta_F = 0$; here the fusion front will be traced as it travels through the qth lump and the temperature of the lump node will be continuously adjusted while the fusion front moves.

In the lump q (that containing the fusion front) a discontinuity in the temperature curve occurs at $x = \epsilon$. Two temperatures are calculated for the lump q, one by interpolation from temperatures in the solid region and the other by interpolation from temperatures in the liquid. In each case the fusion temperature and the location of the fusion front, $\epsilon = q\Delta x + \delta x$, are used to perform the interpolation:

$$\theta_{qs} = -\theta_{q-2}\frac{\delta x/\Delta x}{(2 + \delta x/\Delta x)} + \theta_{q-1}\frac{2\delta x/\Delta x}{(1 + \delta x/\Delta x)} + \theta_\epsilon \frac{2}{(2 + \delta x/\Delta x)(1 + \delta x/\Delta x)} \tag{10a}$$

$$\theta_{qL} = \theta_\epsilon \frac{2}{(2 - \delta x/\Delta x)(1 - \delta x/\Delta x)} - \theta_{q+1}\frac{2\delta x/\Delta x}{(1 - \delta x/\Delta x)} + \theta_{q+2}\frac{\delta x/\Delta x}{(2 - \delta x/\Delta x)} \tag{10b}$$

where again $\theta_\epsilon = 0$. Although δx may be either positive or negative and both equations (10a) and (10b) are mathematically defined over the full range of δx, θq is represented by θ_{qs} when $0 < \delta x$ and by θ_{qL} when $0 > \delta x$.

The temperatures θ_{qs} and θ_{qL} are substituted into the uniform difference equations (3) to permit calculation of θ_{q-1} and θ_{q+1}. This procedure facilitates the computations as compared with the alternate and equivalent procedure of using θ_ϵ in divided difference calculations. (By this latter means the numerical derivatives are obtained over a nonuniform network requiring considerable modification of the equations.)

In order to obtain the expression for fusion front motion, the slopes at the fusion front are developed from the first two terms of the difference form of the Taylor expansion:

$$\left.\frac{\partial\theta_s}{\partial x}\right|_{x=\epsilon} \simeq \frac{\theta_{qs} - \theta_{q-2}}{2\Delta x} + (\Delta x + \delta x)\frac{\theta_{q-2} - 2\theta_{q-1} + \theta_{qs}}{\Delta x^2} \tag{11a}$$

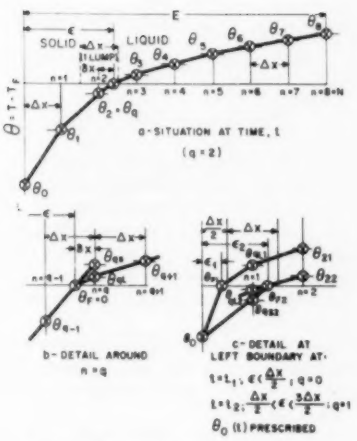

Fig. 2 Description of variables in Method II

$$\left.\frac{\partial\theta_L}{\partial x}\right|_{x=\epsilon} \simeq \frac{\theta_{q+2} - \theta_{qL}}{2\Delta x} - (\Delta x - \delta x)\frac{\theta_{qL} - 2\theta_{q+1} + \theta_{q+2}}{\Delta x^2} \tag{11b}$$

Use of θ_{qs} and θ_{qL} in equations (11) and further substitution into equation (2) results in the fusion front velocity:

$$\frac{d\epsilon}{dt} = \frac{1}{L\rho}\left\{k_s\left[\frac{\theta_{qs} - \theta_{q-2}}{2\Delta x} + (\Delta x + \delta x)\frac{\theta_{q-2} - 2\theta_{q-1} + \theta_{qs}}{\Delta x^2}\right] - k_L\left[\frac{\theta_{q+2} - \theta_{qL}}{2\Delta x} - (\Delta x - \delta x)\frac{\theta_{qL} - 2\theta_{q+1} + \theta_{q+2}}{\Delta x^2}\right]\right\} \tag{12}$$

For the starting and terminating points $q = 0$, 1, $N - 1$, and N, three internal adjacent network points are not available and the equations must be reduced to alternate slope and curvature approximations. The writing of the starting and terminating fusion front equations are dependent on the boundary conditions and both must be resolved together.

As in Method I, conditions at the extreme boundaries can be defined in terms of temperature and/or heat flux. When $\theta_0(t)$ is prescribed [see Fig. 2(c)], and when $q = 0$ $\left(\epsilon < \frac{\Delta x}{2}\right)$, $\theta_{qs} = \theta_0(t)$, by definition. Only two points are available to compute $\left.\frac{\partial\theta_s}{\partial x}\right|_{x=\epsilon}$ and the two-point formula is used:

$$\left.\frac{\partial\theta_s}{\partial x}\right|_{x=\epsilon} = \frac{\theta_\epsilon - \theta_0}{\epsilon} = -\frac{\theta_0}{\epsilon} \tag{13}$$

since $\theta_\epsilon = \theta_F = 0$. θ_{qL} and $\left.\frac{\partial\theta_L}{\partial x}\right|_{x=\epsilon}$ are calculated by the methods of equations (10) and (11).

When $q = 1$ $\left(\frac{\Delta x}{2} < \epsilon < \frac{3\Delta x}{2}\right)$, and when $\theta_0(t)$ is prescribed, θ_{qs} is computed from the two-point interpolation:

$$\theta_{1s} = \theta_0 + \frac{\Delta x}{\epsilon}(\theta_\epsilon - \theta_0) = \frac{\theta_0(\epsilon - \Delta x)}{\epsilon} \tag{14}$$

and again $\left.\frac{\partial\theta_s}{\partial x}\right|_{x=\epsilon}$ is calculated from equation (13).

Similar procedures are used for $q = N - 1$, N, when $\theta_N(t)$ is prescribed:

$$\theta_{N-1,L} = \theta_N \frac{\Delta x - N\Delta x + \epsilon}{N\Delta x - \epsilon} \tag{15}$$

$$\left.\frac{\partial \theta_L}{\partial x}\right|_{x=\epsilon} = \frac{\theta_N}{N\Delta x - \epsilon} \tag{16}$$

For the boundary conditions just given, a starting or termination error results in the calculation of $d\epsilon/dt$ due to the two-point slope approximation. When $Q(t)$ is prescribed, or computed as a part of the problem, three-point approximations for θ_q may be obtained. While the fusion front is in the interior region $q = 2, 3, \ldots N-2$, boundary conditions are identical to those listed for Method I, except that both Δx_s and Δx_L are now fixed rather than varying network spaces.

Again the fusion front must be started at some small, finite distance from the boundary with the starting value, ϵ_0. Selection of the starting value will depend on the computer scaling and will be discussed in the second paper.

4 Sample Solutions

To permit an evaluation of both new methods and the conventional technique, solutions of two sample problems were worked out on both a digital computer and an electronic differential analyzer. The first problem is a Stefan analysis, which is subject to analytical confirmation; the second sample problem covers a finite slab initially at a uniform temperature above the fusion temperature to be solidified with large subcooling.

The physical variables and the boundary conditions selected are summarized in Table 1. The L/c ratio selected may be considered as typical for practical metal solidification problems, which range from a low value of 297 F for lead to a high 950 F for nickel and include aluminum, copper, magnesium, steel, and tin. Water has an L/c value of 144 F; sodium has 165 F.

Eight network spaces, corresponding to seven internal and two boundary nodal points, were selected for all solutions. This number represents a compromise between satisfactory accuracy and computational complexity, and it is near the upper limit that can be effectively programmed on an electronic differential analyzer. The excellent agreement found between the numerical solution and an analytical evaluation of the fusion front travel for the Stefan problem appears to justify this selection.

The digital solutions were carried out on the Burroughs Corp., E-101 computer, while analog simulation was performed on the Electronic Associates, Inc., PACE 16-31-R, augmented. All digital computations were carried out with a time interval determined from $\alpha \dfrac{\Delta t}{\Delta x^2} = 1/5$, which exceeds the stability criterion and provides improved accuracy.

Table 1 Sample freezing problems

	Stefan problem	General problem
Geometry	Semi-infinite slab	Symmetrical finite slab, thickness $2E = 1.6$ (half slab computed)
Initial conditions	$\theta_{s,0} = 0$ (initially at fusion temperature)	$\theta_{s,0} = 500$ F (all in liquid region)
Boundary conditions	$\theta_{0,t} = -1000$ F step-input	$\theta_{0,t} = -1000$ F step-input
Physical constants	$\alpha_s = 0.2778 \times 10^{-3}$ ft^2 sec^{-1} $= \alpha_L$	
	$L/c = 500$ F	
	$L^* = 0.5$	
	$k_s = 0.01389$ Btu-sec^{-1}-ft^{-1} F^{-1} $= k_L$	
	$c_s = 0.1$ Btu-lb^{-1} deg F^{-1} $= c_L$	
	$\rho_s = 500$ lb-ft^{-3} $= \rho_L$	

Fig. 3 shows a plot of fusion front position against time for digital computations using Method I, Method II, and the analytic solution of Stefan. Points resulting from a conventional method are shown for comparison, as are points resulting from Cochran's one lump parameter technique. The error resulting from a two-point approximation of $\left.\dfrac{\partial \theta_s}{\partial x}\right|_{x=\epsilon}$ (similar to an approximation used by Otis) is indicated by the plot with the approximation used in Method II. Analog solutions for Methods I and II showed excellent agreement with the digital calculations throughout and are not plotted on this or any subsequent figure except as noted. A comparison of errors at various times in the solution is shown in Table 2. In Fig. 4, temperature-time plots at the nodal points are presented for the digital solutions by Method II and the conventional method. Temperatures at various times calculated by interpolation from the moving space scale resulting from the digital solution by Method I are shown as are selected points resulting from the analytic solution.

Results of the fusion front motion with time for the second problem are presented in Fig. 5. Here no analytic solution is available for comparison, and the Cochran solution does not apply. Digital solution by Methods I and II, and points determined by the conventional method are shown. Since there was some divergence between the analog and digital results with Method I, particularly in the later stages of computation (presumably due to integration of noise signals and to drift in integrators), the analog solution by this method is also indicated. The analog solution of Method II was again in excellent agreement with the digital results.

Fig. 6 shows temperature histories at nodal points resulting from digital solutions by Method II, and the conventional technique. Temperatures obtained by interpolation from the Method I

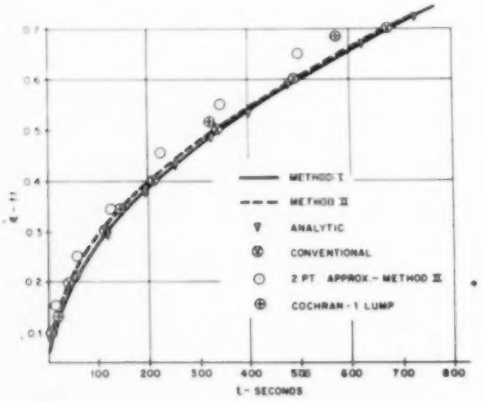

Fig. 3 Fusion front motion with time, Stefan problem

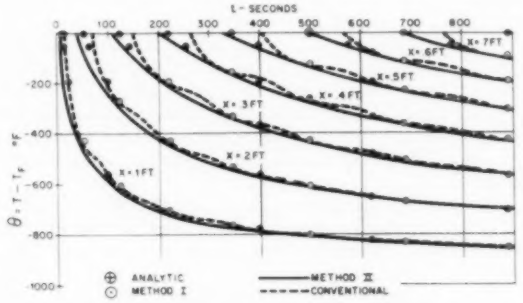

Fig. 4 Temperature histories, Stefan problem

Table 2 Errors resulting from numerical solutions of a typical Stefan problem

Time, sec	13.82	55.3	221.5	498	Notes
ϵ, Analytic solution ft	0.1	0.2	0.4	0.6	...
	Per cent error				
Conventional	13.3	7.5	2	1.5	Time to lose 1/2 latent heat is more accurate (see Ref. [22])
Cochran 1 lump	6	6	6	6	...
Method I (digital)	0	0	0	0	Very small starting error. Started at $\epsilon_0 = 0.01$
Method I (analog)	5	1.5	0	0	Starting error reduced fast. Started at $\epsilon_0 = 0.05$
Method II (digital)	28	13	4	1.5	Starting error due two-point approx. until $\epsilon = 0.15$. Started at $\epsilon_0 = 0.01$
Method II (analog)	31	14	4.5	1.5	Starting error due two-point approx. until $\epsilon = 0.15$. Started at $\epsilon_0 = 0.05$
Method II (2 pt approx.)	28	20	12	9.5	

digital solutions are also shown. These sample calculations serve to demonstrate the continuous evaluation of the fusion front motion made possible in both new methods. Method I yields accurate temperatures throughout the computation. Method II offers accuracy in front travel and temperature history after a starting error due to the two-point approximation for $\left.\frac{\partial \theta_s}{\partial x}\right|_{x=\epsilon}$. This error would be reduced in the case where $Q(t)$ is the boundary condition, since a three-point approximation for $\left.\frac{\partial \theta_s}{\partial x}\right|_{x=\epsilon}$ would then be available.

A comparison of the number of program steps and the time required for a digital solution of the general problem to $\epsilon = 0.6$ ft suggests that the conventional method is fastest and most convenient if there is no demand for an accurate knowledge either of the fusion front travel or of the temperature distribution, especially in the neighborhood of the fusion point, or, alternately, if the latent heat effects are small.

If comparisons were made on the basis of equal digital computing time, the conventional method with twice the number of network points may well lead to the same over-all accuracy as the proposed new approaches, and this operation might be possible on the same size computer. No such check was performed; the remaining objections to the poor representation of temperatures near the fusion point and the lack of continuous calculation of front motion may still make the new methods preferable.

For an inactive analog computer, such as an R-C network analyzer, the mechanization required to allow for the nonlinear fusion front coupling equations generally suggests that the minimum number of network points be used and the new methods appear preferable. The same applies to an electronic differential analyzer; here more than eight to ten network points are likely to lead to poor results due to internally induced drift errors. For a given number of network spaces the new methods require significantly more equipment than does the conventional technique.

Further details on the choice of analog or digital computing equipment, on the problems inherent in a mechanization of all three methods on both types of computers, and questions regarding stability and accuracy will be discussed in the subsequent companion paper.

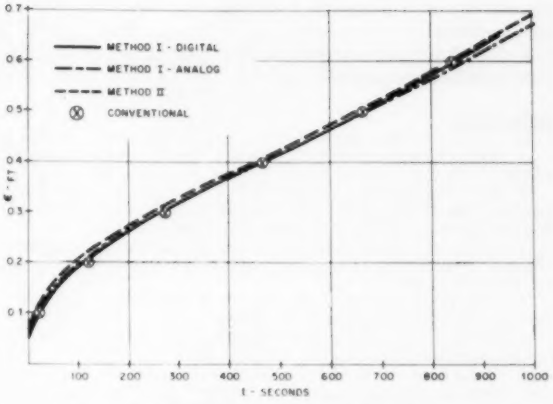

Fig. 5 Fusion front motion with time, general problem

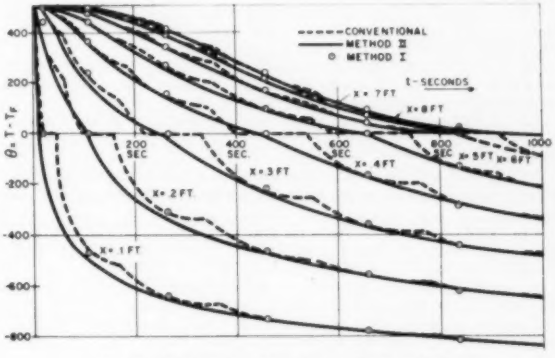

Fig. 6 Temperature histories, general problem

5 Conclusions

The principal results described in this paper may be summarized as follows:

1 The inherent difficulties in formulating analytical methods for freezing problems with practically important boundary conditions suggest the use of analog or numerical solutions in most instances. Even if analytical formulations of the results can be achieved, the actual evaluation generally requires a major computing program, so that their practical advantage over a difference method is doubtful.

2 Most previously published difference methods are limited in their applicability and will lead to inaccurate solutions for materials with marked latent heat effects, unless the space network is highly refined.

3 The new methods presented in this paper are generally applicable and offer the highest over-all accuracy for a given network spacing. In terms of computing time or analog equipment requirements, they are somewhat less advantageous than the conventional numerical method for the same space network.

4 The variable space network is preferable if a continuous evaluation of the fusion front travel is the primary objective, while the fixed space network will lead to a more convenient representation of temperatures. Both methods are superior to the conventional method in describing fusion front travel, al-

though Method II introduces a starting error when temperatures are prescribed at the boundary.

5 The feasibility of both methods on digital and analog equipment has been established.

References

1 H. S. Carslaw and J. C. Jaeger, "Conduction of Heat in Solids," Oxford University Press, London, England, 1947.

2 L. R. Ingersoll, O. S. Zobell, and A. C. Ingersoll, "Heat Conduction With Engineering and Geological Applications," McGraw-Hill Book Company, Inc., New York, N. Y., 1948.

3 J. Stefan, "Über die Theorie der Eisbildung, insbesondere über die Eisbildung im Polarmeere," *Annalen der Physik und Chemie*, vol. 42, 1891, p. 269.

4 C. L. Perkeris and L. B. Slichter, "Problems of Ice Formation," *Journal of Applied Physics*, vol. 10, 1939, p. 135.

5 N. M. H. Lightfoot, "The Solidification of Molten Steels," *London Mathematical Society*, vol. 31, 1929, p. 97.

6 K. Lachmann, "Zum Problems des Erstarrens für den durch zwei parallelen Ebenen begrenzten Körper," *Zeitschrift für Angewandte Mathematik und Mechanik*, vol. 15, 1935, p. 345.

7 L. I. Rubenstein, "On the Solution of Stefan's Problem," *Bulletin del'Academie des Sciences de l'USSR*, vol. 11, 1947, p. 37 (in Russian).

8 A. Huber, "Über das Fortschreiten der Schmelzgrenze in einem linearen Leiter," *Zeitschrift für Angewandte Mathematik und Mechanik*, vol. 19, 1939, p. 1.

9 C. Schwartz, "Zur rechnerischen Behandlung der Erstarrungsvorgänge beim Giessen von Metallen," *Zeitschrift für Angewandte Mathematik und Mechanik*, vol. 13, 1933, p. 202.

10 P. V. Dankwertz, "Unsteady State Diffusion or Heat Conduction With Moving Boundaries," *Trans. Faraday Society*, vol. 46, no. 333, 1950, p. 701.

11 B. Ya. Lyuobov, "Calculation of the Rate of Hardening of a Metallic Ingot," *Doklady Akad. Nauk, SSSR*, vol. 68, 1949, p. 847 (in Russian).

12 G. W. Evans, "A Note on the Existence of a Solution to a Problem of Stefan," *Quarterly of Applied Mathematics*, vol. 8, 1950, p. 312.

13 F. Kreith and F. E. Romie, "A Study of the Thermal Diffusion Equation With Boundary Conditions Corresponding to Solidification or Melting of Materials Initially at the Fusion Temperature," *Proceedings of the Physics Society*, vol. 68, 1955, p. 277.

14 J. H. Weiner, "A Mathematical Investigation of the Solidification of Metals," PhD thesis, Columbia University, New York, N. Y., 1952.

15 A. L. London and R. A. Seban, "Rate of Ice Formation," TRANS. ASME, vol. 65, 1943, p. 771.

16 D. L. Cochran, "Rate of Solidification, Application, and Extension of Theory," Technical Report No. 24, Stanford University, Stanford, Calif., 1955.

17 H. G. Landau, "Heat Conduction in a Melting Solid," *Quarterly of Applied Mathematics*, vol. 8, no. 1, 1950, p. 81.

18 N. R. Eyres, D. R. Hartree, J. Ingham, R. Jackson, R. J. Sargant, and J. B. Wagstaff, "The Calculation of Variable Heat Flow in Solids," *Philosophical Transactions of the Royal Society of London*, vol. 240, series A, 1947, p. 1.

19 W. L. Martin and R. Bromberg, "The Thermal Analyzer, a Special Purpose Computer," Proceedings, 1952 Electronic Computer Symposium, University of California at Los Angeles, 1952.

20 H. P. Aldrich and H. M. Paynter, "Analytic Studies of Freezing and Thawing of Soils," published in "A Palimpsest on the Electronic Analog Art," by H. M. Paynter, Philbrick Researches, Inc., Boston, Mass., 1955, p. 247.

21 G. M. Dusinberre, "Numerical Methods for Transient Heat Flow," TRANS. ASME, vol. 67, 1945, p. 703. See also, G. M. Dusinberre, "Numerical Analysis of Heat Flow," McGraw-Hill Book Company, Inc., New York, N. Y., 1949.

22 P. H. Price and M. R. Slack, "The Effect of Latent Heat in Numerical Solutions of the Heat Flow Equation," *British Journal of Applied Physics*, vol. 5, 1954, p. 285.

23 G. Liebmann, "Solution of Transient Heat-Transfer Problems by the Resistance-Network Analog Method," TRANS. ASME, vol. 78, 1956, p. 1267.

24 D. R. Otis, "Solving the Melting Problem Using the Electric Analog to Heat Conduction," Heat Transfer and Fluid Mechanics Institute, Stanford University, Stanford, Calif., 1956, p. 29.

25 C. A. Forster, "Finite Difference Approach to Some Heat Conduction Problems Involving Change of State," Report of the English Electric Company, Luton, England, 1954.

26 J. Douglas, "On the Numerical Integration of Quasi-Linear Parabolic Differential Equations," Humble Production Research Report, Humble Oil Company, Houston, Texas, 1954.

27 J. Douglas and T. M. Gallie, "On the Numerical Integration of a Parabolic Differential Equation Subject to a Moving Boundary Condition," *Duke Mathematical Journal*, vol. 22, 1955, p. 557.

28 G. C. O'Brien, M. A. Hyman, and S. Kaplan, "A Study of the Numerical Solution of Partial Differential Equations," *Journal of Mathematics and Physics*, vol. 29, 1951, p. 223.

29 W. D. Murray, "Numerical and Machine Solutions of Problems in Transient Heat Conduction," Doctoral thesis, Department of Mechanical Engineering, New York University, New York, N. Y., April, 1958.

E. M. SPARROW
Assoc. Mem. ASME

J. L. GREGG
NASA, Lewis Research Center, Cleveland, Ohio

A Theory of Rotating Condensation

An analysis is made for film condensation on a rotating disk situated in a large body of pure saturated vapor. The centrifugal field associated with the rotation sweeps the condensate outward along the disk surface, and gravity forces need not be involved. The problem is formulated as an exact solution of the complete Navier-Stokes and energy equations. Numerical solutions are obtained for Prandtl numbers between 0.003 and 100 and for $c_p\Delta T/h_{fg}$ in the range 0.0001 to 1.0. Results are given for the heat transfer, as well as for the condensate layer thickness, torque moment, and temperature and velocity profiles.

Introduction

Since the pioneering work of Nusselt in 1916 [1],[1] studies of condensation heat transfer have been largely concerned with the situation of gravity-induced flow. In such natural condensation processes, it is the gravity force alone which brings about the removal of the condensed liquid from the cooled surface and, in this way, controls the condensation rate. Unfortunately, the magnitude of the gravity force is beyond our control, and so it appears that there are definite limits to any natural condensation process. This limitation becomes especially severe when applications at high altitudes are considered, e.g., space vehicle power plants. In these situations, the gravity force diminishes to a negligible value and natural condensation is impossible.

To overcome the limitations inherent in natural condensation, a conventional alternative such as pumping or blowing might be used. But, a more intriguing idea is to create an artificial "gravity" by use of a centrifugal field, and this is the problem on which attention will be focused here. The system to be studied, as shown schematically in the sketch, Fig. 1, is a cooled rotating disk at uniform temperature T_w situated in a large quiescent body of pure saturated vapor. It will be assumed that the condensed liquid forms a continuous film on the disk. Fluid in this film will be moved radially outward along the disk under the action of the centrifugal force field (in qualitatively the same way that gravity causes condensate to flow downward in the natural condensation process).

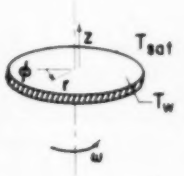

Fig. 1

The prime results of this investigation are the heat-transfer characteristics of the system. Heat-transfer coefficients are presented for fluids having Prandtl numbers in the range 0.003 to 100. Other results which are to be given include the film thickness, temperature profiles, and torque moment requirements. Readers who are primarily interested in results are invited to pass over the section on Analysis.

Aside from the practical aspects of the problem, there is a strong theoretical motivation, namely, that the problem can be formulated as an exact solution of the Navier-Stokes and energy equations. Very few cases are known which permit such rigorous determination of the temperature and velocity fields.

Analysis

General Considerations. To achieve our ultimate goal of finding heat-transfer results, it is first necessary to analyze, in detail, the velocity and temperature distributions in the condensate layer. The problem is, of course, governed by the basic conservation laws: Mass, momentum, and energy; and it is these which constitute the starting point for our study. Since it will be supposed that the condensate is incompressible and that properties are constant, there will be a total of five unknowns to be con-

[1] Numbers in brackets designate References at end of paper.

Contributed by the Heat Transfer Division and presented at the Annual Meeting, New York, N. Y., November 30–December 5, 1958, of The American Society of Mechanical Engineers.

Note: Statements and opinions advanced in papers are to be understood as individual expressions of their authors and not those of the Society. Manuscript received by ASME Headquarters, July 21, 1958. Paper No. 58—A-70.

Nomenclature

c_p = specific heat of condensate
F, G, H = dimensionless velocity variables defined by equation (6*b*)
h = local heat-transfer coefficient, $q/(T_{sat} - T_w)$
h_{fg} = latent heat of condensation
k = thermal conductivity of condensate
M_T = torque moment
P = dimensionless pressure, defined by equation (6*b*)
Pr = Prandtl number, $c_p\mu/k$
p = static pressure
q = local heat-transfer rate per unit area
r = radial co-ordinate
T = temperature; T_w, disk surface temperature; T_{sat}, saturation temperature of vapor; $\Delta T = T_{sat} - T_w$
V_r = radial velocity component
V_ϕ = tangential velocity component
V_z = axial velocity component
z = co-ordinate measuring distance normal to disk surface
δ = thickness of condensate layer
η = dimensionless independent variable, $(\omega/\nu)^{1/2}z$
η_δ = dimensionless condensate layer thickness, $(\omega/\nu)^{1/2}\delta$
θ = dimensionless temperature, $(T_{sat} - T)/(T_{sat} - T_w)$
μ = absolute viscosity of condensate
ν = kinematic viscosity of condensate
ρ = condensate density
τ_{zr} = radial shear stress, $\mu\left(\frac{\partial V_r}{\partial z} + \frac{\partial V_z}{\partial r}\right)$
$\tau_{z\phi}$ = tangential shear stress, $\mu\left(\frac{\partial V_\phi}{\partial z} + \frac{1}{r}\frac{\partial V_z}{\partial \phi}\right)$
ϕ = angular co-ordinate
ω = angular velocity

sidered: The three velocity components, the pressure, and the temperature. Correspondingly, there are five equations at our disposal: Three from the Navier-Stokes equations (momentum conservation), and one apiece from mass and energy conservation. Solving such a set of five nonlinear partial differential equations would appear, at first glance, a too formidable task. Fortunately, we can draw on the experience of von Karman [2], who successfully solved the simpler problem of a disk, rotating in a large quiescent body of single phase fluid.

The Conservation Equations and Their Transformation. The equations expressing conservation of mass, momentum, and energy for an incompressible, constant-property fluid may be written in cylindrical co-ordinates as

$$\frac{1}{r}\frac{\partial}{\partial r}(rV_r) + \frac{1}{r}\frac{\partial V_\phi}{\partial \phi} + \frac{\partial V_z}{\partial z} = 0 \tag{1}$$

$$\rho\left(\frac{DV_r}{Dt} - \frac{V_\phi^2}{r}\right) = -\frac{\partial p}{\partial r} + \mu\left(\nabla^2 V_r - \frac{2}{r^2}\frac{\partial V_\phi}{\partial \phi} - \frac{V_r}{r^2}\right) \tag{2}$$

$$\rho\left(\frac{DV_\phi}{Dt} + \frac{V_r V_\phi}{r}\right) = -\frac{1}{r}\frac{\partial p}{\partial \phi} + \mu\left(\nabla^2 V_\phi + \frac{2}{r^2}\frac{\partial V_r}{\partial \phi} - \frac{V_\phi}{r^2}\right) \tag{3}$$

$$\rho\frac{DV_z}{Dt} = -\frac{\partial p}{\partial z} + \mu\nabla^2 V_z \tag{4}$$

$$\rho c_p\frac{DT}{Dt} = k\nabla^2 T \tag{5}$$

where

$$\frac{D}{Dt} = V_r\frac{\partial}{\partial r} + \frac{V_\phi}{r}\frac{\partial}{\partial \phi} + V_z\frac{\partial}{\partial z}$$

and

$$\nabla^2 = \frac{\partial^2}{\partial r^2} + \frac{1}{r}\frac{\partial}{\partial r} + \frac{1}{r^2}\frac{\partial^2}{\partial \phi^2} + \frac{\partial^2}{\partial z^2}$$

The viscous dissipation terms have been deleted from the energy equation on the assumption that their effect will be negligible. The retention of these terms would still permit the formulation of an exact solution. The gravity force has been omitted, but it could be included in equation (4) as part of the pressure without altering the analysis.

Rather than deal with this formidable array of partial differential equations, we may transform them to a set of ordinary differential equations, which are easier to solve. The new variables which comprise the transformation are:

(a) new independent variable

$$\eta = \left(\frac{\omega}{\nu}\right)^{1/2} z \tag{6a}$$

(b) new dependent variables

$$F(\eta) = \frac{V_r}{r\omega}, \qquad G(\eta) = \frac{V_\phi}{r\omega}, \qquad H(\eta) = \frac{V_z}{(\omega\nu)^{1/2}}$$

$$P(\eta) = \frac{p}{\mu\omega} \tag{6b}$$

$$\theta(\eta) = \frac{T_{sat} - T}{T_{sat} - T_w} = \frac{T_{sat} - T}{\Delta T} \tag{6c}$$

Under the transformation, equations (1) through (5) become

$$H' = -2F \tag{1a}$$

$$F'' = HF' + F^2 - G^2 \tag{2a}$$

$$G'' = HG' + 2FG \tag{3a}$$

$$P' = H'' - HH' \tag{4a}$$

$$\theta'' = (\mathrm{Pr})H\theta' \tag{5a}$$

The primes denote differentiation with respect to η and Pr represents the Prandtl number.

Inherent in the transformation, there are two important suppositions about the nature of the velocity and temperature fields which are worthy of discussion. First, there is the property of angular symmetry, i.e., $\partial/\partial\phi = 0$. Second (and more important) is that, except for a simple stretching of V_r and V_ϕ, the velocity and the temperature profiles do not change *shape* at different values of r. In particular, the assumption that the temperature distribution depends only on z (since $\eta \sim z$) implies the existence of a condensate layer whose thickness is uniform over the disk. The fact that equations (1a) through (5a) are ordinary differential equations shows that the transformation (6) is consistent with the basic conservation laws.

Our prime interest is in the temperature distribution and the heat transfer, and hence our objective is the solution of equation (5a). Unfortunately, the integration of equation (5a) cannot be carried out without a prior (or simultaneous) knowledge of the velocity function $H(\eta)$. But H is intimately connected with the other velocity functions F and G through equations (1a), (2a), and (3a). There is no complete escape from the formidable computational undertaking, but the task may be somewhat lightened by combining equations (1a), (2a), and (3a) to give

$$H''' = HH'' - (H')^2/2 + 2G^2 \tag{7}$$

$$G'' = HG' - H'G \tag{8}$$

Simultaneous solution furnishes G and H, but only the latter is needed for integration of equation (5a) for the temperature distribution.

Boundary Conditions. To complete the statement of the problem, it is necessary to specify the boundary conditions. At the surface of the disk ($z = 0$), the standard viscous flow conditions are imposed, namely, that there is no motion relative to the solid surface. Moreover, the liquid immediately adjacent to the disk is required to take on the surface temperature T_w.

It has already been observed that the condensate forms a layer of uniform thickness, denoted by δ, over the surface of the rotating disk. At the interface between the condensate and the vapor, the usual condition of negligible shear will be imposed. Further, the condensate and vapor will share the common temperature T_{sat} at the interface.

The formal statement of these boundary conditions is

$$\left.\begin{aligned} V_r &= 0 \\ V_\phi &= r\omega \\ V_z &= 0 \\ T &= T_w \end{aligned}\right\} z = 0 \qquad \left.\begin{aligned} \tau_{zr} &= 0 \\ \tau_{z\phi} &= 0 \\ T &= T_{sat} \end{aligned}\right\} z = \delta \tag{9a}$$

The thickness δ of the condensate layer remains to be determined from the analysis. In terms of the new independent and dependent variables pertinent to equations (5a), (7), and (8), these conditions become

$$\left.\begin{aligned} H &= 0 \\ H' &= 0 \\ G &= 1 \\ \theta &= 1 \end{aligned}\right\} \eta = 0 \qquad \left.\begin{aligned} H'' &= 0 \\ G' &= 0 \\ \theta &= 0 \end{aligned}\right\} \eta = \eta_\delta \tag{9b}$$

where η_δ is the value of η corresponding to $z = \delta$.

With these boundary conditions, we then may proceed to solve equations (5a), (7), and (8), provided that numerical values are first chosen for two parameters: Prandtl number and η_δ. From the mathematical standpoint, this is a completely satisfactory situation. But, from the practical view, the problem is incomplete, since the dimensionless condensate thickness η_δ would not be known a priori. So, there still remains the task of relating η_δ to another parameter which contains quantities which are all known. Such a relationship is found later.

The Parameter $c_p\Delta T/h_{fg}$. To relate η_δ (and hence δ) to known physical quantities, we invoke an over-all energy balance as follows

$$h_{fg}\int_0^\delta \rho 2\pi r V_r dz + \int_0^\delta \rho 2\pi r V_r c_p(T_{sat} - T)dz = k\left(\frac{\partial T}{\partial z}\right)_{z=0}\pi r^2 \quad (10)$$

The first term on the left is the energy released as latent heat, while the second term is the energy liberated by subcooling of the condensate. The right hand represents the heat transferred from the condensate to the disk over a span from $r = 0$ to $r = r$. In writing equation (10), the assumption of negligible heat conduction across the vapor-liquid interface, which is standard in condensation theory, has been used. In terms of the variables of the analysis as defined by equations (6), the over-all heat balance becomes

$$\frac{c_p\Delta T}{h_{fg}} = \Pr\frac{H(\eta_\delta)}{\theta'(\eta_\delta)} \quad (10a)$$

where $H(\eta_\delta)$ and $\theta'(\eta_\delta)$ represent the values of H and $d\theta/d\eta$ at $\eta = \eta_\delta$.

From a solution of equations (5a), (7), and (8) corresponding to specified values of Pr and η_δ, the values of $H(\eta_\delta)$ and $\theta'(\eta_\delta)$ are available, and the right side of equation (10a) may be computed. So, $c_p\Delta T/h_{fg}$ is determined. Now, if the Prandtl number is fixed and equations (5a), (7), and (8) are solved for several different values of η_δ, we are able to compute a corresponding set of values for $c_p\Delta T/h_{fg}$. In other words, for a fixed Prandtl number, there is a unique relationship between η_δ and $c_p\Delta T/h_{fg}$. So, if we wish, we can think of our solutions as depending upon Pr and $c_p\Delta T/h_{fg}$, rather than on Pr and η_δ.

Solutions. Numerical solutions of equations (5a), (7), and (8) subject to the boundary conditions (9b) have been carried out on an IBM 653 electronic computer using the numerical integration procedures outlined in reference [3]. The solutions were obtained for Prandtl numbers of 0.003, 0.008, 0.03, 1.0, 10, and 100; the first three span the range of liquid metals, while the last three correspond to ordinary liquids. Values of the parameter $c_p\Delta T/h_{fg}$ ranged from 0.0001 to 0.1 for the liquid metals and from 0.001 to 1.0 for the ordinary liquids. Based on these solutions, results for the heat transfer, condensate layer thickness, torque moment, and temperature and velocity profiles will be given.

Results

Heat-Transfer Coefficients. The most important results of practical interest are the heat-transfer characteristics of the system. The local heat flux *to* the disk may be computed by Fourier's Law:

$$q = \left(k\frac{\partial T}{\partial z}\right)_{z=0} \quad (11)$$

In terms of the transformed variables of the analysis, the expression for q becomes

$$q = -k(T_{sat} - T_w)\left(\frac{\omega}{\nu}\right)^{1/2}(d\theta/d\eta)_{\eta=0} \quad (12)$$

The derivative $(d\theta/d\eta)_{\eta=0}$, obtained from solutions of equations (5a), (7), and (8), depends on the Prandtl number and on $c_p\Delta T/h_{fg}$. For a particular liquid and a fixed temperature difference, equation (12) shows that

$$q \sim \omega^{1/2}$$

It is also worth remarking that q is uniform over the surface of the disk.

Introducing the definition of the local heat-transfer coefficient as follows

$$h \equiv \frac{q}{T_{sat} - T_w} \quad (13)$$

the heat-transfer results may be rephrased in the form

$$\frac{h\left(\frac{\nu}{\omega}\right)^{1/2}}{k} = -(d\theta/d\eta)_{\eta=0} \quad (14)$$

The quotient $(\nu/\omega)^{1/2}$ has the dimensions of a length, and so the left side of equation may be regarded as a Nusselt number. Inasmuch as $(d\theta/d\eta)_{\eta=0}$ depends on Pr and $c_p\Delta T/h_{fg}$, so then do the Nusselt number results. In presenting these results, it is convenient to look first at the higher Prandtl numbers (1, 10, 100) and then at the lower Prandtl numbers (0.003, 0.008, 0.03).

By evaluating equations (14) and (10a) from the numerical solutions, heat-transfer results for the higher Prandtl numbers have been plotted on Fig. 2 for values of $c_p\Delta T/h_{fg}$ between 0.001 and 1.0. The choice of the ordinate variable is noteworthy. Rather than plot the Nusselt number alone, the group

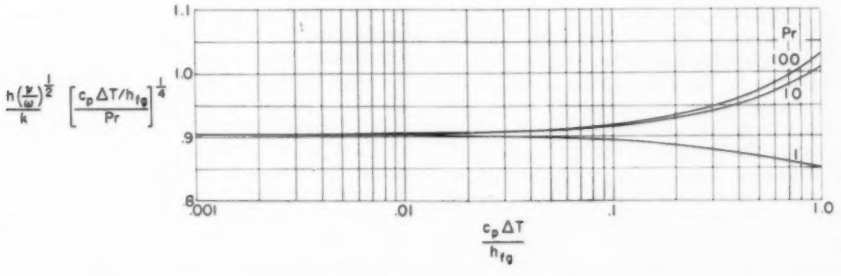

Fig. 2 Heat-transfer results for high Prandtl number fluids

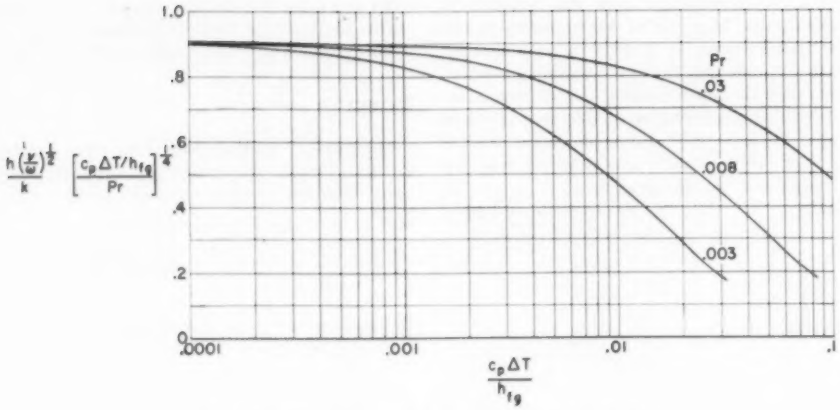

Fig. 3 Heat-transfer results for low Prandtl number fluids

$$\frac{h\left(\frac{\nu}{\omega}\right)^{1/3}}{k}\left(\frac{c_p\Delta T/h_{fg}}{\mathrm{Pr}}\right)^{1/4}$$

has been used. By inspection of the figure, it is seen that for small values of $c_p\Delta T/h_{fg}$, all the results are represented by

$$\frac{h\left(\frac{\nu}{\omega}\right)^{1/3}}{k} = 0.904\left(\frac{\mathrm{Pr}}{c_p\Delta T/h_{fg}}\right)^{1/4} \tag{15}$$

But, as demonstrated in the Appendix, equation (15) corresponds precisely to the heat-transfer result for the situation where *energy convection and acceleration terms are negligible*. So, departures from this relationship represent the effects of convection and inertia, the former tending to increase the heat transfer and the latter tending to diminish it. With increasing Prandtl number, the effect of energy convection becomes relatively more important than the inertia effects. As a consequence, the Pr = 10 and Pr = 100 curves of Fig. 1 tend to exceed (or, in the limit, equal) the limiting value of 0.904. On the other hand, the inertia effects become relatively more important as the Prandtl number decreases, and so the Pr = 1 curve tends to drop slightly below the limiting value of 0.904. It is worth while noting that for a significant part of the technically important range of $c_p\Delta T/h_{fg}$, equation (15) is a good representation of the heat-transfer results of Fig. 2.

Now, we turn to the low Prandtl number heat-transfer results which are plotted on Fig. 3. The ordinate and abscissa variables are the same as on the previous figure, but here we are concerned with smaller values of $c_p\Delta T/h_{fg}$ to correspond to the relatively small values of c_p/h_{fg} for liquid metals. For the smallest values of $c_p\Delta T/h_{fg}$ which are plotted on the figure, the curves tend to approach (but never quite reach) the limiting value of 0.904. The inertia terms play an important role for these low Prandtl number liquids, tending to substantially decrease the heat transfer as the condensate layer thickens (increasing values of $c_p\Delta T/h_{fg}$).

Condensate Layer Thickness. The analysis predicts that the dimensionless condensate layer thickness $\delta(\omega/\nu)^{1/3}$ will be uniform over the disk and will vary with Prandtl number and $c_p\Delta T/h_{fg}$. This dependence may be determined from equation (10*a*) by utilizing the numerical solutions of equations (5*a*), (7), and (8). For the limiting situation of negligible inertia and heat convection effects, the following limiting relationship has been derived (see Appendix).

$$\delta\left(\frac{\omega}{\nu}\right)^{1/3} = 1.107\left(\frac{c_p\Delta T/h_{fg}}{\mathrm{Pr}}\right)^{1/4} \tag{16}$$

Fig. 4 shows the condensate layer thickness results for the high Prandtl numbers. The limiting result of equation (16) is achieved for small values of $c_p\Delta T/h_{fg}$, while the deviations from this limit never appear too great (in common with the high Prandtl number heat transfer). The low Prandtl number results are plotted on Fig. 5. There, substantial upward deviations from the limit of equation (16) may be observed as a consequence of the inertia effects.

By comparing Figs. 4 and 5, it can be seen that for a given value of $c_p\Delta T/h_{fg}$, the magnitude of $\delta(\omega/\nu)^{1/3}$ increases with decreasing Prandtl number. Finally, we note that for a given fluid and a fixed temperature difference

$$\delta \sim \omega^{-1/3}$$

Temperature Profiles. The temperature distribution across the condensate layer may also be of some interest. We will content ourselves with displaying representative results, focusing attention on Pr = 10 for the high Prandtl number group and Pr = 0.008 for the low Prandtl number group.

Dimensionless temperature profiles for Pr = 10 are plotted on Fig. 6. The profiles for $c_p\Delta T/h_{fg} < 0.1$ cannot be distinguished from a straight line on the scale of this figure. The deviations from the straight line profile increase with increasing $c_p\Delta T/h_{fg}$ (i.e., increasing layer thickness), but do not become decisive even for the highest value of $c_p\Delta T/h_{fg}$ plotted here. The effect upon the heat transfer of these deviations has already shown on Fig. 2 to be small. Numerous other cases were available for plotting in the range $0.1 \leq c_p\Delta T/h_{fg} \leq 1$, but they have been omitted for the sake of clear reproduction.

Fig. 7 shows temperature profiles for Pr = 0.008. For values of $c_p\Delta t/h_{fg} < 0.02$, the curves could not be distinguished from a straight line. Even the extreme case on Fig. 7, $c_p\Delta T/h_{fg} = 0.083$, so closely parallels the straight line profile that it was physically impossible to draw other intermediate curves.

It would appear from both Figs. 6 and 7 that, for most technically interesting situations, the temperature profile across the condensate layer closely approximates a straight line.

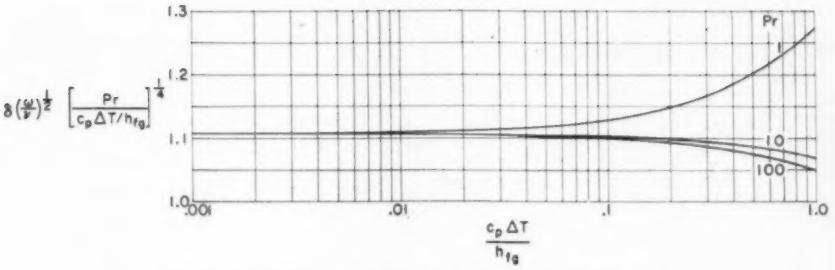

Fig. 4 Condensate layer thickness for high Prandtl number fluids

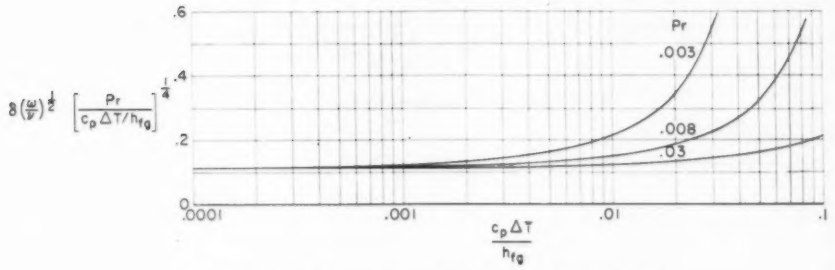

Fig. 5 Condensate layer thickness for low Prandtl number fluids

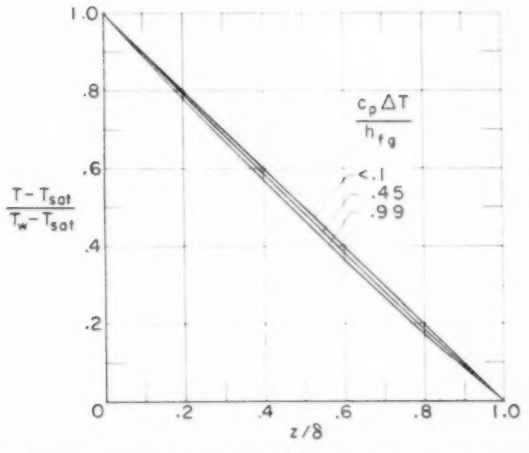

Fig. 6 Representative temperature distributions across condensate layer for Pr = 10

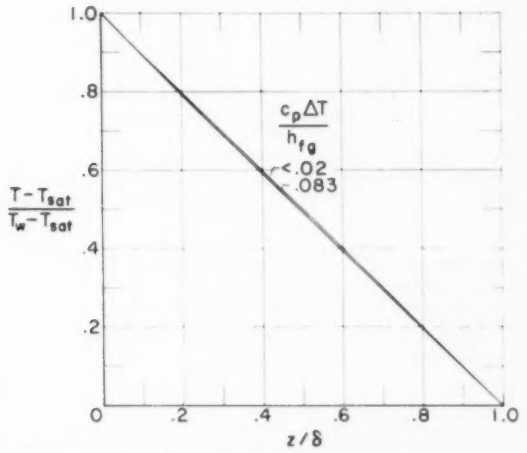

Fig. 7 Representative temperature distributions across condensate layer for Pr = 0.008

Velocity Profiles. A view of some of the hydrodynamic aspects of the problem may be gained by inspection of the velocity distributions. We confine ourselves to representative situations, selecting results for a layer thickness of $\delta(\omega/\nu)^{1/2} = 5$ to typify relatively thick films and those for $\delta(\omega/\nu)^{1/2} = 0.5$ to represent relatively thin films.

Turning first to the relatively thicker films, we present on Fig. 8 the distribution of each of the velocity components across the condensate film. It is seen that the tangential velocity decreases significantly across the layer, and that there is a substantial axial velocity carrying mass inward toward the disk surface. The general shape of the curves is not significantly different from those for von Karman's problem of a rotating disk in an infinite domain of single phase fluid (figure 5.10, reference [2]).[3]

Velocity profiles corresponding to $\delta(\omega/\nu)^{1/2} = 0.5$ (relatively thin films) are shown in Fig. 9. Here it may be noted that the tangential velocity changes very little across the layer, while the axial velocity is appreciably smaller than that for the thicker layers. This reduction in axial velocity in turn leads to a decrease in the effect of energy convection.

[3] For increasingly thicker films, the velocity profiles should approach more and more closely to those of von Karman's problem; while the temperature profiles should approach those of Millsaps and Pohlhausen [4], who solved the heat-transfer portion of von Karman's problem.

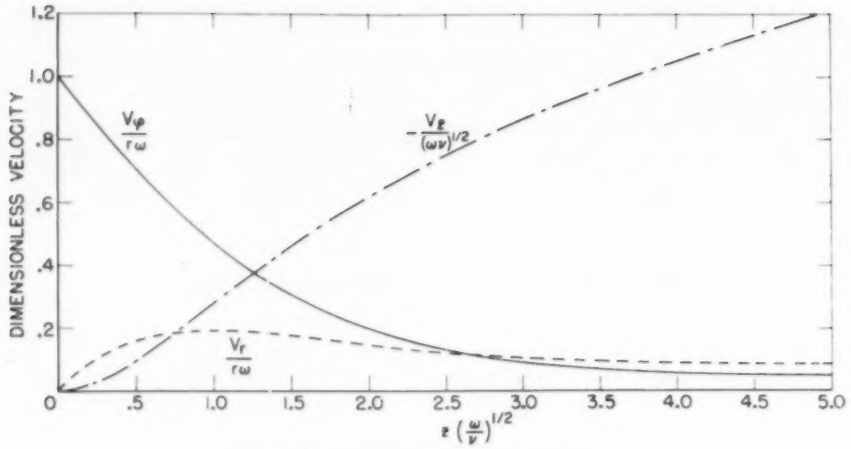

Fig. 8 Velocity distributions for $\delta(\omega/\nu)^{1/2} = 5.0$

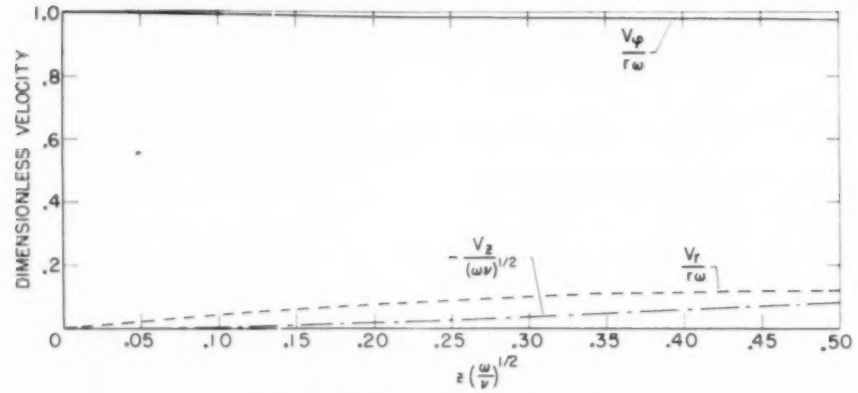

Fig. 9 Velocity distributions for $\delta(\omega/\nu)^{1/2} = 0.50$

Torque Moment. In order to sustain a steady rotation of the disk, it is necessary to provide torque at the shaft. The torque moment required to overcome the shear forces due to the condensate film may be computed as follows: The tangential stress on the surface of the disk $\tau_{z\varphi}$ is given by

$$\tau_{z\varphi} = \left(\mu \frac{\partial V_\phi}{\partial z}\right)_{z=0} \tag{17}$$

In terms of the variables of the analysis, the expression for the stress becomes

$$\tau_{z\phi} = \rho r(\nu\omega^3)^{1/2}(dG/d\eta)_{\eta=0} \tag{17a}$$

The torque moment M_τ associated with condensation on *one side* of a rotating disk of radius r_0 is

$$M_\tau = \int_0^{r_0} r\tau_{z\varphi} 2\pi r dr \tag{18}$$

Integrating equation (18) gives

$$\frac{2M_\tau}{\pi r_0^4 \rho(\nu\omega^3)^{1/2}} = (dG/d\eta)_{\eta=0} \tag{19}$$

The derivative $(dG/d\eta)_{\eta=0}$ depends upon the Prandtl number and $c_p\Delta T/h_{fg}$. To shorten the presentation of the results, the dimensionless torque moment[3] is plotted on Fig. 10 as a function of $\delta(\omega/\nu)^{1/2}$. Inasmuch as Figs. 6 and 7 give $\delta(\omega/\nu)^{1/2}$ as a function of Pr and $c_p\Delta T/h_{fg}$, the torque moment may be computed from Fig. 10 in conjunction with one of these two figures.

It can be easily verified that the dimensionless torque moment increases with increasing $c_p\Delta T/h_{fg}$ at a fixed Prandtl number and with decreasing Prandtl number at a fixed value of $c_p\Delta T/h_{fg}$.

Laminar-Turbulent Transition. If the results of the present analysis were to be applied, the question would immediately arise as to the conditions under which the laminar flow assumption would be valid. In the absence of experimental data on rotating condensation, we must rely on the findings for the somewhat similar system of a rotating disk in an infinite domain of single phase fluid. For that situation, it is observed (reference [2], p. 79) that the laminar results are usable up to a value of

$$\mathrm{Re} = \frac{r^2\omega}{\nu} = 3 \times 10^5$$

Comparison With Natural Condensation

It may be of interest to compare the heat-transfer results for rotating condensation with those for natural gravity condensa-

[3] Left side of equation (19).

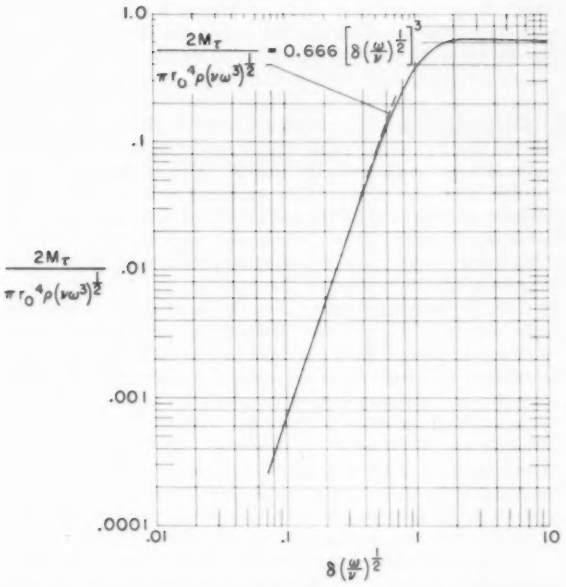

Fig. 10 Torque moment for condensation on one side of rotating disk (radius r_0)—to be used with Figs. 4 and 5

tion. Unfortunately, analytical results for the latter situation are available only for $\mathrm{Pr} \geq 1$, and so the comparison must be limited to that range. The local heat-transfer result for natural condensation on a vertical surface has been analytically determined in references [5 and 6] as

$$\frac{h_x x}{k}\left[\frac{4\nu k}{g c_p(\rho - \rho_v)x^3}\right]^{1/4} = \left(0.68 + \frac{h_{fg}}{c_p \Delta T}\right)^{1/4}, \qquad \mathrm{Pr} \geq 1 \quad (20)$$

where x measures distance downward from the top of the vertical surface, g is the acceleration of gravity, and ρ_v is vapor density. In general, the heat-transfer coefficients from equation (20) would have to be compared with those read from Fig. 2. However, for $c_p \Delta T/h_{fg} \leq 0.1$, the comparison can be made analytically, since equation (15) becomes an adequate description of the results for rotating condensation. Further, we observe that equation (20) approximately reduces to

$$\frac{h_x x}{k}\left[\frac{4\nu k}{g c_p(\rho - \rho_v)x^3}\right]^{1/4} \approx \left(\frac{h_{fg}}{c_p \Delta T}\right)^{1/4}, \qquad \begin{matrix}\mathrm{Pr} \geq 1 \\ c_p \Delta T/h_{fg} \leq 0.1\end{matrix} \quad (20a)$$

Then, taking the ratio of equations (15) and (20a), and attaching subscripts *rot* and *gr* to respectively indicate rotating and gravitational condensation, we find

$$\frac{h_{rot}}{h_{x,gr}} = \left(\frac{8}{3}\frac{x\omega^2}{g}\right)^{1/4} \quad (21)$$

where we have set $(1 - \rho_v/\rho) \approx 1$. So, the local coefficient for the rotating disk exceeds that for the vertical surface when

$$\omega^2 > \frac{3g}{8x} \quad (22)$$

where x is the distance from the top of the vertical surface. If $x = 1$ foot, ω must exceed 3.48 radians/sec (33.2 rpm) to satisfy equation (22).

APPENDIX

Limiting Results for Thin Condensate Layers

For thin condensate layers, the energy convection and inertia tend to become negligible,[4] and the mathematical problem formulated in the Analysis section simplifies considerably. After convection and inertia terms have been deleted, equations (5a), (7), and (8) become

$$\theta'' = 0 \quad (23)$$

$$H''' = 2G^2 \quad (24)$$

$$G'' = 0 \quad (25)$$

where only the centrifugal acceleration represented by G^2 has been retained in equation (24). The solution of these equations subject to the boundary conditions (9b) is

$$\theta = 1 - \eta/\eta_\delta \quad (26)$$

$$H = \eta^3/3 - \eta^3\eta_\delta \quad (27)$$

$$G = 1 \quad (28)$$

In particular,

$$H(\eta_\delta) = -\frac{2}{3}\eta_\delta^3, \qquad \theta'(\eta_\delta) = -\frac{1}{\eta_\delta} \quad (29)$$

Introducing the expressions for $H(\eta_\delta)$ and $\theta'(\eta_\delta)$ into equation (10a), the relationship between δ, Pr, and $c_p \Delta T/h_{fg}$ may be determined as follows

$$\frac{c_p \Delta T}{h_{fg}} = \frac{2}{3}\,\mathrm{Pr}\eta_\delta^4 = \frac{2}{3}\,\mathrm{Pr}\left[\delta\left(\frac{\omega}{\nu}\right)^{1/2}\right]^4$$

or

$$\delta\left(\frac{\omega}{\nu}\right)^{1/2} = \left(\frac{3}{2}\right)^{1/4}\left(\frac{c_p \Delta T/h_{fg}}{\mathrm{Pr}}\right)^{1/4} \quad (30)$$

This equation coincides with equation (16) of the text.

The local heat-transfer coefficient is easily evaluated from equations (14) and (26), giving,

$$\frac{h\left(\frac{\nu}{\omega}\right)^{1/2}}{k} = \frac{1}{\eta_\delta} = \left(\frac{2}{3}\right)^{1/4}\left(\frac{\mathrm{Pr}}{c_p \Delta T/h_{fg}}\right)^{1/4} \quad (31)$$

which is identical to equation (15) of the text.

References

1 W. Nusselt, "Die Oberflächen Kondensation des Wasserdampfes," *Zeitschrift des Vereines Deutscher Ingenieure*, vol. 60, 1916, pp. 541 and 569.

2 H. Schlichting, "Boundary Layer Theory," McGraw-Hill Book Company, Inc., New York, N. Y., 1955, pp. 75–79.

3 J. L. Gregg, "A General Purpose IBM 653 Routine for the Solution of Simultaneous Ordinary Differential Equations," IBM 650 Scientific Computation Seminar, Endicott, N. Y., October, 1957.

4 K. Millsaps and K. Pohlhausen, "Heat Transfer by Laminar Flow From a Rotating Plate," *Journal of the Aeronautical Sciences*, vol. 19, 1952, pp. 120–126.

5 W. M. Rohsenow, "Heat Transfer and Temperature Distribution in Laminar-Film Condensation," TRANS. ASME, vol. 78, 1956, pp. 1645–1648.

6 E. M. Sparrow and J. L. Gregg, "A Boundary Layer Treatment of Laminar Film Condensation," TRANS. ASME, series C, JOURNAL OF HEAT TRANSFER, vol. 81, 1959, pp. 13–18.

[4] It may be of interest to note that these simplifications were precisely those used by Nusselt in his original derivation for natural condensation on vertical surfaces.

DISCUSSION

W. E. Welsh, Jr.[5]

The authors have treated a unique and original problem. It would be very interesting to compare experimental results for this situation with the analytical assumptions and results. In particular, the point of assuming the temperature to be independent of radius seems quite arbitrary. The condensate thickness and heat flux become independent of radius when temperature is independent, and the results of the analysis are heavily biased as a consequence. Further, the von Karman assumption of radial and circumferential velocity components being simply proportional to radius is tacitly accepted as valid for this case of two-phase flow. These temperature and velocity assumptions undoubtedly simplify the analysis considerably, but it is difficult to emphasize the meaning of the results without some physical justification for this analytical model. It would enhance the value of this analysis considerably if the authors could cite physical data of any nature which would tend to support their assumptions.

Authors' Closure

The authors extend their thanks to Mr. Welsh for his interesting comments. Before proceeding to describe some recently published experimental data, we wish first to explore the meaning of the mathematical solutions which have been obtained.

To facilitate this discussion, we turn for a moment to the much-studied and apparently well-understood problem of boundary layer flow over a flat plate. The flow is described by a boundary layer momentum equation and by the continuity equation; both of which are partial differential equations. In seeking a solution, Blasius made the a priori assumption that the *shape* of the velocity profile is similar at all stations along the plate. He found that this assumption was compatible with the governing equations and boundary conditions and was able to find a solution. Now, the solution found by Blasius is *a* solution to the boundary layer equations for flow over a flat plate, but (to the knowledge of the authors) it may not be *the only* solution. That is, uniqueness has not been proved. But, since other solutions have not been found, we are quite content to use Blasius' results.

Now, returning to the rotating disk, von Karman's analysis for the flow in a single phase fluid is again based on the a priori supposition of similar velocity profiles. This assumption is compatible with the conservation equations and boundary conditions; and his solution is a valid solution of the problem. No proof of uniqueness exists; but because other solutions have not been found, we are ready, without reservation, to apply von Karman's analysis to the laminar flow problem.

Now, for rotating condensation, the same point of view has been adopted. The a priori assumption of similarity is compatible with the governing equations and the prescribed boundary conditions and leads to a valid solution. No other solutions currently exist to compete with this similarity solution. The one aspect of the analysis which one may question is the boundary conditions at the edge of the condensate layer. If the liquid-vapor interface is taken to be smooth (and this is a standard assumption in condensation theory), then the authors see no more reason for challenging the similarity assumptions in the two-phase problem than in von Karman's single phase study.

In the period after this report was submitted for publication, an experimental study of condensation on a rotating disk was reported in a PhD thesis at North Carolina State College.[6] By the use of dye injection, the flow was shown to be *axially symmetric*, as was assumed in the analysis. Heat-transfer experiments were carried out using methanol, ethanol, and Freon-113 at atmospheric pressure. The experimentally-determined heat-transfer coefficients fell about 30 per cent below theory. This level of agreement is quite common in condensation studies. The fact that the theorical prediction is higher than experiment is due, at least in part, to the neglect of the shear forces at the liquid-vapor interface. The authors are currently reformulating the analysis to include this effect.

[5] Research Engineer, California Institute of Technology, Jet Propulsion Laboratory, Pasadena, Calif.

[6] S. S. Nandapurkar, "Condensation on Rotating Surface," PhD thesis, Department of Chemical Engineering, 1958.

L. S. HAN

Associate Professor, Department of Mechanical Engineering, The Ohio State University, Columbus, Ohio

Laminar Heat Transfer in Rectangular Channels

Three cases of laminar heat transfer with linear heat input in long rectangular channels have been treated by the method of orthogonal trigonometric series. The boundary conditions of the first two problems are those of laminar and slug flows with two opposite faces as secondary extended surfaces. A new fin parameter K defined as (wk_m/bk_f) has been shown to be the important factor in governing the Nusselt number. The third case discussed is the combined effects of free and forced-convection in vertical rectangular tubes.

Introduction

THE PURPOSE of this paper is to present a theoretical treatment of the heat-transfer problem with fully established velocity profiles in long rectangular channels. The study of the problem is carried out in three main phases. The first phase considers two parallel plates with interconnecting longitudinal ribs forming a series of rectangular channels. The fluid flowing in these channels is assumed to be steady and incompressible and to have a fully established laminar velocity profile. The physical properties of the fluid are assumed constant. The inner surfaces of the parallel plates are assumed to have a constant temperature in any plane transverse to the flow. Heat is transferred to the fluid along the parallel-plate surfaces at a uniform rate with respect to the flow direction. For channels of sufficient length, this results in a linearly increasing temperature of the enclosing walls of the flow passages. On the surface formed by the interconnecting ribs or the secondary surfaces, heat is transferred from the parallel plates on the primary surface. On those fins, the temperature is therefore not uniform in a transverse plane. In the longitudinal direction, however, the temperature is linearly increasing at the same rate as the primary surface.

The problem considered in this paper is in reality a generalization of a previous solution presented in reference [1][1] wherein limiting values of the Nusselt number are given for the case of constant temperature on all surfaces in any transverse plane. The present analysis includes the effectiveness of the transverse fins and includes the results in reference [1] as special cases. The system described here might be found, for example, in a counter-flow heat exchanger with equal thermal capacity for both fluids, resulting in linear temperature variations on both sides.

The second phase of this analysis treats the case of slug flow through the same physical arrangement with identical thermal boundary conditions. The results obtained herein are of use in the case of heat transfer in fully established turbulent flow of liquid metals, since it has been demonstrated in reference [2] that a correlation of the actual Nusselt number, the limiting Nusselt number for slug flow, and the Peclet number agrees quite well with experimental data.

The third problem deals with the superimposed effects of natural and forced-convection heat transfer for fully established laminar flow in vertically mounted rectangular channels. The

Contributed by the Heat Transfer Division and presented at the Annual Meeting, New York, N. Y., November 30–December 5, 1958, of THE AMERICAN SOCIETY OF MECHANICAL ENGINEERS.

NOTE: Statements and opinions advanced in papers are to be understood as individual expressions of their authors and not those of the Society. Manuscript received at ASME Headquarters July 21, 1958. Paper No. 58—A-124.

[1] Numbers in brackets designate References at end of paper.

Nomenclature

A = area, sq ft
a, b = side dimensions, ft
C_p = specific heat at constant pressure, Btu per (slug-deg F)
C_1 = temperature gradient in flow direction, deg F per ft
C_2 = pressure gradient in flow direction, lb_F per cu ft
D = hydraulic diameter, ft
F_c = correction factor, see equation (28), dimensionless
F_B = body force, lb_F per cu ft
F = dimensionless heat generation function, see equation (39)
g = gravitational acceleration, ft per hr^2
h = heat-transfer coefficient, Btu per (deg F-sq ft-hr)
k_m = wall thermal conductivity, Btu per (deg F-ft-hr)
k_f = fluid thermal conductivity, Btu per (deg F-ft-hr)
K = fin parameter, dimensionless, (wk_m/bk_f)
L = pressure drop parameter, equation (39), dimensionless
m, n = dummy indexes, integers
Nu = Nusselt number, (hD/k_f)
P = pressure, psf
Q = heat generation rate, Btu per (hr-cu ft)
R = function as defined in equations (22) and (26)
R_A = Rayleigh number, dimensionless
t = temperature, deg F
u = axial velocity, fph
u_m = mean axial velocity, fph
v = dimensionless velocity (u/u_m)
V_{mn} = Fourier coefficient for velocity function
w = one half of fin width, ft; refers to wall when used as a subscript
x, y = co-ordinates, ft
x_1, y_1 = dimensionless co-ordinates, (x/D), (y/D)
z = axial co-ordinate, ft
γ = aspect ratio, (b/a)
β = coefficient of density contraction, per deg F
∇^2 = Laplace operator
θ = temperature-difference function, deg F
μ = viscosity, lb_F-hr/ft^2
ρ = density, slug per cu ft
ϕ = dimensionless temperature function
ϕ_{ms} = mixed mean function of ϕ
Φ_{mn} = Fourier coefficients for ϕ-function
α = thermal diffusivity, $(k_f/\rho C_p)$

effects of superposition have been discussed in references [3 and 4]. Reference [3] considers a circular tube and presents a solution for circular symmetry in terms of the Bessel functions. Reference [4], however, treats the case of rectangular tubes but neglects the influence of the heat-generation function within the fluid, as is necessary in a number of engineering applications of the heat-transfer data. The same problem of combined effects is also discussed in references [5 and 6]. The problem discussed by Ostrach in reference [5] is concerned with a two-infinite-parallel-plate system, considering the effects of heat generation and frictional heat dissipation. The work of reference [6] is experimental and is valid for a circular tube with uniform wall temperature.

Influence of Secondary Surfaces on Limiting Laminar Nusselt Number for Constant Axial Temperature Gradient

Consider the flow configuration shown in Fig. 1. The problem can be simply stated as follows: Since the interconnecting ribs do not have infinite thermal conductivity, passage of heat from the primary surface to the extension surface and subsequently to the fluid would necessitate a temperature drop along the fin length. The question is: What is the parameter which governs the nonuniformity in the temperature distribution and what is the influence on the heat-transfer coefficient?

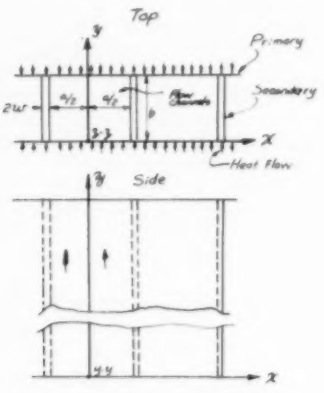

Fig. 1 Flow channel configuration

As a first approximation, one may estimate the heat-transfer coefficient on the basis of the uniform wall-temperature data in reference [1]. Subsequent correction can be made by allowing the effectiveness of the fins as described in any standard heat-transfer book such as reference [7]. Such a procedure is based on the concept that the surface coefficient is uniformly distributed and is unaffected by nonuniform distribution in temperature. Analysis in this section shows that the values and the distribution of the heat-transfer coefficients on all surfaces, primary and secondary, are strongly influenced by the temperature distribution on the secondary surface.

Analysis. The assumptions employed here are summarized as follows:

(*a*) Fluid properties are constant with respect to temperature.

(*b*) The velocity and temperature profiles are fully developed[2] and the motion is laminar.

(*c*) The axial temperature gradient is constant and independent of position in the channel cross section.

[2] The assumption of fully developed flow for laminar motion implies vanishing velocity components transverse to the axis. A rigorous proof can be found in reference [8].

With these assumptions, the basic equations of motion and of energy are reduced to

$$\nabla^2 t = C_1 u/\alpha \tag{1}$$

$$\nabla^2 u = C_2/\mu \tag{2}$$

The boundary condition for velocity u is

$$u_w = 0 \tag{3}$$

For the primary surface the temperature is a function of the axial position only, i.e.

$$t_w = t_0 + C_1 z \tag{4}$$

where t_0 is a reference temperature at $z = 0$.

For the secondary surface the temperature is a function of the axial position z and its location from the primary surface. Assuming that the temperature is uniform across the secondary surface but varies along the heat-flow path, the temperature must obey the following heat-balance equation:

$$wk_m \left(\frac{\partial^2 t_w}{\partial y^2}\right) = \pm k_f \left(\frac{\partial t}{\partial x}\right)_w \tag{5}$$

where + sign applies to $x = +a/2$ and − sign, $x = -a/2$.

Equations (1) through (5) may be transformed by introducing the temperature-difference function θ, defined as

$$\theta = t - (t_0 + C_1 z) \tag{6}$$

Hence equations (1) and (2) become

$$\nabla^2 \theta = C_1 u/\alpha \tag{7}$$

$$\nabla^2 u = C_2/\mu \tag{8}$$

with the following boundary conditions

$$\left.\begin{aligned} u_w &= 0 \\ \theta_w &= 0, \quad \text{for} \quad y = 0, \quad b \text{ only} \\ wk_m \left(\frac{\partial^2 \theta}{\partial y^2}\right) &= \pm k_f \left(\frac{\partial \theta}{\partial x}\right), \quad \text{for} \quad x = \pm a/2 \end{aligned}\right\} \tag{9}$$

Solution. The method of solving the foregoing equations is similar to the procedure recommended in reference [1], i.e., by combining equations (7) and (8) resulting in

$$\nabla^4 \theta = C_1 C_2/\alpha\mu \tag{10}$$

where C_1, C_2, α, and μ are independent of the cross-sectional coordinates, x and y. The corresponding boundary conditions expressed in terms of a single function θ are

$$\left.\begin{aligned} \nabla^2 \theta &= 0, \qquad x = \pm a/2; \; y = 0, b \\ \theta &= 0, \qquad y = 0, b \\ wk_m \left(\frac{\partial^2 \theta}{\partial y^2}\right) &= \pm k_f \left(\frac{\partial \theta}{\partial x}\right), \qquad x = \pm a/2 \end{aligned}\right\} \tag{11}$$

The solution to equation (10) can be assumed to be made up of two functions θ_1 and θ_2 satisfying the following relations

$$\nabla^4 \theta_1 = C_1 C_2/\alpha\mu \tag{12}$$

$$\nabla^2 \theta_2 = 0 \tag{13}$$

with

$$\nabla^2 \theta_1 = 0, \quad \text{and} \quad \theta_1 = 0 \quad \text{on all boundaries}$$

$$\theta_2 = 0 \quad \text{on} \quad y = 0, b$$

$$wk_m\left(\frac{\partial^2\theta}{\partial y^2}\right) = \pm k_f\left(\frac{\partial\theta}{\partial x}\right), \qquad x = \pm a/2 \tag{14}$$

The functions satisfying the foregoing relations can be obtained by the use of double Fourier series and the method of undetermined coefficients. Thus,

$$\theta_1 = \frac{16C_1C_2b^4}{\alpha\mu\pi^6}\sum_{m,\,n=1,3,5\ldots}^{\infty}(-1)^{\frac{m-1}{2}}\frac{\cos(m\pi x/a)}{mn(m^2\gamma^2+n^2)^2}\sin(n\pi y/b) \tag{15}$$

$$\theta_2 = \frac{16C_1C_2b^5}{\alpha\pi^6\mu a}\sum_{n=1,3,5\ldots}^{\infty}\frac{\left[\sum_{l=1,3,5\ldots}^{\infty}\frac{1}{n^2(l^2\gamma^2+n^2)^2}\right]}{\sinh\frac{n\pi}{2\gamma}+\left(\frac{wk_m}{bk_f}\right)n\pi\cosh\frac{n\pi}{2\gamma}}\cosh\frac{n\pi x}{b}\sin\frac{n\pi y}{b} \tag{16}$$

and the velocity function u is given by

$$u = -\frac{16C_2b^2}{\mu\pi^4}\sum_{m,\,n=1,3,5\ldots}^{\infty}(-1)^{\frac{m-1}{2}}\frac{\cos\frac{m\pi x}{a}\sin\frac{n\pi y}{b}}{mn(m^2\gamma^2+n^2)} \tag{17}$$

Results. A commonly used heat-transfer parameter is the Nusselt modulus,

$$\mathrm{Nu} = (hD/k_f) \tag{18}$$

where D is the equivalent or the hydraulic diameter and h is the average peripheral heat-transfer coefficient defined as

$$h = \left[\oint k_f\frac{\partial\theta}{\partial n}\,ds\right]\frac{1}{2(a+b)}\frac{1}{\Delta t} \tag{19}$$

The temperature difference in equation (19) is defined as the difference between the mixed-mean temperature of the fluid and the primary surface temperature at the same cross-section. Hence

$$\Delta t = \theta_m = \int_A \theta u\,dx\,dy \Big/ \int_A u\,dx\,dy \tag{20}$$

Combination of the preceding equations (15) to (20) together with the equivalent diameter D yields the equation for the average Nusselt number,

$$\mathrm{Nu} = \frac{64}{\pi^2}\left(\frac{1}{1+R}\right)\left[\sum_{m,\,n=1,3,5\ldots}^{\infty}\frac{1}{m^2n^2(m^2\gamma^2+n^2)^2}\right]^2\Bigg/\left[\sum_{m,\,n=1,3,5\ldots}^{\infty}\frac{1}{mn(m^2\gamma^2+n^2)^3}\right] \tag{21}$$

where

$$R = \frac{4\gamma^2}{\pi^2}\left\{\sum_{m,\,n=1,3,5\ldots}\frac{(-1)^{\frac{m-1}{2}}}{mn^3(m^2\gamma^2+n^2)^2}\left[\frac{m\gamma(-1)^{\frac{m-1}{2}}-n\tanh\left(\frac{n\pi}{2\gamma}\right)}{\tanh\left(\frac{n\pi}{2\gamma}\right)+n\pi\left(\frac{wk_m}{bk_f}\right)}\right]\left[\sum_{l=1,3,5\ldots}^{\infty}\frac{1}{(l^2\gamma^2+n^2)^2}\right]\right\}\left\{\sum_{m,\,n=1,3,5\ldots}^{\infty}\frac{1}{mn(m^2\gamma^2+n^2)^3}\right\}^{-1} \tag{22}$$

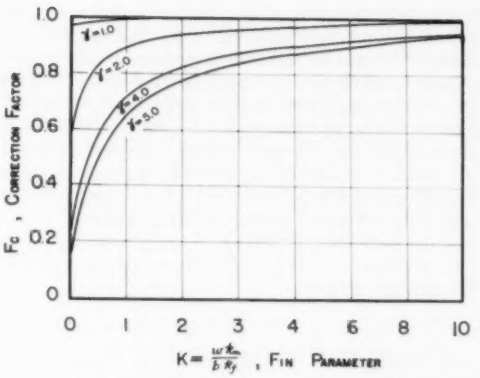

Fig. 2 Correction factor for finite fin conductivity

Thus equations (21) and (22) define the Nusselt number for any aspect ratio and for any combination of the fin geometry and thermal-conductivity ratio. Let

$$K = (wk_m/bk_f)$$

Hence equations (21) and (22) can be expressed as

$$\mathrm{Nu} = (\mathrm{Nu}_{k=\infty})F_c(K,\gamma)$$

where

$$F_c(K,\gamma) = 1/(1+R)$$

Thus, when the thermal conductivity of the fin material is infinite, the peripheral temperature variation becomes zero, by virtue of equation (5), indicating the case of uniform wall temperature at the same cross section. The limiting Nusselt number in this case is given by equation (21) with $R = 0$; the resulting expression is identical to that given in reference [1]. The function $F_c(k,\gamma) = 1/(R+1)$ is therefore the correction factor which indicates the over-all effectiveness of the entire surface, secondary and primary.

The values of the function $F_c(K,\gamma)$ have been calculated and shown in Table 1 for aspect ratios of $\gamma = 1, 2, 4$, and 5 for the fin parameter between 0 and 10.

Table 1 Correction factors for finite fin parameters, laminar flow

K	$\gamma = 1.0$	$\gamma = 2.0$	$\gamma = 4.0$	$\gamma = 5.0$
0	0.968	0.587	0.207	0.138
1	0.993	0.892	0.710	0.645
2	0.996	0.938	0.823	0.777
4	0.998	0.966	0.898	0.873
10	0.999	0.986	0.957	0.944

These data are shown graphically in Fig. 2. It is interesting to observe that, for ordinary fluids, such as air, in a square channel with b/w ratio of 20 and the wall conductivity in the order of 20, the fin parameter would assume a value of the order of 25. For liquid water the K-value would be of the order of 5. For these values, the correction factors are close to 1, representing a small reduction of the Nusselt number. For liquid metals, however, for which the thermal conductivity is comparable to that of the wall, the resulting fin parameter may be of the order of unity. Hence a reduction in the heat-transfer coefficient may be quite appreciable.

Influence of Secondary Surfaces on Limiting Nusselt Number With Slug Flow and Constant Axial Temperature Gradient

Analysis and Results. Although slug flow does not exist in nature

and is only valid as a result of the nonviscous assumption, calculations of the Nusselt number based on the slug velocity distribution have been found to be fruitful in estimating the contribution of molecular conduction in turbulent heat transfer for liquid metals. In the case of a rectangular duct such as shown in Fig. 1, the interconnecting ribs may cause circumferential variations in temperature and the ordinary boundary condition of a uniform wall temperature cannot be maintained. Again in the present problem, the use of a fin effectiveness will not lead to the correct estimate as the result of this section will demonstrate.

Under the same assumptions as for the preceding section and with an additional condition of uniform velocity profile, the problem is simply to solve,

$$\nabla^2\theta = C_1 u/\alpha \tag{1}$$

for which the boundary conditions along the primary and secondary surfaces are

$$\theta = 0, \quad \text{at} \quad y = 0, b$$

$$wk_m \frac{\partial^2\theta}{\partial y^2} = \pm k_f \frac{\partial\theta}{\partial x}, \qquad x = \pm\frac{a}{2} \tag{23}$$

The solution is obtained by including θ_2 satisfying $\nabla^2\theta_2 = 0$ as a part of the general solution. Thus

$$\theta = -\frac{16C_1b^2u}{\alpha\pi^6} \sum_{m,\,n=1,\,3,\,5\,..} (-1)^{\frac{m-1}{2}} \frac{\cos\dfrac{m\pi x}{a}\sin\dfrac{n\pi y}{b}}{mn(m^2\gamma^2+n^2)} - \frac{16C_1b^3u}{\alpha\pi^4 a} \sum_{m,\,n=1,\,3,\,5\,..} \cosh\frac{n\pi x}{b}\sin\frac{n\pi y}{b} \times \frac{}{n^2(m^2\gamma^2+n^2)\left[\sinh\dfrac{n\pi}{2\gamma} + n\pi\left(\dfrac{wk_m}{bk_f}\right)\cosh\dfrac{n\pi}{2\gamma}\right]} \tag{24}$$

Employing the same procedure for evaluating the Nusselt number, the following expression is obtained:

$$\mathrm{Nu} = \left[\frac{64}{\pi^6} \sum_{m,\,n=1,\,3,\,5\,..} \frac{1}{m^2n^2(m^2\gamma^2+n^2)}\right]^{-1} \frac{1}{1+R}\,\frac{1}{(1+\gamma)^2} \tag{25}$$

where

$$R = \gamma^2\left[\sum_{n=1,\,3,\,5\,..} \frac{1}{n^4}\left(\frac{\displaystyle\sum_{l=1,\,3,\,5\,..} \frac{1}{l^2\gamma^2+n^2}}{1+n\pi\left(\dfrac{wk_m}{bk_f}\right)\coth\dfrac{n\pi}{2\gamma}}\right)\right] \left[\sum_{m,\,n=1,\,3,\,5\,..} \frac{1}{m^2n^2(m^2\gamma^2+n^2)}\right]^{-1} \tag{26}$$

Equations (25) and (26) can be rearranged to read

$$\mathrm{Nu} = (\mathrm{Nu}_{k=\infty})F_c(K, \gamma) \tag{27}$$

where $\mathrm{Nu}_{k=\infty}$ are the slug-flow Nusselt numbers for the conditions of uniform wall temperature with respect to peripheral positions. Their values for various aspect ratios can be computed from equation (25) by letting $R = 0$, corresponding to infinite thermal conductivity for the fin material. These values are also contained in reference [2]. A correction factor F_c for finite fin parameters is similarly defined as

$$F_c = 1/(1+R) \tag{28}$$

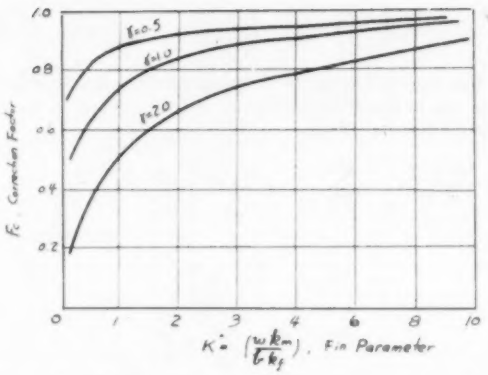

Fig. 3 Correction factor for finite fin conductivity for slug flow

and the numerical results tabulated in Table 2. The values also are plotted in Fig. 3. Again, a typical example involving a liquid metal as the heat-transfer fluid shows a K-value of the order of unity, for which the correction factor to allow for fin inefficiency may be very significant.

Table 2 Correction factors for finite fin parameters, slug flow

$K = \left(\frac{wk_m}{bk_f}\right)$	$\gamma = 0.5$	$\gamma = 1.0$	$\gamma = 2.0$
0	0.672	0.421	0.163
1	0.895	0.764	0.531
2	0.938	0.852	0.674
4	0.955	0.915	0.798
10	0.985	0.962	0.905

Combined Forced and Natural Convection for Laminar Flow in Vertical Channels With Internal Heat Generation

Analysis. The main assumptions in this analysis are that the flow velocity is fully established and that the heat input from the boundary to the fluid is constant in the flow direction. The heat-input distribution varies in the transverse directions in such a manner that the wall temperature becomes uniform in the transverse plane. Because of the uniform heat input with respect to the flow direction, the temperatures of the walls and the fluids in fully established regions become linear along the flow direction. Fluid properties are assumed constant except when the body force is considered. Heat dissipation due to the viscosity effect is assumed negligible. The fluid may contain heat sources which are assumed to have arbitrary but identical distributions in all transverse planes. The flow is in the vertical upward direction, along the positive z-axis.

Under the foregoing restrictions, the equations of motion and temperature distribution are

$$\nabla^2 u = \frac{1}{\mu}\left[\frac{\partial\rho}{\partial z} - F_B\right] \tag{29}$$

$$k_f\nabla^2 t = \rho u C_p \frac{\partial t}{\partial z} - Q \tag{30}$$

The co-ordinate axes shall be those shown in Fig. 4. In equation (29) the term F_B represents the body force in the positive z-direction.

To express the body force per unit volume, the fluid is assumed to obey the following linear law of density variation with temperature:

$$\rho = \rho_0[1 - (t - t_0)\beta] \tag{31}$$

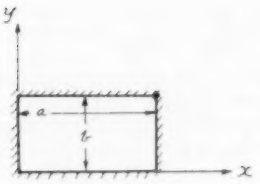

Fig. 4 Flow channel configuration for combined convection

where β is the temperature coefficient for density. The validity of this relationship is of course dependent upon the fact that no phase change of the fluid occurs, and that the temperature variation is small enough to make the temperature coefficient β applicable within the scope of the investigation. Introducing the temperature-difference function θ defined as

$$\theta = (t - t_w) \tag{32}$$

with the wall temperature defined by

$$t_w = t_0 + C_1 z \tag{4}$$

where t_0 represents the wall temperature at the reference station of $z = 0$ and C_1 being the temperature gradient in the axial direction, the state equation (31) is rearranged to read

$$\rho = \rho_0[1 - \beta(\theta + C_1 z)] \tag{33}$$

Noting that

$$\rho_w = \rho_0[1 - C_1\beta z] \tag{34}$$

and assuming $C_1 z\beta$ is less than unity within the scope of the problem, equation (33) can be approximated by

$$\rho = \rho_w(1 - \beta\theta) \tag{35}$$

Hence the body force in the positive z-direction is

$$F_B = -\rho g = -\rho_w(1 - \beta\theta)g \tag{36}$$

and the equations of motion and temperature are now

$$\nabla^2 u = \frac{1}{\mu}\left[\frac{\partial P}{\partial z} + \rho_w g(1 - \beta\theta)\right] \tag{37}$$

$$\nabla^2\theta = [C_1\rho u C_p/k_f] - [Q/k_f] \tag{38}$$

referring to the co-ordinate system shown in Fig. 4.

In order to express results in general terms, the following dimensionless parameters are used:

$$x_1 = x/D; \qquad \phi = \theta \Big/ \left[\frac{\rho u_m C_p C_1 D^2}{k_f}\right]$$

$$y_1 = y/D; \qquad L = -D^2\left[\frac{\partial p}{\partial z} + \rho_w g\right] \Big/ u_m\mu \tag{39}$$

$$F = Q/[\rho C_p C_1 u_m]$$

$$v = u/u_m; \qquad \mathrm{R_A} = [\rho^2 g C_p C_1 \beta D^4/k_f\mu]$$

where D is the equivalent diameter; u_m, the mean fluid velocity. Equations (37) and (38) are therefore simplified to read

$$\frac{\partial^2\phi}{\partial x_1^2} + \frac{\partial^2\phi}{\partial y_1^2} - v = F \tag{40}$$

$$\frac{\partial^2 v}{\partial x_1^2} + \frac{\partial^2 v}{\partial y_1^2} + \mathrm{R_A}\phi = -L \tag{41}$$

The boundary conditions are simply

$$\phi = v = 0, \quad x_1 = 0, \quad (a/D); \quad y_1 = 0, \quad (b/D) \tag{42}$$

Solution: Since there are two simultaneous differential equations, the method of undetermined coefficients using double Fourier series is convenient. The pressure-drop parameter L is independent of x and y and is therefore expressible in terms of the double Fourier series; hence

$$L = \frac{16L}{\pi^2} \sum_{m,n=1,3,5\ldots}^{\infty} \frac{1}{mn} \sin\frac{m\pi x_1}{(a/D)} \sin\frac{n\pi y_1}{(b/D)} \tag{43}$$

for $\dfrac{a}{D} > x_1 > 0$ and $\dfrac{b}{D} > y_1 > 0$.

The heat generation function F, if its distribution across the section is known, can be expressed in the following manner:

$$F = \sum_{m,n=1,2,3,4\ldots}^{\infty} F_{mn} \sin\frac{m\pi x_1}{(a/D)} \sin\frac{n\pi y_1}{(b/D)} \tag{44}$$

where the Fourier coefficients can be obtained easily by the usual rule or some tabulation method. In the case of uniform distribution of heat source, the function F is

$$F = \frac{16F}{\pi^2} \sum_{m,n=1,3,5\ldots}^{\infty} \frac{1}{mn} \sin\frac{m\pi x_1}{(a/D)} \sin\frac{n\pi y_1}{(b/D)} \tag{45}$$

Finally, the functions v and ϕ are assumed to have the following forms:

$$v = \sum_{m,n=1,2,3\ldots}^{\infty} V_{mn} \sin\frac{m\pi x_1}{(a/D)} \sin\frac{n\pi y_1}{(b/D)} \tag{46}$$

$$\phi = \sum_{m,n=1,2,3\ldots}^{\infty} \Phi_{mn} \sin\frac{m\pi x_1}{(a/D)} \sin\frac{n\pi y_1}{(b/D)} \tag{47}$$

which satisfy the boundary conditions prescribed.

Substitution of equations (43), (45), (46), and (47) into equations (40) and (41) and equating coefficients of $\sin m\pi x_1/(a/D)$ sin $n\pi y_1/(b/D)$ terms, the following relations are obtained:

$$\Phi_{mn} = V_{mn} = 0 \quad \text{for} \quad m, n = \text{even integers} \tag{48}$$

and

$$\Phi_{mn} = \left(\frac{16}{\pi^2 mn}\right) \frac{F\mathrm{R_A} + L\left[\dfrac{m^2\pi^2}{(a/D)^2} + \dfrac{n^2\pi^2}{(b/D)^2}\right]}{\left\{\mathrm{R_A} + \left[\dfrac{m^2\pi^2}{(a/D)^2} + \dfrac{n^2\pi^2}{(b/D)^2}\right]^2\right\}} \tag{49}$$

$$V_{mn} = \left(\frac{16}{\pi^2 mn}\right) \frac{F\left[\dfrac{m^2\pi^2}{(a/D)^2} + \dfrac{n^2\pi^2}{(b/D)^2}\right] - L}{\left\{\mathrm{R_A} + \left[\dfrac{m^2\pi^2}{(a/D)^2} + \dfrac{n^2\pi^2}{(b/D)^2}\right]^2\right\}} \tag{50}$$

for $m, n =$ odd integers.

The solution defined by equations (48), (49), and (50) satisfies the governing equations as well as the boundary conditions.

Results and Discussions

The Pressure-Drop Parameter. For prescribed values of the temperature gradient, heat-source intensity, and pumping rate, the pressure gradient is a fixed quantity. Thus one may regard the heat-generation function F and the Rayleigh number as the input functions with L as the resulting function. For arbitrarily given values of F and $\mathrm{R_A}$, the resulting L-value is defined by the following relation:

$$\int_A w dx dy = \int_A dx dy \tag{51}$$

Substitution of equations (43), (45), (46), (47), (49), and (50) into the integral (51) and performing the indicated operation, the following algebraic relation is obtained:

$$L = 1 - \frac{64}{\pi^4} F R_A \sum_{m,n=1,3,5\ldots} \frac{1}{m^3 n^3 \left\{R_A + \left[\frac{m^2\pi^2}{(a/D)^2} + \frac{n^2\pi^2}{(b/D)^2}\right]\right\}} \Bigg/ \frac{64}{\pi^4} \sum_{m,n=1,3,5\ldots} \frac{\left[\frac{m^2\pi^2}{(a/D)^2} + \frac{n^2\pi^2}{(b/D)^2}\right]}{m^3 n^3 \left\{R_A + \left[\frac{m^2\pi^2}{(a/D^2)} + \frac{n^2\pi^2}{(b/D)^2}\right]^2\right\}} \tag{52}$$

where the indexes assume values of positive odd integers.

Inspection of equation (52) shows that the pressure-drop parameter is a linearly decreasing function of the heat-generation parameter F. Heat generation (positive F) reduces the pressure-drop requirement and heat absorption (negative F) increases the necessary pressure gradient. For an aspect ratio of unity, i.e., $a = b = D$, the following expressions have been obtained from equation (52) by assigning various values to R_A. The linear equations containing F and L follow:

$$\left.\begin{aligned} L &= 28.46 && \text{for} \quad R_A = 0 \\ L &= 35.13 - 4.707\,F && \text{for} \quad R_A = \pi^4 \\ L &= 90.73 - 44.77\,F && \text{for} \quad R_A = 10\pi^4 \\ L &= 441.8 - 357\,F && \text{for} \quad R_A = 100\pi^4 \end{aligned}\right\} \tag{53}$$

The foregoing parametric representations are graphically shown in Fig. 5.

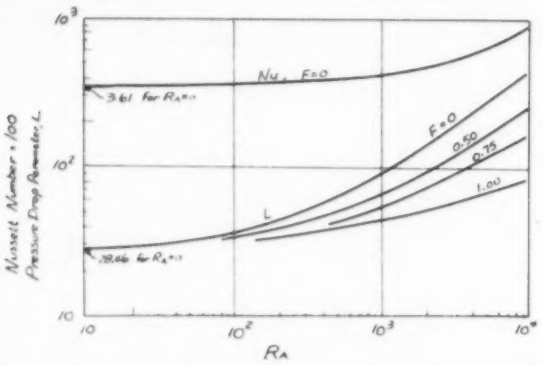

Fig. 5 Nusselt number and pressure-drop parameter at various Rayleigh numbers. Square tube only.

The Nusselt Number. The Nusselt number when evaluated in the usual manner is given by the following expression:

$$\mathrm{Nu} = (F - 1)/(-4\phi_{mx}) \tag{54}$$

where ϕ_{mx} is the dimensionless mixed mean temperature difference between the fluid and the wall at the same location, i.e.

$$\phi_{mx} = \int_A \phi w dA \Big/ \int_A dA \tag{55}$$

for which the following expression is obtained:

$$\phi_{mx} = -\frac{64}{\pi^4} \sum_{m,n=1,3,5\ldots} \frac{1}{m^3 n^3} \frac{\left\{L - F\left[\frac{m^2\pi^2}{(a/D)^2} + \frac{n^2\pi^2}{(b/D)^2}\right]\right\}\left\{L\left[\frac{m^2\pi^2}{(a/D)^2} + \frac{n^2\pi^2}{(b/D)^2}\right] + FR_A\right\}}{\left\{R_A + \left[\frac{m^2\pi^2}{(a/D)^2} + \frac{n^2\pi^2}{(b/D)^2}\right]^2\right\}} \tag{56}$$

For an aspect ratio of 1 and a heat generation parameter of zero and for selected R_A-values, the Nusselt-number values are tabulated in Table 3, where the Nu at $R_A = 0$ is identical to the case of pure laminar forced convection. The values in Table 3 are plotted in Fig. 5.

Table 3 Influence of free-convection on forced convection Nusselt number without heat source, square tubes

R_A	Nu
0	3.61
π^4	3.69
$10\pi^4$	4.27
$100\pi^4$	9.46

Zero Rayleigh Number. When dealing with the combined effects of free and forced convection of the present problem, it is possible to have a zero Rayleigh number by either one of the two conditions; $\beta = 0$ and $C_1 = 0$. The former corresponds to an incompressible fluid and consequently no free-convection effects can occur. The latter case denotes zero axial temperature gradient. Under this condition, free-convective current can exist if the heat generation Q is not zero. Of course, with zero heat generation and zero temperature gradient, the problem leads to a trivial solution.

Inspection of the variables defined by equation (39), however, indicates that they do not admit the case of $C_1 = 0$ as a possibility since, for $C_1 = 0$, F and ϕ become infinitely large. For the case of pure free convection with zero axial temperature gradient, the governing equations may be directly obtained from equations (37) and (38) as

$$\nabla^2 u = -\rho_w g \beta \theta / \mu \tag{57}$$

$$\nabla \theta = -Q/k_f \tag{58}$$

for which the solutions are simply

$$\theta = \frac{Q}{k_f} \frac{16}{\pi^2} \sum_{m,n=1,3,5\ldots} \frac{1}{mn\left[\frac{m^2\pi^2}{a^2} + \frac{n^2\pi^2}{b^2}\right]} \sin\frac{m\pi x}{a} \sin\frac{n\pi y}{b} \tag{59}$$

$$\frac{u}{u_m} = \frac{\rho_w g \beta Q}{k_f u_m \mu} \frac{16}{\pi^2} \sum_{m,n=1,3,5\ldots} \frac{1}{mn\left(\frac{m^2\pi^2}{a^2} + \frac{n^2\pi^2}{b^2}\right)^2} \sin\frac{m\pi x}{a} \sin\frac{n\pi y}{b} \tag{60}$$

For a given Q, equation (59) defines the temperature distribution and equation (60) defines the induced flow rates. It is of interest to note that the specific heat has no effect on the present problem.

Negative Rayleigh number. The Rayleigh number is defined as

$$R_A = [\rho^2 g C_p C_1 \beta D^4 / k_f \mu]$$

A negative value for the Rayleigh number would result if the temperature gradient should become negative along the flow

direction. Under this condition, the flow field is referred to as heating from below which leads to the Rayleigh's instability as discussed in reference [5].

Inspection of equations (46) through (50) indicates that for all positive values of R_A, the solutions are valid. Whereas for negative R_A, there are numerous R_A-values for which the solutions as given by equations (46) through (50) break down. This occurs when

$$R_A + \left[\frac{m^2\pi^2}{(a/D)^2} + \frac{n^2\pi^2}{(b/D)^2}\right]^2 = 0$$

or

$$-R_A = \frac{16\pi^4}{(1+\gamma)^4}(m^2\gamma^2 + n^2)^2 \qquad (61)$$

For a square tube, the critical values of the Rayleigh number are $4\pi^4$, $100\pi^4$, $676\pi^4$ . . . . It is difficult within the scope of the present paper to ascertain the implications of these critical values since the equations employed herein do not apply to this type of nonlinear study.

Insulated Walls. The case of zero heat transfer from the walls can be represented by $F = 1$. For nonuniform heat generation, the equivalent condition will be $\int_A F dA = \int_A dA$. The Nusselt number as defined by equation (54) will be zero. In this manner, one has the condition of "insulated" walls. Inspection of the temperature expressions (47) and (49) indicates, however, that the temperature gradient on the boundaries is not identically zero for the case of $F = 1$. In fact, the temperature gradient changes sign along the boundaries. This indicates a reversal in the heat-flow direction, resulting in zero net heat transfer while the walls are maintained at a uniform temperature without peripheral variation.

From a consideration of heat conduction, existence of heat-flow reversals requires that the thermal conductivity of the materials of the walls be infinitely large so that heat may be conveyed along the secondary surface without change in its temperature. On the other hand, the case of truly insulated walls is one for which the fluid-temperature gradient in the normal direction is identically zero on the walls. It can be shown that the condition of identically zero normal gradient is not compatible with the requirement of uniform wall temperature with respect to peripheral locations. If the walls are truly insulated which can be represented by a zero wall conductivity, then the wall temperature must vary along the boundaries in the peripheral directions. The solution to this problem can be obtained by some approximate procedures such as the collocation method.

Finally, it may be stated that, if the wall conductivity is neither zero nor infinity, the resulting temperature distribution for the case of zero heat transfer must lie between the two extreme cases discussed previously. It is apparent that in a circular pipe with symmetry, an identically zero temperature gradient is the only condition for zero heat transfer, while the peripheral variation of the wall temperature is zero, by reason of circular symmetry.

Conclusions

The following conclusions may be drawn:

1 For laminar flow in channels with secondary surfaces, the over-all limiting Nusselt number or heat-transfer coefficient for fully established flow conditions is greatly influenced by the fin parameter (wk_m/bk_f), as shown in Figs. 2 and 3 for laminar flow and slug flow, respectively.

2 For small values of the fin parameter, the peripheral variation of the wall temperature is quite appreciable. For rectangular channels, the controlling factors are the aspect ratio and the fin parameter.

3 For heat transfer in vertical channels with combined-convection effects and heat generation within the fluid, the general trend is comparable to that in a circular tube investigated by Hallman and reported in reference [3].

Acknowledgment

The author wishes to thank Prof. R. H. Zimmerman for his advice and criticism during the preparation of this paper.

References

1 S. M. Marco and L. S. Han, "A Note on the Limiting Laminar Nusselt Number," TRANS. ASME, vol. 77, 1955, pp. 625–630.

2 J. P. Hartnett and T. F. Irvine, Jr., "Nusselt Values for Estimating Turbulent Liquid Metal Heat Transfer in Noncircular Ducts," *Journal American Institute of Chemical Engineers*, vol. 3, no. 3, 1957, pp. 313–317.

3 T. M. Hallman, "Forced and Free-Laminar Heat Transfer in Vertical Tubes," TRANS. ASME, vol. 78, 1956, pp. 1831–1844.

4 L. S. Han, "Laminar Heat Transfer in Rectangular Tubes With Combined Free and Forced-Convection," *Journal of the American Society of Naval Engineers*, vol. 67, no. 1, 1955, pp. 163–167.

5 Simon Ostrach, "Combined Natural and Forced-Convection Laminar Flow and Heat Transfer of Fluids With and Without Heat Sources in Channels With Linearly Varying Wall Temperatures," NACA TN 3141.

6 T. W. Jackson, W. B. Harrison, and W. C. Boteler, "Combined Free and Forced-Convection in a Constant-Temperature-Vertical Tube," TRANS. ASME, vol. 80, 1958, pp. 739–745.

7 Max Jakob, "Heat Transfer," John Wiley & Sons, Inc., New York, N. Y., vol. 1, 1949.

8 S. H. Maslen, "Transverse Velocities in Fully Developed Flows," *Quarterly of Applied Mathematics*, vol. 16, 1958, p. 173.

ADDENDUM

After the manuscript of this paper was reviewed, the author received comments relative to the subject matter. Aside from editorial comments with respect to typographical errors and some obscure parts of the paper which the author has corrected and clarified, the following points are of significance:

1 That, in the case of three-dimensional flow, the assumption of fully established flow does not necessarily lead to equations (2), (29), and (30) of this paper.

2 That the case of zero Rayleigh number is not necessarily identical to pure convection flow.

3 That equations (12), (13), and (14) can be solved by relaxation methods.

With respect to the first point, the mathematical definition of fully established flow is simply $\partial u/\partial z = 0$. A recent publication by Maslen [8] gave proof that the assumption of fully developed flow implies zero velocities transverse to the flow axis for incompressible viscous flow in laminar motion.

Regarding the case of zero Rayleigh number, the author has added a paragraph explaining the possibility of pure free-convective current with zero axial temperature gradient and heat generation. As to the third comment on relaxation methods, the author is aware of the availability of approximation methods. Since the exact solutions were obtained, no effort was made to use the relaxation methods in the present application. However, it may be mentioned that the solution of equations by relaxation methods might be indeed convenient in solving the problem of insulated walls as mentioned in the paper. Finally, the author would like to thank the reviewers for their comments which materially contributed to the completeness of the paper.

DISCUSSION

P. C. Lu[3]

The writer is particularly interested in the third problem dealt with in this paper. A thesis[4] has recently been submitted to Kansas State College, in which the writer solved the same problem by employing the finite Fourier double sine transform. The results check with those presented in this paper, although different parameters are used. Basically, the finite Fourier transform and the classical Fourier method are of the same origin; but usually the method of Fourier transform is considered to be more straightforward in procedure.

In the thesis mentioned, the writer also was able to solve the problem when the channel is of ring or full-sector cross section by using finite Fourier single sine transform.

With reference both to this paper and a previous paper[5] by the author, the writer would like to point out that an analogy exists between some special cases of the problem under discussion and the deflection of plates lying on an elastic foundation.

When $C_1 = 0$, an analogy to the ordinary thin-plate theory exists just as in pure forced convection. Results for triangular pipes have been obtained by observing this analogy.

[3] Graduate Research Assistant, Department of Mechanical Engineering, Kansas State College, Manhattan, Kan.; now, Graduate Assistant, Department of Mechanical Engineering, Case Institute of Technology, Cleveland, Ohio.

[4] P. C. Lu, "A Theoretical Investigation of Combined Free and Forced-Convection Heat-Generating Laminar Flow Inside Vertical Pipes With Prescribed Wall Temperatures," MS thesis, Kansas State College, Manhattan, Kan.

[5] S. M. Marco and L. S. Han, "A Note on the Limiting Laminar Nusselt Number in Ducts With Constant Temperature Gradient by Analogy to Thin-Plate Theory," TRANS. ASME, vol. 77, 1955, pp. 625–630.

Author's Closure

The author is pleased to learn that the problems for combined convection in channels of ring or full-sector cross sections have been treated in Mr. Lu's thesis. The uses of the classical Fourier method or of the Fourier transforms are extensively discussed in mathematical literature and is not the center of discussion here. It is, however, not impertinent here to recall the basic structure of the equations governing the third problem dealt with in the present paper. If one combines equations (40) and (41), assuming uniform heat generation, the following equation in terms of ϕ is obtained:

$$\nabla^4\phi + R_A\phi = -L \tag{62}$$

with the boundary conditions

$$\phi = 0$$

$$\nabla^2\phi = F \tag{63}$$

To these equations, an analogous problem in the thin plate theory is obvious; namely, a plate resting on an elastic foundation with elastic constant R_A, with zero deflection on the boundaries and acted upon by a constant bending moment (in the case of plates of polygonal shapes). Solutions in this case can be best handled by the use of the energy method.

The author would like to thank Mr. Lu for his discussion and Professor Hoagland of the Massachusetts Institute of Technology for pointing out a misprint which was the result of an oversight in the original analysis. Fig. 2 and Table 1 have been accordingly revised, in the final form.

Heat Transfer to Water in Thin Rectangular Channels

S. LEVY[1]
R. A. FULLER[2]
R. O. NIEMI[1]

Heat-transfer coefficients are presented for water flowing vertically in thin rectangular channels (0.1 × 2.5 in.) 18 and 36 in. long and heated electrically around the entire periphery. The range of variables covered is: 65 to 200 psia pressure, 90 to 200 F subcooling, and 4 to 50 fps water velocity. Heat-transfer correlations are given for data along the narrow and wide faces of the rectangular test section. Burnout data also are reported with steam blanketing occurring first at the corner of the test section. The proposed correlating equation, valid at the narrow face of the test section, gives values considerably lower than those obtained in a circular pipe.

HIGH NEUTRON FLUXES, typical of nuclear test reactors, require unusually large specific powers; i.e., large heat productions per unit volume of reactor core. This requirement is often met by utilizing flat-plate fuel elements of the type shown in Fig. 1. The fuel elements consist of several thin plates of uranium-aluminum alloy clad on both sides with aluminum. The plates, held in position by two side plates, are normally cooled by downward flow of water at rather low temperature and pressure. The heat-transfer problems associated with this kind of fuel elements are:

1 Use of thin rectangular channels of high aspect ratio, measuring about 0.1 × 2.5 in.

2 Continuous variation of bulk-coolant properties in the flow direction.

3 High film-temperature drop from surface of fuel plate to bulk of the coolant and, therefore, large changes of water properties close to the heated plate.

4 Entrance effects where for a short distance beyond the inlet of the fuel element the velocity and temperature profiles are not fully developed.

5 Possibility of "burnout" or steam blanketing of the fuel element during transient power increases or flow reductions.

Yet, as pointed out in the literature survey that follows, data are often lacking when two or three of the foregoing conditions exist simultaneously. In particular, rectangular geometries have not been studied for circumstances encountered in a nuclear test reactor. For this reason, late in 1955 the Atomic Power Equipment Department of the authors' company initiated an extensive heat-transfer program. A heat-transfer and burnout loop was especially erected to study flat-plate fuel elements of the type used in test reactors. This paper covers the experimental results obtained. Following a summary review of available data, the test equipment is described and the test data are presented and discussed.

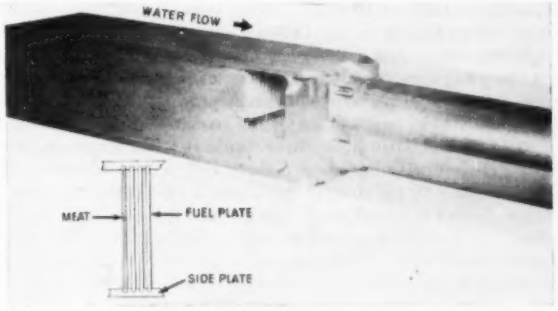

Fig. 1 Typical flat-plate fuel element

[1] General Electric Company, Atomic Power Equipment Department, San Jose, Calif. Assoc. Mem. ASME.
[2] General Electric Company, Knolls Atomic Power Laboratory, Schenectady, N. Y.

Contributed by the Heat Transfer Division and presented at the Annual Meeting, New York, N. Y., November 30–December 5, 1958, of THE AMERICAN SOCIETY OF MECHANICAL ENGINEERS.
NOTE: Statements and opinions advanced in papers are to be understood as individual expressions of their authors and not those of the Society. Manuscript received at ASME Headquarters, September 7, 1958. Paper No. 58—A-127.

Nomenclature

A = heat-transfer area, sq ft
A_P = flow area, ft²
c = specific heat, Btu/lb deg F
D = hydraulic diameter, ft
f = deflection, in.
G = mass flow rate per unit area, lb/hr sq ft
h = heat-transfer coefficient, Btu/hr sq ft deg F
J = current in test section, amp
k = thermal conductivity, Btu/hr ft deg F
N_{Nu} = Nusselt number, nondimensional, (hD/k)
N_{Pr} = Prandtl number, nondimensional, $(\mu c/k)$
N_{Re} = Reynolds number, nondimensional, (GD/μ)
p = average test section perimeter, ft
Q = heat generation in test section, Btu per hr
$(Q/A)_{BO}$ = burnout heat flux, Btu/hr sq ft
r = resistivity of test section, ohm-ft
T_b = bulk temperature, deg F
T_O = test-section, thermocouple-temperature reading, deg F
T_{out} = outlet-water temperature, deg F
T_{sat} = saturation temperature at outlet of test section, deg F
T_w = surface temperature of test section, deg F
V = water velocity, fps
Y_T = total deflection, in.
μ = absolute viscosity, lb/hr ft

Subscripts

b = bulk
f = film
w = wall

Literature Survey

The problem of heating and cooling fluids inside tubes has received considerable theoretical and experimental attention [1].[2] Test data for turbulent flow have been correlated in several references. They include the equations of the following:

1 The Dittus-Boelter [2] type where all physical properties are evaluated at the bulk fluid temperature

$$\frac{hD}{k} = 0.0243 \left(\frac{DG}{\mu}\right)^{0.8} \left(\frac{c\mu}{k}\right)^{0.4}$$

for heating, and (1)

$$\frac{hD}{k} = 0.0265 \left(\frac{DG}{\mu}\right)^{0.8} \left(\frac{c\mu}{k}\right)^{1/3}$$

for cooling.

2 The Colburn [3] form where properties are taken at the so-called film temperature or arithmetic mean of surface and bulk temperature

$$\frac{hD}{k_f} = 0.023 \left(\frac{DG}{\mu_f}\right)^{0.8} \left(\frac{c\mu}{k}\right)_f^{1/3} \quad (2)$$

3 The Sieder-Tate [4] kind which utilizes both bulk and surface properties

$$\frac{hD}{k} = 0.027 \left(\frac{DG}{\mu}\right)^{0.8} \left(\frac{c\mu}{k}\right)^{1/3} \left(\frac{\mu_b}{\mu_w}\right)^{0.14} \quad (3)$$

Yet, as pointed out by McAdams [1], equations of the foregoing form are proving to be inadequate. A coefficient of 0.023 has been suggested [5] for Equation (1). Similarly, a coefficient of 0.023 is recommended [1] for Equation (3) and some data for air employ a value of 0.021 [6]. Recent tests [7] with gases would place the coefficient in the Colburn equation at 0.019. Even when only considering data for heating water, the correlations are not always in agreement. Test results for pipe flow at pressures from 500 to 2000 psi and with small property variation have been correlated by means of the Colburn equation with coefficients of 0.023 [8] and 0.019 [9]. Experiments at lower pressures and with large property variation include the data of Kreith and Summerfield [10] for circular tubes which agree with Equation (3); those of McAdams, et al. [11] for flow in an annulus which satisfy the Sieder-Tate equation with a coefficient of 0.026; and those of Stein, et al. [12] for an annular geometry which are best correlated by a Colburn equation with a coefficient of 0.020 [13].

Equivalent correlations for turbulent flow in rectangular channels are practically unavailable. Besides the data of Bailey and Cope [14] which are somewhat uncertain due to a nonadiabatic mixing device at the outlet, there are the test results of Kays [15] for heating air in a rectangular passage with an aspect ratio of 5.85. Kays' values are for Reynolds numbers of less than 10,000 and fall 24 per cent below those predicted from Equation (2). Also, Washington and Marks [16] reported heat-transfer coefficients in rectangular channels substantially below the predictions of Equations (1), (2), or (3). Test data for Reynolds numbers less than 10,000 may be in a transitional region and the turbulent-flow, heat-transfer-correlating equations may not be applicable.

Similarly, entrance effects in rectangular channels have not been studied previously. Results, however, can be found for circular tubes. Recent test results for water flow in pipes have been presented by Hartnett [17] and they agree with the analysis of Deissler [18].

Heat-transfer burnout data approaching the range of interest in test reactors have been obtained by McAdams, et al. [11] and Gunther [19]. McAdams, et al. [11] have reported burnout-flux values for degassed distilled water flowing upwards in a vertical annulus containing a central tube heated electrically. Pressures ranged from 30 to 90 psi, water velocities from 1 to 12 fps, subcooling from 20 to 100 deg F. The diameter of the annulus was not varied in the tests and the data apply to a 0.25-in. central heater in a 0.77-in. glass tube. Gunther [19] carried out similar measurements in a horizontal glass passage $^1/_2$ in. high, $^3/_{16}$ in. wide, and 6 in. long containing a horizontal electrically heated metal strip at the axis. Water velocities varied from 5 to 40 fps, subcooling from 22 to 282 deg F, pressures from 15 to 160 psia. These tests, however, do not cover the case of downward flow of water in very thin rectangular channels with high heat production in the corners of the rectangular section (to simulate gamma and neutron heat generation in the side plates of Fig. 1).

[2] Numbers in brackets designate References at end of paper.

Description of Equipment

Test Loop. The heat-transfer burnout loop is shown in Fig. 2. It is built entirely of stainless steel and designed for 1000 psi. A schematic representation of the experimental system is shown in Fig. 3. It consists of:

1 Primary loop, where water is circulated in a closed system by means of a centrifugal pump through a preheater, along the steam pressurizer connection, upward or downward through two parallel test sections, and on to a vertical or horizontal heat exchanger.

2 Demineralized water system, utilizing a demineralizer and associated cooling equipment to yield the desired water purity.

3 Heat-exchange system, consisting of a horizontal heat exchanger for low temperature and low pressure, and a vertical heat exchanger for high temperatures and net steam generation.

4 Test sections, where heat is generated by electrical heating of the test section walls up to 9 ft in length.

5 Power supply, using six General Electric d-c arc welders rated at 40 volts and supplying 1540 amp each to the test section.

6 Instrumentation and controls, consisting of temperature, pressure, flow, current, and voltage-measuring equipment.

Fig. 2 Heat-transfer and burnout loop

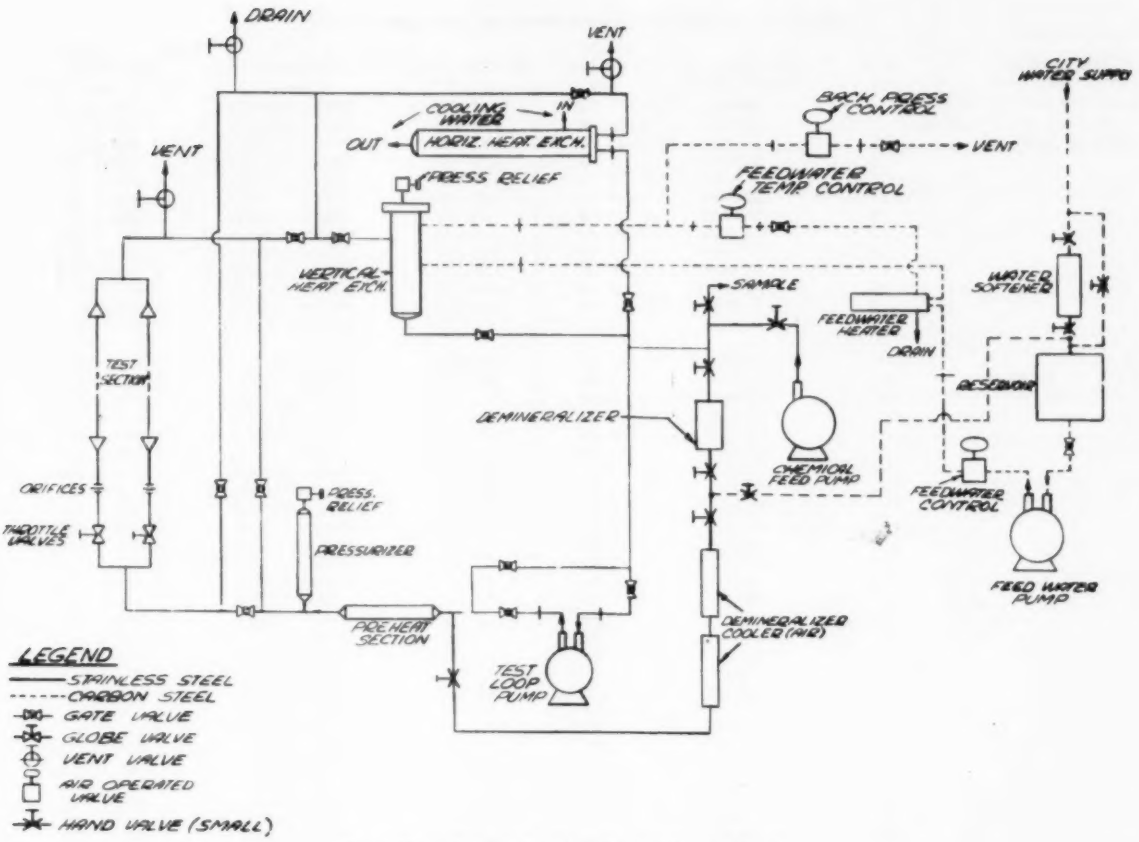

Fig. 3 Flow diagram (heat-transfer and burnout loop)

Test Sections. A typical test section is shown in Fig. 4. It consists of a rectangular channel about 0.100 in. × 2.500 in. fabricated of stainless steel. A copper flange is attached to each end of the test section and it is connected to the current-carrying bus bars by means of flexible connections. Two side plates spanning the entire length and width of the test section are provided to resist internal pressure forces. The side plate as well as the rest of the loop are electrically insulated from the test section and copper flanges.

The heating-element size varied slightly from one test section to another. The exact dimensions of test sections 4 and 11 are shown in Table 1. Test section 5, also listed in Table 1, is a distorted test section used to find the effects of dimension variation in rectangular geometries. Its dimensions are given in a later part of the paper. Test sections used for burnout tests measured 0.118 in. × 2.405 in. They were also 18 in. long and 0.028 in. thick. On the other hand, test sections 4, 5, and 11 were 36 in. long and 0.056 in. thick.

Twenty-eight thermocouples were installed at various positions on the test section. The test sections also were instrumented with two pressure taps at each end of the heating element. The thermocouples, insulated from the test section by 0.0015-in. thick mica tape, were distributed lengthwise, and around the periphery of the rectangular cross section. Their exact location is given in Fig. 5 which illustrates a typical set of thermocouple measurements. It should be noted that thermocouples labeled C_1 and C_2 were placed at the centers of the narrow sides of the test section, while thermocouples M_F, M_B, S_1, and S_2 were located on

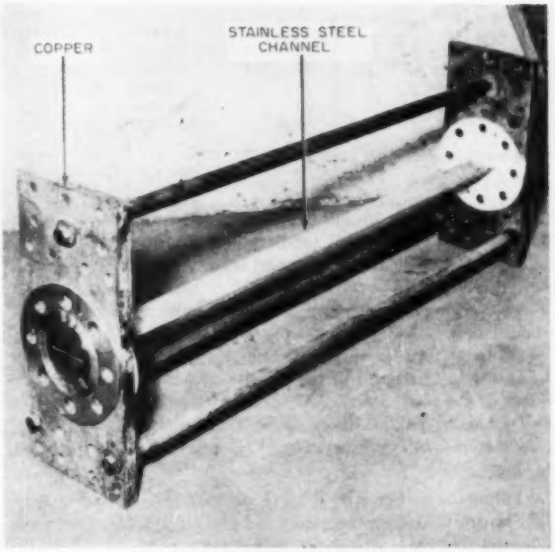

Fig. 4 Heat-transfer test section

the 2.500-in. faces of the heating element. Thermocouples M_F and M_B are on the center line of these two faces, and thermo-

Table 1 Heat-transfer runs for water flow in thin rectangular channels

Test section no.	Run no.	Heat flux Q/A, Btu/hr sq ft	Water velocity, fps	Bulk temp, T_b, deg F	Bulk Reynolds no., $N_{RE(Bulk)}$	Ratio of surface to bulk temp, T_w/T_b, deg F/deg F
4	8	265000	37.70	112–130	104000–124000	1.348–1.282
	9	550000	38.10	112–152	103000–152000	1.715–1.468
0.118 × 2.405 in.	10	267000	37.70	112–132	104000–125000	1.416–1.344
	11	572000	37.70	112–154	104000–151000	1.768–1.500
	12	268000	33.30	113–134	93000–112000	1.400–1.345
	13	574000	30.20	112–158	94000–141000	1.895–1.608
	14	269000	35.40	116–140	89000–110000	1.483–1.395
	15	579000	28.40	113–168	79000–126000	1.782–1.560
	16	173000	14.70	113–146	41000–56000	1.468–1.383
	17	162000	37.50	113–124	104000–117000	1.238–1.200
	18	1,010000	39.40	114–187	110000–195000	2.09–1.542
	19	990000	39.10	114–186	109000–196000	2.08–1.542
	20	983000	38.80	113–184	106000–190000	2.04–1.542
11	100	815000	26.10	118–212	73000–146000	2.31–1.589
0.114 × 2.349 in.	101	630000	26.40	126–194	81000–135000	1.930–1.535
	102	530000	23.90	113–172	72000–118000	1.975–1.587
	103	999000	36.20	126–209	110000–200000	2.175–1.635
	104	547000	36.00	97–141	85000–128000	1.990–1.632
	105	440000	36.00	90–124	78000–111000	1.869–1.550
	108	740000	39.40	129–184	125000–191000	1.853–1.599
	109	1040000	40.90	102–175	100000–186000	2.380–1.753
	110	802000	43.90	107–161	113000–192000	2.360–1.870
	111	600000	45.00	94–133	103000–150000	2.190–1.829
	112	447000	45.50	86–114	93800–127000	2.000–1.720
	113	1018000	45.40	101–165	110000–194000	2.395–1.849
	114	27000	5.54	79–92	10600–12400	1.278–1.172
	115	60000	4.75	79–114	9000–13300	1.648–1.316
	116	103000	4.76	82–144	8400–17300	2.080–1.432
	117	154000	16.70	72–97	29400–39700	1.723–1.391
	118	446000	24.40	91–143	53200–87900	2.090–1.645
	119	449000	16.55	92–169	36400–72500	2.400–1.658
	120	331000	12.62	85–138	34800–59600	2.180–1.623
	121	240000	16.90	78–117	32000–48800	2.00–1.545
	122	822000	33.50	118–190	95200–168300	2.10–1.585
	123*	244000	12.95	73–127	22900–40900	2.26–1.562
	124*	113000	12.95	68–93	21600–29400	1.735–1.465
	125*	174000	12.90	70–108	22100–33500	2.03–1.555
	126*	65000	11.55	66–81	18800–22700	1.455–1.345
	127	59000	4.32	88–126	9300–13700	1.612–1.302
	128	58000	3.76	87–131	7900–12400	1.701–1.322
	129	107000	3.68	88–171	7700–16300	2.195–1.438
	130	122000	3.05	102–221	7300–17900	2.315–1.421
	131	159000	2.90	107–273	7100–21400	2.645–1.375
5	24	650000	24.6	117–165	105000–157000	1.985–1.605
	25	308000	24.3	113–135	101000–125000	1.630–1.488
(For dimensions see Fig. 8)	27	440000	22.2	115–152	96000–131000	1.492–1.390
	28	615000	25.0	115–162	105000–157000	1.630–1.445
	29	302000	19.8	114–142	83000–107000	1.385–1.275
	34	1000000	25.3	116–191	107000–193000	2.060–1.345

* Upward waterflow

couples S_1 and S_2 are on either side of the center line M_F and 0.735 in. away from it. Bulk temperatures were measured at the inlet and outlet of the test section and are assumed to have varied linearly from one end to the other.

The test sections were equipped with a burnout detector. This burnout control system was capable of turning off the power supply before peak fluxes could damage the test section. It consisted of balancing the resistance of the exit end against the resistance of the rest of the test section. As burnout occurs, the bridge becomes unbalanced and shuts off the electrical power supply.

Loop Operation. The experimental procedure consisted of the following:

1 Filling the system with demineralized water.

2 Starting the circulating pump and pressurizing the system to the desired pressure.

3 Applying the desired power to the test section after adjusting the flow and pressure setting.

4 Regulating the inlet-water temperature by changing the secondary flow in the heat exchanger or utilizing the preheater.

5 Recording surface temperature, system pressure, pressure difference across the flow orifice, water inlet and outlet temperatures, current and voltage to the test section, and pressure drop along the test section.

6 Reducing the data. The inside wall temperature T_w is computed first from the measured value T_O at the outer surface according to the expression [10]

$$T_O - T_w = \frac{3.413I^2}{2p^2}\frac{r}{k} \tag{4}$$

where I = current in test section, amp
r = resistivity of test section, ohm-ft
k = thermal conductivity, Btu/hr-ft deg F
p = average test-section perimeter, ft

In the present case there is no need to correct for the variation of electrical resistivity and thermal conductivity with temperature since their ratio for 304SS, used in the test section, remains practically constant and varies only 0.33 per cent, well within the range of the accuracy of the data.

Table 1 (cont'd)

Heat balance, per cent	RUN	SYMBOL	RUN	SYMBOL	RUN	SYMBOL
Run 8(0.3)	8	△	29	⊡	115	s
9(0.6)	9	□	34	⊛	116	~
10(0.1)	10	×			117	<
11(0.5)	11	◑	100	⊥	118	>
12(0.43)	12	▲	101	⊕	119	÷
13(12.5)*	13	■	102	+	120	( )
14(14.4)*	14	☆	103	‡	121	(=)
Run 15(6.2)	15	⊖	104	‖	122	(=)
16(22.2)*	16	●	105	‖	123	(-)
17(4.1)	17	○	106	■	124	(·)
18(1.3)	18	▲	108	⊥	125	(†)
19(1.9)	19	◨	109	⊥	126	(‡)
20(1.4)	20	+	110	⊎	127	(≈)
	24	⊟	111	⊎	128	(×)
	25	⊡	112	⊹	129	(•)
	27	⊠	113	c	130	(‖)
	28	⊞	114	ɔ	131	(=)

* Flow based on electrical Q.

Next, the mean temperature of each segment of the test section is determined and the corresponding heat output obtained from the measured current and an extrapolation of the measured resistance at room temperature. The fluid temperature at any position along the test section is derived by integrating the heat generated to the desired point. A knowledge of the heat flux, bulk and surface temperatures in turn determines a heat-transfer coefficient.

Error Analysis. The heat-transfer coefficient is calculated from

$$h = (Q/A) / (T_w - T_b)$$

From the Sieder-Tate equation

$$h = 0.023\,(k/D)\,(DV/\mu)^{0.8}\,(c\mu/k)^{1/3}\,(\mu/\mu w)^{0.14}$$

or

$$h = 0.023\,k\,(\rho/\mu)^{0.8}\,(c\mu/k)^{1/3}\,(\mu/\mu w)^{0.14}\,(V^{0.8}/D^{0.2})$$

Since the measured and calculated heat-transfer coefficients differ, the factors involved in the experiments and in the correlating equation must be examined. In the experimental heat-transfer coefficient, the factors are:

1 Heat flux, Q/A
2 Surface temperature, T_w
3 Bulk temperature, T_b

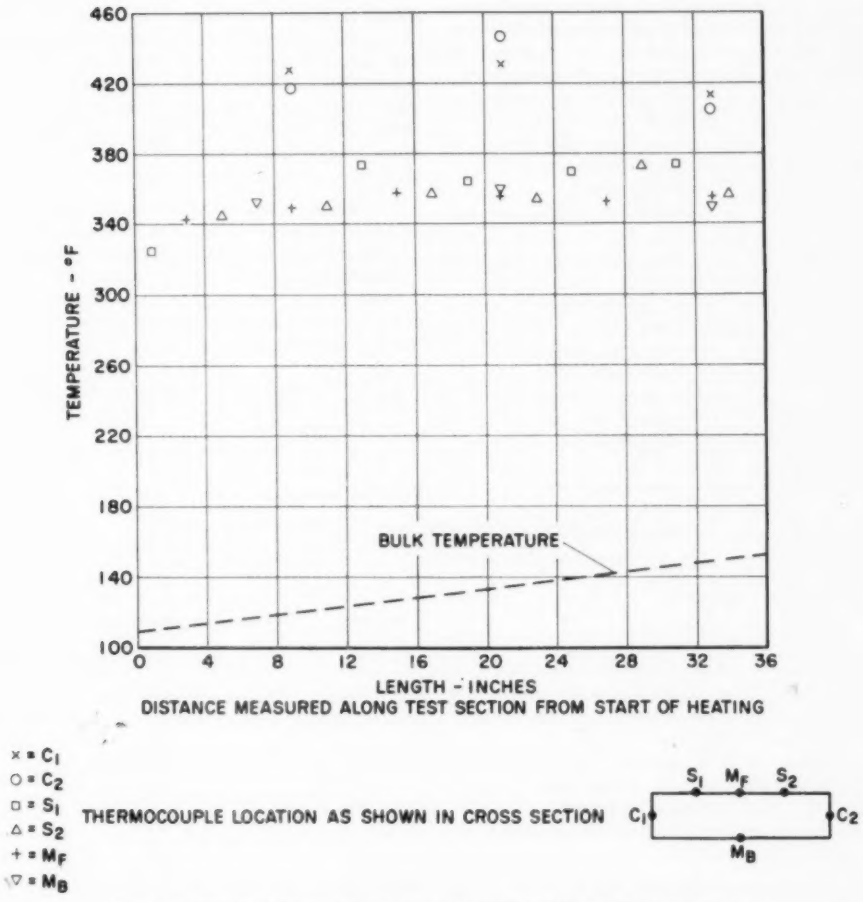

Fig. 5 Typical set of thermocouple measurements for test section No. 4, run No. 11

The heat flux Q/A is determined from the heat input Q and the heat-transfer area A. The heat-transfer area can be measured and calculated to a high degree of accuracy. An error of 0.020 in. in a 5-in. perimeter corresponds to an error of 0.4 per cent. The heat input was determined from electrical measurements of the voltage and current with instruments of $^1/_4$ per cent of full-scale deflection error. Parallax reading errors were minimized by the usual reflecting mirror in the instrument. At a half-scale reading the instrument errors would be $^1/_2$ per cent and a reading error of 1 per cent give an error of $1^1/_2$ per cent. This error, however, would vary from reading to reading. Nonuniformity of thickness of the test section would yield variations in I^2R heating. Commercially drawn tubing is uniform to within 1 mil, but the forming operation used to make the test section probably produced a nonuniform thickness at the corners. Ordinary visual inspection did not yield any detectable thickness changes.

The temperature measurements are expected to be the critical ones. The factors involved in the temperature measurements will be considered:

1 Thermocouples. The thermocouples were made by the General Electric Engineering Laboratory using a helium arc-welding procedure. These thermocouples were calibrated to an accuracy of 1 deg to 400 F.

2 Error due to Conduction Loss. There is a $1^1/_2$-mil thickness of mica electrical insulating tape between the outside surface of the test section and the thermocouples. Heat conduction due to external losses would give a temperature drop across the mica tape. To minimize the drop, a 2-in-thick block of magnesia insulation was installed over the thermocouples. It should be emphasized that the temperature error introduced by conduction losses reduces the temperature and yields *increased* values of the heat-transfer coefficient. Radiation losses enter only in increasing the insulation exterior film heat-transfer coefficient and, since the insulation is so thick, radiation effects are small.

3 Thermocouple System. An ice-bath cold junction was used for the series of tests with test section No. 4. A Leeds and Northrup precision laboratory-type potentiometer made specifically for thermocouple installations was used. The instrument itself is accurate to 0.1 per cent. Later, an automatic Brown recorder was substituted and temperatures were recorded graphically with an automatic plotter. The data duplicated the ice-bath precision-potentiometer arrangement and further test data were recorded graphically. The recorders were guaranteed to $^1/_4$ per cent of full-scale deflection. Up to 600 F the error would be $1^1/_2$ deg F. For a 50-F temperature differential this would correspond to a 3 per cent error. Higher temperature differentials would have a correspondingly smaller percentage error.

4 Wall Temperature-Drop Correction. Since the outside wall temperature was measured, the temperature drop across the test section wall must be known. The correction was given by

$$T = \frac{3.413\, I^2 r}{2p^2 k}$$

The I^2 error is about twice the error in current I and therefore is about 1 per cent maximum. The maximum error in p^2 would be 0.8 per cent. The ratio (r/k) is determined from other experimenters' data. The error in thermal conductivity is the controlling error. An estimate of the accuracy of (r/k) is 1 per cent. The maximum error would then be about 2.8 per cent. A wall-temperature drop of 100 F would yield a 3-deg-F error.

Summary. The errors in determining the heat-transfer coefficient are:

(*a*) (Q/A) = error in reading volts and amperes = 1.5 + 1.5 = 3 per cent.

(*b*) Surface temperature, T_w

(1) thermocouple, 1 deg
(2) conduction loss, $^1/_2$ deg
(3) thermocouple recorder, $1^1/_2$ deg
(4) temperature drop through wall, 3 deg for 100-F differential.

Error for 100-deg-F wall conduction drop = 6 deg.

The surface temperature rise is of the order of 200 F or greater when the wall correction is 100 deg. The error is 3 per cent.

The total cumulated error could be 6 per cent.

In the calculated heat-transfer coefficient, the factors involved are:

(*a*) $k(\rho/\mu)^{0.8}$, $(c\mu/k)^{1/3}$, $(\mu/\mu w)^{0.14}$, all dependent on temperature. The values are determined from other experimenters' values. Accuracy estimated at greater than 1 per cent.

(*b*) V, velocity. A calibrated orifice was used to measure flow. The initial accuracy was about $^1/_4$ of 1 per cent but with operation may decrease in accuracy to about 1 per cent. A reading error of 0.05 in. at a 30-in. reading corresponds to an error of $^1/_2$ of 1 per cent. The flow-measurement accuracy is between 1 and 2 per cent.

Now, the velocity is determined in the test section from

$$W = (\rho A V)_{\text{orifice}} = (\rho A V)_{\text{test section}}$$

Errors in determining the flow area would affect the velocity. The heat-transfer coefficient will have 0.8 the error in the velocity.

(*c*) D, hydraulic diameter. The hydraulic diameter could be determined to about 2 mils accuracy in the unpressurized state. The channel size was not measured in the pressurized state. The test section was backed with a $^1/_{16}$-in-thick hard-asbestos gasket, which was backed with a steel supporting section about $^1/_4$-in. thick. The whole assembly was bolted together. Compression of the backing gasket and deflection of the support plate would allow the channel spacing to change.

The gasket compression can be estimated. For compressed asbestos, a 100-psi pressure will give a 3 per cent compression.

Deflection y is: $y = (0.03)(0.0625) = 0.001875$

(Gasket) $y = 0.002$ in.

Deflection of backup plate: Assume plate to be simply supported at bolting lines. The plate will act as a uniformly loaded, simply supported beam.

$$f(\text{deflection} - \text{maximum}) = \left(\frac{5}{384}\right)\frac{Wl^3}{EI}$$

$$I = \frac{bd^3}{12} \quad \text{where} \quad b = 1 \text{ in. (assumed)}, \quad d = {}^1/_4 \text{ in.}$$

Then, for 100-psi pressure

$$f = \left(\frac{5}{384}\right)\frac{(100 \times 3)(3)^3}{(30 \times 10^6)\dfrac{1 \times (^1/_4)^3}{12}} = 0.0027 \text{ in.} \quad l = 3 \text{ in.}$$

The total of the plate and gasket deflections is

$$Y_T = Y(\text{total}) = 2[0.002 + 0.0027] = 0.0094 \text{ in.}$$

If the middle third is assumed to have the maximum deflection and a linear taper of deflection to zero at the ends, then

$$A_F = \frac{w}{3}\left[\left(c + \frac{Y_T}{2}\right) \times 2 + (c + Y_T)\right]$$

$$A_F = wc + w\left(\frac{2Y_T}{3}\right)$$

Neglecting the slight increase in perimeter due to stretching of the test section,

$$D_H = \frac{4A_F}{p} = \frac{4[wc + w(2Y_T/3)]}{2(w + c)}$$

$$= \left[\frac{wc + w(2Y_T/3)}{w + c}\right] 2$$

$$= \frac{\{2[2.5 \times 0.108 + 2.5(2 \times 0.0094/3)]\}}{2.5 + 0.108}$$

$$D_H = 0.219 \text{ in.}$$

The undeformed test section hydraulic diameter was 0.207 in. The test section hydraulic diameter could have changed due to deflection of the backing plate and compression of the gasket:

$$\frac{0.012}{0.207} \text{ or } +5.8 \text{ per cent}$$

The velocity change is inversely proportional to the flow-area change.

$$+100\left(\frac{\Delta V}{V}\right) = \frac{-100\left(\frac{1}{wc} - \frac{1}{wc + w(2Y_T/3)}\right)}{\frac{1}{wc}}$$

$$= -6.7 \text{ per cent}$$

Then, the error in the calculated heat-transfer coefficient due to test-section deformation is

$$-0.8(6.7) + -(0.2)(5.8) = -6.5 \text{ per cent at 100 psi}$$

The deformation of the test section is the one factor which would reduce the heat-transfer coefficient.

Test Results

All the heat-transfer runs are summarized in Tables 1 and 2. Table 1 lists the tests performed to obtain the heat-transfer coefficients while Table 2 shows the runs which determined burnout heat flux.

Over 40 runs were carried out to measure heat-transfer coefficients in thin rectangular sections. The range of variables was

Water velocity, fps	2.90 – 45.5 fps
Heat-transfer rate, Btu/hr sq ft	58,000 – 1,040,000
Bulk water temperature, deg F	66 – 273
Ratio of surface to bulk temp, deg F/deg F	1.17 – 2.65

With the exception of four runs marked with asterisks in Table 1, all runs were performed with downward water flow. Also, boiling was not permitted in any of the tests in Table 1.

A total of 16 burnout runs were performed with downward water flow. They cover the following set of conditions:

Water velocity, fps	6 – 53
Outlet pressure, psia	60 – 140
Subcooling, deg F	90 – 200

Only 16 runs were completed because rupture of the test section happened every two to three runs despite the burnout detector. Data of interest involved such high water subcooling and large water velocities that excessive thermal shocking of the test section resulted after the detector turned off the power supply.

In all such cases of rupture of the test section it was noted that the failure was localized in the corner. The burnout data as reported here, therefore, apply to steam blanketing at the corner of a thin rectangular section with large heat production at the corner. This phenomenon was verified further during a voluntary burnout test carried out without the detector to check its accuracy.

Discussion of Results—Heat-Transfer Coefficients

A plot of all the heat-transfer coefficients on the 2.5-in. faces is given in Fig. 6, with the exception of those for test section No. 5. The data, including those points in the entrance region, are plotted in terms of Sieder-Tate parameters and compared to the original Sieder-Tate Equation (3). Examination of Fig. 6 reveals that:

1 The heat-transfer coefficients are 30 to 45 per cent below those predicted from Equation (3), the deviation increasing with Reynolds number. A lower coefficient of 0.023 in Equation (3), as suggested in reference [1], would still yield values 15 to 30 per cent too high. One concludes that rectangular channels for the conditions tested exhibit poorer heat-transfer characteristics than those accepted for circular pipes. This reduction in heat-transfer coefficient is small enough not to lessen the ability of flat-plate elements to operate at very high heat-transfer rates.

2 A correlation with a constant exponent on the Reynolds numbers is not adequate. Even though simultaneous consideration of all runs indicates that the Reynolds number exponent may be below 0.8, close examination of the runs in Fig. 6 shows that the exponent for each run is larger than 0.8 and varies from run to run, increasing slowly with reduced heat rates. A major reason for the variation in the exponent could be the continuous change in fluid properties as the water and surface temperatures vary along the heated length. In particular, the viscosity continually

Table 2 Burnout data for subcooled water flow in thin rectangular channels

Run no.	Heat generation Q, Btu/hr	Heat flux Q/A, Btu /hr sq ft	Outlet pressure, psia	Saturation temp T_{sat}, deg F	Outlet bulk temp T_{out}, deg F	Subcooling $T_{sat} - T_{out}$, deg F	Water velocity V, fps	$\frac{Q/A}{400{,}000 + 4800}{(T_{sat} - T_{out})}$	$\frac{Q/A}{T_{sat} - T_{out}}$
1B	368604	600332	74.0	306.7	218.0	88.7	7.29	0.7270	6768
2B	325000	530000	70.0	302.9	204.5	98.4	7.05	0.6075	5386
3B	432000	735000	67.0	300.0	173.3	126.7	12.25	0.7290	5801
4B	Run no. 4	no burnout at 50.5 fps, 1,708,000 Btu/sq ft hr							
5B	965000	1575000	75.0	341.2	167.7	173.5	42.2	1.278	9078
6B	1058000	1725000	75.0	307.6	137.6	170.0	53.0	1.418	10147
7B	879000	1430000	75.0	307.6	143.5	164.1	36.8	1.204	8714
8B	659000	1075000	70.0	302.9	138.1	164.8	28.3	0.9025	6523
9B	527000	859000	70.0	302.9	146.5	156.4	21.4	0.7464	5492
10B	398000	648000	65.0	298.0	139.0	159.0	15.2	0.5570	4070
11B	346000	564000	65.0	298.0	166.5	131.5	9.8	0.5470	4280
12B	Run no. 12	no burnout at 45 fps, 1,725,000 Btu/sq ft hr							
13B	501000	817000	120.0	341.2	139.6	201.6	19.7	0.5960	4050
14B	676000	1100000	120.0	341.2	148.8	192.4	23.8	0.8940	5730
15B	388000	633000	115.0	338.1	202.8	135.3	5.6	0.6031	4678
16B	525000	857000	138.0	351.9	196.0	155.9	7.8	0.7528	5497

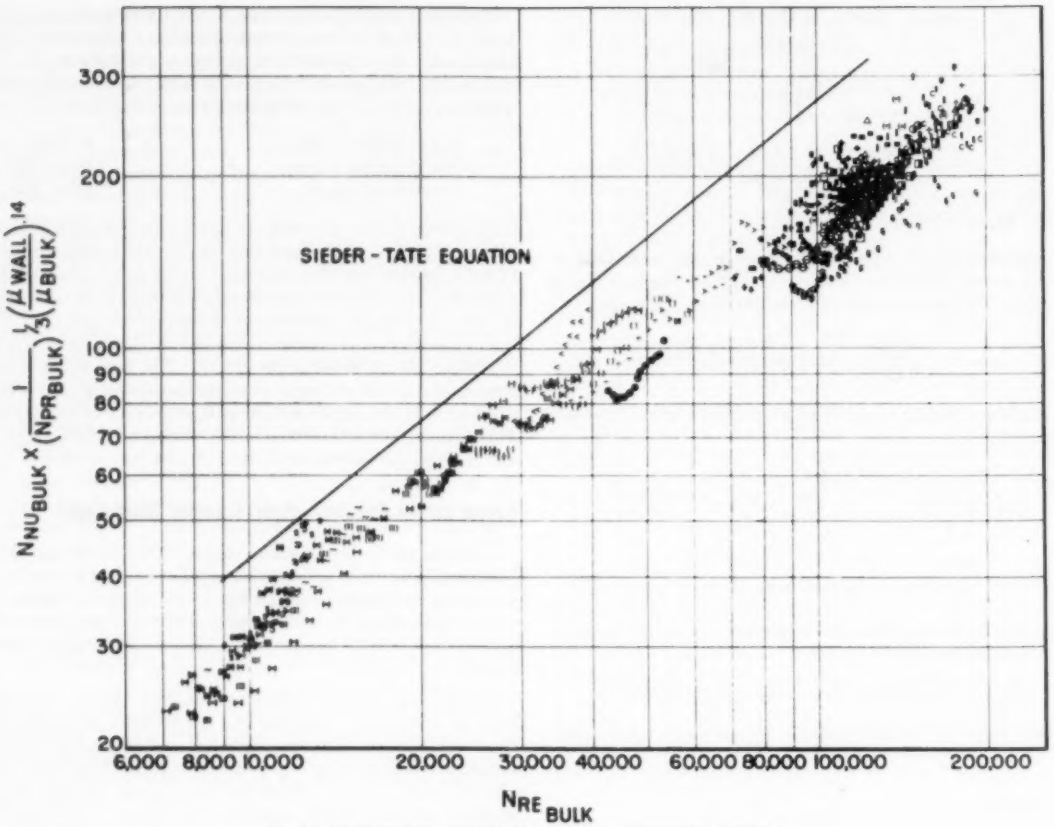

Fig. 6 Heat-transfer coefficients for thin rectangular channels

decreases in the direction of flow, i.e., the corresponding water-velocity distribution changes from inlet to outlet. These "secondary thermally produced" hydraulic entrance effects could account not only for the Reynolds number exponent variation with heat rate, but also for the spread in the experimental measurements.

3 Entrance effects are noticeable in each run of Fig. 6. The heat-transfer coefficients at the inlet of the test section correspond to the lower Reynolds numbers values of each run. They are seen first to decrease, then reach a minimum, and finally increase. The thermal-entrance length may be defined as the distance from start of heating to the point where the Nusselt number increases as the Reynolds number, raised to a fixed power. This thermal-entry length is seen to be about one fourth of the test section and to vary but slightly with water velocity. Each of the foregoing effects will now be considered in more detail.

Effect of Rectangular Cross Section. As already noted, lower coefficients were obtained in the rectangular test sections. However, proper understanding of these reduced heat-transfer conditions must await measurement of velocity and temperature distribution in rectangular cross section. To date, velocity measurements have been carried out only in triangular ducts in the low Reynolds number range; less than 25,000. The most recent tests of Eckert and Irvine [20] reveal that in a limited range the flow may be turbulent near the base of the triangular duct, but laminar near the apex of the cross section. A similar pattern of laminar-turbulent flow or of low turbulence–high turbulence flow coexistence may be anticipated at the edges of a rectangular cross section. The higher surface temperatures measured at the edges of the present heating elements tend to verify this assumption. A plot of heat-transfer coefficients at the center of the short side of the rectangular channels is given in Fig. 7. Two values are shown for each run corresponding to positions 12 and 24 in. away from the inlet of the heated section. Higher coefficients are noted for test section No. 4. These may be due to slight differences in geometry. Test section No. 4 was made up of two L strips and had very sharp corners, while test section No. 11 was fabricated from a circular tube and had rounded edges. In both cases, however, the heat-transfer coefficients are considerably lower than those from Equation (3). The values are 60 to 70 per cent below the Sieder-Tate prediction and about 15 to 30 per cent below the data given in Fig. 6. The exact extent of this region of reduced heat transfer was not determined. However, Fig. 5 indicates that it must have been confined to the edges of the section since thermocouples S_1, S_2, and M_F, were reading the same.

Another way of tracing the lower coefficients of Fig. 6 to the rectangular geometry was obtained with test section No. 5. Test section No. 5 was a distorted test section deformed by applying internal pressure to it without installing the backing plates. It was recognized early in the program that fuel-element channels cannot be expected to remain flat in the reactor. Some bowing will happen as pressure differential and heating are applied to them. A series of runs therefore was performed with test section No. 5 to determine the seriousness of small variations in geometry. The exact changes in geometry were not determined from run to run. Once the test section was originally deformed, the backing plates were placed in position. However, the backing plates were flat and did not match the test-section curvature so

that further geometry distortion may have happened with changes in system pressure and temperature.

Relative dimensions of the test section were obtained after the last run and are given in Fig. 8. They were taken 2, 12, 20, and 32 in. from the inlet of the test section. An average cross section used to calculate the hydraulic diameter is also shown. It is important to note that the cross section varies in the flow direction and that its average hydraulic diameter is 50 per cent larger than that of test sections Nos. 4 and 11. Typical heat-transfer data for test section No. 5 are given in Fig. 9. They are based upon the average hydraulic diameter of Fig. 8. It is seen that the coefficients are higher than those of test sections Nos. 4 and 11. The increased roundness in the geometry, therefore, brings the heat-removal properties close to those in circular pipes. Further correlation of the data in Fig. 9 cannot be attempted owing to velocity changes and variation in cross section from run to run. The hydraulic diameter is not known for the tests plotted in Fig. 9 and the spread between the data indicates that it must have varied with time.

Type of Correlating Equation. Data from test section No. 4 were used to determine the best type of correlation. Plots corresponding to Equations (1), (2), and (3) were attempted. Fig. 10 utilizes the Sieder-Tate parameters, Fig. 11 uses film properties, while Fig. 12 is based upon bulk conditions. Heat balances are given in Table 1 to show the relative accuracy of each run. In three runs shown with check marks, the heat balances did not agree within 10 per cent and the flow rates used in the Reynolds numbers were based on the electrical input rather than the orifice reading.

Figs. 10 to 12 show that Sieder-Tate and Dittus-Boelter types of equation bring the runs closest together, and are to be preferred to a Colburn kind of equation. Relations identical to Equations (1) and (2), but with reduced coefficients probably could be used to correlate satisfactorily all the runs of test section No. 4. However, upon closer examination it is noted that each run satisfies a different equation, and in particular the exponent of the Reynolds number varies considerably. The exponents are all greater than 0.8 reaching the highest values when properties are evaluated at film conditions. Intermediate exponents are obtained for the Sieder-Tate parameters, and lowest values result when all properties are taken at bulk conditions. For all three types of correlation, the exponent on the Reynolds number decreases with heat flux. For instance, from Fig. 10, runs 18, 19, and 20 at about 1,000,000 Btu/hr sq ft, have an exponent of 1.1, while runs 8, 10, 12, and 14 at 270,000 Btu/hr sq ft have an exponent of 2.2. As previously noted, the water-velocity distribution is expected to vary over the entire test section due to the constant change in water temperatures. It is anticipated that these circumstances, not previously treated analytically, could account for the variation and increased values of the exponents.

Entrance Effects. The thermal-entrance effects are illustrated in Fig. 13, which shows runs 11, 14, and 19 of test section No. 4.

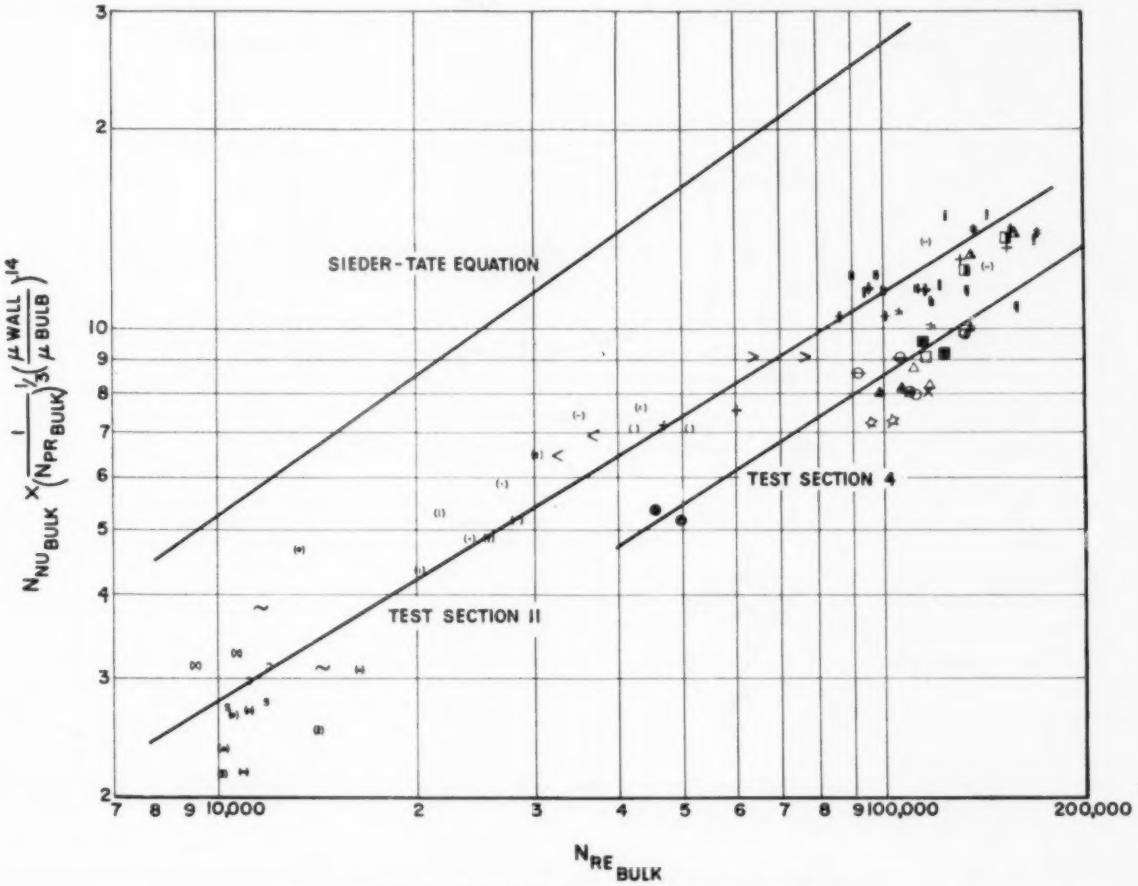

Fig. 7 Heat-transfer coefficients for edges of thin rectangular cross section

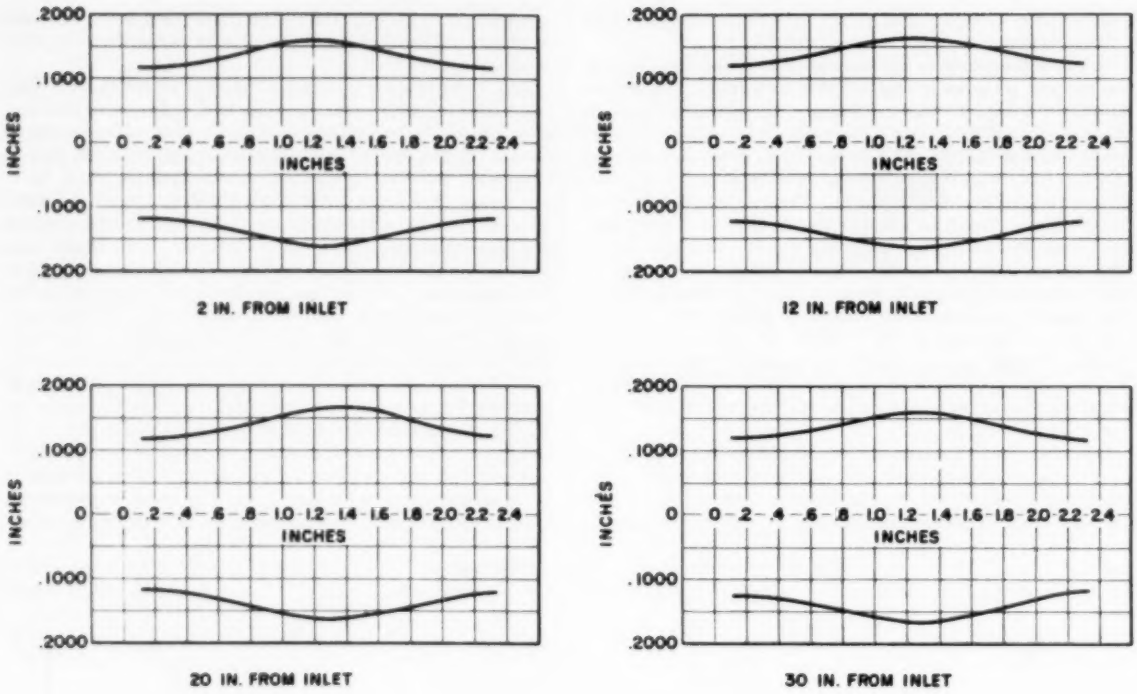

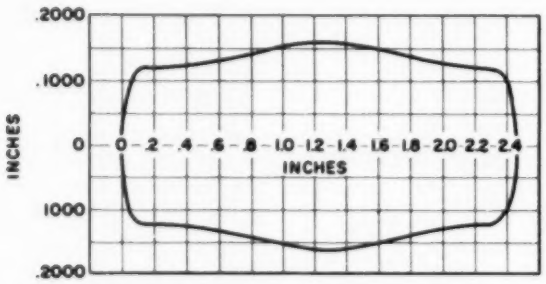

AVERAGE CROSS SECTION

Fig. 8 Dimensions of distorted rectangular test section No. 5

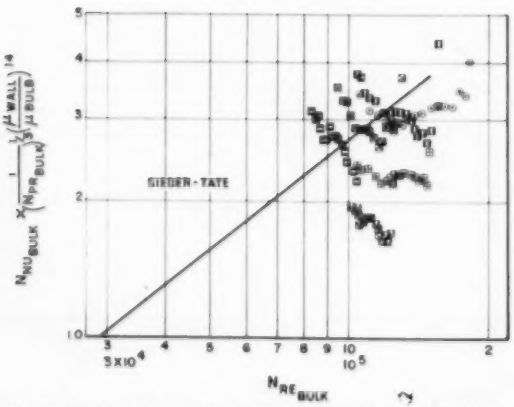

Fig. 9 Heat-transfer coefficients for deformed test section No. 5

The entry length for these three runs is about 10 to 12 in. The corresponding entry length-to-diameter ratio is 55 to 65 and is considerably larger than the value of 15 reported by Hartnett for pipe flow [17] at this Reynolds number. It is important to note that Hartnett's data apply to a fully established velocity distribution, while in the present test section only 1 in. of calming hydraulic section was provided. Deissler's analysis for turbulent flow, however, indicates that even with simultaneous initiation of the hydraulic and thermal boundary layers, the ratio of thermal-entry length to diameter should not exceed 15. It is expected that Deissler's results for pipe flow cannot be applied to rectangular cross sections. For instance, in the case of triangular ducts, Eckert and Irvine [20] found from pressure-gradient measurements that the flow did not develop completely at a distance of 70 diameters from the inlet.

Even though the obtained entry lengths are considerably larger than those of reference [17], the effects of Reynolds number upon entry length appear preserved. Hartnett [17] obtained only a re-

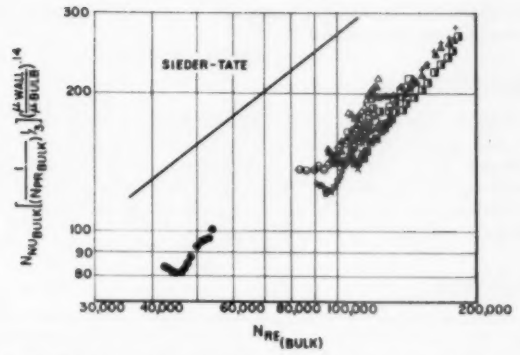

Fig. 10 Correlation of heat-transfer data for rectangular test section No. 4 in terms of Sieder-Tate parameter

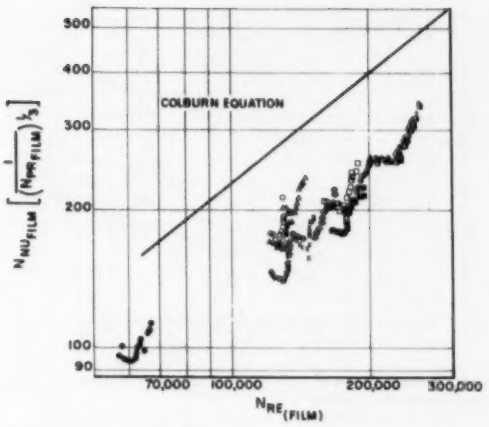

Fig. 11 Correlation of heat-transfer data for rectangular test section No. 4 in terms of film properties

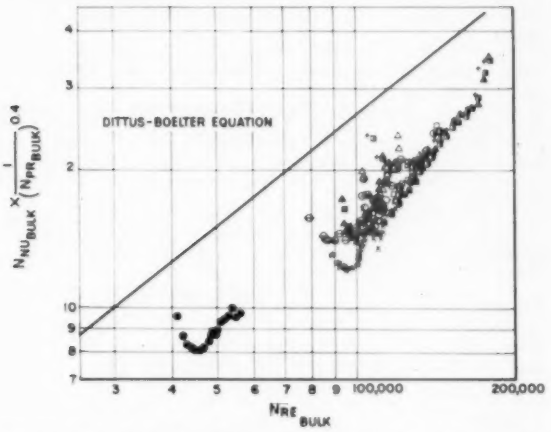

Fig. 12 Correlation of heat-transfer data for rectangular test section No. 4 in terms of bulk properties

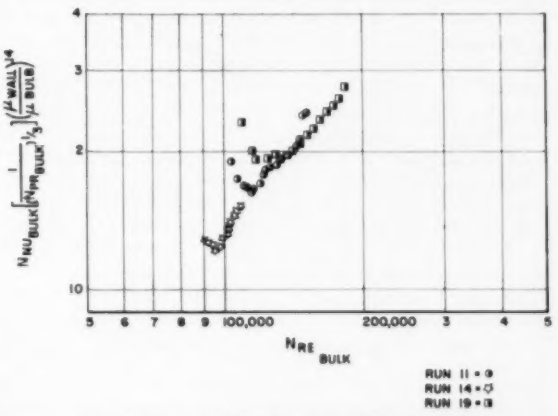

Fig. 13 Entrance effects for rectangular test section

duction of 30 per cent in entry length when decreasing his Reynolds number from 100,000 to 10,000. The present data shown in Figs. 13 and 6 indicate that the entry length varies but slightly with Reynolds number, decreasing slowly with Reynolds number. Values of 40 to 60 diameters are recommended in design for Reynolds number between 10,000 and 100,000.

Flow Direction. Four test runs were carried out with upward flow of water. As shown in Fig. 6, reversal of flow direction did not affect the heat-transfer coefficients. This can be expected since at the high Reynolds numbers of the tests the natural-convection effects are negligible.

Discussion of Results—Burnout Heat Transfer

Insufficient data on peak heat fluxes were obtained to warrant an attempt at dimensionless correlations. Instead, data were plotted using groupings developed in references [11] and [19]. Fig. 14 shows a plot of the experimental results as compared to the equation proposed by McAdams, et al. [11]. Fig. 15 gives a similar comparison between the present data and Gunther's [19]. Both figures reveal that the obtained burnout fluxes are approximately one third those previously reported. However, as it was already pointed out, the data given in Table 2 give the heat-transfer flux needed to produce burnout at the corner of the test section. Since the heat-transfer coefficient at the shorter face is considerably lower than on the larger face of the section, lower burnout fluxes may be expected. In other words, without heat generation in the corners, much higher heat fluxes would be attained before steam blanketing occurs.

Examination of Fig. 14 shows that the use of an equation of the form proposed by McAdams gives an over-all correlation of the data within plus or minus 25 per cent. The recommended equation is

$$\left(\frac{Q}{A}\right)_{BO} = 0.29[400{,}000 \text{ plus } 4800(T_{sat} - T_b)]V^{1/3} \quad (5)$$

Application of Equation (5) to a typical test reactor will now be considered. At the hottest point in the reactor the maximum heat flux is assumed to be 1,150,000 Btu/hr sq ft, corresponding to a heat generation in the fuel of 1.38×10^3 Btu/hr cu ft. If it is assumed that 7 per cent of this heat is generated in the water and side plates immediately adjacent to the fuel plates, it is found that the heat generation in the side plates is 2.44×10^2 Btu/hr cu ft. If heat from the side plate is transferred in its entirety to the water flowing along the fuel plates, the maximum heat flux at the corner of the rectangular flow channel is then found to be 560,000 Btu/hr sq ft. Fig. 14 gives a corresponding burnout flux of 1,400,000 Btu/hr sq ft based upon water velocity of 35 fps and subcooling of 200 F. This means that the reactor power must increase to at least 240 per cent before any possibility of steam blanketing needs to be considered. Similarly, it is found that flow

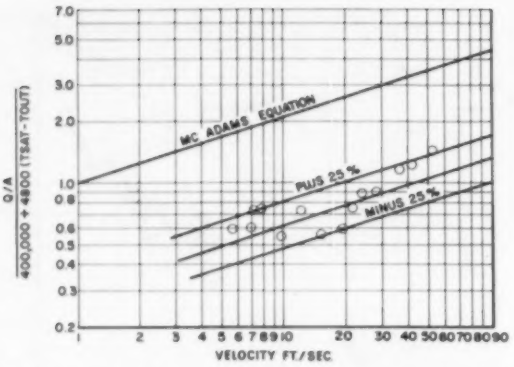

Fig. 14 Burnout fluxes at various pressures and degrees of subcooling in rectangular test section

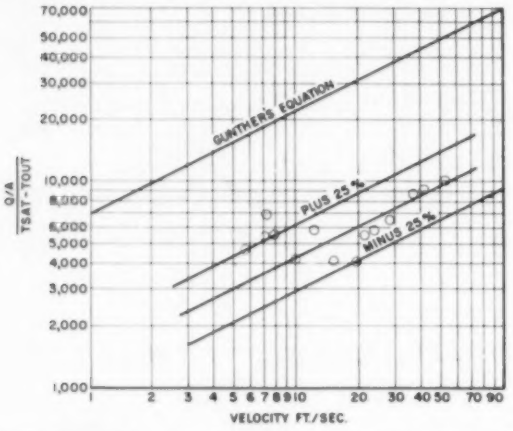

Fig. 15 Burnout fluxes at various pressures and degrees of subcooling in rectangular test section

reduction to 22 per cent of the original value decreases subcooling enough to produce burnout at the normal corner flux of 560,000 Btu/hr sq ft.

Conclusions

1 Reduced heat-transfer coefficients were obtained for turbulent water flow in thin rectangular channels measuring about 0.1 × 2.5 in. The heat-transfer rates are 30 to 45 per cent below those predicted from the Sieder-Tate equation and 15 to 30 per cent below most of the reported values for circular pipe flow.

2 The use of bulk properties or Sieder-Tate parameters gives best correlation of the data from several runs. However, equations with constant exponent on the Reynolds number are inadequate. Test runs, when examined one at a time, have exponents above 0.8, the value of the exponent increasing as the heat rate is reduced at constant water velocity.

3 Heat-transfer coefficients decreased at the short side of the rectangular section. Values 15 to 30 per cent below those on the 2.50-in. face were measured.

4 Thermal entry lengths-to-hydraulic diameter ratios vary from 40 to 60 for Reynolds number between 10,000 and 100,000.

5 Burnout heat fluxes were measured with heat generation around the entire periphery of the rectangular channels. Burnout occurs at the corners and the values there are correlated by a McAdams type equation. Values one third of those obtained for circular pipes were measured.

Acknowledgments

The authors wish to acknowledge the help of several members of the Atomic Power Equipment Department and their assistance during the design, construction, and operation of the test loop. A. J. Borgese, J. Boyle, R. D. Brooks, W. J. Clabaugh, J. Dickson, H. E. Grantz, K. L. Hanson, W. A. Pitt, and G. F. Rieger contributed to the over-all project.

References

1 W. H. McAdams, "Heat Transmission," third edition, McGraw-Hill Book Company, Inc., New York, N. Y., 1954, pp. 202–251.

2 F. W. Dittus and L. M. K. Boelter, "Heat Transfer in Automobile Radiators of the Tubular Type," University of California Publications in Engineering, vol. 2, 1930, pp. 443–461.

3 A. P. Colburn, E. M. Schoenborn, and C. S. Sutton, "Effect of Local Boiling and Air Entrainment on Temperatures of Liquid-Cooled Cylinders," U. S. NACA Report UD-NI, 1945; TN 1498, March, 1948.

4 E. N. Sieder and G. E. Tate, "Heat Transfer and Pressure Drop of Liquid in Tubes," *Industrial and Engineering Chemistry*, vol. 28, 1936, pp. 1429–1435.

5 W. H. McAdams, "Heat Transmission," second edition, McGraw-Hill Book Company, Inc., New York, N. Y., 1942, p. 168.

6 R. E. Drexel and W. H. McAdams, "Heat-Transfer Coefficients for Air Flowing in Round Tubes, in Rectangular Ducts, and Around Finned Cylinders," U. S. NACA Wartime Report 108, February, 1945.

7 L. G. Desmon and E. W. Sams, "Heat-Transfer Data for Air-Flowing in Smooth Platinum Tube With Long-Approach Entrance at High Surface and Inlet-Air Temperatures," U. S. NACA Research Memorandum E 50 H 23, November, 1950.

8 H. Buchberg, F. Romie, R. Lipkis, and M. Greenfield, "Heat Transfer, Pressure Drop, and Burnout Studies With and Without Surface Boiling for Deaerated and Gassed Water at Elevated Pressures in a Forced Flow System," Heat Transfer and Fluid Mechanics Institute, Stanford University Press, 1951, pp. 177–191.

9 W. M. Rohsenow and J. A. Clark, "Heat Transfer and Pressure Drop Data for High Heat Flux Densities to Water at High Sub-Critical Pressures," Heat Transfer and Fluid Mechanics Institute, Stanford University Press, 1951, pp. 193–207.

10 F. Kreith and M. Summerfield, "Heat Transfer to Water at High Flux Densities With and Without Surface Boiling," TRANS. ASME, vol. 71, 1949, pp. 805–815.

11 W. H. McAdams, W. E. Kennel, C. S. Minden, R. Carl, P. M. Picornell, and J. E. Dew, "Heat Transfer at High Rates to Water With Surface Boiling," *Industrial and Engineering Chemistry*, vol. 41, 1949, pp. 1945–1953.

12 R. P. Stein, J. W. Hoopes, Jr., M. Markels, Jr., W. A. Selke, A. J. Bendler, and C. F. Bonilla, "Pressure Drop and Heat Transfer to Nonboiling and Boiler Water in Turbulent Flow in an Internally Heated Annulus," Nuclear Engineering, Part I, AIChE, Chemical Engineering Progress Symposium, series 11, 1954.

13 R. P. Stein, personal communication, 1956.

14 A. Bailey and W. F. Cope, "Heat Transmission Through Circular, Square, and Rectangular Pipes," Aeronautical Research Committee, Great Britain, Technical Reports, 1933–1934, vol. 1, pp. 199–209 (R. and M. No. 1560).

15 W. M. Kays, "Basic Heat Transfer and Flow Friction Design Data for Gas Flow in Circular and Rectangular Cylindrical Tube Heat Exchangers," Technical Report 14, prepared for Office of Naval Research, NR-035-104, Stanford University, 1951.

16 L. Washington and W. M. Marks, "Heat Transfer and Pressure Drop in Rectangular Air Passages," *Industrial and Engineering Chemistry*, vol. 29, 1937, pp. 337–345.

17 J. P. Hartnett, "Experimental Determination of the Thermal-Entrance Length for the Flow of Water and of Oil in Circular Pipes," TRANS. ASME, vol. 77, 1955, pp. 1211–1220.

18 R. G. Deissler, "Turbulent Heat Transfer and Friction in the Entrance Regions of Smooth Passages," TRANS. ASME, vol. 77, 1955, pp. 1221–1233.

19 F. C. Gunther, "Photographic Study of Surface-Boiling Heat Transfer to Water With Forced Convection," TRANS. ASME, vol. 73, 1951, pp. 115–123.

20 E. R. G. Eckert and T. F. Irvine, Jr., "Flow in Corners of Passages With Noncircular Cross Sections," TRANS. ASME, vol. 78, 1956, pp. 709–718.

DISCUSSION

S. J. Green[4] and B. W. LeTourneau[5]

The authors are to be commended for undertaking a difficult experimental program in a relatively unexplored area. However, in view of their somewhat drastic conclusions concerning the relative inefficiency of rectangular channels as compared with circular tubes from the heat-transfer standpoint, a rather critical examination of the data would appear to be in order.

The authors' conclusion that the heat-transfer coefficients for rectangular-channel geometry are substantially lower (15 to 30 per cent) than those for circular tubes is in disagreement with all applicable data known to the writers. In particular, if only those data of Washington and Marks [16] with $N_{Re} > 10{,}000$ are considered, their values satisfy the Dittus-Boelter type of equation [authors' equation (1)] using an average coefficient of 0.0239. Also, it might be noted that additional rectangular-channel heat-transfer data, presented at the same meeting as the paper under discussion [21][6] agreed well with the Colburn equation [authors' equation (2)].

Also, Lowdermilk, Weiland, and Livingood [22] have published heat-transfer and friction-factor data for flow of air through square, rectangular, and triangular ducts at Reynolds numbers from 1000 to 330,000 and at temperatures from 80 to 1320 F. For rectangular channels, their data were correlated by an equation which was the same equation as that used for correlating their round-tube data.

It might have been desirable if the authors had conducted a few heat-transfer runs with round tubes to show agreement with published data. This would have helped to confirm the experimental validity of their data on rectangular channels.

The authors estimate that their accumulated error in inside surface temperature T_w could be as much as 6 per cent, but do not indicate the error in heat-transfer coefficient which would result from such an error in T_w. It is worth while to estimate this error for run 11, which is described in Fig. 5 and Table 1 of the paper. Near the middle of the channel we can take, approximately, $T_0 = 360$ F, $T_B = 130$ F, and $T_w/T_B = 1.7$. For these conditions, $T_w = 221$ F $\pm$ 6 per cent or 221 $\pm$ 13.2 deg F, and $T_w - T_B = 91 \pm 13.2$ deg F or 91 F $\pm$ 14.5 per cent. Thus in this case a 6 per cent error in wall temperature would result in a 14.5 per cent error in heat-transfer coefficient. If the errors in flux ($\pm$3 per cent) and bulk temperature (not stated) are included, then the possible error in experimental heat-transfer coefficient will be near 20 per cent. It is noted that the 6 per cent error in T_w would be 8 per cent if the 1 1/2 per cent error in current, given elsewhere in the paper, were used rather than 1/2 per cent in the authors' estimate of the wall temperature-drop error.

Further, the possible error in the thermal conductivity of the test section wall is believed to be $\pm$5 per cent rather than the 1 per cent stated in the paper [23]. For run 11 this would correspond to an additional possible error of 0.05(360 − 221) = 7 deg F. This could result in an additional 8 per cent error in the heat-transfer coefficient.

In the case of the calculated heat-transfer coefficients, the largest error is that (6.5 per cent at 100 psi) due to the gasket compression, which is of such a nature as to decrease the calculated coefficients, thus bringing the experimental and calculated values into closer agreement. The combination of these errors is of such a magnitude that, if the error were consistent rather than random, the conclusion of heat-transfer coefficients 15 to 30 per cent lower than those for circular tubes could be entirely due to experimental error rather than to the rectangular channel geometry.

It is noted that although the authors measured both the voltage and current, only the current and published values of resistivity were used to calculate the heat generation. Would the authors like to comment on why this technique was used and what was the agreement between the three possible methods (EI, I^2R, and E^2/R).

The writers would be interested to know the results of any isothermal measurements. Here any difference between the inlet and exit water thermocouples gives a measure either of errors in calibration or of estimated heat loss. Similarly, a comparison between the water and outside-wall thermocouples determines the accuracy of the wall thermocouples. Finally, measurements of the exit-water thermocouples under net steam-generation conditions also would confirm the accuracy of these thermocouples. Were such measurements made?

The authors state that the experimentally determined exponent on Reynolds number, for a given run, is higher than 0.8 and reaches values as high as 2.2 for some runs. This is very difficult to believe. If the velocity profile were to approach the extreme value associated with complete hydraulic roughness, then the Reynolds analogy could predict exponents as high as 1.0, and such values might not be surprising at very high Reynolds numbers. Values as high as 2.2, however, suggest possible errors due to experimental techniques, such an electrical thermocouple pickup. The authors' explanation that the continuously-varying bulk temperature and hence velocity profile can account for such high exponents is difficult to understand, especially since the highest exponents are associated with the small temperature gradients, and the lowest exponents with the larger temperature gradients.

The paper states that the deviation of the data below equation (3) increases with increasing Reynolds number. It would be worth while to compare this trend with trends predicted by the available semitheoretical methods such as those given by Deissler [24] and by Martinelli [25]. It might be noted here that the Martinelli analysis predicts heat-transfer coefficients for rectangular channels which are essentially the same as those for round tubes, particularly for $N_{Pr} > 0.7$.

The authors' method of illustrating entrance effects, Fig. 13, is not clear. It is usual to plot h_{Loc}/h_0 versus L/D, where

h_{Loc} = local heat-transfer coefficient
h_0 = fully established heat-transfer coefficient
L = distance from inlet
D = hydraulic equivalent diameter

Since, in this experiment, the fluid properties vary significantly with length, it might be well to correct h_0 to local fluid properties.

One source of rectangular-channel, thermal-entrance-effect information known to the writers is the data of Weiland and Sams [26]. While in their experiment fully established flow was not reached, the data for both average and local heat-transfer coefficients in short rectangular channels were slightly higher than the values predicted from established round-tube correlations for the same L/D ratio.

With regard to the burnout data, it would be interesting to calculate the circumferential heat-flux distribution in the rectangular channels, assuming uniform volumetric heat generation and using conventional analog or digital techniques for solving two-dimensional heat-conduction problems. Nucleate boiling wall superheat correlations may be used, or the surface temperature may be assumed constant. (To calculate the circumferential heat flux distribution under forced-convection conditions, estimates of the local heat-transfer coefficients relative to the average could be taken from the work of Eckert and Low [27], who indicate

[4] Bettis Plant (operated by the Westinghouse Electric Corporation for the U. S. Atomic Energy Commission under AEC Contract AT-11-1-Gen-14), Pittsburgh, Pa. Mem. ASME.
[5] Bettis Plant, Pittsburgh, Pa. Assoc. Mem. ASME.
[6] Numbers in brackets designate References at end of discussion.

that the local heat-transfer coefficient approaches the average value at a distance of 0.05 to 0.10 of the equivalent diameter from a 90-deg corner.) It would not surprise the writers if conventional burnout heat-flux correlations would fit the present data satisfactorily if the maximum local heat flux were used.

It would seem overly conservative in most cases to apply these data directly to rectangular coolant channels in nuclear reactors. In conventional reactor fuel plates, the fueled region is of slightly less width than the coolant channels. While there is a significant amount of gamma heating in the extreme ends of the fuel plates and in the side plates, this geometry and heating rate are normally such that the heat flux through the narrow edges, and the portions of the wide sides nearest the corners, is much less than that opposite the fueled region.

For this reason, the rectangular channel test sections used for electrically heated burnout tests [28, 29] at the Bettis Plant have been designed with a reduced metal cross section in the corners, such that the heat flux on the narrow edges and on the part of the wide faces nearest the corner was about 20 per cent of that in the main part of the channel. With this type of channel (and at pressures from 2000 to 600 psia) the burnout heat flux was found to be in fact higher than that for a round tube at the same conditions, and the burnouts did not occur preferentially at the corners.

Three minor errors which might be pointed out are that the ordinate scales of Figs. 7, 9, 12, and 13 are incorrect, the left-hand side of equation (4) should read $T_O - T_{wi}$ and the value of Y_T in the calculation of the adjusted D_H should be 0.0094 rather than 0.094.

Table 2 also contains some apparent numerical errors. The ratio of heat-generation to heat-flux values indicates a heat-transfer area of 0.613 sq ft, while the test-section dimensions given indicate a heat-transfer area of only 2(0.118 + 2.045) (18)/(144) = 0.541 sq ft for average heat flux, or an equivalent heat-transfer area (test section volume ÷ thickness) of (0.028) [2(0.118 + 2.045) + 4(0.028)] (18)/(144) (0.028) = 0.555 sq ft for local values of heat flux far from the corners, assuming uniform volumetric heat generation. For runs 15B and 16B, the inlet temperatures necessary for consistency of the data are below freezing. For example, in run 16B the 196 F outlet bulk temperature at 138 psia corresponds to an exit enthalpy of 164 Btu per lb. The mass-flow rate may be calculated as $W = \rho AV$ = [(7.8) (3600) (0.118) (2.045) (60.3)]/144 = 2840 lb per hr, so that the channel enthalpy rise is Q/W = 525,000/2840 = 185 Btu per lb. Thus the inlet enthalpy is calculated to be 164 − 185 = −21 Btu per lb!

The writers conclude by pointing out that it is very difficult to obtain accurate heat-transfer coefficients for water at high Reynolds numbers, where the coefficients are very large. It is necessary to use the most refined experimental techniques, including the use of individually calibrated thermocouples for both surface and water-temperature measurements, extreme precaution to eliminate heat losses, thermocouple electrical pickup, and thermocouple lead-wire conduction effects, minimization of wall-temperature-drop correction by the use of thin, high-thermal conductivity walls, and precautions to insure accurate knowledge of the channel dimensions during test. In the paper, the large cumulative effect of the many experimental errors on the accurate determination of forced convection heat-transfer coefficients may be seen clearly.

References

21 R. T. Lancet, "The Effect of Surface Roughness on the Convection Heat-Transfer Coefficient for Fully-Developed Turbulent Flow in Ducts With Uniform Heat Flux," ASME Paper No. 58—A-122.

22 W. H. Lowdermilk, W. F. Weiland, and J. N. B. Livingood, "Measurement of Heat Transfer and Friction Coefficients for Flow of Air in Noncircular Ducts at High Surface Temperatures," NACA RM E53J07, January 25, 1954.

23 N. L. Dickinson and C. P. Welch, "Heat Transfer to Supercritical Water," TRANS. ASME, vol. 80, 1958, p. 746.

24 R. G. Deissler, "Analysis of Turbulent Heat Transfer, Mass Transfer, and Friction in Smooth Tubes at High Prandtl and Schmidt Numbers," NACA Report 1210, 1955.

25 R. C. Martinelli, "Heat Transfer to Molten Metals," TRANS. ASME, vol. 69, 1947, p. 947.

26 E. W. Sams and W. F. Weiland, "Experimental Heat Transfer and Friction Coefficients for Air Flowing Through Stacks of Parallel Flat Plates," NACA RM E54F11, August, 1954.

27 E. R. G. Eckert and G. M. Low, "Temperature Distribution in Internally Heated Walls of Heat Exchangers Composed of Noncircular Flow Passages," NACA Report 1022, 1951.

28 H. S. Jacket, J. D. Roarty, and J. E. Zerbe, "Investigation of Burnout Heat Flux in Rectangular Channels at 2000 Psia," TRANS. ASME, vol. 80, 1958, p. 391.

29 R. A. DeBortoli, S. J. Green, B. W. LeTourneau, M. Troy, and A. Weiss, "Forced Convection Heat Transfer Burnout Studies for Water in Rectangular Channels and Round Tubes at Pressures Above 500 Psia," WAPD-188, October, 1958. (Available from the Office of Technical Services, Department of Commerce, Washington 25, D. C.)

Authors' Closure

The authors wish to thank Messrs. S. J. Green and B. W. Le Tourneau for their extensive comments. Because many of the questions they raise deal with the "lower" heat-transfer coefficients reported in the paper, it is worth while to restate here that the present work deals with the *simultaneous* effects of (1) a rectangular cross section of high aspect ratio, (2) large variation of bulk properties in the flow direction, (3) large film temperature drops, and (4) undeveloped flow and thermal conditions at the inlet of the test section. Experimental and analytical studies are lacking in the case of a water-cooled channel for the specific test conditions reported herein. It is, therefore, important to avoid using preconceived relations or explaining the reduction in heat-transfer coefficients in terms of any one of the four test variables outlined.

Green and Le Tourneau mention the work of references [16, 21, and 22]. These tests do not exactly correspond to the conditions at hand. For instance, in references [21 and 22] the data are concerned with flow of air in rectangular channels of aspect ratio of only 5 to 1. Further, in reference [22] the flow is fully developed at the entrance of the test section and the surface conditions rough.

The discussers' attempt to explain the low heat-transfer coefficients in terms of experimental errors is not justified for several reasons:

(1) Green and Le Tourneau assumed a 6 per cent error in the wall temperature. The 6 per cent mentioned in the paper is the sum of a 3 per cent error in surface temperature plus a 3 per cent error in heat flux measurements, as stated in the previous paragraph. Instead of the 13.2 deg F error calculated, one has a maximum error of 5.5 deg F in film temperature drop.

(2) Random errors such as reading errors should be neglected since they can lead only to data scatter. For instance, the 1 1/2 per cent error used for the current includes an assumed 1 per cent reading error.

(3) The errors stated for the thermal conductivity are maximum errors according to reference [23] and Dickinson and Welch concluded that the accuracy of their equivalent Equation (4) was ±3 per cent in spite of the quoted accuracy of the thermal conductivity.

(4) The errors were maximized by the authors whenever they contributed to reducing the heat-transfer coefficient. The gasket compression calculation is typical of such instances. Further, errors contributing to an increase in the heat-transfer coefficient such as conduction along thermocouple wires and through the test section insulation should not be added when considering the maxi-

mum errors because they lead to reduced coefficients; in reality they should be subtracted.

(5) The same experimental methods have been applied to circular pipes in another test loop and satisfactory comparison was obtained with the Colburn equation.

The discussers note that the heat generation was calculated from values of current and local resistance. This technique was selected to account for local variation in heat flux along the test section. In every run the total heat generation calculated by this method was checked against the value obtained from voltage and current readings. The agreement was always excellent. It is also worth noting that the temperature instrumentation was checked out at ambient conditions before startup and that agreement was obtained within expected thermocouple calibration error within one degree. Similar checkouts were not performed at higher temperatures and the discussers' suggestion is a worthwhile one to consider in future experimental work.

The variation in exponent of the Reynolds number with heat flux or ratio of surface to bulk temperature could be prematurely attributed to variation in the experimental errors with heat flux. Indeed, at the lower heat flux the film temperature drop is small and more susceptible to error but even at low heat flux the errors are not large enough to explain the high exponent on the Reynolds number. It is worth noting that in reference [30] the exponent on the Reynolds number varies and is greater than 0.8 at the exit end of the test section. In Fig. 5(*a*) of that reference the exponent starts to change at Reynolds number of 50,000 and the effect of heat flux upon exponent is not clear, some runs even showing an increase in exponent at the lower Reynolds range with heat flux. Close examination of the same figure also reveals good agreement with the data shown in Fig. 12. For instance, at a bulk Reynolds number of 150,000 for a 2.1 value of T_w/T_b (about an equivalent 1.3 ratio in °R/°R) the ordinate in Fig. 12 is about 240 in agreement with the value given in reference [30] for a 1.4 temperature ratio (°R/°R). This agreement partially serves to establish the validity of the present tests and data. It also points to property variation as the potential reason for the reduction in the heat transfer coefficients. Unfortunately, the effects of the property variation could not be as firmly established as in reference [30]. The use of film properties did not bring all the data together as in reference [30] and the other variables used in the tests cannot be excluded as potential contributors to the reduction in heat-transfer coefficient. Theoretical solutions such as those given in references [24 and 25] are of no assistance in clarifying the picture. The solutions are based upon simplified models and upon *pipe velocity distribution* so that they can be expected to yield results in agreement with those for round tubes.

The discussers note that the authors report greater deviation of the data from Equation (3) at increasing Reynolds number. The authors' statement refers to Fig. 6 where the effects of all the test variables are compounded. On the other hand, examination of one run at a time in Fig. 12 shows smaller deviation of the data from Equation (3) at higher Reynolds numbers in agreement with the trend noticeable in reference [30]. Also, the entrance effects were not illustrated by means of usual plots because the authors *do not know how to exactly calculate* the fully established heat-transfer coefficient or to accurately account for fluid variation.

With regard to the burnout data it is very hard to see how the local heat flux can be three times as large as the average heat flux. Conduction effects along a 28-mil wall could never produce such extreme peaking. It is also important to note that the proposed data apply to test reactors as noted in the first sentence of the introduction and not to power or propulsion reactors referred to by the discussers.

The authors cannot disagree with the discussers' comment that large heat-transfer coefficients are difficult to measure. They feel, however, that they have achieved data repeatability (see Fig. 12) and that the scatter is not necessarily tied to experimental errors and techniques but rather to the large number of variables considered. They would recommend separation of the variables and the use of another method besides electrical heating to study high heat-transfer coefficients.

The authors thank the discussers for pointing out the errors in Figs. 7, 9, 12, and 13, Equation (4), and the value of Y_T. The last two typographical errors were corrected in this last proof reading.

However, Table 2 stands correct as is. Due to a typographical error the burnout test section dimensions appeared as 0.118 in. × 2.045 in. The dimensions are 0.118 × 2.405 in. as now shown in the text (or as one could have deduced from Table 1, Fig. 8, and even Table 2). With these dimensions, the heat fluxes are correct in Table 2. In runs 15B and 16B, the use of the dimension 2.045 in. and the lack of an allowance for an error in the heat balance at low velocities are responsible for the below-freezing temperatures computed by the discussers. The authors feel that they have considered enough variables without the added complication of icy water.

Additional Reference

30 Leroy V. Humble, Warren H. Lowdermilk, Leland G. Desmon, "Measurements of Average Heat-Transfer and Friction Coefficients for Subsonic Flow of Air in Smooth Tubes at High Surface and Fluid Temperatures," NACA Report 1020, 1051.

VICTOR PASCHKIS

Director, Heat and Mass Flow Analyzer Laboratory, Columbia University, New York, N. Y. Mem. ASME

Combined Geometric and Network Analog Computer for Transient Heat Flow

A method to analyze three-dimensional transient heat flow is described, which comprises a continuous resistance medium but discrete capacitances. After describing the principles of the technique, the several components and their criteria are discussed, and the accuracy is illustrated by comparing the results of several simple problems with analytically determined values.

1 Background and Purpose

The term "analog computer" as used in this paper describes a device which permits the solution of a problem in one field of physics by interpretation of measurements carried out in an "analogous" other field. For example, a problem in heat conduction is solved by appropriate interpretation of electrical measurements on an analogous system. The basis for such computers is the identity of mathematical expresions describing the problem and its "analog"; if the same equation describes several fields (as the Fourier equation, which describes heat conduction, diffusion, and electric currents in noninductive cables), a multiple analogy exists, and the choice in which field to make measurements is strongly influenced by the convenience with which measurements can be made.

The relative ease and accuracy of electrical measurements makes the electrical analog computer a versatile and powerful tool.[1] One can distinguish between two types of analogs: The geometric and the network computer. While the paper deals with analogs for heat flow, the remarks have (in view of multiple analogies) broader applicability.

In geometric analogs the body in which heat flow occurs (henceforth called "the object") is represented by a "model" which is geometrically similar to the object and related to the latter by a (geometric) scale factor. Langmuir [1][2] suggested the electrolytic tank, Bruckmeyer [2] used metallized paper; Beuken [3] described a method to represent finite boundary resistance values in Langmuir's tank, while Kayan [4] introduced a method to include such resistances when using metallized paper.

In network analogs the continuous system is broken down into discrete sections, with properties lumped at center or surface of each section. Such analogs have found wide and deversified applications. But here only the use of resistance networks with capacitances connected to the nodes and capable of handling transient problems are of interest. Beuken [5] first introduced this technique which was later extended and used by the author [6].

The geometric analog is limited to the solution of steady-state problems; whereas the main limitation of the lumped network lies in its complexity if three-dimensional (or even complex two dimensional) shapes are to be handled.

It is tempting to combine the two techniques, and this has been suggested by the author [7]. A brief report of an attempt to carry out such combined study has been given by A. V. Clark [8]. This paper presents results of work by this laboratory on such a "combined method," carried out over many years and still continuing.

2 Principle and Problems

The Principle. Since no resistance medium is known which would show appropriate electric capacity against a reference, a method was sought in which the resistance medium is continuous, but capacitances are introduced in lumped form. Also, if there is a boundary conductance between the surface of the body and the ambient, such conductance can best be represented by discrete external resistors. This method, though on the surface very simple, presents a number of difficulties both conceptual and experimental.

The two conceptual difficulties are both concerned with the transition from the continuous to the finite system: From capacitance to body resistance and from the latter to boundary resistance. The problem of transition from lumped capacitance to continuous resistance is explained, using a simple case (Fig. 1) for the solution of which no computer of any kind is required. The problem is that of heating a slab, initially at zero temperature, by imposing on one surface a step increase of temperature; the other surface faces the reference ambient across a boundary conductance; the sides of the slab are perfectly insulated, so that heat flow is one-directional (perpendicular to the surface). In the mixed systems (continuous resistance-lumped capacitance) the problem can be handled by the arrangement shown schematically in Fig. 1.

A tank T is filled with a resistance medium R in which connectors C are immersed, each connector leading to a capacitance C_a (C_{a1} to C_{a4}). The power supply is connected to electrodes E+ and E−. Initially the switch S is open and the system is not charged. At time zero, S is closed and the condensers start to charge. But while the differential equation requires that at time

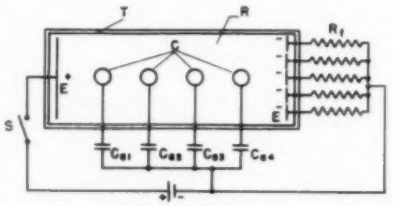

Fig. 1 Lumped capacitance—continuous resistance system

[1] It should be remembered here that the term analog is frequently used to describe differential analyzers, particularly electric differential analyzers. In this paper the term analog computer will be used only as defined above and will always refer to electric analogs.

[2] Numbers in brackets designate References at end of paper.

Contributed by the Heat Transfer Division and presented at the Annual Meeting, New York, N. Y., November 30–December 5, 1958, of The American Society of Mechanical Engineers.

Note: Statements and opinions advanced in papers are to be understood as individual expressions of their authors and not those of the Society. Manuscript received at ASME Headquarters, June 13, 1958. Paper No. 58—A-69.

0^+ capacitances C_{s5}–C_{s4} receive only an infinitesimally small current, in the system, Fig. 1, all capacitances receive finite values of current as soon as S is closed.

The second difficulty related to the finite boundary resistance occurs both in steady and transient state, and is explained with regard to the "cold surface" of the model, Fig. 1.

The methods [3, 4] are all similar in that the boundary resistance which by definition is uniform for the surface is broken down into a finite number of discrete resistances. The voltage distribution in the liquid represents the temperature distribution in the slab. In view of the one dimensional heat flow the voltage at any distance x from the (arbitrarily chosen) origin 0 should be the same for all positions y.

But the electrodes e_1, e_2, . . . e_n connecting the individual boundary resistance R_f (film) to the continuous resistance R, which represents the body, result in a distortion of the voltage distribution particularly near e_1 . . . e_n. In corners and in case of other two-dimensional problems this may cause serious errors.

The Problems. Solution of a problem by means of the combined method, i.e., with distributed resistance and lumped capacitance, requires answers to a number of questions as follows:

a. Resistance Material. The three main requirements for a suitable resistance material are: That it must easily accept a shape, that it must be usable with d-c, and that the resistivity must be in an acceptable range.

The last requirement rules out all commonly used metals. Mixtures of mercury and glass beads proved unmanageable. Finally, a solution of tetra-butyl-ammonium picrate (hereafter abbreviated tbap) in Dowtherm was tried, based on suggestions of C. A. Kraus and R. M. Fuoss [9], and found acceptable.

The electric resistivity was measured in a glass cell with palladium electrodes $1^{13}/_{32}$ in. apart; the electrodes were $1^{13}/_{32}$ in. wide and immersed $1^1/_4$ in. deep using 200 v d-c.

The resistivity changes also characteristically with temperature and therefore the solution must be used at constant temperature. Fig. 2 shows the resistivity versus temperature for several values of concentration. If plotted on semilog paper (concentration on logarithmic abscissa) the resistivity decreases at a temperature of 22 C from 140 megohm-in. (at 27 mg/1000 cc) linearly to 20 megohm-in. at 270 mg/100 cc; then the curve flattens out to reach a value of 3.9 megohm-in. at 618.4 mg/100 cc. At such high concentration solution of the liquid takes a long time and, although saturation may be reached only somewhat higher, it is not practical to use concentrations in excess of about 600–620 mg/100 cc. Obviously, being a liquid the mixture satisfies the requirement of easy forming, and the resistivity range is appropriate. The third requirement, usability with direct current, requires explanation.

The solution is slightly electrolytic; under influence of d-c a slow dissociation takes place. This makes itself felt in form of a deviation from Ohm's law: A plot of current measurements made in the afore-mentioned cell at different voltages does not go through zero; instead, a finite voltage is needed to achieve any current flow. This limiting voltage is sometimes called the "back-emf" and depends to a considerable extent on the electrode material.

A number of electrode materials have been investigated, and the following values have been found for the back-emf, when used in tbap:

nickel	1.471 v
platinum	1.131 v
palladium	1.027 v
platinized palladium	0.546 v
palladinized palladium	0.509 v
platinized platinum	0.444 v

The difference between the performance of the last two metals is not big enough to warrant the much higher cost of the platinized platinum; palladinized palladium is suitable.

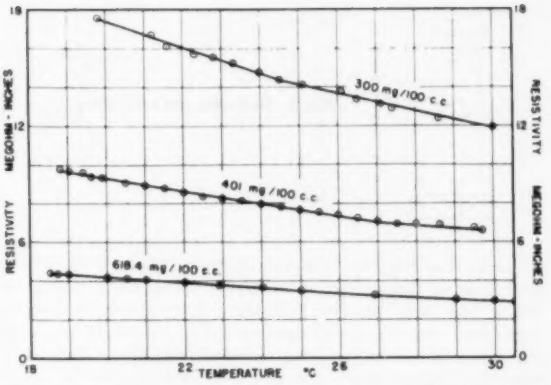

Fig. 2 Resistivity-temperature relationship for a solution of tbap in Dowtherm

b. The Electrodes. The choice of the electrode material cannot be separated from that of the resistance material. Thin sheets and strips can be used for the surface electrodes, which can be bent so as to fit any desired surface contour. The "electrodes" connecting to the capacitances present a special problem, and are therefore given a special name (capacitance connectors) and are dealt with later. Suffice it here to say that for the sake of economy in the trial runs nickel electrodes and steel capacitance connectors were used; in spite of this conscious choice of less than the best materials results were good (see Section 4).

c. The Tank. Any material that does not react with the resistance liquid and which has sufficiently high electric resistivity is acceptable. Because of the ease of working to any shape, wood was used and made impermeable on the inside by an appropriate coating, Bakelite BL3128 of the Bakelite Corp., and Weldwood Waterproof Resorcinal glue made by the U. S. Plywood Corp., were found acceptable; since the former requires baking at elevated temperatures the experiments described in Section 4 were carried out in tanks coated on the inside with several layers of Weldwood.

Capacitance Connectors. In steady-state (electrolytic) tanks, wires can be used as probes to determine the potential distribution because no current flows through the probe. But in transient experiments current flows through the capacitance connectors, and thus the resistance of the connector becomes significant; the resistance is that between the liquid and the connector. If a wire is used as connector, the resistance from the latter to the bath approaches infinity as the diameter approaches zero. To understand this, consider a hollow cylinder of liquid resistance material; the outside diameter can be at any reasonable distance from the axis of the cylinder, while the inner surface is given by the diameter of the wire. The resistance of this liquid cylinder is proportional to the logarithm of the diameter ratio which approaches infinity as the wire diameter approaches zero. Conversely an increase of the diameter of the capacitance connectors shorts out increasingly large areas of the resistance medium. The diameter of a cylinder (in case of two-dimensional work) or of a sphere (for three-dimensional work) has been selected to date on an empirical basis only; the experiments are reported under Section 4.

Boundary Electrodes and Boundary Resistance. Accepting the concept of discrete resistors to be connected by individual electrodes, the question arises as to how many electrodes should be used; obviously, theoretically, the greater the number, the better the results. But as the number increases, the required value of

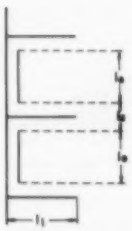

Fig. 3 Electrodes and separation

the individual discrete resistance increases, thus putting a practical limit on the number of electrodes. The question thus becomes, how large an error is introduced by a finite number of electrodes? Fig. 3 is an enlarged view of a straight surface, a few electrodes, and the surrounding resistance medium. Contrary to theoretical requirements each electrode imposes over its length the condition of an isothermal face. Thus even for a given number of electrodes, the size of l_e, of the electrode, and thus the uncovered space l_d between them remains an open question. If the distance between two electrodes, l_d, becomes small, the resistance of the liquid connecting the two electrodes also becomes very small; thus through the liquid a near-short is created. Electrodes can be placed nearer if between the electrodes an isolating fin is placed which protrudes into the liquid. Then the size, l_i, of the insulator is open.

In connection with this electrode-boundary resistance problem, the optimum solution can be sought from the viewpoint of a correct value for the rate of heat flow (represented by the current) or the temperature distribution either at the surface itself or in the body near the surface (represented by voltages). These problems are mentioned here only for the sake of completeness. Work on these aspects is in progress and not part of this paper.

3 Test Body

In order to examine the usefulness of the several techniques selected, it was decided to solve several problems of two and three-dimensional nature, for which analytical solutions were available or were developed. These problems are listed hereafter.

a) A square bar of sufficient length to be treated as two-dimensional problem is initially at zero temperature. At time zero the four surfaces are subjected to a step increase in temperature. What is the temperature rise in the body?
b) The same bar is heated from two adjacent sides, while the two other sides were kept at zero temperature.
c) A cube, initially at zero temperature, is heated by subjecting the six surfaces to a step increase of temperature.
d) The same cube is heated by providing for a step increase on four faces, placed symmetrically, while the other two faces are kept at zero temperature.

The two-dimensional problems were analyzed in a wooden tank with an inside opening of 8 × 8 in., with 100 capacitance connectors spaced at 0.8-in. center distance. Steel cylinders of $^1/_8$, $^1/_4$, and $^3/_8$-in. diameter were used as condenser connectors.

The three-dimensional tests were carried out in a cubic tank of 8-in. inside length. Steel spheres of $^3/_4$-in. diameter were provided with $^3/_{16}$-in. holes along one diameter; the spheres were strung on glass rods and held at proper distance from each other by glass tubes slipped over the rods. The rods in turn were held in place by a board provided with regularly drilled holes at the bottom of the tank and by a spacer plate at the top. Teflon insulated wire was soldered to each sphere, and all wires of one vertical row of spheres were brought to a plug-in connector. A total of 125 spheres provided 5 nodes in each direction. Because of symmetry the cubic tank was used to represent $^1/_8$ of the actual cube. Thus, for problem *c*, three faces joining in one corner were equipped with electrodes and subjected to the step increase in voltage, while the other three faces were insulated. In problem *d*, investigating again one eighth of the cube, two "heating faces" are now adjacent to the cold face; thus at some edges discontinuities occur. An edge separating a heated from a cold face belongs to both and should at the same time be connected to full voltage and to ground. To overcome this difficulty in the tank, such electrodes were cut back at the edges, so that the "zero electrode" and the "hot electrodes" do not touch.

4 Results

Two-Dimensional Tests. In order to separate the errors incurred by lumping and by the bypassing of the capacitance connectors by the liquid resistance medium computing experiments were compared with the analytical solutions, and in part with the solution obtained on a lumped resistance–capacitance network. Fig. 4 indicates the position of the points in question; Figs. 5 and 6 show the temperature (or voltage) rise as function of N_{Fo} for problem *a*. Results with $^3/_8$-in. capacitance connectors check very closely with analytical results, while curves based on $^1/_4$ and $^1/_8$-in. connectors are much less accurate. Also for point E the

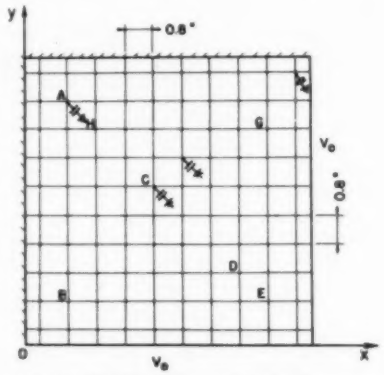

Fig. 4 Position of measured points (square bar)

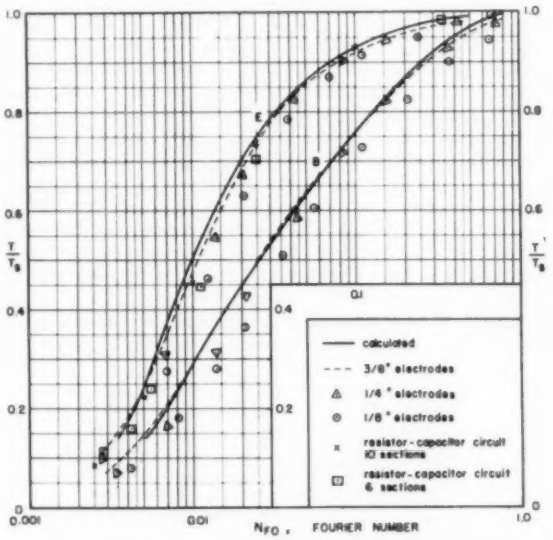

Fig. 5 Temperature versus time; points B and E (problem *a*)

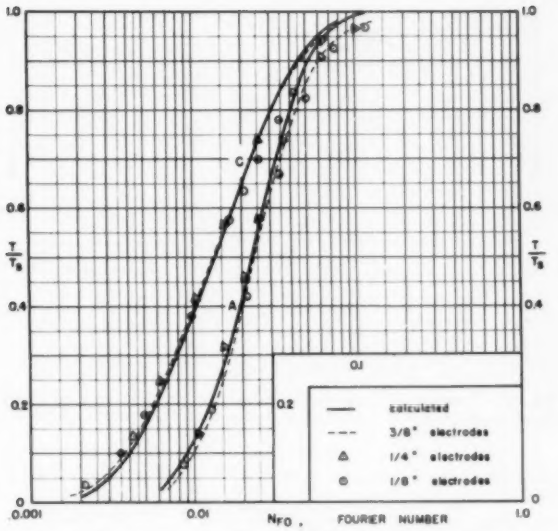

Fig. 6 Temperature versus time; points A and C (problem *a*)

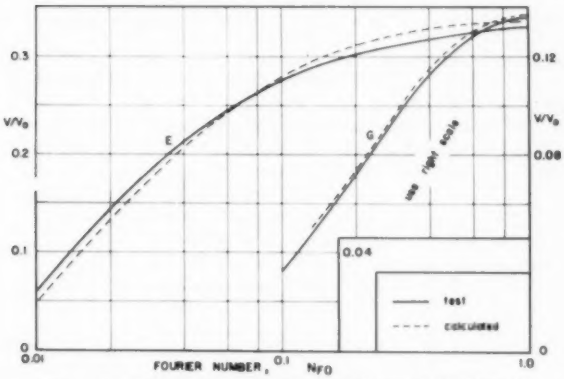

Fig. 7 Temperature versus time; points E and G (problem *b*)

check between the lumped network and the analytical values are very good, particularly for 10 nodes. Fig. 7 shows the results for problem *b*, points E and G. Errors are appreciably smaller than in problem *a;* but results appeared encouraging enough as to warrant proceeding to three-dimensional problems.

Three-Dimensional Tests

a. Cube Heated From All Sides—Problem c. The potential rise of points on the space diagonal was computed analytically and compared with values found from the model tests. The points on the space diagonal are numbered 5-5-5 (next to the hot corner) to 1-1-1 (next to the center of the cube). Results are shown in terms of fractions of the steady-state temperature of each point. Results at point 5-5-5 are poor, improving rapidly as one progresses toward the inside (see Fig. 8). For comparison values of a 5 node R-C network are included. The error in case of the tank method far exceeds that of the lumped network. In Fig. 9 two further pairs of curves compare the analytical with tank values, the latter taken by means of a probe at a point A very near the "hot corner," and at a point B very near the center of the cube; neither point had a capacitance connector. The errors at point B are very small, in case of point A large. But it can be seen that the major influence is in the position rather than in the presence or absence of a capacitance connector.

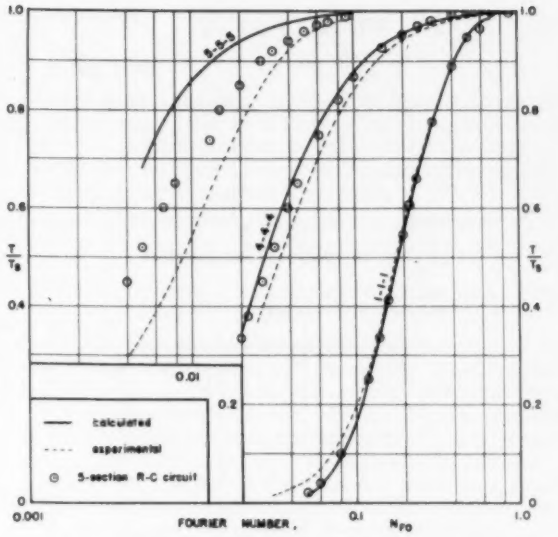

Fig. 8 Temperature versus time; node 5-5-5 (problem *c*)

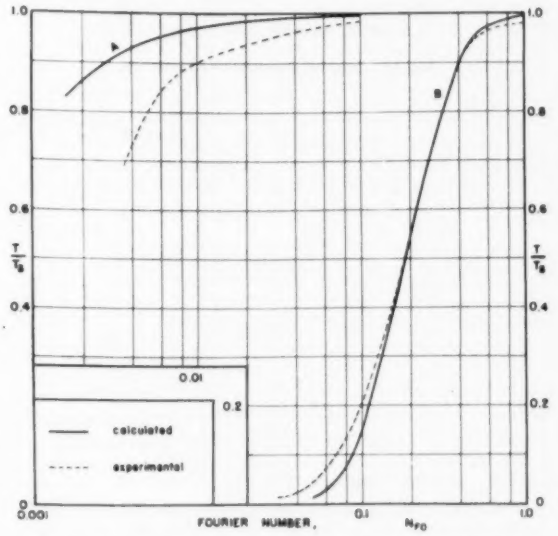

Fig. 9 Temperature versus time; points A and B (problem *d*)

Obviously, the proximity of the electrodes is detrimental to accuracy. If the potential at a given point, e.g., at node 5-5-5, should be determined, one should see to it that this point is not at the first node. But an increase of nodes is expensive; e.g., if point 5-5-5 should be the third instead of the first node from the corner, the total number of nodes (provided uniform lumping is used) would be $15^3 = 1335$! One way to provide for uneven lumping is to provide two tanks made to uneven scale: a smaller tank representing the hot corner, including the node 5-5-5, and the other representing the balance of the cube.

The relationship of the two tanks is shown in Fig. 10; the insert tank had a side of five inches and was equipped with nine electrode connectors. In the large tank a solid cube of 1.6-in. side length was put in the hot corner to displace the liquid resistor. The corresponding faces a, b, e, f; a, b, c, d; and a, d, h, e, on both

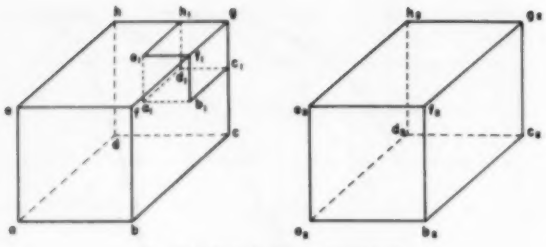

Fig. 10 Main tank and insert tank

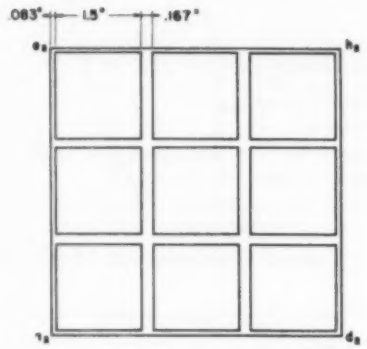

Fig. 11 Transfer electrodes on insert tank

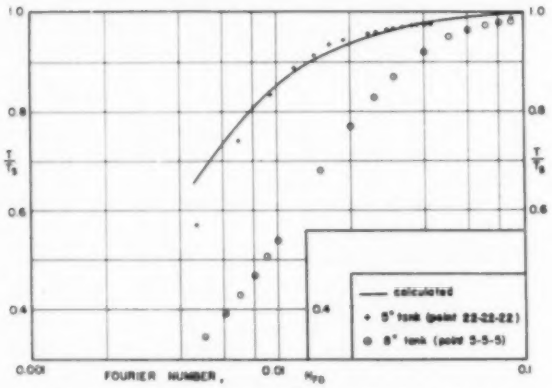

Fig. 12 Comparison of results for node 5-5-5 (problem c)

tanks were covered with metal squares as shown in Fig. 11 for the insert tank. Corresponding plates were connected with wires.

In the insert tank nodes along the diagonal were characterized by double numbers 11-11-11, 22-22-22, and 33-33-33, the latter being in the new hot corner, and the first near the point a, in Fig. 10. Point 22-22-22 corresponds exactly to point 5-5-5 in the 8-in. tanks. Fig. 12 compares the results for this point found in the 8-in. tank (repeated from Fig. 8) with those found in the insert tank and with analytically determined values. The insert tank gives satisfactory results.

Fig. 13 shows that results for the two other nodes are less satisfactory. The large error is easily understandable for point 33-33-33. With regard to the innermost point 11-11-11, it is surprising that the direction of the error is reversed as compared with node 4-4-4 in the 8-in. tank. In the latter (Fig. 8) the potential value in the model was at any time N_{Fo} below the analytical value, while for node 22-22-22 the analytical value was below the model value.

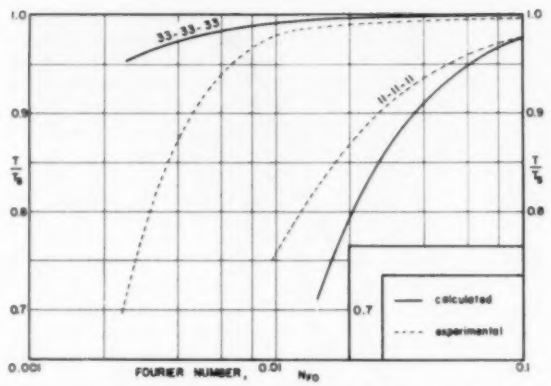

Fig. 13 Temperature time curves for points 11-11-11 and 33-33-33 (problem c)

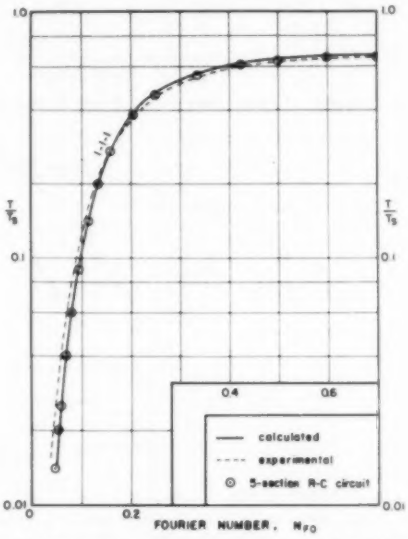

Fig. 14 Temperature versus time; points 1-1-1 (problem d)

A possible explanation may be seen in the use of the plates, as shown in Fig. 10, which provide a relatively short path from the power electrode on faces e_2, f_2, g_2, h_2, and b_2, c_2, f_2,' g_2 to the capacitance connector.

b. Cube Heated From Four Sides—Problem d. Figs. 14 and 15 show the results for the several nodes, again in comparison both with analytical results and with lumped-network results. Point 5-5-5, now receiving heat only from two instead of from three sides, heats up slower in comparison with conditions of problem c (compare Fig. 8). In light of the more favorable results of this problem, no tests were run with the small insert tank.

Conclusion and Further Work

The problem mentioned with regard to the finite boundary resistance and the connectors is obviously also relevant for the connections between the main tank and the insert tank. A study along the lines indicated in Section 2 is under way. Further problems with cubes, possibly in connection with node and electrode size should be studied, including arrangement and size of the insert tank. Also the replacement of cylinders and spheres by square bars and cubes (for symmetry in square sections)

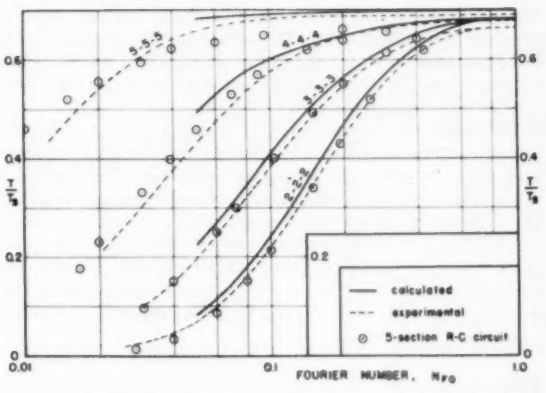

Fig. 15 Temperature versus time; points 2-2-2; 3-3-3; 4-4-4; and 5-5-5

might be considered. The concept of separate tanks connected across sets of corresponding electrodes can be extended to make possible handling of three-dimensional problems in bodies consisting of materials with different conductivities.

Acknowledgments

The development reported here was carried out over many years, and a number of persons were involved.

Joan Borowik-Sobel did much work in connection with the liquid resistance medium; M. P. Heisler was concerned with the size and shape of electrodes; H. G. Landau developed the analytical expressions used for comparison; A. Yang and S. Dicker carried out three-dimensional tests.

The latter stages of the program were in part supported by contributions, gratefully acknowledged, from: General Electric Co., Harrison Radiator Division of General Motors Corporation, Pittsburgh Plate Glass Co., Thompson Products Co., Union Carbide Corp.

References

1 I. Langmuir, E. Q. Adams, and F. S. Meikle, "Flow of Heat Through Furnace Walls," *Trans. American Electrochemical Society*, vol. 24, 1913, pp. 53–84.

2 F. Bruckmeyer, "Elektrisches Modellmessverfahren für Wärmebrücken im Kuehlraumbau," *Zeitschrift, VDI*, vol. 88, 1944, pp. 270–272.

3 C. L. Beuken, "Die Wärmeströmung durch die Ecken von Ofenwandungen," *Wärme- und Kältetechnik*, vol. 39, 1937, no. 7, pp. 1–3.

4 C. F. Kayan, "Heat-Transfer Temperature Patterns of a Multicomponent Structure by Comparative Methods," TRANS. ASME, vol. 71, 1949, pp. 9–16.

5 C. L. Beuken, "Wärmeverluste bei periodisch betriebenen Elekrischen Ofen," Compte Rendu, First International Congress on Electric Heating and Electrochemistry, 1936, Scheveningen, pp. 204–213.

6a V. Paschkis and H. D. Baker, "A Method for Determining Unsteady-State Heat Transfer by Means of an Electrical Analogy," TRANS. ASME, vol. 64, 1942, pp. 105–112.

6b M. Avrami and V. Paschkis, "Application of Electric Model to Study of Two-Dimensional Heat Flow," *Trans. AICE*, vol. 38, 1942, pp. 631–652, 723.

7 V. Paschkis, "Heat and Mass Flow Analyzer," *Scientific Monthly*, vol. 73, 1951, pp. 81–88.

8 A. V. Clark, "Simplified Method for Study of Two-Dimensional Transient Heat Flow Using Resistance Paper," ASME Paper No. 57—S-9.

9 Personal communications.

DISCUSSION

R. P. Benedict[3]

In this paper, the author introduces an interesting technique for approximating solutions to transient heat-transfer problems. The author has indicated not only the various advantages inherent in the subject geometric-network analog, but he points out at least three basic difficulties. These are:

1 Back-emf phenomena which opposes impressed emf.
2 Necessary transition from lumped-capacitors to distributed resistances.
3 Unavoidable currents through capacitance connectors which complicate connector designs.

Since the writer has worked with the Liebmann type of resistance network analog[4] and with the electrolytic tank analog,[5] it might be appropriate to make a few remarks along these lines.

While electrolytic tank analogs offer the distinct advantage of distributed resistances and facility in representing complex geometric boundaries, their use is nevertheless attended by many complications. Foremost is the chemical reaction which always takes place at the electrode-electrolyte interface as an outcome of the transition from an electronic to an ionic mode of electrical conduction. As mentioned by the author, this polarization effect means that locally the electrolyte is not an ohmic conductor, a fact quite important when it is remembered that all the electric field equations on which the various analogies depend are based on Ohm's law. It is evident that the polarization effect must be minimized. This may be accomplished by proper choice of electrode, electrolyte, and power supply. The following suggestions are offered in this connection:

a Inexpensive electrodes of practically zero transition resistance may be obtained by coating electrodes of any material with a colloidal dispersion of graphite such as Aquadag.

b Tap water has been found to be quite satisfactory as an electrolyte.

c To avoid the back-emf phenomena associated with d-c tanks, a-c power supplies usually have been employed. While the use of a-c is accompanied by its own peculiar polarization phenomena (i.e., the appearance of an unwanted capacitive reactance) this effect may be reduced by going to the higher frequencies (500 to 1000 cps).

It is realized that the R-C networks, as used in this paper with the geometric analog, require a d-c power supply. However, if a Liebmann resistance network were used in place of the R-C network in the combined geometric-network analog, certain advantages would accrue; for in bypassing polarization effects, we avoid also the transient measuring problems associated with capacitors charging and discharging. This latter advantage is realized because in the Liebmann method, time is handled as a stepwise variable so that at any instant we have a steady-state problem.

It is true that by combining a Liebmann network with an electrolytic tank we do not avoid the use of lumped circuit elements, nor do we resolve the problem of unavoidable currents through the connectors from these lumped circuit elements to the electrolyte. In fact, in view of these difficulties and considering

[3] Development Engineer, Westinghouse Electric Corp., Lester, Pa.

[4] R. P. Benedict, "Liebmann Network Approximations to One-Dimensional Transient Heat Conduction Problems," ASME Paper No. 58—A-221.

[5] R. P. Benedict and C. A. Meyer, "Electrolytic Tank Analog for Studying Fluid Flow Fields Within Turbomachinery," ASME Paper No. 57—A-120.

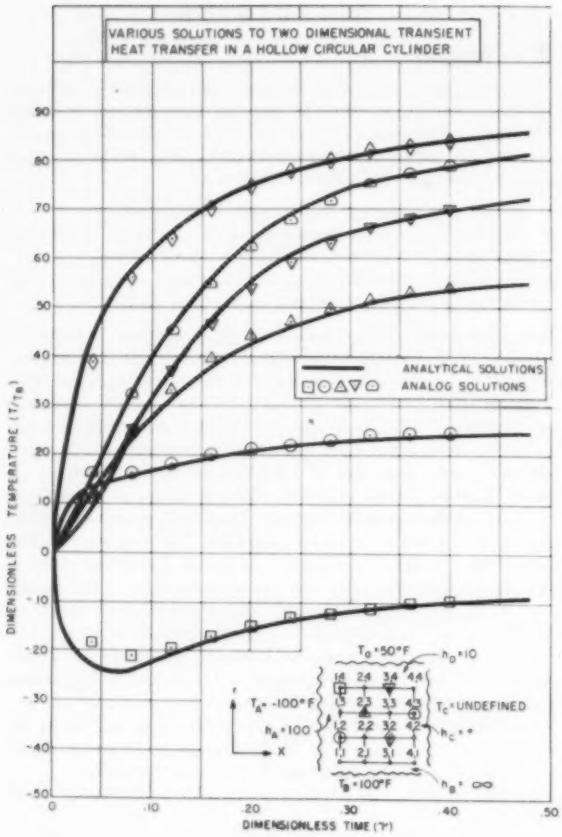

Fig. 16

also such items as uniform resistivity, ph, leakage, and evaporation of the electrolyte, as well as model building, leveling, and size of connectors, it is the feeling of the writer that at present the increased difficulties encountered probably more than offset the gains to be realized by the use of the proposed geometric-network analog.

As a matter of interest, a problem similar to problem *a* of the paper was solved by a two-dimensional Liebmann network. Programming consists simply of evaluating resistance ratios at each of the nodes of the problem. Results are presented in Fig. 16 and these are seen to compare favorably with the numerical solutions (programmed for high-speed digital computers) of Dr. Y. S. Tang of the Westinghouse Electric Corporation.

H. P. Fullerton[6]

The development of techniques for applying the electrolytic tank to three-dimensional transient problems is a valuable contribution in a difficult field. The author and his associates are to be commended for their ingenuity in meeting the problems which they faced and for the guidance this paper extends to others who may attempt work in this area.

One wonders, however, whether in using the insert tank in problem *c*, care was taken to choose the resistivity for the insert tank so as to retain the proper scale relation. No mention is made of this in the paper and it appears that this may account for the anomaly at point 11-11-11 mentioned in the text and shown in Fig. 13. If electrolyte of the same resistivity as that in the main tank were used in the insert tank, the effect would be the same as though a fluid of lower resistivity had been placed in that portion of the main tank. A corresponding distortion of the potential field would result.

Author's Closure

Mr. Benedict suggests the use of "steady-state" tanks, operated with a-c, using the Liebmann techniques. The writer's enumeration of difficulties encountered in such procedure seem sufficient to make the R-C method of the paper the more attractive. This leaves as alternative for the handling of three-dimensional problems a straight Liebmann technique, using a three-dimensional resistor grid with "drain resistors" taking the place of capacitances, or the combined technique suggested in this paper. If the three-dimensional shapes are simple, e.g., cubes, the Liebmann method may become attractive, even if the number of resistors required would be large. But for irregular shapes, or for regular shapes with irregular boundary resistances, the number of resistors required for the Liebmann technique becomes prohibitive and the method proposed in the paper seems to be clearly in the advantage; the good results for point E (Fig. 7) indicate that it will not be necessary to place too many capacitors, and the use of insert tanks (Fig. 10) may also be used at points of irregularities of shape.

The reason for choosing simple geometries and two-dimensional cases as examples in the paper is that only for such cases are analytic solutions available for comparison. Therefore the example in Mr. Benedict's Fig. 16 is not helpful for a comparison, even of two-dimensional cases between the combined techniques and the Liebmann method. The latter is in distinct disadvantage for complex two-dimensional shapes.

Mr. Fullerton is correct in saying that the different size of the insert requires a different time constant of the system in the insert. However, this time constant can be achieved by changing resistivity *or* capacity (capacitance per unit volume). Experimentally it was easier to use the same resistance liquid as in the main tank, changing the capacity. The capacitance of each node in the insert tank was reduced to $^1/_9$ of the value of that in the large tank, corresponding to the square of the length ratio. In this manner the Fourier numbers (dimensionless times) in main and insert tanks remained identical.

As mentioned in the paper, the anomaly at point 11-11-11 is probably due to the proximity of the two electrodes with different potentials.

[6] Switchgear and Control Division, General Electric Company, Philadelphia, Pa.

H. H. KELLER

Steam Division,
Westinghouse Electric
Corporation, Lester, Pa.

E. V. SOMERS

Research Laboratories,
Westinghouse Electric
Corporation, Pittsburgh, Pa.

Heat Transfer From an Annular Fin of Constant Thickness[1]

The two-dimensional solution for annular fins, given in graphical form with the efficiency plotted versus the design-parameter group, $(b - a)[(2h)/(kw)]^{1/2}$, supplies needed design information for fins of small height-to-thickness ratio and large height-to-inner radius ratio. The one-dimensional solutions previously given for annular fins are accurate for height-to-width ratios of the order of 10 or more, while the two-dimensional results for rectangular fins are useful as approximations to annular fins when curvature is not large. With height-to-width ratios less than 10 and for annular fins with large curvature, design of fins can be computed with the results presented in this paper.

A PROBLEM of practical engineering interest is that of the diffusion of heat through an annular fin of constant thickness. Interest in fins is prevalent in the many fields of engineering, such as air conditioning, heat-exchanger apparatus, electric motors, and electronics, where, using extended surfaces, engineers have been able to build more compact and efficient heat-transfer apparatus.

The effect of adding fins to a surface immersed in a fluid depends upon a number of factors of which the most important is the increase of exposed surface area. For heat transfer from an interior isothermal surface to an external fluid, there are two factors which determine the rate of heat exchange:

1 Resistance to heat flow through the convective film of the ambient fluid.

2 Conductive resistance to heat flow within the metal fin itself.

Numerous solutions to the problem of diffusion of heat in an annular fin of constant thickness have been presented, but all cases refer to one-dimensional heat flow [1–5].[2] An assumption inherent in these solutions is that the fin thickness is sufficiently small compared to its height that temperature gradients normal to the length direction of the fin may be neglected. For fins of large height and small thickness this assumption produces negligible error. For fins with a small height-to-thickness ratio, the error introduced by the one-dimensional assumption becomes important.

Avrami and Little [6] have applied a two-dimensional analysis to a flat rectangular fin. Their results should approximate closely an annular fin of small height-to-thickness ratio and large inner diameter; effectively, a fin where the curve is unimportant. The work reported here supplies the solution for annular fins of small height-to-thickness ratio where curvature is important; i.e., where the fin height is comparable to the inner diameter

Treatment of the Problem

The diffusion of heat in an annular fin of constant thickness reduces to the problem of obtaining the steady-state temperature distribution in a finite, hollow, circular cylinder representing the annular fin. Several restrictions and assumptions are inherent in solving this fin problem:

1 The flow of heat and temperature distribution throughout the fin are independent of time.

2 The fin material is isotropic.

3 There is no heat source in the fin.

4 The flow of heat is both radial and axial; i.e., two-dimensional.

These establish the Laplace differential equation as describing

[1] This paper is based on an MS thesis submitted by H. H. Keller to the Mechanical Engineering Department of the University of Pittsburgh.

[2] Numbers in brackets designate References at end of paper.

Contributed by the Heat Transfer Division and presented at the Annual Meeting, New York, N. Y., November 30–December 5, 1958, of THE AMERICAN SOCIETY OF MECHANICAL ENGINEERS.

NOTE: Statements and opinions advanced in papers are to be understood as individual expressions of their authors and not those of the Society. Manuscript received at ASME Headquarters, August 5, 1958. Paper No. 58—A-116.

Nomenclature

A_e' = surface of end of fin
A_f' = surface of side of fin
a = inner radius of fin
b = outer radius of fin
h = heat-transfer coefficient
$I_n(x)$ = modified Bessel function of first kind of order n and of argument x
$K_n(x)$ = modified Bessel function of second kind of order n and of argument x
k = thermal conductivity of fin material
n = an integer
Q' = heat-flow rate
Q = dimensionless heat-flow rate
r' = radius of any point in fin
r = ratio of radius of any point in fin to height of fin, $r = r'/(b - a)$
S = function of $\left(\alpha_n, \mu, \beta, \frac{a}{b-a}\right)$; equation (12)
V' = temperature
V = dimensionless temperature distribution in fin
V_s' = temperature at base of fin
w = fin thickness
α_n = roots of characteristic equation (7)
β = ratio of fin height to thickness
z' = axial position of any point in fin
z = dimensionless axial position at any point in fin, $z = z'/w$
μ = ratio of heat-transfer coefficient times fin height to thermal conductivity of fin material, $\mu = h(b - a)/k$
φ = fin efficiency
ψ = function defined in equation (8)

the heat flow within the fin, which in dimensionless form is given by

$$\frac{\partial^2 V}{\partial r^2} + \frac{1}{r}\frac{\partial V}{\partial r} + \beta^2 \frac{\partial^2 V}{\partial z^2} = 0 \tag{1}$$

The restrictions on the boundary conditions for the fin are:

1 The heat-flux rate from the fin surface at any point is directly proportional to the temperature difference between the surface at that point and the ambient fluid; i.e., Newton's law of cooling applies with a constant convection coefficient.

2 The ambient temperature of the fluid is constant at an arbitrary temperature of zero.

3 The base of the fin is isothermal at temperature V_i'.

4 The fin is of constant thickness.

These restrictions lead to the following dimensionless-boundary-condition equations:

At the base of the fin

$$V\left(\frac{a}{b-a}, z\right) = 1 \tag{2}$$

At the end of the fin

$$\frac{\partial V\left(\frac{b}{b-a}, z\right)}{\partial r} + \mu V\left(\frac{b}{b-a}, z\right) = 0 \tag{3}$$

At the sides of the fin

$$-\frac{\partial V(r, 0)}{\partial r} + \frac{\mu}{\beta} V(r, 0) = 0 \tag{4}$$

and

$$\frac{\partial V(r, 1)}{\partial r} + \frac{\mu}{\beta} V(r, 1) = 0 \tag{5}$$

The solution to equations (1) through (5) yields the dimensionless temperature distribution in the finite hollow cylinder representing an annular fin [7]

$$V = 2\beta \sum_{n=1}^{\infty} \frac{\left\{\alpha_n \cos\left(\frac{\alpha_n z}{\beta}\right) + \mu \sin\left(\frac{\alpha_n z}{\beta}\right)\right\} \left\{\sin\left(\frac{\alpha_n}{\beta}\right) + \frac{\mu}{\alpha_n}\left[1 - \cos\left(\frac{\alpha_n}{\beta}\right)\right]\right\} \psi(r, n)}{\{\alpha_n^2 + \mu^2 + 2\mu\beta\}\psi\left(\frac{a}{b-a}, n\right)} \tag{6}$$

where the $\{\alpha_n\}$ are the positive roots of

$$\tan\left(\frac{\alpha_n}{\beta}\right) = \frac{2\mu\alpha_n}{\alpha_n^2 - \mu^2} \tag{7}$$

and

$$\psi(r, n) = I_0(\alpha_n r)\left\{\frac{\alpha_n}{b-a} K_1\left(\frac{\alpha_n b}{b-a}\right) - \frac{\mu}{b-a} K_0\left(\frac{\alpha_n b}{b-a}\right)\right\} + K_0(\alpha_n r)\left\{\frac{\alpha_n}{b-a} I_1\left(\frac{\alpha_n b}{b-a}\right) + \frac{\mu}{b-a} I_0\left(\frac{\alpha_n b}{b-a}\right)\right\} \tag{8}$$

The heat rate at the base of the fin can be found by integrating the Fourier law for conducted heat-flux rate across the base of the fin

$$\int_0^{Q'} dQ' = -\int_0^W k\left(\frac{\partial V'}{\partial r'}\right)_{r=a} 2\pi a dz' \tag{9}$$

From equations (6) through (9), in dimensionless form

$$Q = -\beta \sum_{n=1}^{\infty}$$

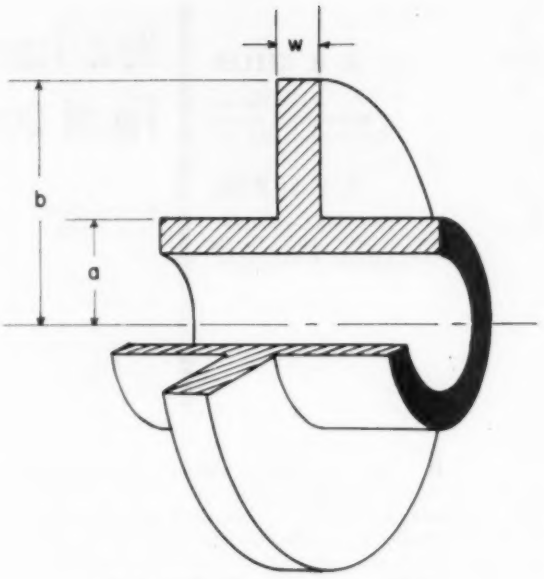

Fig. 1 Annular fin of constant thickness

$$\frac{\left\{\sin\left(\frac{\alpha_n}{\beta}\right) + \frac{\mu}{\alpha_n}\left[1 - \cos\left(\frac{\alpha_n}{\beta}\right)\right]\right\}^2 \frac{\partial \psi\left(\frac{a}{b-a}, n\right)}{\partial r}}{\{\alpha_n^2 + \mu^2 + 2\mu\beta\}\psi\left(\frac{a}{b-a}, n\right)} \tag{10}$$

The fin efficiency, used as the basis for determining a fin design, is defined as the ratio of actual heat-flow rate to the heat-flow rate that would exist if the entire fin were at the temperature of the base of the fin. This definition in equation form is

$$\varphi = \frac{\int_0^{A_f' + A_e'} V' dA'}{V_i'(A_f' + A_e')} = \frac{Q'}{hV_i'(A_f' + A_e')} \tag{11}$$

Let

$$S = \sum_{n=1}^{\infty} \frac{\left\{\sin\left(\frac{\alpha_n}{\beta}\right) + \frac{\mu}{\alpha_n}\left[1 - \cos\left(\frac{\alpha_n}{\beta}\right)\right]^2\right\} \frac{\partial \psi\left(\frac{a}{b-a}, n\right)}{\partial r}}{\{\alpha_n^2 + \mu^2 + 2\mu\beta\}\psi\left(\frac{a}{b-a}, n\right)} \tag{12}$$

from which

$$Q' = -4\pi a k V_i' \beta S$$

The fin efficiency then becomes

$$\varphi = -\frac{2\beta S}{\mu\left\{\frac{b+a}{a} + \frac{b}{a\beta}\right\}} = \frac{2Q}{\mu\left\{\frac{b+a}{a} + \frac{b}{a\beta}\right\}} \tag{13}$$

Numerical Reduction of Solution

The fin efficiency φ was evaluated with the geometrical and operating variables given, i.e., b, a, h, and k given; this required the determination of φ per equation (13). The dimensionless heat-flow rate Q was found in equation (10) to be

$$Q = -\beta \sum_{n=1}^{\infty} \frac{\left\{\sin\left(\frac{\alpha_n}{\beta}\right) + \frac{\mu}{\alpha_n}\left[1 - \cos\left(\frac{\alpha_n}{\beta}\right)\right]^2\right\} \frac{\partial \psi\left(\frac{a}{b-a}, n\right)}{\partial r}}{\{\alpha_n^2 + \mu^2 + 2\mu\beta\}\psi\left(\frac{a}{b-a}, n\right)} \quad (14)$$

where

$$\psi\left(\frac{a}{b-a}, n\right) = I_0\left(\frac{\alpha_n a}{b-a}\right)\left\{\frac{\alpha_n}{b-a} K_1\left(\frac{\alpha_n b}{b-a}\right) - \frac{\mu}{b-a} K_0\left(\frac{\alpha_n b}{b-a}\right)\right\} + K_0\left(\frac{\alpha_n a}{b-a}\right)\left\{\frac{\alpha_n}{b-a} I_1\left(\frac{\alpha_n b}{b-a}\right) + \frac{\mu}{b-a} I_0\left(\frac{\alpha_n b}{b-a}\right)\right\} \quad (15)$$

and

$$\frac{\partial \psi\left(\frac{a}{b-a}, n\right)}{\partial r} = \alpha_n I_1\left(\frac{\alpha_n a}{b-a}\right)\left\{\frac{\alpha_n}{b-a} K_1\left(\frac{\alpha_n b}{b-a}\right) - \frac{\mu}{b-a} K_0\left(\frac{\alpha_n b}{b-a}\right)\right\} - \alpha_n K_1\left(\frac{\alpha_n a}{b-a}\right)\left\{\frac{\alpha_n}{b-a} I_1\left(\frac{\alpha_n b}{b-a}\right) + \frac{\mu}{b-a} I_0\left(\frac{\alpha_n b}{b-a}\right)\right\} \quad (16)$$

The Bessel functions contained in Q are evaluated by interpolation of tabulated values when the value of the argument is less than 20. For values of the argument greater than 20, an asymptotic approximation of the Bessel functions [8] was used. For $x > 20$

$$I_0(x) \simeq \frac{x^{-1/2}\epsilon^x}{(2\pi)^{1/2}}$$

$$I_1(x) \simeq \frac{\epsilon^x}{(2\pi)^{1/2}}\left\{x^{-1/2} - \frac{1}{2}x^{-3/2}\right\}$$

$$K_0(x) \simeq \left(\frac{\pi}{2}\right)^{1/2}\epsilon^{-x}x^{-1/2}$$

$$K_1(x) \simeq \left(\frac{\pi}{2}\right)^{1/2}\epsilon^{-x}\left\{x^{-1/2} + \frac{1}{2}x^{-3/2}\right\}$$

The roots of the characteristic equation, equation (8), were computed roughly in graphical form and the values were then refined by Newtonian interpolation. A graphical plot of the right-hand and left-hand sides of equation (7) is shown in Fig. 2 for $\mu = 0.2$ and $\beta = 10$.

A simplification of the solution may be made by noting that the expression

$$\frac{\alpha_n I_1\left(\frac{\alpha_n a}{b-a}\right)\left\{\alpha_n K_1\left(\frac{\alpha_n b}{b-a}\right) - \mu K_0\left(\frac{\alpha_n b}{b-a}\right)\right\} - \alpha_n K_1\left(\frac{\alpha_n a}{b-a}\right)\left\{\alpha_n I_1\left(\frac{\alpha_n a}{b-a}\right) + \mu I_0\left(\frac{\alpha_n b}{b-a}\right)\right\}}{I_0\left(\frac{\alpha_n a}{b-a}\right)\left\{\alpha_n K_1\left(\frac{\alpha_n b}{b-a}\right) - \mu K_0\left(\frac{\alpha_n b}{b-a}\right)\right\} + K_0\left(\frac{\alpha_n a}{b-a}\right)\left\{\alpha_n I_1\left(\frac{\alpha_n a}{b-a}\right) + \mu I_0\left(\frac{\alpha_n b}{b-a}\right)\right\}}$$

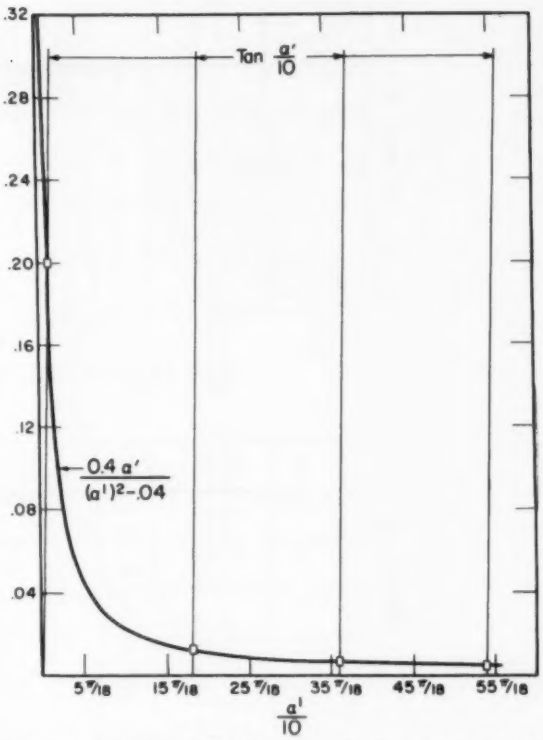

Fig. 2 Graphic solution of $(\alpha'/\beta) = (2\mu\alpha')/[(\alpha')^2 - \mu^2]$ for $\mu = 0.2$, $\beta = 10$

may be approximated closely by

$$\frac{-\alpha_n K_1\left(\frac{\alpha_n a}{b-a}\right)}{K_0\left(\frac{\alpha_n a}{b-a}\right)}, \quad (\alpha_n > 5)$$

and may be approximated by

$$\alpha_n + \frac{1}{2}\frac{b-a}{a}, \quad (\alpha_n > 20)$$

The results are plotted in Figs. 3, 4, 5, 6, 7 for five values of b/a. The selection of $a/(b-a)$ determines $b/(b-a)$ and b/a. The values chosen for $a/(b-a)$ are

$$\frac{a}{b-a} = 0.2,\ 0.5,\ 1.00,\ 5.00,\ \text{and}\ 10.00$$

These values cover a range from tall fins on small-diameter tubes to short fins on large-diameter tubes.

The values chosen for β were picked to cover a practical range from a short wide fin to a long and narrow fin. The values chosen for β are

$$\beta = 1/3,\ 1.00,\ 3.00,\ 10.00,\ \text{and}\ 50.00.$$

The values chosen for μ were such as to keep the magnitude of

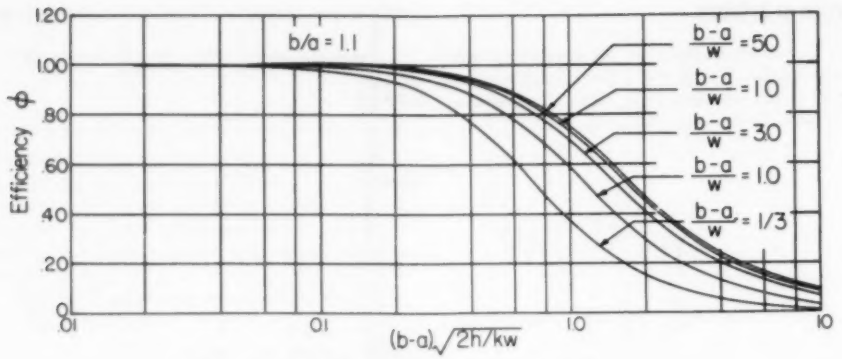

Fig. 3 Efficiency of annular fin of constant thickness

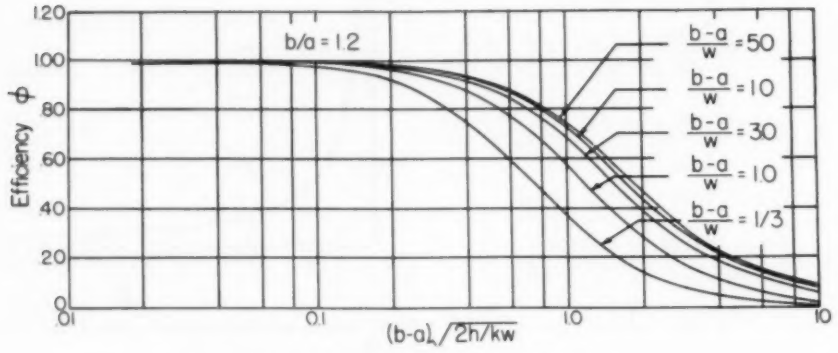

Fig. 4 Efficiency of annular fin of constant thickness

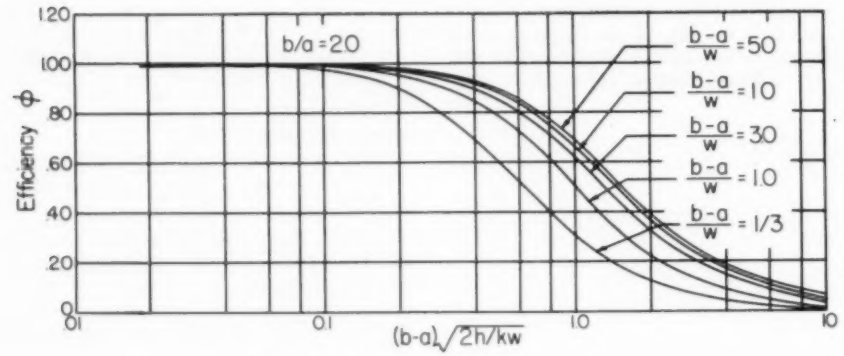

Fig. 5 Efficiency of annular fin of constant thickness

$(2\mu\beta)^{1/2}$ (where $[2\mu\beta]^{1/2} = b - a[2h/kw]^{1/2}$) within the limits of 0.05 to 10. For $(2\mu\beta)^{1/2}$ less than 0.05 the efficiencies are almost unity and for $(2\mu\beta)^{1/2}$ greater than 10 the efficiencies are almost zero.

Discussion

The results of this paper have been compared to the results obtained by Avrami and Little [6] for the two-dimensional rectangular bar and to the results obtained by Gardner [5] for a one-dimensional annular fin.

Comparison with the results obtained by Avrami and Little indicate that theirs could be used in designing an annular fin of small height-to-width ratio and small b/a ratio; as the b/a ratio increases, the results of Avrami and Little deviate from those obtained here. The values are compared in Table 1.

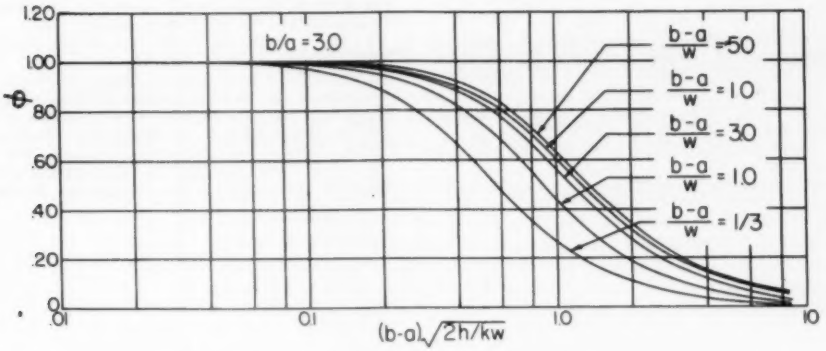

Fig. 6 Efficiency of annular fin of constant thickness

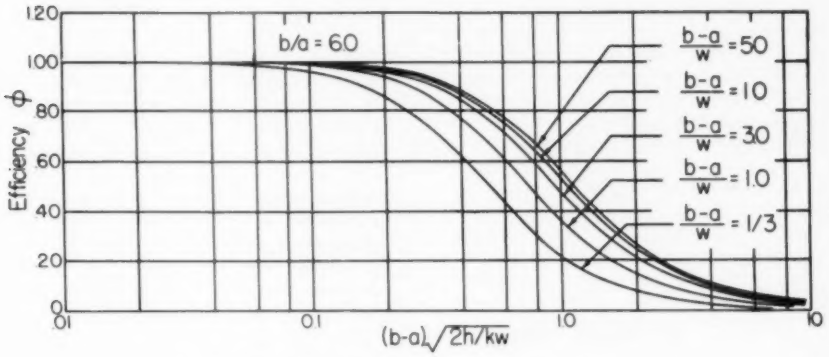

Fig. 7 Efficiency of annular fin of constant thickness

Table 1 Comparison of two-dimensional rectangular and radial cases

b/a	$(b-a)\left(\frac{2h}{kw}\right)^{1/2}$	φ(two-dimensional) $\frac{b-a}{w}=50$	$\frac{b-a}{w}=10$	$\frac{b-a}{w}=\frac{1}{3}$
1.00[a]	0.50	0.925	0.915	0.732
1.00	2.00	0.480	0.476	0.151
1.00	5.00	0.196	0.182	0.038
1.10	0.50	0.915	0.906	0.685
1.10	2.00	0.468	0.445	0.150
1.10	5.00	0.190	0.178	0.038
1.20	0.50	0.912	0.902	0.665
1.20	2.00	0.465	0.438	0.140
1.20	5.00	0.190	0.178	0.038
2.00	0.50	0.895	0.880	0.600
2.00	2.00	0.390	0.370	0.126
2.00	5.00	0.150	0.138	0.032
3.00	0.50	0.875	0.855	0.560
3.00	2.00	0.340	0.318	0.110
3.00	5.00	0.118	0.110	0.027

[a] $b/a = 1.00$ infers rectangular results of Avrami and Little; compare efficiencies given for rectangular results at $b/a = 1.00$ with efficiencies given for radial results at other values of b/a, at constant $b - a/w$ and constant $(b - a)(2h/kw)^{1/2}$.

Comparison with the results obtained by Gardner indicate that his results are satisfactory for large height-to-width ratios Shown in Table 2 is a comparison of Gardner's one-dimensional values with the two-dimensional values of this paper. As can be seen, Gardner's results apply with decreasing accuracy as the length-to-width ratio is reduced below 10.

Table 2 Comparison of one and two-dimensional radial cases

$\frac{b}{a}$	$(b-a)\left(\frac{2h}{kw}\right)^{1/2}$	φ (one-dimensional)	φ (two-dimensional) $\frac{b-a}{w}=50$	$\frac{b-a}{w}=10$	$\frac{b-a}{w}=\frac{1}{3}$
1.10	0.50	0.920	0.915	0.906	0.685
1.10	2.00	0.470	0.468	0.445	0.150
1.10	5.00	0.195	0.190	0.178	0.038
1.20	0.50	0.920	0.912	0.902	0.665
1.20	2.00	0.465	0.465	0.438	0.140
1.20	5.00	0.190	0.182	0.172	0.035
2.00	0.50	0.900	0.895	0.880	0.600
2.00	2.00	0.390	0.390	0.370	0.126
2.00	5.00	0.150	0.150	0.138	0.032
3.00	0.50	0.875	0.875	0.855	0.560
3.00	2.00	0.340	0.340	0.318	0.110
3.00	5.00	0.120	0.118	0.110	0.027

References

1 D. R. Harper and W. B. Brown, "Mathematical Equations for Heat Conduction in the Fins of Air-Cooled Engines," NACA Report No. 158, 1922.

2 W. H. Carrier and S. W. Anderson, "The Resistance to Heat Flow Through Finned Tubing," *Heating, Piping, and Air Conditioning*, vol. 10, 1944, pp. 304–320.

3 Max Jakob, "Heat Transfer," John Wiley & Sons, Inc., New York, N. Y., 1949, p. 229.

4 W. M. Murray, "Heat Dissipation Through an Annular Disk or Fin of Uniform Thickness," *Journal of Applied Mechanics*, vol. 5, TRANS. ASME, vol. 60, 1938, p. A-78.

5 K. A. Gardner, "Efficiency of Extended Surface," TRANS. ASME, vol. 67, 1945, pp. 621–631.

6 Melvin Avrami and J. B. Little, "Diffusion of Heat Through a Rectangular Bar and the Cooling and Insulating Effects of Fins, I. The Steady State," *Journal of Applied Physics*, vol. 13, 1942, p. 255.

7 H. S. Carslaw and J. C. Jaeger, "Conduction of Heat in Solids," Oxford University Press, London, England, 1947, p. 192.

8 E. T. Whittaker and G. N. Watson, "A Course of Modern Analysis," Cambridge Press, Cambridge, England, 1950, p. 373.

E. M. SPARROW
R. SIEGEL

NASA, Lewis Research Center, Cleveland, Ohio, Assoc. Mem. ASME

A Variational Method for Fully Developed Laminar Heat Transfer in Ducts

A variational method is presented for determining fully developed velocity and temperature distributions for laminar flow in noncircular ducts. The heat addition to the fluid is taken to be uniform in the axial direction, but a variety of thermal boundary conditions are considered around the periphery of the duct cross section. Several illustrative examples are given, and comparisons are made which show good agreement with available exact solutions. These examples include ducts of rectangular and circular-sector cross sections.

Introduction

THE UTILITY of variational methods as a tool for the solution of complex problems in the theory of elasticity and other fields of applied science is well established. The power of the variational technique has yet to be brought to bear on problems in heat transfer, except for recent work on unsteady conduction, e.g., Biot [1].[1]

In this report we are concerned with forced convection heat transfer, and our aim is to formulate and apply a variational procedure for solving the problem of fully developed heat transfer in noncircular ducts. To demonstrate the method, velocity and heat-transfer solutions will be found for laminar flow in passages of rectangular and of circular sector cross section. In all cases, the heat input per unit length will be taken as constant along the passage, but a variety of thermal conditions around the boundary of the cross section will be considered.

Attention is focused here on noncircular ducts because of their increasing application in the design of high performance heat exchange equipment. In particular, such noncircular configurations may be found in the cores of nuclear reactors, where fuel elements may be arranged in various patterns.

A brief description of the general variational procedure will be given in the next section, and this will be followed by the specific problems. More detailed information on the mathematical fundamentals may be found in a number of texts, for example, Hildebrand [2].

[1] Numbers in brackets designate References at end of paper.

Contributed by the Heat Transfer Division and presented at the Annual Meeting, New York, N. Y., November 30–December 5, 1958, of THE AMERICAN SOCIETY OF MECHANICAL ENGINEERS.

NOTE: Statements and opinions advanced in papers are to be understood as individual expressions of their authors and not those of the Society. Manuscript received at ASME Headquarters, August 4, 1958. Paper No. 58—A-92.

The Variational Procedure

General Considerations. The basis of the variational method to be applied here may be stated as follows: Suppose that the physical principles involved in a problem are expressed mathematically as a differential equation, e.g., a conservation law. Then, the solution of the problem is given by the function which satisfies

Nomenclature

A = cross-sectional area of duct
a = half-length of the short side of rectangular duct, or half-length of the side of square duct
b = half-length of the long side of rectangular duct
C = a constant, $\frac{1}{\mu}\frac{dp}{dz}$
c_f = friction factor
c_p = specific heat at constant pressure
D_e = hydraulic diameter, $4A$/wetted perimeter
F = integrand of the variational integral
h = fully developed heat-transfer coefficient
I = variational integral
k = thermal conductivity
Nu = Nusselt number, hD_e/k
p = static pressure
Q = heat-transfer rate to fluid per unit length of duct
R = dimensionless radial co-ordinate, r/r_0
r = radial co-ordinate; r_0, duct radius
T = temperature; T_b, bulk fluid temperature; T_w, wall temperature
u = fluid velocity; $\bar{u}$, mean fluid velocity
V = representation of a dependent variable
X = dimensionless co-ordinate, x/a
x = co-ordinate along the short side of rectangular duct, or along the side of square duct
Y = dimensionless co-ordinate; y/b for rectangular duct or y/a for square duct
y = co-ordinate along the long side of rectangular duct, or along the side of square duct
z = axial co-ordinate along duct length
β = dimensionless temperature in circular-sector duct, $\frac{T - T_w}{Q/k\theta_0}$; β_b, bulk fluid temperature
γ = aspect ratio of rectangular duct, b/a
Θ = dimensionless angular co-ordinate, θ/θ_0
θ = angular co-ordinate in circular-sector duct; θ_0, half of opening angle, radians
μ = absolute viscosity
ρ = fluid density
Φ = dimensionless temperature, $\frac{T - T_w}{Q/8k}$; Φ_b, bulk fluid temperature
ϕ = dimensionless temperature, $\frac{T}{Q/4(\gamma+1)k}$; ϕ_b, bulk fluid temperature; $\bar{\phi}_w$, average wall temperature

Subscripts

x, y, r, θ = partial differentiation

both the differential equation and the given boundary conditions. Now, according to the calculus of variations, there corresponds to this differential equation an integral with a very particular characteristic. Namely, that the value of the integral is a minimum when it is evaluated using that function which satisfies the differential equation and boundary conditions. As discussed later these boundary conditions must be of certain permissible types. When other functions satisfying the boundary conditions but not the differential equation are introduced, the value of the variational integral exceeds the minimum. These properties suggest a procedure for obtaining approximate solutions of differential equations by utilizing the variational integral. The simplest scheme would be to select a number of trial functions which satisfy the boundary conditions, and then introduce them successively into the variational integral. That function leading to the least value of the integral would then be regarded as most closely approximating the correct solution. More sophisticated schemes, e.g., the Ritz method, provide systematic ways of finding trial functions with good minimum properties.

We now proceed to express mathematically the discussion of the preceding paragraphs. The initial item to be considered is the correspondence between a differential equation and its variational integral. For convenience, rectangular co-ordinates will be used.

Consider a function V which may depend upon x and y; for example, V may represent the velocity or the temperature. Suppose that the physical problem has been mathematically formulated, so that we know the differential equation which V must satisfy. Then, according to the calculus of variations, we must first find (by inspection, experience, or other means) a function $F(x, y, V, V_x, V_y)$ which when inserted into the relation[2]

$$\frac{\partial}{\partial x}\left(\frac{\partial F}{\partial V_x}\right) + \frac{\partial}{\partial y}\left(\frac{\partial F}{\partial V_y}\right) - \frac{\partial F}{\partial V} = 0 \tag{1}$$

yields the differential equation for V. When F is known we can write the variational integral I,

$$I = \iint_{\text{area}} F(x, y, V, V_x, V_y)dx\,dy \tag{2}$$

The variational method states that the solution of the differential equation for V also gives a minimum value for I.

As a simple illustration, suppose that V is governed by

$$V_{xx} + V_{yy} = 0 \tag{3a}$$

From experience, we propose that the F function be

$$F = \frac{1}{2}\left[(V_x)^2 + (V_y)^2\right] \tag{3b}$$

Inserting this expression into equation (1) and differentiating yields equation (3a); so our choice for F is a proper one. The variational integral corresponding to equation (3a) is then written in accordance with equation (2) as

$$I = \frac{1}{2}\iint_{\text{area}} \left[(V_x)^2 + (V_y)^2\right]dx\,dy \tag{3c}$$

Leaving this illustration and returning to the general situation, it is important to note that the correspondence between variational integrals and differential equations is contingent upon particular boundary conditions being satisfied. Specifically, V must be either constant on the boundary or else the normal derivative of V must be zero on the boundary. We will later show that these restrictions provide no obstacle for the types of problems considered in this report.

[2] This is often called the Euler Equation.

Once a variational integral has been found, it may then form the basis of an approximation method for finding V. The procedure is to choose trial functions for V which make the integral as small as possible (the exact solution gives the absolute minimum). A well-known technique for minimizing a variational integral is called the Ritz method. According to this approach, V is written as a linear combination of functions, *each* of which satisfies the boundary conditions, i.e.,

$$V = A_0V_0(x, y) + A_1V_1(x, y) + A_2V_2(x, y) + \ldots = \sum_{k=0}^{r} A_kV_k(x, y) \tag{4}$$

With this choice of V, the function F may be evaluated and the integration in equation (2) carried out. The result is an expression containing the $A_0, A_1, \ldots A_r$. To achieve a minimum value of the integral I, this expression is differentiated separately with respect to each A_k and each result is set equal to zero. This provides $(r + 1)$ simultaneous equations which can be solved for the unknown constants $A_0, \ldots A_r$. In practice, this procedure may be applied successively using an increasing number of terms in the series (4) until convergence to a desired accuracy is achieved. The convergence is hastened by choosing the form of the V_k in accordance with any intuition or knowledge that one may have about the physical form of the solution.

Application of these ideas to forced convection flow and heat transfer will be made in later sections.

The Conservation Equations. Heat transfer involving fluid motion is governed by three conservation laws: Mass, momentum, and energy. For the situation of fully developed heat transfer in passages, the velocity is taken to be unchanging along the length. Under these conditions, the conservation of mass equation is identically satisfied, and conservation of momentum reduces to a single equation which, in rectangular co-ordinates, is

$$\frac{\partial^2 u}{\partial x^2} + \frac{\partial^2 u}{\partial y^2} = \frac{1}{\mu}\frac{dp}{dz} = C \tag{5}$$

This equation expresses the fact that the pressure forces must exactly balance the viscous forces in a nonaccelerating flow. The viscous flow boundary conditions require that the velocity vanish on all solid surfaces.

Now we turn to the energy equation for fully developed flow, which, when written in rectangular co-ordinates, is

$$\rho c_p u\frac{\partial T}{\partial z} = k\left(\frac{\partial^2 T}{\partial x^2} + \frac{\partial^2 T}{\partial y^2} + \frac{\partial^2 T}{\partial z^2}\right) \tag{6}$$

Fluid property variations and viscous dissipation have been neglected. For the situation of uniform heat input per unit length, the condition of fully developed heat transfer is that the axial temperature gradient, $\partial T/\partial z$, is constant. An over-all energy balance gives

$$\frac{\partial T}{\partial z} = \frac{Q}{\rho A\bar{u}c_p}$$

where A is the cross-sectional area of the passage and Q is the heat input per unit length. Using this expression for the temperature gradient and $\partial^2 T/\partial z^2 \equiv 0$, equation (6) becomes

$$\frac{u}{\bar{u}}\frac{Q}{A} = k\left(\frac{\partial^2 T}{\partial x^2} + \frac{\partial^2 T}{\partial y^2}\right) \tag{7}$$

The thermal conditions around the boundary of a given cross section may take on a variety of forms, e.g., uniform temperature, uniform heat flux, partially insulated, etc. Specific choices will be made in the examples given later.

For cylindrical co-ordinates, the conservation laws analogous to equations (5) and (7) are

$$\frac{\partial^2 u}{\partial r^2} + \frac{1}{r}\frac{\partial u}{\partial r} + \frac{1}{r^2}\frac{\partial^2 u}{\partial \theta^2} = \frac{1}{\mu}\frac{dp}{dz} = C \qquad (5a)$$

$$\frac{u}{\bar{u}}\frac{Q}{A} = k\left(\frac{\partial^2 T}{\partial r^2} + \frac{1}{r}\frac{\partial T}{\partial r} + \frac{1}{r^2}\frac{\partial^2 T}{\partial \theta^2}\right) \qquad (7a)$$

Variational Principles for the Velocity and Temperature Distributions. We are now in a position to write the variational integrals corresponding to the conservation laws of the previous paragraphs.

Consider a rectangular duct as shown in Fig. 1. We deal first with the differential equation (5) for the velocity. According to the rules for the variational procedure, the initial task is to find a function F which, when inserted into equation (1), yields equation (5). It is easily verified that the following choice for F is the proper one

$$F = (u_x^2 + u_y^2) + 2Cu$$

The variational integral corresponding to equation (5) is then

$$I = \int_{-a}^{+a}\int_{-b}^{+b} (u_x^2 + u_y^2 + 2Cu)\,dx\,dy \qquad (8)$$

The physical requirement that the velocity be zero on the boundaries satisfies the mathematical restrictions on the boundary conditions needed to assure correspondence between the differential equation and the variational integral.

Next, we go to the energy equation for the rectangular duct. By inspection, the function F which leads to equation (7) is found to be

$$F = T_x^2 + T_y^2 + 2\left(\frac{Q}{kA}\right)\frac{u}{\bar{u}}\,T$$

and the corresponding variational integral is

$$I = \int_{-a}^{+a}\int_{-b}^{+b}\left[T_x^2 + T_y^2 + 2\left(\frac{Q}{kA}\right)\frac{u}{\bar{u}}\,T\right]dx\,dy \qquad (9)$$

It has already been noted that in order for the variational integral (9) to correspond to the differential equation (7), the permissible boundary conditions are that the temperature is constant or that the normal derivative is zero. Since the zero derivative case is trivial (all walls insulated), equation (9), as it stands, is only usable for ducts with uniform peripheral wall temperature. To treat a situation where the peripheral heat flux is specified, i.e., prescribed normal derivative, a modification will be made in the formulation. This will be demonstrated later when illustrative examples are given.

Finally, we give the form of the variational integrals in cylindrical co-ordinates. The specific geometry to be considered is a passage whose cross section, as shown in Fig. 2, is a circular sector.

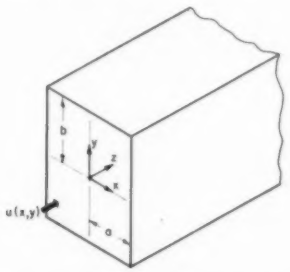

Fig. 1 Co-ordinate system for rectangular duct

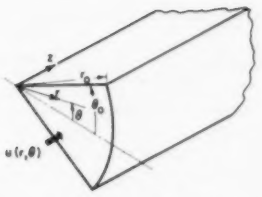

Fig. 2 Co-ordinate system for circular-sector duct

The variational integral for the velocity, corresponding to equation (5a), is

$$I = \int_0^{r_0}\int_{-\theta_0}^{+\theta_0}\left(u_r^2 + \frac{1}{r^2}u_\theta^2 + 2Cu\right)r\,dr\,d\theta \qquad (8a)$$

Further, the variational integral corresponding to the energy equation (7a) is

$$I = \int_0^{r_0}\int_{-\theta_0}^{+\theta_0}\left[T_r^2 + \frac{1}{r^2}T_\theta^2 + 2\left(\frac{Q}{kA}\right)\frac{u}{\bar{u}}\,T\right]r\,dr\,d\theta \qquad (9a)$$

The comments with respect to boundary conditions which have been made in connection with equations (8) and (9) also apply to equations (8a) and (9a).

Applications of the Variational Procedure

Velocity Distribution in a Square Duct. It is seen from the energy equation (7) or its variational integral (9) that a knowledge of the velocity distribution is required before the temperature problem can be solved. Hence we shall first direct our attention to the velocity distribution.

In solving the velocity problem, we are able to benefit from knowledge accumulated in the solution of the torsion problem in elasticity theory. There is a direct correspondence between equation (5) and the differential equation for the stress function in the torsion problem. Further, equation (8) is analogous to the "energy integral" for the stress function. Thus, from the results given by Timoshenko (reference [3], p. 283) for torsion of a square bar, we can write a first approximation to the laminar velocity distribution in a square duct as follows

$$\frac{u}{\bar{u}} = \frac{1}{0.2808\,a^6}(x^2 - a^2)(y^2 - a^2)[0.5844\,a^2 + 0.1185(x^2 + y^2)] \qquad (10)$$

To test the accuracy of this expression, a comparison with the exact velocity solution [4] is made in Fig. 3. Profiles are plotted along a co-ordinate axis and along a diagonal. The agreement is generally very good, except for deviations near the corners.

With the thought of improving the approximation, the variational method was reapplied using an expression of slightly greater complexity than equation (10). The steps in the calculation will be shown in some detail, so that future calculations which proceed in the same manner may be described only in outline form. The profile chosen for the improved approximation is

$$u = (x^2 - a^2)(y^2 - a^2)[A_0 + A_1(x^2 + y^2) + A_2x^2y^2] \qquad (11)$$

The factors $(x^2 - a^2)$ and $(y^2 - a^2)$ assure that each of the three terms satisfies the condition of zero velocity at the boundaries $x = \pm a$, $y = \pm a$. The constants A_0, A_1, and A_2 remain to be determined.

Substitution of equation (11) into the variational integral (8) leads to the result

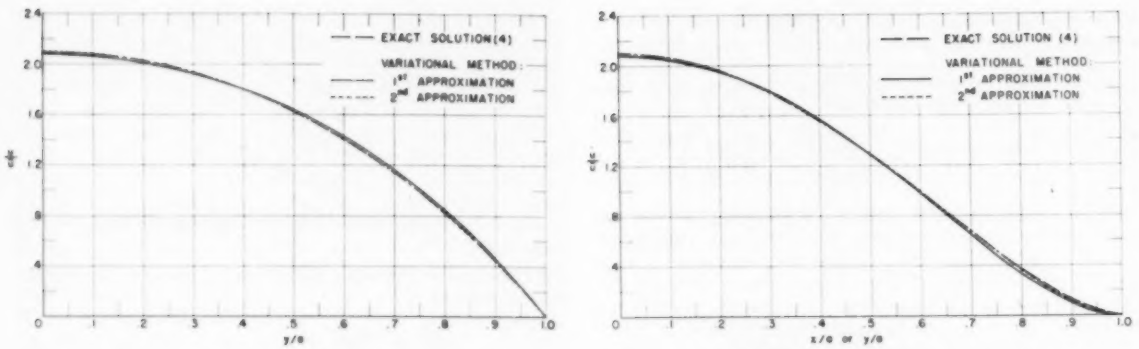

(a) Profile along axis of symmetry $\left(x = 0,\ 0 \leq \frac{y}{a} \leq 1\right)$ (b) Profile along diagonal ($x = y$)

Fig. 3 Laminar velocity distribution in a square duct

$$\frac{I}{4a^6} = 0.71111\,A_0^2a^2 + 0.29799\,A_1^2a^6 + 0.010642\,A_2^2a^{10} + 0.48762\,A_0A_1a^4 + 0.040635\,A_0A_2a^6 + 0.077400\,A_1A_2a^8 + C\left(\frac{8}{9}\,A_0 + \frac{16}{45}\,A_1a^2 + \frac{8}{225}\,A_2a^4\right) \quad (12)$$

To find the values of A_0, A_1, and A_2 which will make I a minimum, we differentiate equation (12) with respect to each A and set the resulting equations equal to zero. This operation yields

$$\frac{\partial I}{\partial A_0} = 0 \rightarrow 1.4222\,A_0a^2 + 0.48762\,A_1a^4 + 0.040635\,A_2a^6 + \frac{8}{9}\,C = 0$$

$$\frac{\partial I}{\partial A_1} = 0 \rightarrow 0.48762\,A_0a^2 + 0.59598\,A_1a^4 + 0.077400\,A_2a^6 + \frac{16}{45}\,C = 0$$

$$\frac{\partial I}{\partial A_2} = 0 \rightarrow 0.040635\,A_0a^2 + 0.077400\,A_1a^4 + 0.021284\,A_2a^6 + \frac{8}{225}\,C = 0$$

Simultaneous solution of this group of linear algebraic equations provides the following values

$$A_0 = -\frac{0.58984\,C}{a^2}, \qquad A_1 = -\frac{0.082030\,C}{a^4}, \qquad A_2 = -\frac{0.24610\,C}{a^6}$$

The mean velocity is computed from its definition, giving

$$\bar{u} = \frac{1}{a^2}\int_0^a\int_0^a u\,dxdy = \frac{4}{9}\,A_0a^6 + \frac{8}{45}\,A_1a^8 + \frac{4}{225}\,A_2a^{10} = -0.28111\,Ca^4$$

After substituting the A values into equation (11) and dividing by the mean velocity, we find

$$\frac{u}{\bar{u}} = \frac{1}{0.28111\,a^6}(x^2 - a^2)(y^2 - a^2)[0.58984\,a^4 + 0.082030\,a^2(x^2 + y^2) + 0.24610\,x^2y^2] \quad (11a)$$

Velocity profiles evaluated from equation (11a) are compared with the exact solution in Fig. 3. The agreement is very good, and it is seen that the exact solution is approached more and more closely as more terms are added to the approximating polynomial for u.

Now that accurate velocity distributions have been computed for the square duct, we may proceed to solve the heat-transfer problem.

The Square Duct With Uniform Peripheral Temperature. The first heat-transfer situation to be considered is a square duct whose walls have a uniform temperature around each cross section, while the heat transfer per unit length in the axial direction is constant. Under these conditions it is clear that the wall temperature will increase from section to section along the length of the passage.

For this situation, we may use the variational integral (9) without essential modification. For convenience, we introduce dimensionless variables

$$\Phi = \frac{T - T_w}{Q/8k}, \quad X = x/a, \quad Y = y/a$$

and rewrite equation (9) as

$$I = \int_{-1}^{+1}\int_{-1}^{+1}\left(\Phi_X^2 + \Phi_Y^2 + 4\,\frac{u}{\bar{u}}\,\Phi\right)dX\,dY \quad (9a)$$

where the condition at the duct boundaries is that $\Phi = 0$. When the temperature around the boundary is uniform, the temperature distribution across the section would be expected to have a shape not too different from the velocity. So, as a first approximation for Φ, we select a simple polynomial having a form similar to equation (10), i.e.,

$$\Phi = (X^2 - 1)(Y^2 - 1)[c_0 + c_1(X^2 + Y^2)] \quad (13)$$

Then, this expression for Φ is introduced into the variational integral (9a) along with $u/\bar{u}$ from equation (10). After carrying out the integration and minimizing (by differentiation), there results two linear algebraic equations for computing the unknown c_0 and c_1. When these constants have been determined, the expression for Φ becomes

$$\Phi = (X^2 - 1)(Y^2 - 1)[-0.9276 + 0.1368(X^2 + Y^2)] \quad (13a)$$

Once the temperature distribution is known, we may proceed to find the Nusselt number. Using the definitions[3]

$$\mathrm{Nu} \equiv \frac{hD_e}{k}, \qquad h \equiv \frac{Q}{\text{Perimeter} \times (T_w - T_b)} \quad (14)$$

[3] The perimeter appearing the definition of h is the *heated* perimeter.

and noting that for a square duct: $D_e = 2a$, perimeter $= 8a$; the Nusselt number expression becomes

$$\mathrm{Nu} = \frac{Q/k}{4(T_b - T_w)} \equiv \frac{2}{\Phi_b}$$

The dimensionless bulk temperature Φ_b may be computed from the usual definition

$$\Phi_b = \int_0^1 \int_0^1 \Phi(u/\bar{u})dX\,dY = -0.5555$$

Then, the final result for the square duct with uniform peripheral wall temperature is

$$\mathrm{Nu} = 3.60 \tag{15}$$

An exact calculation by Marco and Han [5] gives a value in precise agreement (to three significant figures) with equation (15). Hence there is no need to use more complex approximations for Φ or for $u/\bar{u}$.

The Square Duct With Uniform Peripheral Heat Flux. The next situation to be considered is the square duct with a uniform heat flux around the walls of each cross section, as well as uniform heat input per unit length in the axial direction. The condition of uniform heat flux is equivalent to the requirement that the normal derivative of the temperature be constant at all the duct walls. This type of boundary condition is not consistent with the variational integral as given in equation (9). However, there is no difficulty in deriving an alternate variational integral which will apply for the situation under consideration.

To accomplish this, we write the temperature T as the following sum

$$T = T_1 + \frac{Q}{16ka^2}(x^2 + y^2) \tag{16}$$

Now, the condition of uniform heat flux requires that

$$(\partial T/\partial n)_{\text{wall}} = Q/8ka$$

where n is direction of the (outward) normal to the duct walls. It then follows by differentiation of equation (16) that $\partial T_1/\partial n$ is identically zero on all the boundaries. The differential equation for T_1 is found by substitution in equation (7), giving

$$\frac{\partial^2 T_1}{\partial x^2} + \frac{\partial^2 T_1}{\partial y^2} = \frac{Q}{4a^2}\left(\frac{u}{\bar{u}} - 1\right) \tag{17}$$

The variational integral corresponding to this differential equation is found by inspection to be

$$I = \int_{-1}^{+1}\int_{-1}^{+1}\left[(\phi_{1X})^2 + (\phi_{1Y})^2 + 4\left(\frac{u}{\bar{u}} - 1\right)\phi_1\right]dX\,dY \tag{18}$$

where $\phi_1 = T_1/(Q/8k)$ and X and Y are dimensionless co-ordinates. That the differential equation (17) actually corresponds to the integral (18) is assured because T_1 possesses proper boundary conditions.

To use the variational integral (18) we must select a trial function which has zero normal derivatives at the boundaries. For example, we might choose

$$\phi_1 = (X^2 - 1)^2(Y^2 - 1)^2[d_0 + d_1(X^2 + Y^2)] \tag{19}$$

This, however, would be an unfortunate choice, since not only do the normal derivatives vanish at $X = \pm 1$, $Y = \pm 1$, but also ϕ_1 itself vanishes. Hence equation (19) does not provide any freedom in the variation of the temperature around the bounding walls and, in fact, this variation is already specified by the last term on the right side of equation (16).

As a more suitable first approximation, we select the following expression for ϕ_1:

$$\phi_1 = e_0[(X^2 - 1)^2 + (Y^2 - 1)^2] + e_1(X^2 - 1)^2(Y^2 - 1)^2 \tag{20}$$

Since the simple velocity expression of equation (10) led to favorable Nusselt number results in the last example, we shall use it again, at least for a first approximation. Inserting equations (20) and (10) into the variational integral (18) leads to

$$I = \frac{512}{315}\left(6e_0^2 + \frac{32}{5}e_0e_1 + \frac{256}{105}e_1^2 + 2.7743\,e_0 + 1.6741\,e_1\right)$$

Differentiating with respect to e_0 and e_1 to determine the values which minimize I gives the two equations

$$\frac{\partial I}{\partial e_0} = 0 \rightarrow 12e_0 + \frac{32}{5}e_1 + 2.7743 = 0$$

$$\frac{\partial I}{\partial e_1} = 0 \rightarrow \frac{32}{5}e_0 + \frac{512}{105}e_1 + 1.6741 = 0$$

which are satisfied by $e_0 = -0.16032$, $e_1 = -0.13290$. Using these constants in conjunction with equations (16) and (20) provides the temperature distribution as follows:

$$\phi = \frac{T}{Q/8k} = \phi_1 + \frac{X^2 + Y^2}{2}$$

$$= \frac{X^2 + Y^2}{2} - 0.16032[(X^2 - 1)^2 + (Y^2 - 1)^2] - 0.13290(X^2 - 1)^2(Y^2 - 1)^2 \tag{21}$$

The Nusselt number and heat-transfer coefficient are again defined as in equation (14), except that T_w must now be regarded as the average value of the wall temperature which varies around the periphery. Introducing the dimensionless temperature ϕ and using a bar to denote an average, the Nusselt number becomes

$$\mathrm{Nu} = \frac{2}{\bar{\phi}_w - \phi_b} \tag{22}$$

The average wall temperature and the bulk temperature which appear in equation (22) are found by integrating the temperature distribution (21) as follows:

$$\bar{\phi}_w \equiv \frac{1}{2}\left[\int_0^1 (\phi)_{X=1}\,dY + \int_0^1 (\phi)_{Y=1}dX\right] = 0.5814 \tag{23}$$

$$\phi_b \equiv \int_0^1\int_0^1 \phi\left(\frac{u}{\bar{u}}\right)dX\,dY = -0.06803 \tag{24}$$

With these values, the Nusselt number result is

$$\mathrm{Nu} = 3.09 \tag{25}$$

To check the accuracy of this result, we proceed to reapply the variational method with more complex expressions for the velocity and temperature distributions. For the velocity, equation (11a) will be used, while the temperature distribution is written as follows:

$$\phi = \frac{X^2 + Y^2}{2} + \phi_1$$

$$= \frac{X^2 + Y^2}{2} + f_0[(X^2 - 1)^2 + (Y^2 - 1)^2] + f_1(X^2 - 1)^2(Y^2 - 1)^2 + f_2[(X^2 - 1)^2 + (Y^2 - 1)^2]$$

Evaluating the variational integral (18) and following the same minimizing procedure as before, it is found that

$f_0 = -0.17532, \qquad f_1 = -0.14003, \qquad f_2 = -0.020761$

The values of $\bar{\phi}_w$ and ϕ_b needed in computing the Nusselt number may be evaluated from the defining equations (23) and (24), giving

$$\bar{\phi}_w = 0.5826 \qquad \phi_b = -0.0654$$

Finally, substitution into equation (22) leads to

$$\mathrm{Nu} = 3.09 \tag{26}$$

This result is identical (to three significant figures) to that obtained by use of the simpler velocity and temperature profiles [see equation (25)]. Hence there is no need to continue the problem by using still more complex profiles.

The square duct with uniform peripheral heat flux was studied by Cheng [6] using separation of variables, and this led to rather involved results in the form of infinite series. He computed a Nusselt number of 3.82, but this value appears inconsistent with his results for rectangular ducts of higher aspect ratios and hence may be in error. A computation by Irvine [7] using a finite difference procedure yielded a Nusselt number of 2.9, a deviation of 6 per cent from the current results.

Flat Rectangular Duct With Uniform Peripheral Heat Flux. Next, we turn to flow in a flat rectangular duct and, in particular, to a duct with aspect ratio $\gamma = b/a = 10$. The situation of uniform peripheral heat flux will be considered first.

An approximation for the velocity distribution in a flat rectangular duct can be taken directly from the solution of the corresponding torsion problem (ref. [3], p. 285), i.e.,

$$\frac{u}{\bar{u}} = \frac{3}{2}(1 - X^2)\,\frac{1 - e^{-\gamma\sqrt{\frac{5}{2}}(1-Y)}}{1 - 0.632/\gamma} \tag{27}$$

where $X = x/a$ and $Y = y/b$.

It is noted that this form is not symmetric in Y, and as written only applies when Y is positive. A comparison with the tabulation of the exact solution given in reference [4] shows that equation (27) is a good representation of the velocity, and its use poses no special problems if care is exercised with regard to signs.

To formulate the problem for a rectangular duct with uniform peripheral heat flux, it is only necessary to retrace the steps already taken for the square duct. In a manner analogous to equation (16), we write the temperature T as

$$T = T_1 + \frac{Q}{8(1+\gamma)k}(X^2 + \gamma Y^2) \tag{28}$$

For $\gamma = 1$ (square duct), equations (28) and (16) coincide. It is easily verified that $\partial T_1/\partial n$ must vanish on all the boundaries of the rectangle in order that the condition of uniform peripheral heat flux be satisfied $\left(\text{i.e., } \left.\frac{\partial T}{\partial n}\right|_{\text{wall}} = \frac{Q}{4(a+b)k}\right)$. Further, the variational integral corresponding to equation (18) becomes

$$I = 4\int_0^{+1}\int_0^{+1}\left[(\phi_{1X})^2 + \frac{1}{\gamma^2}(\phi_{1Y})^2 + \frac{2(1+\gamma)}{\gamma}\left(\frac{u}{\bar{u}} - 1\right)\phi_1\right]dX\,dY \tag{29}$$

where $\phi_1 = T_1\Big/\dfrac{Q}{4(1+\gamma)k}$. We are now in a position to use this integral to find the temperature distribution.

As a first approximation for ϕ_1, we select a function of the same form as has already been used for the square, i.e.,

$$\phi_1 = g_0(X^2 - 1)^2 + g_1(Y^2 - 1)^2 + g_2(X^2 - 1)^2(Y^2 - 1)^2 \tag{30}$$

This expression is introduced in integral (29) along with the velocity (27). After minimizing the integral, the constants in the resulting simultaneous equations were determined for an aspect ratio $\gamma = 10$. This yielded the following temperature distribution

$$\phi = \frac{T}{Q/4(1+\gamma)k} = \frac{X^2 + 10Y^2}{2} - 0.11703(X^2 - 1)^2 - 3.0660(Y^2 - 1)^2 - 0.038328(X^2 - 1)^2(Y^2 - 1)^2 \tag{31}$$

The Nusselt number is again defined by equation (14), where T_w is interpreted as the average wall temperature. For a rectangular duct heated on all boundaries

$$D_e = 4a\left(\frac{\gamma}{\gamma+1}\right), \quad \text{heated perimeter} = 4(a+b)$$

In terms of ϕ, the Nusselt number becomes

$$\mathrm{Nu} = \frac{4}{\bar{\phi}_w - \phi_b}\,\frac{\gamma}{1+\gamma} \tag{32}$$

The average wall temperature and the bulk fluid temperature may be computed from

$$\bar{\phi}_w = \frac{1}{a+b}\left[\int_0^b (\phi)_{x=a}\,dy + \int_0^a (\phi)_{y=b}\,dx\right] = \frac{1}{1+\gamma}\left[\gamma\int_0^1 (\phi)_{X=1}\,dY + \int_0^1 (\phi)_{Y=1}\,dX\right] \tag{33}$$

$$\phi_b = \int_0^1\int_0^1 \frac{u}{\bar{u}}\,\phi\,dX\,dY \tag{34}$$

The numerical values of these quantities corresponding to equation (31) for ϕ and equation (27) for $u/\bar{u}$ are

$$\bar{\phi}_w = 0.9472, \qquad \phi_b = -0.2537$$

The corresponding Nusselt number is 3.03.

In addition to the Nusselt number, which represents an averaging of the heat-transfer performance around the periphery, it is of interest to know the wall temperature variation around the boundary. This has been evaluated from equation (31) and is plotted in Fig. 4. The hot spot in the duct corner is strikingly displayed there.

Higher order approximations for the temperature profile were then employed to investigate the accuracy of the predictions of Nusselt number and wall temperature variation. Since the temperature variation in the y-direction is much larger than that in the x-direction, the original expression (30) was modified by adding polynomials in y to provide more degrees of freedom. For the second approximation, a term $g_3(Y^2 - 1)^3$ was added to equation (30). After evaluation of the constants $g_0, \ldots g_3$, by application of variational method, the expression for the temperature distribution became

$$\phi = \frac{T}{Q/4(1+\gamma)k} = \frac{X^2 + 10Y^2}{2} - 0.11703(X^2 - 1)^2 - 6.9554(Y^2 - 1)^2 - 0.038328(X^2 - 1)^2(Y^2 - 1)^2 - 3.8894(Y^2 - 1)^3 \tag{35}$$

Computation of $\bar{\phi}_w$ and ϕ_b from equations (33) and (34) leads to values of 0.67779 and -0.58018, respectively. This yields a Nusselt number of 2.89, which is 4.5 per cent lower than that found for the first approximation.

This change in the Nusselt number suggests that still another

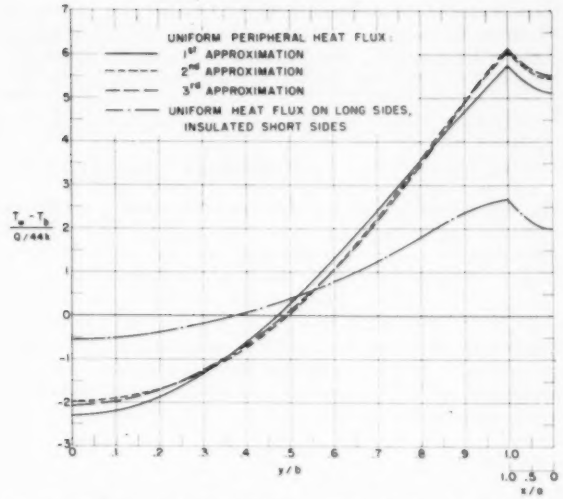

Fig. 4 Wall temperature distribution for fully developed heat transfer in a rectangular duct of aspect ratio 10

term be added to the approximation for the temperature distribution. After affixing the term $g_4(Y^2 - 1)^4$ and following through the variational procedure to determine the constants, the resulting temperature distribution is

$$\phi = \frac{X^2 + 10Y^2}{2} - 0.11703(X^2 - 1)^2 - 10.291(Y^2 - 1)^2 - 0.038328(X^2 - 1)^2(Y^2 - 1)^2 - 12.05(Y^2 - 1)^3 - 4.9697(Y^2 - 1)^4 \quad (36)$$

This gives an average wall temperature, $\bar{\phi}_w = 0.6143$, and a bulk temperature $\phi_b = -0.6379$; with a corresponding value of 2.90 for the Nusselt number. The very close agreement of this result with that of the previous approximation indicates that further refinement of the temperature distribution is not necessary. It is worth while noting that this Nusselt number agrees closely with the value 2.88 given by Cheng's [6] exact solution.

The wall temperature variations corresponding to the successive variational calculations are shown in Fig. 4. The figure illustrates the manner in which the sequence of solutions converges to the final result.

As has already been pointed out in reference [6], the Nusselt number for rectangular ducts with uniform peripheral heat flux remains at a value of about 3 as the aspect ratio increases from 1 to 10. This is in contrast to the situation of uniform peripheral wall temperature (with constant heat input per unit length), where the Nusselt number increases from 3.60 to 6.79 as the aspect ratio changes from 1 to 10, and approaches 140/17 (8.23) as the aspect ratio approaches infinity. The Nusselt number for flow between infinite parallel plates with uniform axial heat flux is also 140/17. So, the parallel plate channel represents the limiting situation for the rectangular duct with uniform peripheral wall temperature. An important practical consequence is that the parallel plate model cannot be used to predict hot spot (corner) temperatures when the heat flux is uniform around the periphery.

The Flat Duct With Partially Insulated Walls. The severe corner hot spots which are indicated in Fig. 4 are in some part due to the stipulation of uniform heat flux on the short end walls. In some applications, e.g., reactor core assemblies,[4] it is likely that the short end walls would essentially be insulated. We now proceed to investigate, using variational techniques, the situation where there is uniform heat flux along the long sides of the rectangle, with the short sides being insulated. The aspect ratio γ will again be taken as 10. The analysis follows closely that which has been already presented for the flat duct with uniform heat flux all around the periphery.

To reduce the problem to one which is suitable for the variational method, we write the temperature as

$$T = T_1 + \frac{Q}{8\gamma k} X^2 \quad (37)$$

where X represents x/a as before. In order to satisfy the conditions that

$$\frac{\partial T}{\partial x} = \pm\frac{Q}{4bk} \text{ at } x = \pm a, \qquad \frac{\partial T}{\partial y} = 0 \text{ at } y = \pm b$$

it is necessary that $\partial T_1/\partial n$ be zero on all the boundaries. For convenience, we may rephrase equation (37) as

$$\phi = \phi_1 + \frac{\gamma + 1}{\gamma}\frac{X^2}{2} \quad (38)$$

where $\phi = T \Big/ \frac{Q}{4(1 + \gamma)k}$ and $\phi_1 = T_1 \Big/ \frac{Q}{4(1 + \gamma)k}$. It is easily verified that the variational integral for ϕ_1 is again given by equation (29). Inasmuch as ϕ_1 must satisfy the same equations and boundary conditions as in the preceding illustrative problem, we may make direct use of the previous results. Then, the result for the temperature distribution corresponding to $\gamma = 10$ may immediately be written as

$$\phi = \frac{11}{10}\frac{X^2}{2} - 0.11703\,(X^2 - 1)^2 - 10.291(Y^2 - 1)^2 - 0.038328(X^2 - 1)^2(Y^2 - 1)^2 - 12.05(Y^2 - 1)^3 - 4.9697(Y^2 - 1)^4 \quad (39)$$

The average wall temperature and fluid bulk temperature can be computed from equations (33) and (34), giving: $\bar{\phi}_w = -1.3038$ and $\phi_b = -2.1095$. The Nusselt number is then evaluated from the basic definition (14). After noting that the *heated* perimeter is $4b$, the Nusselt number expression becomes

$$\text{Nu} = \frac{4}{\bar{\phi}_w - \phi_b} = 4.96$$

This value for the Nusselt number lies between those for uniform peripheral heat flux and uniform peripheral wall temperature.

The wall temperature variation as computed from equation (39) is plotted in Fig. 4. On that figure there also appear curves giving the corresponding results for uniform heating all around the periphery. A comparison may be made at the same heat input per unit length (i.e., same Q). It is seen that insulating the end walls leads to a significant decrease in the hot spot temperature at the duct corners.

Velocity Distribution in a Circular Sector. The problems heretofore considered have been concerned with rectangular geometry. Now, we turn to a very different configuration: The case of heat transfer in a duct whose cross section is a circular sector. The co-ordinate system is shown in Fig. 2.

The velocity distribution will be considered first. Using dimensionless variables $\Theta = \theta/\theta_0$ and $R = r/r_0$, we write a first approximation for the velocity distribution as

$$u = (\Theta^2 - 1)R^2(1 - R^2)(m_1 + m_2R) + (\Theta^4 - 1)R^2(1 - R^2)(m_3 + m_4R) \quad (40)$$

[4] An often-used reactor core assembly is composed of parallel fuel plates, producing essentially uniform heat flux, supported at their edges by unheated structural materials.

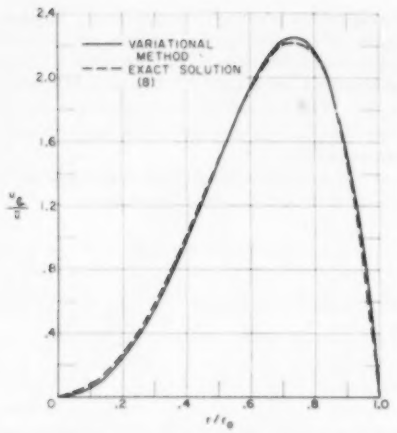

Fig. 5 Velocity distribution along symmetry line ($\theta = 0$) for laminar flow in a circular-sector duct, opening angle 33.4 deg

where the $m_1, \ldots m_4$ are constants to be determined by application of the variational method. Equation (40) is introduced into the variational integral (8*a*), and the minimizing process is carried out by differentiating with respect to each of the m's and setting the resulting equations equal to zero. In this way, four equations are provided for computing the $m_1, \ldots m_4$. The numerical calculations were carried out for a duct of *33.4-deg opening angle* so that a direct comparison could be made with the exact solution of reference [8].

The mean velocity may be computed by integrating as follows

$$\bar{u} = \int_0^{r_0}\int_0^{\theta_0} u\, r\, dr\, d\theta \Big/ \int_0^{r_0}\int_0^{\theta_0} r\, dr\, d\theta \qquad (41)$$

Then, the normalized velocity distribution resulting from the variational procedure is

$$\frac{u}{\bar{u}} = \frac{1}{0.007575}\left[(\Theta^2 - 1)R^2(1 - R^2)(-0.05724 - 0.004605\,R) + (\Theta^4 - 1)R^2(1 - R^2)(0.01675 - 0.033873\,R)\right] \quad (40a)$$

The velocity distribution along the symmetry line ($\theta = 0$) has been calculated from equation (40*a*) and is plotted in Fig. 5. Also included is a curve representing the exact solution [8]. The agreement is seen to be very good.

The relationship between the friction factor and Reynolds number may also be evaluated once the velocity distribution is known. Based on equation (40*a*), we find that

$$c_f \cdot \mathrm{Re} = 53.79$$

The exact solution gives a value of 53.75 for the constant.

Circular Sector With Uniform Peripheral Temperature. Having determined the velocity distribution, we now turn to the heat-transfer problem. We shall consider the situation where the walls have a uniform temperature around each cross section, while the heat transfer per unit length in the axial direction is a constant. Under these conditions, the variational integral of equation (9*a*) applies without modification.

For convenience, let T in this equation represent the difference between the temperature at any point in the fluid and the wall temperature; consequently, $T = 0$ on the boundaries. It is expected that the reduced temperature distribution would have a shape generally similar to that of the velocity. So, we select a function of the same form as equation (40). This expression, along with the velocity (40*a*), is introduced into the variational integral (9*a*). The end result of the computational process is

$$\frac{T - T_w}{Q/k\theta_0} \equiv \beta = (\Theta^2 - 1)R^2(1 - R^2)(0.037613 + 0.12061R) + (\Theta^4 - 1)R^2(1 - R^2)(-0.010928 - 0.010200\,R) \quad (42)$$

The bulk fluid temperature is obtained by integrating as follows

$$\beta_b = \frac{\int_0^{r_0}\int_0^{\theta_0} u\beta\, r\, dr\, d\theta}{\int_0^{r_0}\int_0^{\theta_0} u\, r\, dr\, d\theta} = -0.01629$$

Finally, the Nusselt number may be evaluated from the basic definition (14) after observing that the equivalent diameter and heated perimeter for a circular sector are $2r_0\theta_0/(\theta_0 + 1)$ and $2r_0(\theta_0 + 1)$, respectively. So,

$$\mathrm{Nu} = -\left(\frac{\theta_0}{\theta_0 + 1}\right)^2 \frac{1}{\beta_b} = 3.12$$

This is about 3 per cent higher than the value given by the exact solution in reference [8].

Concluding Remarks

The specific problems considered here are meant to illustrate the method and by no means exhaust the situations to which the variational technique may be applied. In addition to numerous other laminar flow configurations, it may be possible to make application to the turbulent situation, provided that suitable choices are made for the trial functions.

The authors are currently extending the variational method to the thermal entrance region of ducts.

Acknowledgment

The authors would like to acknowledge the very valuable discussions on variational methods with Dr. Stephen H. Maslen of the NASA Lewis Research Center.

References

1 M. A. Biot, "New Methods in Heat Flow Analysis With Application to Flight Structures," *Journal of Aeronautical Sciences*, vol. 24, 1957, pp. 857–873.

2 F. B. Hildebrand, "Methods of Applied Mathematics," Prentice-Hall, Inc., New York, N. Y., 1952, chapter 2.

3 S. Timoshenko and J. N. Goodier, "Theory of Elasticity," second edition, McGraw-Hill Book Company, Inc., New York, N. Y., 1951, p. 280.

4 R. W. Smith, Jr., H. E. Edwards, and S. R. Brinkley, Jr., "Tables of Velocity of Steady Laminar Flow in Channels of Rectangular Cross Section," Bureau of Mines Report 4885, July, 1952.

5 S. M. Marco and L. S. Han, "A Note on Limiting Laminar Nusselt Number in Ducts With Constant Temperature Gradient by Analogy to Thin-Plate Theory," TRANS. ASME, vol. 77, 1955, pp. 625–630.

6 H. M. Cheng, "Analytical Investigation of Fully Developed Laminar-Flow Forced Convection Heat Transfer in Rectangular Ducts With Uniform Heat Flux," MS thesis, M.I.T., 1957.

7 Personal correspondence with Prof. Thomas F. Irvine, Jr., Department of Mechanical Engineering, University of Minnesota.

8 E. R. G. Eckert, T. F. Irvine, Jr., and J. T. Yen, "Local Laminar Heat Transfer in Wedge-Shaped Passages," TRANS. ASME, vol. 80, 1958, pp. 1433–1438.

DISCUSSION

Andrew A. Fejer[5]

The variational method developed in this interesting paper represents a valuable addition to techniques being used currently in solving heat-transfer problems. The authors demonstrate that this method can be used effectively to calculate heat-transfer rates and temperature distributions in laminar flows occurring in ducts of various shapes and for various types of thermal boundary conditions. And, as indicated by the authors, the method will, no doubt, be found useful also in connection with other types of heat-transfer problems. However, there are some questions suggesting themselves regarding the results obtained in some of the illustrative problems. In the case of the rectangular duct with uniform peripheral wall temperature and uniform axial heat flux, i.e., for $\partial T_w/\partial x = \partial T_w/\partial y = 0$ and $dT_b/dx = c$, the authors find that the Nusselt number increases from 3.6 at aspect ratio 1 to 6.79 at aspect ratio 10, approaching 8.23 as the aspect ratio goes to ∞. This result is in good agreement with the results of the numerical solution of Clark and Kays.[6]

On the other hand, for uniform peripheral and axial heat flux, i.e., $\partial T_w/\partial n = \text{const}$ and $dT_b/dx = \text{const}$, the authors find a Nusselt number of about 3 over a range of aspect ratios from 1 to 10. It is difficult to reconcile this finding with the fact that for infinite aspect ratio (i.e., the two-dimensional case) both temperature and heat flux are constant along the periphery of the duct and Nu = 8.23 in this case. In this connection it may be of interest to examine the form of the Nusselt number as defined by the authors for the case of uniform peripheral heat flow:

$$\text{Nu} = \frac{4}{\bar{\phi}_w - \phi_b} \frac{\gamma}{1 - \gamma}$$

where $\bar{\phi}_w$ is the average wall temperature along the duct periphery. In view of the fact that Nusselt number may be considered as a ratio of the temperature gradient at the wall to the temperature difference across the fluid in the duct, it would, perhaps, be more meaningful physically to define a local Nusselt number along the periphery and to use its average to describe heat-transfer processes when peripheral variations of temperature occur.

William C. Reynolds[7]

Comments based on research work in progress on Foundations of Irreversible Thermodynamics under sponsorship of Air Force Office of Scientific Research Contract AF49(638)-201. Reproduction in whole or in part for any purpose of the U. S. Government is authorized.

The Ritz-Galerkin method is indeed a powerful one, and it is gratifying to see it used effectively in convection problems.

To the uninitiated, variational methods may seem rather like magic, particularly if the physical significance is not apparent. The variational formulations of elasticity phenomena can be developed from notions of "minimum strain energy"; one might expect that the variational equations for laminar flow might also be derived from some sort of a physical extremum principle, and this is in part true. There is a particular type of variational problem called the "isoperimetric" problem in which an extremum is sought for one integral, subject to the condition that another integral is a *constant* [1].[8] Classically one seeks the curve of fixed length which encloses the biggest area, and the isoperimetric solution is the circle. The hydrodynamic portion of the laminar flow problem [authors' equation (8)] can be formulated in this manner, with an extremum being sought for the integral

$$D = \int_A \mu(u_x^2 + u_y^2)dA = \min \tag{43}$$

subject to the restraint imposed by continuity that

$$\int_A \rho u dA = Au_m\rho = w = \text{const} \tag{44}$$

By formulating the problem in this manner a certain physical significance can be seen; the rate of *dissipation* of mechanical energy D [2] is to be a *minimum*, subject to the condition that the total *flow rate* is *constant*. That is to say, one examines all possible velocity profiles which have the same total flow rate, and zero velocity at the wall; the *actual* velocity profile is the one for which the *rate of dissipation is the least*! This physical formulation is quite appealing, and not too unreasonable; it can be looked upon as a "path-of-least-resistance" statement. Several well-known laminar flow problems have been handled by W. L. Rogers [3] using minimum dissipation as a basic postulate instead of the momentum principle. These include essentially the whole class of fully established laminar flows.

This physical picture may provide the insight which will eventually let *turbulent* flow problems be treated in the same manner. It may be easily shown from friction factor measurements that the dissipation in a given tube for turbulent flow is considerably *greater* than the dissipation in laminar flow at the same flow rate. Malkus [4] has proposed a theory for fully developed turbulent flow between infinite parallel plates in which he extremizes the dissipation rate. He suggests that the flow is such that the dissipation rate is a *maximum*. It may well be that it is in reality again a *minimum*, this time selected from a *different family* of admissible flows. As an analogy, consider the classical "soap film" problem in which a soap film is stretched between two co-axial opposed wire hoops; elasticity theory says that the soap film is shaped such that the surface area is a minimum. The variational formulation yields a *catenary* as the surface of revolution for the film connecting the two hoops. However, as the hoops are moved farther and farther apart, the catenary film becomes unstable; the film eventually breaks, and the soap forms a thin circular membrane inside each hoop. The resulting discontinuous surface consisting of two disks is another surface of least area, but it is decidedly different in character. Perhaps the same sort of thing happens in transition from laminar to turbulent flow. Initially the laminar flow is the one of least dissipation; as the flow rate is raised, the laminar flow becomes unstable, and another flow of minimum dissipation appears. In a sense the laminar dissipation is the "minimum-minimum" and the turbulent dissipation is the "maximum-minimum." It can be hoped that continued effort will lead to a variational formulation of turbulent flow phenomena which will complement the laminar formulation presented by the authors.

The heat-transfer part of the problem may also be formulated in an isoperimetric manner. If the flow is isothermal, the variational formulation is equivalent to seeking the temperature profile which provides *minimum production of entropy* [5, 6] subject to the condition that the heat input is fixed. But this is not very satisfying, since heat transfer requires temperature variations. Perhaps continued effort in the area of irreversible thermodynamics will shed more light on the physical significance of the variational formulation for the temperature profile.

Finally, it should be pointed out that the authors fail to verify that their integrals are *minimums* and not *maximums*. This is quite important, for the relative accuracy of solutions can be readily determined by comparison of the values of the corresponding integrals, the best solution being the one for which the integrals are *least* (or biggest, as the case may be). The

---

[5] Director, Department of Mechanical Engineering, Illinois Institute of Technology, Chicago, Ill.

[6] S. H. Clark and W. M. Kays, TRANS. ASME, vol. 75, 1953, p. 859.

[7] Assistant Professor, Department of Mechanical Engineering, Stanford University.

[8] Numbers in brackets designate References at end of this discussion.

condition that the integrals be a *minimum* is given by the *second variation* [7] and in the authors' nomenclature is

$$F_{V_x V_x} > 0$$

$$F_{V_y V_y} > 0$$

By inspection of the integrals of the authors' equations (8) and (9), it is seen that both extremals are indeed minimums.

References

1 Weinstock, "Calculus of Variations," McGraw-Hill Book Company Inc., New York, N. Y., 1952.
2 Lamb, Hydrodynamics.
3 W. L. Rogers, "An Introduction to the Study of Extremum Principles and Thermodynamic Equilibrium," PhD dissertation, Stanford University, being prepared.
4 W. V. R. Malkus, "Outline of a Theory for Turbulent Shear Flow," *Journal of Fluid Mechanics*, vol. 1, part 5, November, 1956.
5 I. Prigogine, "Introduction to Thermodynamics of Irreversible Processes," C. C. Thomas, Springfield, Ill., 1955.
6 M. A. Biot, "Variational Principles in Irreversible Thermodynamics With Application to Viscoelasticity," *Physical Review*, vol. 97, no. 6, March, 1955, p. 1463.
7 R. Courant and D. Hilbert, "Methods of Mathematical Physics," vol. 1, Interscience Publishers, New York, N. Y., 1953, p. 214.

Myron Tribus[9]

The method used by the authors is of greater generality than they claim. Two problems which can be solved by their methods are as follows: Consider the square duct shown in Fig. 1; but let there be a nonuniform temperature on the periphery. It is only necessary to invent a function $f(x, y)$ such that $f(x, y)$ is analytic inside the duct and is equal to the prescribed wall temperature on the duct wall. Then one considers that the temperature is composed of two parts according to $T = T_1 + f$ substituted in Equation (7) to give

$$k\left(\frac{\partial^2 T_1}{\partial x^2} + \frac{\partial^2 T_1}{\partial y^2}\right) = \frac{u}{\bar{u}}\,\frac{Q}{A} - k\left(\frac{\partial^2 f}{\partial x^2} + \frac{\partial^2 f}{\partial y^2}\right)$$

for which the boundary condition is $T_1 = 0$ on the walls. Instead of Equation (9), one obtains

$$I = \int_{-a}^{+a}\int_{-a}^{+a}\left\{T_x^2 + T_y^2 + \left[2\left(\frac{u}{\bar{u}}\,\frac{Q}{Ak}\right) - 2\left(\frac{\partial^2 f}{\partial x^2} + \frac{\partial^2 f}{\partial y^2}\right)\right]T\right\}dxdy \quad (45)$$

which may, of course, be solved by the methods given in the paper. Therefore the methods given can be used in the case where the wall temperature is nonuniform.

The authors' method may also be used for nonhomogeneous boundary conditions. Again consider the duct of Fig. 1 but let there be external thermal conductances such that around each boundary

$$\frac{\partial T}{\partial n} - hT = 0$$

For example, let $h = h_1$ along $x = +a$, $h = h_2$ along $x = -a$, $h = h_3$ along $y = +a$, $h = h_4$ along $y = -a$.

To handle this kind of boundary condition substitute $T = g(x, y)\cdot T_1(x, y)$ in Equation (7) to get

$$g\nabla^2 T_1 + 2\nabla g\cdot\nabla T_1 + T_1\nabla^2 g - G(x, y) = 0 \quad (46)$$

where

$$\nabla^2 \equiv \frac{\partial^2}{\partial x^2} + \frac{\partial^2}{\partial y^2} \qquad \nabla \equiv i\,\frac{\partial}{\partial x} + j\,\frac{\partial}{\partial y}$$

$$G \equiv \frac{u}{\bar{u}}\,\frac{Q}{A}$$

Dr. Sparrow has pointed out to me that, if we choose for our function g a function such that $\partial g/\partial n = gh$ on the contour, the boundary condition on T_1 becomes $\partial T_1/\partial n = 0$. This condition on g is the same as $\partial \ln g/\partial n = h$, hence it is usually not difficult to find the needed function g. It can be verified by the use of Equation (1) that letting

$$F = \frac{g^2}{2}\,(T_{1x}^2 + T_{1y}^2) + gGT_1 - \frac{g\nabla^2 g}{2}\,T_1^2 \quad (47)$$

leads to Equation (46). For the case considered a suitable function for g is

$$\ln g = \frac{1}{4a}\,[(x - a)^2 h_2 + (y - a)^2 h_4 + (x + a)^2 h_1 + (y + a)^2 h_3] \quad (48)$$

Using Equations (47) and (48), the authors' methods may therefore be applied to nonhomogeneous boundary conditions. By appropriate choice of the function g, other more complicated boundary conditions may be handled. It is probable that methods for doing so are already well described in the literature of other fields. The use of these methods in heat transfer is not common and the authors have rendered an important service in bringing this powerful technique to the attention of the readers of this journal. Applications to steady-state conduction are of course obvious. The writer looks forward to learning how the methods of Biot can be applied to convection-problems and hopes that the authors will report on this work soon.

Authors' Closure

The authors would like to thank the discussers for their very worth-while comments and additions to the content of the paper.

We agree with Professor Fejer that physical reasoning is deceiving in regard to the limiting case of infinite aspect ratio for a duct with uniform peripheral heat flux. Evidently, the heat addition at the short sides of a flat rectangular duct influences the fluid temperature distribution in such a way that the temperatures along the long sides of the duct become quite nonuniform. Thus, in the limit, the case of infinite parallel plates is not approached, since for this configuration the wall temperature would be uniform even for uniform wall heat flux. The Nusselt number defined in the paper is one of practical interest in that it provides a means for computing the average heat-transfer performance. Actually for the uniform peripheral wall heat flux case, the *details* of the wall temperature are of greatest significance, and it is for this reason that Fig. 4 has been included.

Professor Reynolds' comments on the general physical interpretation of variational methods are very interesting, especially in relation to turbulent flows. We are looking forward to seeing more of this work in the literature.

We would like to thank Professor Tribus for adding appreciably to the generality of the variational treatment by considering other types of wall boundary conditions. There are several qualifying remarks which appear appropriate to Professor Tribus' condition

$$\frac{\partial T}{\partial n} - hT = 0 \quad (49)$$

First, it should be noted that h is a conductance; that is, a heat-

[9] Associate Professor, Department of Engineering, University of California, Los Angeles, Calif. Mem. ASME.

transfer coefficient divided by a thermal conductivity. Also, the negative sign in the equation implies that n is the inward normal rather than the outward normal used in the paper. Of even greater importance are the restrictions which are imposed on the external temperature by the requirement of uniform axial heat transfer. To explore this, we rewrite condition (49) displaying the external temperature T_e and using k and h for thermal conductivity and heat-transfer coefficient, and n for the outward normal,

$$k \left.\frac{\partial T}{\partial n}\right|_w + h\,(T_w - T_e) = 0 \qquad (49a)$$

To prepare uniform axial heat transfer, the integral of the local heat flux around the duct periphery must be a constant independent of axial position. So, we have

$$\oint k \frac{\partial T}{\partial n}\, ds = \text{constant} = -\oint h(T_w - T_e) ds \qquad (50)$$

Now, the wall temperature is of the form

$$T_w = \left(\frac{\partial T}{\partial z}\right) z + m\,(x, y)$$

where $\partial T/\partial z$ is a constant for fully developed heat transfer. Thus the integral on the right side of equation (50) yields the condition

$$\oint h \left[\frac{\partial T}{\partial z}\, z + m(x, y) - T_e\right] ds = \text{constant}$$

In order for this to be satisfied, we have the restriction that T_e must vary linearly with z with the same slope as T_w. This may significantly limit the practical applicability of Professor Tribus' development relating to the condition (49).

In reference to his question about future work, we hope, as previously mentioned, to show how variational methods can be applied to the thermal entrance region of ducts.

The Effect of Surface Roughness on the Convection Heat-Transfer Coefficient for Fully Developed Turbulent Flow in Ducts With Uniform Heat Flux[1]

R. T. LANCET

Los Angeles, Calif.
Assoc. Mem ASME

Experimental data are presented for the heat-transfer coefficient and friction factor in a smooth and a rough duct with a hydraulic diameter of approximately 0.035 in. The flow was fully developed and turbulent, and the heat addition was uniform over the length of the tube. The rough tube indicated appreciable increases in heat-transfer coefficient and friction factor. The smooth-tube friction factors corresponded to rough-tube values, indicating the difficulty involved in obtaining smooth surfaces for very small ducts.

In some industrial applications it becomes necessary to make heating or cooling ducts so small that the roughness resulting from normal manufacturing techniques becomes large with respect to the tube radius. In such cases the heat-transfer coefficient and pressure drop may increase appreciably over that for a smooth pipe. In still other cases, it might be desirable to provide a rough surface to increase the heat-transfer rate where space is more important to power loss as a result of increased pressure drop.

The heat-transfer data for rough pipes is meager and of necessity limited to specific types of roughness. To date the primary type of roughness studied was of a continuous-ring type or thread type [5 and 6].[2] These tests indicated an increase in heat-transfer rate but also gave an even greater increase in friction factor.

The object of this experiment was to obtain some data on the effect of roughness in a very small duct and particularly to evaluate the effect of finite protrusions as compared to the continuous-ring type of roughness.

Description of Equipment

A cutaway view of the test section is shown in Fig. 1. The plenum chamber is preceded by a dense screen to provide a relatively uniform inlet velocity. It is insulated on the inside by teflon (which has a thermal conductivity of about 1/60 of the surrounding steel) to keep the air-temperature rise from the thermocouples to the test piece to a minimum, Fig. 1. Furthermore, the outside of the plenum chamber is not insulated to provide a heat sink for the heat conducted to the plenum chamber. Armstrong A-1 cement was used to insulate the air while passing out of the plenum chamber to the test piece, Fig. 1. Three chromel-alumel thermocouples were installed in the plenum chamber as well as two static-pressure taps. One thermocouple was tack-welded to the outside for check-calculation purposes.

The smooth test piece consists of a 4.5-in-long tube with a 0.025-in. × 0.125-in. duct with 0.050 in. thick walls, rounded at the outside corners with approximately a 0.05 -in. radius. The surface roughness in the direction of air flow varied from 3 to 6 microin. (based on an arithmetical average) and 21 to 24 microin. in the direction normal to the air flow. The former corresponds

[1] This work was performed for General Electric Company and as part of a Master of Science thesis for the University of Cincinnati.

[2] Numbers in brackets designate References at end of paper.

Contributed by the Heat Transfer Division and presented at the Annual Meeting, New York, N. Y., November 30–December 5, 1958, of The American Society of Mechanical Engineers.

Note: Statements and opinions advanced in papers are to be understood as individual expressions of their authors and not those of the Society. Manuscript received at ASME Headquarters, August 5, 1958. Paper No. 58—A-122.

Nomenclature

A = fluid free-flow area
A_c = tube-wall cross-sectional area
A_{LN} = tube-wall log-mean area
C_p = specific heat at constant pressure
D_H = effective hydraulic diameter
f = Fanning friction factor
g = gravitational constant
h_m = heat-transfer coefficient based on local wall-surface temperature and mixed mean local fluid temperature
k = fluid thermal conductivity
k_w = tube-wall thermal conductivity
k_s = mean protrusion height
L = tube length
M = Mach number
Nu_m = Nusselt number (based on local mixed fluid temperature and local wall temperature), $Nu_m = h_m D_H/k$
P_H = heated perimeter, for rough surface use maximum perimeter
Pr = Prandtl number, $Pr = \mu C_p/k$
P_s = static pressure
p_t = total pressure
Q = corrected radial heat flow
q = radial heat flow per unit area
R = maximum tube radius, for rough tube taken as 1/2 duct maximum height
Re = Reynolds number, $Re = \rho \bar{u} D_H/\mu$
t = tube-wall thickness
T_f = fluid temperature
T_w = wall-surface temperature at maximum radius
T_{wo} = outside-tube-surface temperature
$\bar{u}$ = mean axial velocity
W = cooling air flow
X = co-ordinate parallel to pipe axis
λ = Darcy friction factor
μ = absolute viscosity
ν = kinematic viscosity
ρ = fluid density

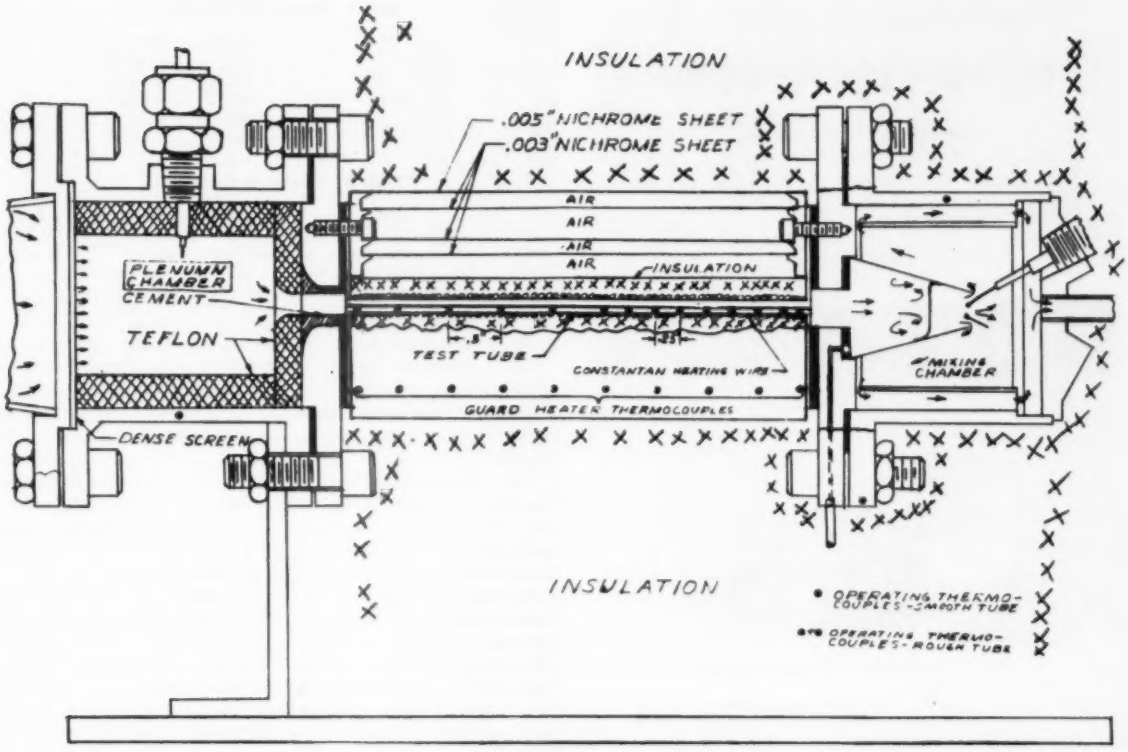

Fig. 1 Test section

to a radius to mean protrusion height ratio of approximately 800 which will be considered smooth (the radius used here was half the maximum duct height). The tube was made in two pieces and brazed together along with a 0.030-in-thick disk on each end to fasten to the plenum and mixing chambers. Gaskets were placed between the test piece and the chambers and the test piece was screwed in place using a relatively heavy back-up plate. The back-up plate had four concentric rings to hold the nichrome strips which provided radiation and convection insulation since the spacing between the rings was sufficient to adequately inhibit free convection.

The tube was instrumented with twelve thermocouples, two of which were lost during assembly, Fig. 1. The tube was then wrapped with two insulated 0.013-in-diam constantan wires, paralleled for the desired resistance. This was then wrapped with asbestos chord to provide insulation and make the unit more rugged during assembly. The tube was wrapped with 4 concentric layers of nichrome sheet (0.003 and 0.005 in. thick). The final layer was instrumented with 10 thermocouples and wrapped with 9 coils of nichrome wire (the second tube had 8 coils of nichrome ribbon) each connected to terminal boards overhead. This was again wrapped with asbestos chord and some cement applied.

The rough tube was 4.5 in. long and the maximum width and height were 0.145 in. and 0.045 in., respectively. The protrusions were approximately 0.010 in. × 0.010 in. × 0.010 in. and were spaced approximately 0.010 in. apart, leaving an open duct area of 0.025 in. × 0.125 in., Fig. 2. Fig. 3 shows the protrusions at the completion of the tests.

Based on the maximum radius, the radius to protrusion height ratio R was 2.5. The relatively large protrusions were selected primarily for ease of manufacture and to show whether the relatively high heat-transfer coefficients indicated as possible by a previous analysis (not discussed here) could actually be achieved. The wall thickness was again 0.050 in. (exclusive of the protrusions) and the edges were rounded to about a 0.025-in. radius. The disks at the tube ends were increased in thickness to 0.060 in. because of manufacturing and resulting sealing difficulty experienced with the first tube.

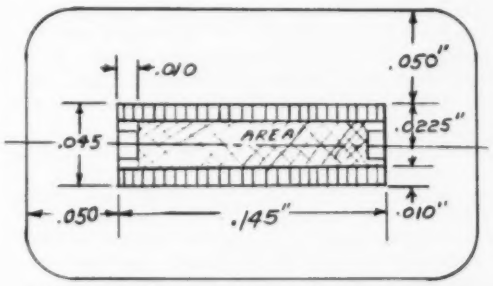

Fig. 2 Rough duct cross section taken normal to axis

The tube was assembled in a fashion similar to the smooth tube with the exception of having 16 operating thermocouples, an improved guard heater including nichrome ribbon instead of wire, and appreciable insulation around the guard heater. This was done in an attempt to improve the low Reynolds-number results. (A comparison of Figs. 8 and 9 indicates that the end effects were reduced.)

The main function of the mixing chamber was to provide an accurate value of the exit-gas temperature. The air leaving the duct impinged on a flat mixing strip. A nozzle of 0.003-in-thick L-605 sheet metal directed the air at three CA thermo-

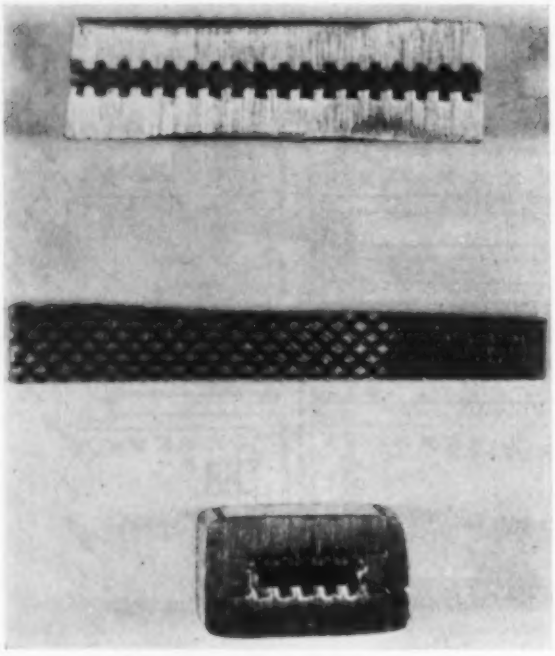

Fig. 3 Protrusions at completion of tests

couples. The air then flowed over the thermocouple shank twice while following a path to minimize the heat losses of the tube exit air before reaching the thermocouples, Fig. 1. The mixing chamber was further insulated on the outside with about 1 in. of insulation. For the second tube the insulation was improved and increased in thickness to about 2.5 in. In addition, thermocouples were installed on the flange and outer wall of the mixing chamber.

The downstream static pressure was measured and a static tap placed in the upstream wall of the mixing chamber as shown in Fig. 1.

Bottled air (dew point, 60 F) was used. The pressure was reduced by two regulators to about 100 psia at the plenum chamber.

The electrical system for the second tube differed from the first tests only in that 8 guard heater coils were used rather than 9 and that a constant-voltage transformer was included in the guard-heater system. The 8 guard-heater coils were controlled by 8 separate variacs. The sensitivity of these secondary variacs was increased by feeding them by a 9th primary variac which was connected to the 110-volt a-c supply. The tube electrical system was similar to the guard-heater supply but had a single variac for control. Ammeters and voltmeters were installed and the experimental tube power was computed from the current and resistance of the constantan wire.

Reduction and Analysis of Data

The actual dimensions of both the smooth and rough tubes differed from the design value. Only the measured values were used and they are given in Tables 1 and 2.

The evaluation of the local heat-transfer coefficient was made by considering a differential portion of the duct as shown in Fig. 4. The details are given in [1]. The resulting equation is

$$h_m = \frac{Q}{P_H(T_w - T_c)} + \frac{k_w A_c \dfrac{d^2T_w}{dx^2}}{P_H(T_w - T_c)} \qquad (1)$$

Table 1 Smooth-tube dimensions

Item	Design	Measured
Height, in.	0.025	0.0229
Width, in.	0.125	0.1297
Area, sq in.	0.00312	0.00297
P_w, in.	0.300	0.305
D_H, in.	0.0417	0.0389

Table 2 Rough-tube dimensions

Item	Design	Measured
Maximum height, in.	0.045	0.045
Minimum height, in.	0.025	0.025
Maximum width, in.	0.145	0.1474
Minimum width, in.	0.125	0.1274
Minimum area, sq in.	0.00312	0.00318
Minimum D_H, in.	0.0417	0.0418
Maximum P_w, in.	0.380	0.385
Minimum P_w, in.	0.300	0.305

The second term on the right accounts for the net heat conducted along the tube rather than to the cooling air in the differential length dx.

The heat generated per unit length was calculated from the measured resistance of the coil divided by the length of the winding. The resistance change due to temperature was calculated and neglected when found to be negligible (the temperature coefficient for constantan at 25 C is 2×10^{-6} ohm/ohm deg C).

The heat generated was then corrected by the over-all heat-balance deficiency. That is, the heat picked up by the cooling air plus that conducted out the ends of the tube was subtracted from the total heat generated and the difference was assumed to be lost uniformly along the tube length to the surroundings. The heat picked up by the cooling air was calculated from the inlet and exit-air temperature measurements, the measured weight flow, and the average specific heat. The corrections varied from 1 to 3 per cent for runs equal to and above Re = 8000, from 7 to 8 per cent for Re = 5000 and from 12 to 13 per cent for Re = 3000. The corrections increased to 33 per cent for Re = 1000, and, as a result, all values for Re < 3000 were discarded. The values for Re = 3000 are included in Fig. 5 as indicating the transition region and are not used further.

The heated perimeter was taken as the inside tube perimeter normal to the air-flow direction.

The wall temperature was calculated from the following equation:

$$T_w = T_{wo} - \frac{Qt}{K_w A_{la}} \qquad (2)$$

The local cooling air temperature was calculated in a stepwise manner as shown in the following for a portion of the duct lying between two thermocouples a distance x apart as in Fig. 4.

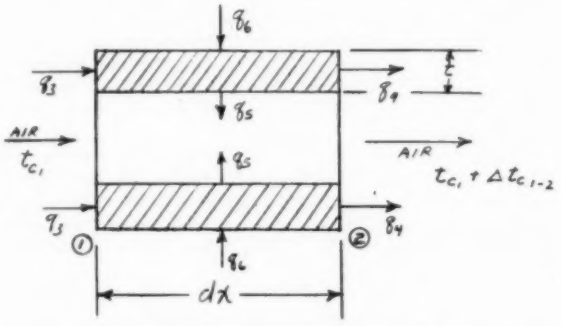

Fig. 4 Duct cross section taken parallel to axis

The resulting equation is

$$T_{ci} = T_{c\,\text{inlet}} + \sum_{j=0}^{j=i} \Delta T_{ci-1\,\text{to}\,i} \tag{3}$$

where

$$T_{ci-1\,\text{to}\,i} = \frac{1}{wc_p}\left[Q\Delta x + k_w A_c \left(dTw_0/dx\Big|_i - \frac{dT_{w0}}{dx}\Big|_{i-1}\right)\right.$$

The details of the analysis are in reference [1]. The remaining term $(d^2T_w)/(dx^2)$ was measured from a graph of $(dT_w)/(dx)$ versus X.

All the fluid properties were evaluated at the local film temperature using [2] which contained data obtained from [3].

The friction factor was calculated assuming the fluid was compressible, that there was an entrance pressure loss equal to 1/2 the difference between the total and static pressure at the inlet, and that the exit static pressure was equal to the mixing-chamber pressure: In addition, the flow area for the rough tube was taken as that between the tips of the protrusions (shaded portion of Fig. 2).

Results and Discussion

The dimensionless heat-transfer coefficients (Nu_m) for the smooth and rough tubes are graphically presented in Fig. 5 and tabulated in Tables 5 and 6. The increase in Nusselt number for the rough tube is almost twice that of the smooth tube. Included in Fig. 5 is the Colburn equation (4) for smooth round ducts in turbulent flow, and it is seen to fit the smooth-duct experimental data very well in the turbulent-flow range. The dashed curve was fitted to the rough-tube data, assuming it should be parallel to the smooth curve and that the data for Re = 5000 was in the transition region. The resulting equation is

$$Nu_m = 0.042\ Re^{0.8}\ Pr^{1/3} \tag{4}$$

as compared to the Colburn equation for smooth round pipes

$$Nu_m = 0.023\ Re^{0.8}\ Pr^{1/3} \tag{5}$$

where the fluid properties are evaluated at the fluid film temperature.

W. Nunner [5] assumed (based on his experimental results) that the protrusion size, shape, and spacing had the same type of effect on the friction factor as on the heat-transfer coefficient and concluded that he could express the Nusselt number as a function of Re, Pr, λ, and λ_0 alone (where λ_0 is the friction factor for a smooth pipe). On this basis he derived the following equation:

$$Nu_m = \frac{\lambda/8\ Re\ Pr}{1 + 1.5\ Re^{-1/6}Pr^{-1/6}(Pr\ \lambda/\lambda_0 - 1)} \tag{6}$$

Equation (6) is plotted in Fig. 5 for the experimentally determined friction factor λ and can be seen to compare favorably with the experimental results. This is particularly interesting since the equation also agreed well with the continuous ring type of roughness considered in [5] although various rings and spacings were tested.

The friction data are presented in Fig. 6 and it becomes immediately apparent that the "smooth tube" was not as smooth as assumed. When these results were obtained the smooth tube was reassembled and additional data taken, but no significant deviation from the previous data was found. The tube was then cut open and the surface finish rechecked and again the results agreed with the previous measurements.

Apparently the fine surface scratches, which run in the direction of the tube axis, were sufficient to cause the smooth tube to act like a rough tube. Even though these scratches are barely

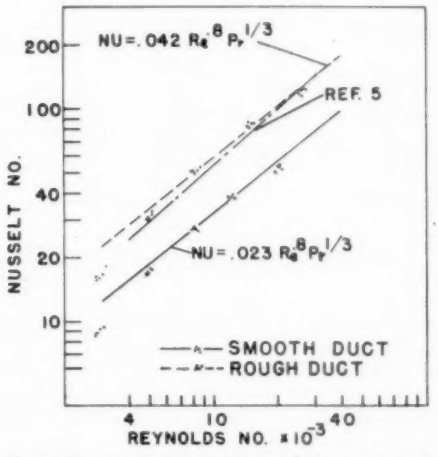

Fig. 5 Comparison of smooth and rough-duct experimental results. (Heat-transfer data.)

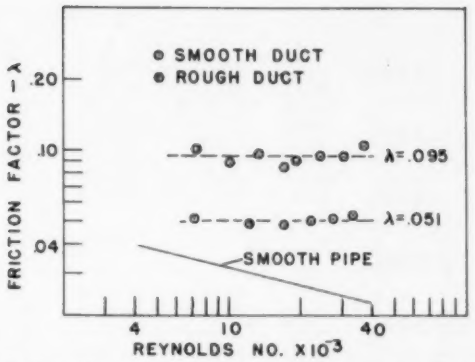

Fig. 6 Comparison of smooth and rough-duct experimental results. (Friction data.)

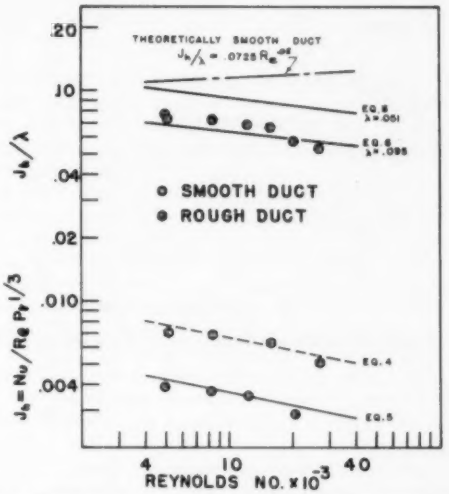

Fig. 7 Comparison of smooth and rough-duct experimental results. (j_m factor and j_h/λ ratio.)

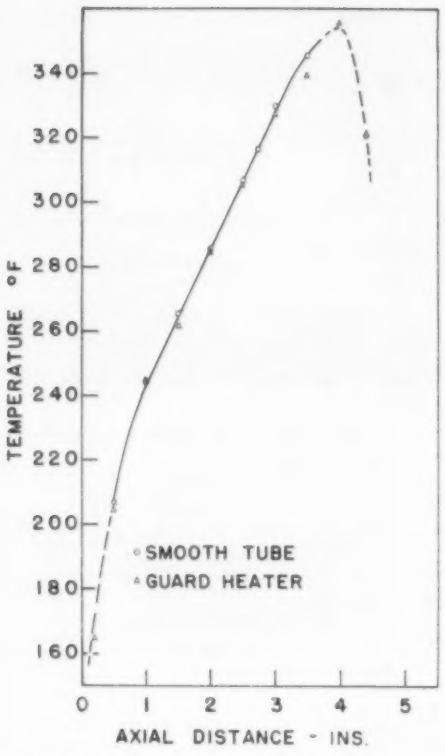

Fig. 8 Smooth duct and guard heater temperature distribution for Re ≅ 8200

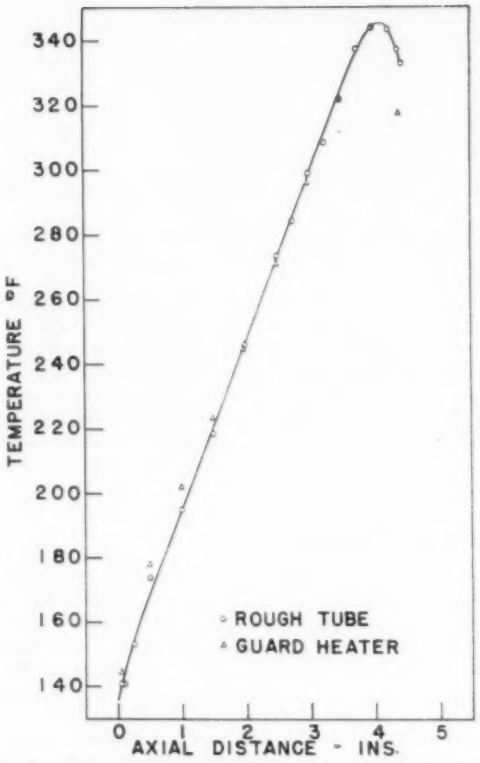

Fig. 9 Rough duct and guard heater temperature distributions for Re ≅ 8400

Table 3 Heat-transfer results—smooth tube

X, in.	Nu_m	Re	Nu_m	Re	Nu_m	Re	Nu_m	Re	Nu_m	Re
1.5	9.46	3010	17.4	5160	26.7	8510	38.1	12600	51.9	21200
2.0	9.26	2930	17.7	5040	27.2	8316	39.5	12400	54.3	20700
2.5	8.81	2870	16.8	4950	27.2	8169	38.5	12200	52.5	20400
2.75	8.85	2820	17.2	4905	27.7	8090	38.9	12200	53.4	20200
3.0	8.52	2790	16.52	4820	27.0	7950	37.4	11900	49.8	19800
3.25			16.9	4770	27.0	7860	38.1	11800	50.4	19700
Weighted mean values	9.07	2910	17.2	4980	27.1	8212	38.5	12300	52.3	20500

Table 4 Heat-transfer results—rough tube

X, in.	Nu_m	Re	Nu_m	Re	Nu_m	Re	Nu_m	Re	Nu_m	Re
1.5	18.25	3110	33.0	5190	53.3	8760	85.5	15430	123.3	27700
2.0	16.87	3020	31.7	5150	51.5	8460	84.7	15210	123.6	27300
2.5	16.00	2920	29.9	4960	49.8	8230	81.9	14900	114.3	26600
2.75	16.14	2880	30.9	4910	51.4	8100	86.9	14800	122.6	26200
3.0	15.73	2830	30.2	4870	51.2	7980	83.1	14690	114.7	25800
Weighted mean values	16.85	2980	31.4	5050	51.6	8380	84.4	15080	120.3	26900

visible to the naked eye and cover a relatively small portion of the duct surface, they are apparently the controlling factor. As noted previously, the measured surface finish normal to the tube axis was 21 to 24 microin., which corresponds to an average peak-to-valley height of about 74 to 84 microin. This corresponds to a radius-to-protrusion-height ratio of about 150. In addition, there were very small traces of braze material in one of the tube corners. As pointed out to the author in [7] this roughness may explain why the results agree with the Colburn equation with a coefficient of 0.023 rather than with the lower values of 0.019 to 0.021 now accepted for air.

Fig. 7 shows that the ratio of j-factor to the friction factor (which is given as constant by the usual Reynolds' analogy) is appreciably higher for the really smooth tube (as given by the Blasius friction factor) than for the rough tubes of this experiment. In general, this agrees with the previous concept that generally the gain in heat transfer due to surface roughness is smaller than the loss due to increased friction. The closeness of

Table 5 Friction-factor results—smooth tube

W, lb/hr	P_{t_0}, in. Hg	P_{t_2}, in. Hg	M_1 Ent.	M_2 Exit	f Fanning	λ Darcy	Re
3.839	70.8	41.0	0.283	0.445	0.0125	0.0494	12300
6.877	120.2	58.7	0.298	0.549	0.0126	0.0503	22100
8.585	150.1	69.9	0.298	0.575	0.0130	0.0519	27500
10.31	181.8	82.3	0.297	0.587	0.0133	0.0531	33100
5.315	93.5	49.0	0.297	0.510	0.0120	0.0481	17100
3.828	70.0	41.0	0.283	0.443	0.0123	0.0491	12300
2.223	48.0	34.2	0.236	0.309	0.0130	0.0520	7131

Table 6 Friction-factor results—rough tube

W, lbs/hr	P_{t_0}, in. Hg	P_{t_2}, in. Hg	M_1 Ent.	M_2 Exit	f Fanning	λ Darcy	Re
3.173	70.3	38.0	0.213	0.370	0.0224	0.0894	10190
4.187	91.7	43.3	0.215	0.428	0.0242	0.0967	13450
5.323	110.5	48.5	0.229	0.482	0.0214	0.0858	17100
6.057	127.5	53.3	0.225	0.500	0.0229	0.0916	19460
7.560	160	63.0	0.223	0.525	0.0236	0.0955	24280
9.577	202	76.0	0.225	0.550	0.0237	0.0947	30760
11.59	251	91.5	0.216	0.555	0.0264	0.1055	37230
2.282	55.5	34.4	0.193	0.300	0.0256	0.1022	7330

the smooth-tube results to the rough tube indicates that the roughness of the smooth tube is inefficient. (This is primarily because the roughness was unintentional.) In other words, it appears that a tube surface roughness can be designed which would have a greater Nusselt number for the same friction factor as the smooth tube (presumably reducing the height of the protrusions of the rough tube would result in such a tube).

Conclusions and Recommendations

(*a*) The equation derived in [5] appears to be sufficiently accurate for predicting the Nusselt number and is recommended for use at the present time.

(*b*) Very small tubes (D_H of the order 0.040 in.) will act like rough tubes unless extreme care is taken to insure a smooth surface.

(*c*) Appreciable gains in the dimensionless heat-transfer coefficient (Nu_m) can be made by increasing the tube-surface roughness but generally at the cost of an even greater increase in friction factor.

References

1 R. T. Lancet, "The Effect of Surface on the Convection Heat Transfer Coefficient for Fully Developed Turbulent Flow in Ducts," MS thesis, University of Cincinnati, Cincinnati, Ohio, 1957.

2 "General Electric Design Data Books," Section G-513.1, p. 1.

3 National Bureau of Standards Circular Number 564, November 1, 1955.

4 W. H. McAdams, "Heat Transmission," third edition, McGraw-Hill Book Company, Inc., New York, N. Y., 1954.

5 Wolfgang Nunner, "Warmeabergang and Dreeckabfall in Rauhen Rohren," *VDI Forschungsheft*, 445, 1956.

6 E. W. Sams, "Experimental Investigation of Average Heat Transfer and Friction Coefficients for Air Flowing in Circular Tubes Having Square-Thread-Type Roughness, NACA RM E52 D 17.

7 R. H. Norris, memorandum to author, March 20, 1958.

DISCUSSION

G. A. Sterbutzel[3]

This very interesting paper illustrates the large effects on heat transfer that can result from surface roughness. Of some concern to the author in his discussion is the flow which existed in the smooth tube and the effects of the relatively minute circumferential roughness. A point in question in the case of the smooth tube is the state of the boundary-layer development. Even at Reynolds numbers as small as 3000, for an appreciable portion of the length, fully developed tube flow will not have been achieved. Perhaps this can explain a deviation from fully developed flow equations for smooth tubes.

The 0.023 constant used in the Colburn correlation does not seem to be unusually high, although perhaps it is higher than the latest data. Because it is on the high side, it is interesting to compare the thickness of the laminar sublayer in turbulent flow with the height of the surface roughness in the smooth tube. If the surface roughness is greater than the thickness of the laminar sublayer, the results probably will be somewhat affected. Unfortunately, the computation of the sublayer thickness is clouded by the need to estimate the shear stress and the existence of entrance conditions. Results show that in some of the test runs the height of the roughness may approach the thickness of the laminar boundary layer, but it is believed that generally the surface-roughness height will be less than the normal thickness of the laminar sublayer. This is not necessarily inconsistent with the relatively high friction factors found using the smooth tube since short tubes sometimes give apparent friction factors which are higher than would normally be expected.

Since the foregoing discussion is centered around the results in the smooth tube, it illustrates the need for more work in the area of marginal roughness; that is, the thresholds of roughness which will produce increased heat-transfer characteristics in a tube of this general size.

Myron Tribus[4]

Just before "Conclusions and Recommendations," the author states: "In other words, it appears that a tube-surface roughness can be designed which would have a greater Nusselt number for the same friction factor as the smooth tube."

The writer has always believed that whereas one can obtain an increase in heat transfer through the addition of roughness, the increase in pressure drop always exceeds the increase in heat transfer and therefore, the smooth tube is always the best heat-transfer surface if one is comparing heat transfer and pressure drop only. The writer would therefore like a clarification of what is meant by the foregoing statement.

Author's Closure

While for low Prandtl number fluids in laminar flow the inlet

[3] Head, Heat Transfer Section, Cornell Aeronautical Laboratories, Inc., Buffalo, N. Y.

[4] Professor of Engineering, University of California, Los Angeles, Calif. Mem. ASME.

length required to obtain fully developed flow will be of the order of 50 to 150 tube diameters, shorter lengths are required in turbulent flow. For example, Deissler (NACA Report 1210) shows analytically (for Prandtl number = 1 and Reynolds numbers from 10^4 to 2×10^5) that heating rates reach 99 per cent of the fully developed turbulent value in 5 to 7 diameters. Furthermore, Boelter, Young, and Iverson (NACA TN 1451) give experimental data for air flowing in a tube with sharp edge entrance conditions which indicate that fully developed heating rates will be obtained in 15 to 17 diameters for Reynolds numbers as high as 36,000. Since local heat-transfer coefficients were determined in the range of 35 to 75 diameters, it is unlikely that they were influenced by entrance effects.

The friction factors, however, represent average values for the entire tube and must therefore be influenced by the entrance effects. However, the extent of the entrance effect can be estimated, for the smooth pipe, by considering the effect of the entrance on the average heating rates. Using the experimental data of NACA TN 1451 it was found by the writer that after 17 diameters the average heating rate was approximately 18 per cent greater than the local value. Extending these data to a tube with an L/D of 115 (corresponding to this experiment) the entrance effect would cause the average value to be only 2.6 per cent greater than the local value. Therefore entrance effects alone cannot explain the high smooth tube friction factors which were from 33 per cent to 122 per cent greater than truly smooth tube. While the writer does not completely understand these high values of friction factor, it is felt that they may result from phenomenon which cannot be directly scaled down to the small diameters encountered in this paper.

As it was pointed out in the last paragraph of the paper before the "Conclusions and Recommendations" ". . . . . the gain in heat transfer due to surface roughness is smaller than the loss due to increased friction." This can be seen more clearly in the revised Fig. 7 where both the experimental data of this paper and equation (6) from reference [5] show the ratio of the $j(= \mathrm{Nu}/\mathrm{RePr}^{1/3})$ factor to friction factor for the rough ducts to be less than the theoretically smooth duct. Thus the data of this paper are in concurrence with the literature and Professor Tribus. The statement in question (see comment by Myron Tribus) is based on the assumption that not all types of roughness produce the same heat-transfer rates for a given pressure drop. Referring again to the revised Fig. 7 we see that equation (6) agreed reasonably well with the rough tube data. However, equation (6) indicated appreciably higher values of heating rates could have been obtained for the so-called smooth tube of this experiment if the roughness were properly designed. In other words, if one must accept surface roughness, proper design will produce the maximum heat-transfer rate for the given pressure drop. However, this value will be less than the theoretically smooth value shown in Fig. 7.

Journal of HEAT TRANSFER

Information for Authors

• Manuscripts should be submitted in final form to the Editor. Each manuscript must be accompanied by a statement that it has not been published elsewhere nor has it been submitted for publication elsewhere. A paper which would occupy more than 8 pages of the Journal may be returned to the author for abridgment.

• The author should state his business connection, the title of his position, and his mailing address. A short abstract (50 to 100 words) should be included on the first page immediately preceding the introductory paragraph of the paper.

Three copies of the manuscript are required. One of these must be a carefully prepared printer's copy, typed in double spacing, on one side of the page only, with wide margins, on $8^1/_2$ by 11-in. opaque white paper. Mimeographed manuscripts, if prepared with exceptional care, can be accepted provided they are completely edited.

• As far as possible, all mathematical expressions should be typewritten. Greek letters and other symbols not available on the typewriter should be carefully inserted in ink. Care should be taken to distinguish between capital and lowercase letter, between zero (0) and the letter (*O*), between the numeral (1) and the letter (*l*), etc. A letter representing a vector cannot be printed with an arrow above or below it. The letter should be underscored with a single wavy line, wherever it appears in the text, to designate boldface type.

• A list of symbols carefully marked for the use of the editor (thus: κ, Greek l.c. kappa), if it has not been included in the body of the paper, should accompany the manuscript on a separate page.

• Before preparing a manuscript the author should study printed articles in the Journal, with special attention to the form and style of mathematical expressions, tables, footnotes, references, and abstract. Numbers that identify mathematical expressions should be enclosed in parentheses. Numbers that identify references at the end of the paper should be enclosed in brackets. Care should be taken to arrange all tables and mathematical expressions in such a way that they will fit into a single column when set in type. Equations that might extend beyond the width of one column (fractions that should not be broken or long expressions enclosed in parentheses) should be rephrased to go on two or more lines within column width. Fractional powers are preferred to root signs and should always be used in more elaborate formulas. The solidus should be used instead of the horizontal line for fractions wherever possible.

• A normal paper should not exceed 8 pages in the Journal. It is about 8000 words or 20 double-spaced typewritten pages exclusive of drawings. A Technical Brief should not exceed 750 words or about one page in the Journal inclusive of drawings.

• Originals and two copies of figures must accompany the manuscript. Line drawings should not be larger than $8^1/_2 \times 11$ in. and should be planned for reduction to column width. Lettering should be large enough to be clearly legible when the illustration is reduced. The originals of line drawings must be in India ink on white or pale blue tracing paper or tracing cloth. Photographs of equipment or test specimens must be glossy prints and should be used sparingly. Captions for figures should be typed double-spaced and included as the last page of the manuscript. The figure number and author's name should be written in the margin or on the back of each illustration.

• Titles of papers should be brief.

• Authors can obtain copies of the ASME Manual MS-4, "An ASME Paper," from the Editor and are urged to do so before drafting their papers in final form.

• Papers published in Journals of the Transactions of the ASME must be presented at a Meeting, either in person or by title. Scheduling of papers is in the hands of the Publications Committee.

• An author is entitled to 25 preprints free of charge (in the case of two authors, 15 each; three or more authors, 10 each). Larger quantities of preprints or reprints can be ordered from Editorial Department, The American Society of Mechanical Engineers, 29 West 39th Street, New York 18, N. Y. Quotations will be sent on request.

Please address all communications to:

Editor, ASME,

29 West 39th Street,

New York 18, N. Y.

ASME Publications Committee

Engineers' Reference Books

PROCEEDINGS, 3rd U. S. NATIONAL CONGRESS OF APPLED MECHANICS

Published 1958. $20.00 to members and nonmembers.—Within this 904-page volume are reports of important studies in the fields of dynamics, vibration, elastic waves, elasticity, elastic structures, plasticity, viscoelastic flow, fracture, fluid flow, aerodynamics, and heat transfer. There are also discussions of new concepts and methods, and a large amount of new data which will aid in generating new ideas and new approaches toward solving other problems of the applied mechanics field. The information was presented by 155 well-known engineers at the June 1958 congress.

MECHANICAL IMPEDANCE METHODS FOR MECHANICAL VIBRATIONS

Published 1958. $5.50.—Shows how impedance methods apply to lumped and continuous systems of simple and moderate complexity, reviews measurement techniques, demonstrates the power of digital computers by comparing the calculated and measured characteristics of a highly symmetrical system of moderate complexity, gives measured values of typical structures of large size and high complexity, discusses the importance of the impedance in influencing shock and vibration spectra measured in field service, indicates how to apply impedance methods to the calculation of vibration insolator effectiveness, treats impedance of some disordered systems, and illustrates how impedance methods may be used to find the response to random excitation.

SHOCK AND VIBRATION INSTRUMENTATION

Published 1956. $5.00.—This book provides a fund of useful information on recent advances and new concepts in the technology of shock and vibration. Among the subjects discussed are random vibration, effect of non-rigid structures on vibration isolation, hysteresis and slip damping, vibration and shock testing, design approaches and analog methods. CONTENTS: Evaluation of Mounts Isolating Nonrigid Machines from Nonrigid Foundations. Experimental Study of the Effects of Foundation Resilience on Vibration Isolating. Effect of Material and Slip Damping on Resonance Behavior. Shock and Vibration Environments. Mechanical Design for Random Vibration and Shock. Influence of Electrical and Motional Impedance on the Control and Performance of Some Vibration Machines. Shock Testing Machines and Procedures. Damaging Potential of Shock and Vibration. High Speed Computing Methods for Shock and Vibration Problems.

METALS ENGINEERING: PROCESSES

Published 1958. $13.50.—Presents detailed data on the various processes by which metals are converted into finished products. For each of the manufacturing methods, there is a compilation of the basic physical characteristics to be considered and the general advantages and limitations usually encountered. Concise, parallel data concerning the suitability of various metals for each process, and the tolerances on size and surface finish obtainable are included.

ENGINEERING TABLES

Published 1956. $12.00.—A collection of tables often wanted by engineers but not commonly found in handbooks covering: Bar Stock and Shafting. Conversion Factors. Formulas for Stress and Strain. Properties of Sections and Cylinders. Bearings. Bearing Load Analysis. Spur Gears. Helical and Herringbone Gears. Bevel Gears. Worm Gears. Cylindrical Fits. Standard Tapers. Keys and Keyseating. Bolts. Counterbores. Screw Threads. Slots. Serrations and Splines. Nuts. Pins. Snaprings. Washers. Wrench Openings. Springs. Aircraft and Mechanical Tubing. Pressure Tubes. Pipe. Pipe Threads and Fittings. Electric Motors. Graphical Symbols. Welding. Gaskets. Hydraulic Standards and Symbols. O-Rings. Packings. Seals. Bibliography.

THERMODYNAMIC AND TRANSPORT PROPERTIES OF GASES, LIQUIDS AND SOLIDS

Published1959. $12.50.—Provides a wealth of information that can be profitably applied to the solution of many problems in various areas demanding a knowledge of thermal properties of materials. Specifically, the book surveys the present theoretical and experimental state of the science; reports a large amount of data on experimental and theoretical techniques; reviews and evaluates the present state of knowledge in the specific areas covered; and indicates the gaps of knowledge existing in both transport and thermodynamic properties, particularly at high temperatures and at high or even moderate pressures. The information was originally presented at a Symposium sponsored by the Standing Committee on Thermophysical Properties of the ASME Heat Transfer Division in February, 1959.

PROCEEDINGS OF THE CONFERENCE ON LUBRICATION AND WEAR

Published 1958. $23.00—Here is the complete record of the 1957 Conference arranged by the Institution of Mechanical Engineers with the collaboration of the ASME for the purpose of evaluating current lubrication knowledge, bringing out the findings of important experiments conducted in the United States, Canada, United Kingdom, and Europe; and obtaining the views of those participating in the discussion. Subjects dealt with include hydrodynamic lubrication, boundary friction, boundary lubrication, bearing metals, novel bearing materials, glands and seals, solid lubricants, surface treatments, ball and roller bearings, gear lubrication, engine lubrication, miscellaneous lubricants and applications, additives, and wear. The 34 papers on the latter subject cover laws of wear rate; mechanism of wear; testing of materials for resistance to wear; surface films; effective temperature and environment; wear due to abrasion, fretting, scuffing, pitting; wear on cutting tools; wear in engines, gears, etc.; influence and nature of rubbing surfaces.

THERMODYNAMIC PROPERTIES OF COMPRESSED WATER

Published 1957. $2.50.—Here is a chart that fills the need for an accurate and convenient presentation of the thermodynamic properties of compressed water. These properties which include temperature, pressure, specific volume, enthalpy and entropy, are presented graphically in a large scale chart broken up into fifteen plates. The temperature range covered is from 32 to 705.4°F and the pressure range, from 0.08854 to 6000 PSIA.

METALS ENGINEERING: DESIGN

Published 1953. $10.00.—This book discusses the essential properties which need to be evaluated by the design engineer in his selection of one material over another. Comprising 48 sections and written by 43 well-known authorities, it deals with the over-all problem of selection of material and takes up such specific items as high temperature considerations, plasticity, residual stresses, vibration, fatigue, shot peening, cold working, nitriding, flame strengthening, impact, corrosion, non-destructive testing, surface finish and mass production, and design theory and practice.

METALS PROPERTIES

Published 1954. $11.00.—Provides, in convenient charts and tables, data on a broad range of metals in common industrial use —AISI steels, ASTM steels, cast copper alloys, aluminum alloys, tin, magnesium, etc. Tabulated under each of the more than 500 metals listed is such information as the chemical composition of the metal; its brittleness, heat treatment and other characteristics; its industrial uses; treatment temperatures for forging, annealing, quenching, etc.; such technological properties as recrystallization temperature and hot working temperature, and a great deal of other pertinent information to help the designer choose the proper metal for each part or product.

FLUID METERS, THEIR THEORY AND APPLICATION

Published 1959. $8.00.—This Fifth Edition includes information on a number of new types of fluid meters and metering procedures that have been developed in recent years. It is divided into three sections with the first giving the classification and nomenclature of fluid meters, together with definitions of special terms and other general information. The theory of fluid measurement and the steps taken to develop practical working equations from the theoretical relations are set forth in the second section. Figures and tables for use in solving practical fluid measurement problems, along with examples illustrating their proper use, are contained in the third section.

FLOW MEASUREMENTS (*Chapter 4, Part of 5 Instruments and Apparatus*)

Published 1959. $5.00.—These rules apply when the primary element is an orifice, a flow nozzle, or a Venturi tube. The fluid may be compressible or incompressible. The primary element may be installed within a continuous section of pipe flowing full, or at the inlet or exit of a plenum chamber. Specifically this Chapter includes information on the construction of these three primary elements, the recommended techniques governing tests, the necessary equations for computing rate of flow, examples to illustrate the application of typical data, a discussion of tolerances applicable to certain of the factors involved in the measurements, and an outline of the major advantages and disadvantages of various types of primary elements.

77-YEAR INDEX TO ASME TECHNICAL PAPERS

Published 1957. $20.00.—This is an index to the technical papers published in the ASME Transactions, the Journal of Applied Mechanics, and Mechanical Engineering for the past seventy-seven years. It is divided into two parts with the first covering the papers published between 1880 and 1939, and the second, indexing those published from 1940–1956. Each part has a subject and an author index. The former lists the titles of the papers chronologically under as many headings as are necessary and includes numerous cross-references to direct attention to related material. The alphabetically arranged authors' index gives the headings and the year under which each paper is listed in the subject index.

VISCOSITY OF LUBRICANTS UNDER PRESSURE

Published 1954. $3.00.—This publication reviews and coordinates twelve experimental investigations, made over a period of thirty-five years, on 148 lubricants comprising of 25 fatty oils, 94 petroleum oils, 17 compounded oils and 12 other lubricants. Data are coordinated by means of sixty tables in which the results originally appearing in diversified units are compared. The methods proposed for correlating viscosity-pressure characteristics of oils with properties determined at atmospheric pressures are reviewed and illustrated. Experimental work on heavily loaded bearings, lubrication calculations, and additional techniques for viscosity are covered. Conclusions, and recommendations are presented. Computation of the temperature coefficients of viscosity and the method of computing pressure coefficients are also given.

DIAPHRAGM CHARACTERISTICS, DESIGN AND TERMINOLOGY

Published 1958. $3.75.—This Manual defines a diaphragm and its performance characteristics, describes methods of measuring and representing them, shows how they are related and used, describes and illustrates the effects of design details and manufacturing methods on the characteristics. In the appendixes, the terms and notation used are defined, the equipment and methods of testing described, applications of the diaphragms classified and equations given.

20% Discount to ASME members

THE AMERICAN SOCIETY OF MECHANICAL ENGINEERS **29 W. 39th St., New York 18, N. Y.**